2017

RAD GTPASE: IDENTIFICATION OF NOVEL REGULATORY MECHANISMS AND A NEW FUNCTION IN MODULATION OF BONE DENSITY AND MARROW ADIPOSITY

Catherine Nicole Kaminski Withers
University of Kentucky, kaminski.withers@yahoo.com
Digital Object Identifier: https://doi.org/10.13023/ETD.2017.326

STUDENT AGREEMENT:

I represent that my thesis or dissertation and abstract are my original work. Proper attribution has been given to all outside sources. I understand that I am solely responsible for obtaining any needed copyright permissions. I have obtained needed written permission statement(s) from the owner(s) of each third-party copyrighted matter to be included in my work, allowing electronic distribution (if such use is not permitted by the fair use doctrine) which will be submitted to UKnowledge as Additional File.

I hereby grant to The University of Kentucky and its agents the irrevocable, non-exclusive, and royalty-free license to archive and make accessible my work in whole or in part in all forms of media, now or hereafter known. I agree that the document mentioned above may be made available immediately for worldwide access unless an embargo applies.

I retain all other ownership rights to the copyright of my work. I also retain the right to use in future works (such as articles or books) all or part of my work. I understand that I am free to register the copyright to my work.

REVIEW, APPROVAL AND ACCEPTANCE

The document mentioned above has been reviewed and accepted by the student's advisor, on behalf of the advisory committee, and by the Director of Graduate Studies (DGS), on behalf of the program; we verify that this is the final, approved version of the student's thesis including all changes required by the advisory committee. The undersigned agree to abide by the statements above.

Catherine Nicole Kaminski Withers, Student

Dr. Douglas A. Andres, Major Professor

Dr. Trevor P. Creamer, Director of Graduate Studies

RAD GTPASE: IDENTIFICATION OF NOVEL REGULATORY MECHANISMS AND A NEW FUNCTION IN MODULATION OF BONE DENSITY AND MARROW ADIPOSITY

DISSERTATION

A dissertation submitted in partial fulfillment of the requirements for the degree of Doctor of Philosophy in the College of Medicine at the University of Kentucky

By
Catherine Nicole Kaminski Withers

Lexington, Kentucky

Director: Dr. Douglas A. Andres

Professor of Molecular and Cellular Biochemistry

Lexington, Kentucky

2017

ABSTRACT OF DISSERTATION

RAD GTPASE: IDENTIFICATION OF NOVEL REGULATORY MECHANISMS AND A NEW FUNCTION IN MODULATION OF BONE DENSITY AND MARROW ADIPOSITY

The small GTP-binding protein Rad (*RRAD,* Ras associated with diabetes) is the founding member of the RGK (Rad, Rem, Rem2, and Gem/Kir) family that regulates voltage-dependent calcium channel function. Given its expression in both excitable and non-excitable cell types, the control mechanisms for Rad regulation and the potential for novel functions for Rad beyond calcium channel modulation are open questions. Here we report a novel interaction between Rad and Enigma, a scaffolding protein that also binds to the E3 ubiquitin ligase Smad ubiquitin regulatory factor 1 (Smurf1). Overexpression of Smurf1, but not of a catalytically inactive mutant enzyme, results in ubiquitination of Rad and down regulation of Rad protein levels. The Smurf1-mediated decrease in Rad levels is sensitive to proteasome inhibition and requires the ubiquitination site Lys204, suggesting that Smurf1 targets Rad for degradation. Rad protein levels, but notably not mRNA levels, are increased in the hearts of Enigma$^{-/-}$ mice, leading to the hypothesis that Enigma may function as a scaffold to enhance Smurf1 regulation of Rad.

In addition to ubiquitination, phosphorylation of RGK proteins represents another potential means of regulation. Indeed, Rem phosphorylation has been shown to abolish calcium channel inhibition. We demonstrate that β-adrenergic signaling promotes Rad phosphorylation at Ser39. Rad Ser39 phosphorylation is correlated with a decrease in the interaction between Rad and the $Ca_V\beta$ subunit of the calcium channel and an increase in Rad binding to 14-3-3. Interestingly, Enigma overexpression promotes an increase in Rad Ser39 phosphorylation as well. Despite an interaction between Enigma and the $Ca_V1.2$ calcium channel subunit, overexpression of Enigma had no effect on Rad-mediated channel inhibition. Thus, Rad Ser39 phosphorylation alters its association with the calcium channel, but its impact on calcium channel regulation has yet to be determined.

Finally, we report a novel function for Rad in the regulation of bone homeostasis. Rad deletion in mice results in a significant decrease in bone mass. Dynamic histomorphometry *in vivo* and primary calvarial osteoblast assays *in vitro* demonstrate that bone formation and osteoblast mineralization rates are depressed in the absence of Rad. Microarray analysis revealed that canonical osteogenic gene expression is not altered in $Rad^{-/-}$ osteoblasts; instead robust up-regulation of matrix Gla protein (MGP, +11-fold), an inhibitor of mineralization and a protein secreted during adipocyte differentiation, was observed. Strikingly, Rad deficiency also resulted in significantly higher bone marrow adipose tissue (BMAT) levels *in vivo* and promoted spontaneous *in vitro* adipogenesis of primary calvarial osteoblasts. Adipogenic differentiation of WT osteoblasts resulted in the loss of endogenous Rad protein, further supporting a role for Rad in the control of BMAT levels. These findings reveal a novel *in vivo* function for Rad signaling in the complex physiological control of skeletal homeostasis and bone marrow adiposity.

In summary, this dissertation expands our understanding of Rad regulation through identification of a novel binding partner and characterization of post-translational regulatory mechanisms for Rad function. This work also defines a new role for Rad that may not depend upon its calcium channel regulatory properties: regulation of the bone-fat balance. These findings suggest that the regulation of Rad GTPase is likely more complex than guanine nucleotide cycling and that functions of Rad in non-excitable tissues warrant further study.

KEYWORDS: Rad GTPase, Ubiquitination, Osteoblast, Adipocyte, Bone

Catherine Nicole Kaminski Withers

July 18, 2017

RAD GTPASE: IDENTIFICATION OF NOVEL REGULATORY MECHANISMS AND A NEW FUNCTION IN MODULATION OF BONE DENSITY AND MARROW ADIPOSITY

By

Catherine Nicole Kaminski Withers

Douglas A. Andres, Ph.D.
Direction of Dissertation

Trevor P. Creamer, Ph.D.
Director of Graduate Studies

July 18, 2017
Date

To my husband, Brad Withers, and our children, Sylvia and Bennett

ACKNOWLEDGEMENTS

I would first like to thank my mentor and the chair of my dissertation committee, Dr. Doug Andres. He has encouraged me to think creatively and has supported me as my project extended into new, unfamiliar fields for our laboratory. I am very grateful for the ways he has pushed and challenged me over the years. I also appreciate all the advice and critiques I have received from the other members of my committee, Dr. Wally Whiteheart, Dr. Craig Vander Kooi, and Dr. Jonathan Satin. The work in this dissertation has benefited greatly from their thoughtful suggestions and feedback, and they have each contributed to my development as a scientist. I would also like to thank my outside examiner, Dr. Chris Norris, for taking the time to read this dissertation and attend my defense.

Next, I want to extend my gratitude to past and present members of the Andres lab. Dr. Geng-Xian Shi and Dr. Weikang Cai helped me to get started in the lab and provided an environment where hard work and fun happened simultaneously. Megan Pannell has been by my side since my second year of graduate school, and I appreciate her companionship along the way. Jeff Smith was a source not only of technical assistance in the lab but also of advice about science and life and fun conversations (especially during football season, Go Steelers!). Dr. Carole Moncman provided invaluable assistance (and patience) with microscopy as well as interesting conversation and delicious cookies. I also thank Dr. Janet Manning, Dr. Zhaiyi Zhang, Dr. Sajad Mir, and Landon Simpson for their company in the lab and for helpful scientific discussions. Finally, I had

the privilege of working with two talented REU students, Linda Castillo and Mariana Sandoval.

We had a number of collaborators who were essential to completion of the work described in this dissertation. The microcomputed tomography core facility at Rush University and the bone histology core facility at IUPUI provided bone assays that were unavailable at UK and allowed us to generate the preliminary data that motivated all of my other studies of $Rad^{-/-}$ mouse bones, and for that I owe them greatly. Dr. Subramanya Pandruvada at UK provided me with the protocol for isolating and differentiating calvarial osteoblasts and splenic pre-osteoclasts and was very responsive to any technical questions I brought to him. The Genomics Core Laboratory at UK helped us to analyze gene expression changes in primary osteoblasts. Dr. Brian Delisle patiently taught me how to patch clamp HEK293 cells, and he generously allowed me to use the electrophysiology rig in his laboratory to perform my experiments. Dr. Wendy Katz showed me how to perform the Echo-MRI analyses. The contributions of each of these individuals made the work described in this dissertation possible, and I am immensely grateful for their assistance.

I am also thankful that I had the opportunity to conduct my graduate training in the Molecular and Cellular Biochemistry department. Thank you to all the faculty, staff, and students that have contributed to my success as a graduate student. I appreciate Dr. Sabire Ozcan, Dr. Yvonne Fondufe-Mittendorf, and Dr. Matthew Gentry allowing me to perform rotations in their laboratories. Many thanks to Dr.

Kevin Sarge, Dr. Michael Mendenhall, and Dr. Trevor Creamer for their work as Director of Graduate Studies during my graduate career. I also sincerely thank Dr. Yvonne Fondufe-Mittendorf, Dr. Emilia Galperin, and Dr. Becky Dutch for their advice as fellow moms in science. Finally, I am thankful for the other friends I have made along the way in Dr. Kara Larson, Megan Pannell, Dr. Caitlyn Riedmann, Smita Joshi, Dr. Stacy Webb, Erica Littlejohn, Satrio Husodo, Marisa Kamelgarn, and many others.

I would also like to acknowledge those who have funded my work along the way. My work was made possible by funding from the National Institutes of Health T32 Interdisciplinary Cardiovascular Training Grant at UK, a Graduate Research Fellowship from the National Science Foundation, and a PEO Scholar Award.

Last but not least, I cannot put into words how appreciative I am for the support and encouragement of my family, without whom none of this would have been possible. My parents, Steve and Glenda Kaminski, have always believed in me and encouraged me when I have doubted myself. They continue to push me to be successful and, most of all, to do what makes me happy. I also want to acknowledge my two sisters, Holly and Kimmi Kaminski, who have brought plenty of laughter into my life. I have been fortunate to inherit two wonderful parents-in-law in Marline and Raymond Withers, and they have been so supportive of Brad and me while we pursued our graduate and medical studies. Our daughter Sylvia and our newest addition, our son Bennett, have brought so much joy into my life and help to keep me grounded when I get stressed with

experiments and science. Most of all, I am so very thankful for my husband, Brad Withers, and for his constant, unswerving love and support. Raising a child in graduate school and medical school, respectively, has not always been easy, and there is no one else I would have wanted by my side to face the challenge.

Table of Contents

List of Tables

List of Figures

Chapter 1

Introduction

Ras superfamily of small GTPases

The Ras superfamily of small monomeric GTP-binding proteins consists of over 170 structurally related proteins that regulate a diverse array of signal transduction cascades and cellular functions [1]. All Ras-related GTPases contain five conserved domains known as G1-G5 and function as guanine nucleotide-dependent switches that are in an active state when bound to guanosine triphosphate (GTP) and an inactive state when bound to guanosine diphosphate (GDP) [2]. Guanine nucleotide exchange factors (GEFs) promote GTP loading of these small G-proteins by facilitating the release of GDP, while GTPase activating proteins (GAPs) catalyze the hydrolysis of GTP to GDP and thus promote inactivation [2]. The small GTPases of the Ras superfamily are divided into five large families, Ras, Rab, Rho, Arf, and Ran, which are further classified into subfamilies based on structural and functional conservation [1]. The studies in this dissertation will focus primarily on Rad, a member of the RGK subfamily within the Ras family.

RGK subfamily of the Ras-related small GTPases

The RGK subfamily of small GTPases consists of four members: Rad (Ras associated with diabetes; also known as Rrad) [3], Rem (Rad- and Gem-like; also known as Rem1 or Ges) [4], Rem2 (Rad- and Gem-like 2) [5], and Gem/Kir (gene expressed in mitogen-stimulated T-cells, or tyrosine kinase-inducible Ras-like) [6]. RGK subfamily G-proteins share a number of unique structural features that are distinct compared to other Ras-related proteins [7-9]. For instance, RGK proteins contain non-conservative substitutions within regions of the Ras core domain that are required for nucleotide binding and hydrolysis. Moreover, proteins of the RGK subfamily have long N- and C-terminal extensions compared to other members of the Ras superfamily, and the C-terminus of these proteins lacks the -CAAX motif that permits lipid modification and directs membrane association of most Ras-related GTPases [10]. Instead, RGK proteins have a conserved polybasic C-terminal motif that directs membrane association without lipid modification, and the C-terminal extension also serves to regulate RGK protein function. The N-terminal extensions range in length from 44-88 amino acids and are not conserved within the RGK family, and the putative G2 effector domains also differ among RGK proteins [11]. This lack of conservation observed within RGK effector domains implies that the regulatory proteins and downstream effector proteins with which RGK proteins interact may be distinct. Established functions for RGK proteins include inhibition of the activity of voltage-dependent calcium channels (VDCCs) through an interaction with the accessory $Ca_V\beta$ subunit [11-18] and regulation of cytoskeletal dynamics through control of

the Rho/Rho kinase signaling axis [19-22], and a growing literature suggests the potential for novel functions of RGK family proteins in processes including metabolism [23-27], tumorigenesis [24-39], transcriptional regulation [25, 40-42], and stem cell differentiation [42-46]. The means by which RGK protein function is regulated in each of these settings is an active area of investigation in the field. Interestingly, RGK proteins exhibit distinct tissue expression profiles [11], and expression of RGK proteins is regulated at the transcriptional and posttranscriptional levels in a variety of contexts [3, 4, 6, 20, 26, 30-32, 34, 35, 37, 41, 43, 44, 46-74]. This chapter will review the structural and functional properties of RGK subfamily proteins, discuss the regulation of RGK proteins through subcellular localization, post-translational modifications, and expression level changes, and delve into the physiological significance of RGK proteins with a specific emphasis on the Rad GTPase. Following an introduction to RGK proteins, osteoblast differentiation and bone biology will be briefly outlined as these are pertinent to data presented in Chapter 5 expanding our current understanding of Rad GTPase function.

RGK proteins have a unique primary structure compared to other Ras family GTPases

The amino acid sequences of RGK proteins contain a number of non-conservative substitutions at positions important for guanine nucleotide binding and hydrolysis [4, 5] (**Figure 1.1**). First, RGK proteins contain substitutions within the G1 motif involved in phosphate binding. The residue equivalent to

Gly12 in Ras is highly conserved among Ras-related GTPases, and mutation of this residue results in constitutive activation of Ras and Rho family GTPases. Notably, this residue is substituted in all four RGK proteins (to proline in Rad and Rem2, to serine in Rem, and to glutamine in Gem; **Figure 1.1**). Moreover, the highly conserved Thr35 residue within the Ras switch I domain, which senses the γ-phosphate and facilitates the conformational change of Ras family proteins in response to nucleotide cycling, is absent in the RGK subfamily (**Figure 1.1**). Furthermore, the highly conserved phenylalanine residue in the switch I motif responsible for capping the guanine ring to promote high affinity nucleotide binding is substituted in each of the RGK proteins (**Figure 1.1**). Mutation of the equivalent Phe28 in H-Ras to leucine resulted in a higher rate of nucleotide dissociation. The RGK protein G2 and G3 domains, which promote the conformational change within Ras family proteins in response to GTP binding, also exhibit key sequence divergences compared to other Ras family GTPases. All four RGK proteins share a conserved DXWEX G3 motif with a bulky tryptophan and charged glutamate residue that are in striking contrast to the small alanine and glycine residues in the conserved DTAGQ motif of other Ras-related G-proteins [75] (**Figure 1.1**). The glutamine residue in this motif, which is critical for GTP hydrolysis in Ras, is conserved in Rad and Rem2 but is substituted for alanine and asparagine in Rem and Gem, respectively (**Figure 1.1**). Despite its conservation in Rad, however, mutation of this glutamine residue appears to have no effect on GTPase activity [76]. Finally, the G2 domain, which serves as the primary docking site for downstream effector

proteins, is characteristically highly conserved within Ras subfamilies. Intriguingly, this putative G2 effector domain differs across the RGK subfamily, suggesting that individual RGK effector proteins may be distinct. The differences in RGK protein G2 effector domains also imply that interactions that are shared by each of the RGK proteins, such as binding to the $Ca_V\beta$ subunit of the calcium channel, may not be nucleotide dependent.

The differences in RGK protein primary structure when compared to other Ras family GTPases first suggested that RGK proteins might not function as canonical GTPases subject to regulation by GTP/GDP cycling [11]. However, despite the sequence divergences observed in the RGK subfamily, all RGK proteins exhibit intrinsic, albeit low, GTPase activity and can bind to GTP and GDP. Notably, nucleotide binding for RGK proteins is in the micromolar range, much weaker than what is observed for other Ras-related GTPases [3, 4, 6-9, 77]. Despite efforts at identifying regulatory proteins, GEFs and GAPs for RGK protein regulation *in vivo* have not been found [11]. Early *in vitro* studies indicated that the nucleotide binding status of Rad is modified by the tumor suppressor nm23, which can phosphorylate GDP or dephosphorylate GTP bound to Rad, but it remains unclear whether nm23 regulates Rad, or other RGK proteins, *in vivo* [28, 78]. Evidence for RGK control through the classical GTPase cycle is lacking, and there is no clear indication to date that any known RGK binding partners associate in a GTP-dependent fashion [11]. These reasons, coupled with the identification of other unique means of RGK regulation including transcriptional control, post-translational modifications, and alteration of

subcellular localization, question the importance of GTP-binding to RGK activation and downstream signaling [11].

Structure of RGK subfamily GTPases

Crystal structures of the core G-domains of Rad, Gem, and Rem2 in the GDP-bound state indicate that the overall RGK G-domain structure is similar to Ras and other small GTPases with a central β-sheet of six strands (β1-β6) and five surrounding α-helices (α1-α5) [7-9, 79]. In each of these structures, the GDP nucleotide was present in the canonical nucleotide-binding pocket observed for other Ras family GTPases; however, in contrast to Ras, there are fewer contacts between RGK proteins and the bound nucleotide. In particular, the switch I region, which covers the bound nucleotide in Ras, is further from the bound nucleotide in the structures of Gem and Rad [7-9, 79]. The switch I and switch II regions of each of the RGK proteins are conformationally flexible in the GDP-bound state [7-9, 79]. Intriguingly, the recent crystal structures of the Rad and Rem2 G-domains bound to GNP, a non-hydrolyzable GTP analog, revealed almost no difference in conformation compared to the GDP-bound structures [77]. Specifically, the conformational change in the switch I region of Ras in response to GTP binding was absent in the Rad:GNP and Rem2:GNP structures, suggesting that RGK proteins may not undergo the canonical nucleotide-dependent molecular switching characteristic of other small GTPases [77]. One caveat to such a conclusion is that these structures were obtained from the isolated RGK GTP-binding domains, without the N- and C-terminal extensions.

The contributions of these extensions to the structure of RGK proteins, particularly of the switch regions, remain unclear. It is worth noting that Splingard and colleagues reported the structure of the G-domain of Gem along with the majority of the C-terminal extension and observed that a portion of this extension folds into an α-helix that makes contacts with the G-domain [8] in a manner that is similar to the N-termini of GDP-bound Arf proteins and the C-terminus of Ran [80, 81]. While this region is conserved in Rad, it differs in Rem and Rem2, which instead contain a Src homology 3-binding motif (PXXP) that cannot form an α-helical fold. The N- and C-terminal extensions of Gem influenced its intrinsic GTPase activity but not its affinity for nucleotides [8]. Additional crystal structures of full-length RGK proteins bound to GDP and GTP are necessary to clarify whether these extensions may undergo rearrangements in response to nucleotide binding and modulate the overall RGK structure.

One other important observation in these biochemical and structural analyses is that the putative dominant negative mutation, equivalent to Ras S17N, in RGK proteins must be approached with caution. The Ras S17N mutant is locked in a GDP-bound state and is thought to form non-productive, stable interactions with GEF proteins and thereby sequester them away from wildtype GTPases in the cell [82, 83]. This serine residue is conserved in RGK subfamily proteins and has been mutated to asparagine in order to generate a “dominant negative” RGK protein in a number of studies in the literature [84-90]. However, Opatowsky et al. and Sasson et al. reported that Gem S89N and Rad S105N may in fact be non-native proteins that fail to bind nucleotide or exhibit only partial occupancy of

nucleotide [7, 77]. In addition, they reported that these mutants express quite poorly [7, 77], which is an observation we have made in the laboratory as well. Hence, these mutants may not represent a dominant-negative protein as expected.

RGK protein function: regulation of cytoskeletal dynamics

RGK proteins, especially Rad and Gem, have been reported to promote cell shape remodeling through regulation of the cytoskeleton. Rad- and Gem-mediated changes in cell morphology are mediated through direct and indirect modulation of Rho/Rho kinase signaling [19, 22, 91, 92]. Both Gem and Rad directly bind and antagonize Rho kinase (ROK), with Gem specifically binding and inhibiting ROKβ and Rad showing specificity for ROKα [19]. Ectopic expression of Rad or Gem induced cell flattening and neurite extension through inhibition of ROK-mediated cell rounding and neurite retraction [19, 93]. In epithelial and fibroblastic cells, blunting of ROK signaling through ectopic Rad or Gem expression caused disassembly of stress fibers and focal adhesions [19, 20]. In addition to direct inhibition of ROK activity, recent yeast-two hybrid studies have identified another cytoskeletal regulatory pathway in which Gem associates with the novel Gem-interacting protein (Gmip), which serves as a GAP for Rho GTPase, and Ezrin, which is a membrane-cytoskeleton linker protein [22]. The interaction between Gem and Ezrin at the interface between the plasma membrane and the cytoskeleton is required for the recruitment and activation of Gmip, which in turn serves to inhibit Rho signaling [22]. More recent

studies have highlighted the importance of the Gem-Ezrin-Gmip interaction to Gem-mediated cytoskeletal rearrangements, as knockdown of Gmip or introduction of constitutively active RhoA rescued the Gem overexpression phenotype [92]. Notably, although Ezrin has only been reported as a binding partner for Gem [22], co-immunoprecipitation and mass spectrometry studies conducted in our laboratory suggest that Rad also associates with Ezrin and the related proteins Radixin and Moesin (data not shown).

Gem has also been studied in its regulation of the microtubule cytoskeleton [94-96]. Kinesin-like protein (KIF9) is a microtubule-associated protein that binds to Gem, and these two proteins together induce changes in cell morphology [95] and regulate spindle length and chromosome alignment during mitosis [94]. Interestingly, Gem expression is up regulated in the brains of tau-deficient mice, and Gem overexpression in Chinese hamster ovary cells induced cell elongation that was inhibited by the microtubule-associated tau protein [96], further suggesting a role for Gem in the microtubule cytoskeleton.

Although they have been less studied, both Rem and Rem2 have been reported to regulate cytoskeletal dynamics as well [69, 89, 97-99]. Rem overexpression induced endothelial cell sprouting [89], and Rem2 is a negative regulator of dendritic complexity in neurons [69, 97-99]. Notably, Rem and Rem2 do not bind to or regulate either ROK isoform [19], and it remains unclear whether these proteins associate with Ezrin to control the activity of Gmip. Thus, further studies

are necessary to clarify the mechanisms of RGK-mediated regulation of cytoskeletal dynamics.

RGK protein function: inhibition of voltage-dependent calcium channels

Voltage-dependent calcium channels (VDCCs) transduce changes in membrane potential at the cell surface into an increase in intracellular calcium concentration that can initiate a number of downstream physiological processes [100]. These processes include muscle contraction, hormone secretion, synaptic transmission, and gene transcription [100]. VDCCs are classified as high voltage-activated (HVA) channels or low voltage-activated (LVA) channels based upon their activation threshold [100]. HVA calcium channels are composed of a complex of proteins, which include a pore-forming $Ca_V\alpha1$ subunit and auxiliary β, $\alpha2\delta$, and in some cases γ subunits [100]. In contrast, LVA channels consist of only the $Ca_V\alpha1$ subunit [100].

The pore-forming $Ca_V\alpha1$ subunits are large, 190 kD proteins composed of four homologous domains (I-IV) that each include six transmembrane segments (S1-S6) [100]. In HVA channels, the accessory $Ca_V\beta$ subunit binds with high affinity to a conserved region of $Ca_V\alpha1$ in the intracellular loop connecting domains I and II (I-II loop) known as the α interaction domain (AID) [100]. There are ten genes encoding $Ca_V\alpha1$ subunits, and these are divided into three families based upon sequence similarity and pharmacological properties [100]. The Ca_V1 family contains the L-type calcium channels $Ca_V1.1$ (α_{1S}), $Ca_V1.2$ (α_{1C}), $Ca_V1.3$ (α_{1D}),

and $Ca_V1.4$ (α_{1F}), and the Ca_V2 family contains the P/Q-type channel $Ca_V2.1$ (α_{1A}), the N-type channel $Ca_V2.2$ (α_{1B}), and the R-type channel $Ca_V2.3$ (α_{1E}) [100]. The Ca_V1 and Ca_V2 families are HVA calcium channels. L-type calcium channels are expressed in skeletal muscle, smooth muscle, ventricular myocytes, neuronal dendrites, and osteoblasts in the bone, while P/Q-, N-, and R-type calcium channels are primarily expressed in the nervous system [100]. The LVA calcium channels comprise the third family of $Ca_V\alpha1$ subunits, the Ca_V3 family, which contains the T-type calcium channels $Ca_V3.1$ (α_{1G}), $Ca_V3.2$ (α_{1H}), and $Ca_V3.3$ (α_{1I}) [100]. T-type calcium channels are expressed in neurons, pacemaker cells, and osteocytes in the bone [100].

There are four genes encoding $Ca_V\beta$ subunits, designated $Ca_V\beta1$-4, and each of these has a variety of splice variants [101]. The $Ca_V\beta2a$ isoform is expressed highly in the heart and will be used for experiments in this dissertation. Each of the $Ca_V\beta$ subunits contains three variable regions separated by conserved Src homology 3 (SH3)-like and guanylate kinase (GK)-like domains [102]. The AID domain of the pore-forming $Ca_V\alpha1$ subunit, described above, binds with high affinity to a region within the $Ca_V\beta$ GK-like domain [100]. The interaction of auxiliary $Ca_V\beta$ subunits with $Ca_V\alpha1$ contributes to the proper forward trafficking of $Ca_V\alpha1$ to the plasma membrane and also modulates the gating properties of VDCCs resident at the membrane [100].

The linkage between the RGK subfamily and voltage-dependent calcium channels was established when an interaction between Gem and $Ca_V\beta3$ was

identified in MIN6 cells [14]. All four RGK proteins have since been shown to function as potent inhibitors of VDCCs, with ectopic expression of RGK proteins in a variety of experimental settings ranging from heterologous expression systems to primary cells consistently causing almost complete blockade of VDCC current (I_{Ca}) [12-14]. RGK protein-mediated inhibition has been reported for L-type, P/Q-type, and N-type calcium channels [11]. Notably, RGK proteins have no effect on T-type calcium channels, which do not require $Ca_V\beta$ for current expression [12, 103]. In line with a physiological role for RGK proteins in inhibiting calcium current, RNA interference and transgenic knockout mouse models also indicate that loss of function of RGK proteins in cardiac myocytes promotes an increase in VDCC current [104, 105], although the effect was more pronounced with loss of function of Rad than Rem.

The interaction between RGK proteins and the calcium channel complex and its likely contributions to RGK-mediated I_{Ca} inhibition have been further investigated. Each of the four RGK proteins has been shown to bind to $Ca_V\beta$ isoforms [14-16, 106], and deletion-mapping studies indicate that RGK proteins, like $Ca_V\alpha1$, bind within the GK-like domain of $Ca_V\beta$ [15]. However, the site for RGK binding to $Ca_V\beta$ is structurally distinct from the AID, as evidenced by the identification of $Ca_V\beta$ mutants that are null for $Ca_V\alpha1$ binding yet retain Rem binding and by the observation of simultaneous binding of $Ca_V\beta$ to RGK proteins and $Ca_V\alpha_1$ [15, 106]. Interestingly, RGK proteins were subsequently shown to interact directly with the $Ca_V\alpha1$ pore-forming subunit [18, 107, 108]. Specifically, Gem co-

immunoprecipitated with $Ca_V2.1$ in the absence of $Ca_V\beta$ subunit [108], and three RGK family proteins, Rem, Rad, and Gem, were shown to bind to the proximal and distal regions of the $Ca_V1.2$ C-terminus [107]. Yang and colleagues also reported a $Ca_V\beta$-independent interaction between Rem and $Ca_V1.2$, but they identified a Rem-binding site within the N-terminus of $Ca_V1.2$ [18]. Interestingly, Rem2 and Gem failed to bind to the $Ca_V1.2$ N-terminus, and Rem did not bind to the N-terminus of $Ca_V2.2$, suggesting that distinct regulatory mechanisms may be at play for different RGK proteins and $Ca_V\alpha1$ isoforms [18].

While it is well established that RGK proteins physically associate with the VDCC complex and negatively regulate calcium current, there is debate as to the mechanism(s) responsible for this effect. One model contends that RGK proteins inhibit I_{Ca} by preventing trafficking of the channel to the surface of the cell through interference with the interaction between $Ca_V\alpha1$ and $Ca_V\beta$ subunits [14, 16, 64, 90, 109]. Proponents of this $Ca_V\beta$ sequestration model cite the findings that 14-3-3 and calmodulin binding alter the subcellular localization of RGK proteins, with RGK mutants that are null for binding to 14-3-3 or calmodulin accumulating in the nucleus along with co-expressed $Ca_V\beta$ [16]. A second, opposing model suggests that RGK proteins bind to and inhibit $Ca_V\alpha1$ and $Ca_V\beta$-containing channels present at the plasma membrane [12, 13, 15, 87, 103, 106, 110, 111]. This model is supported by the observations that RGK protein binding to $Ca_V\beta$ subunits does not block $Ca_V\alpha1$ binding [15, 106] and that the C-terminus of RGK proteins, which targets them to the plasma membrane, is required for I_{Ca}

inhibition but not for $Ca_V\beta$ binding [12, 110]. Furthermore, biochemical studies demonstrate far higher binding affinity between $Ca_V\alpha1$ and $Ca_V\beta$ subunits than between RGK proteins and $Ca_V\beta$; thus, RGK proteins are not abundant enough to block or sequester $Ca_V\alpha1$:$Ca_V\beta$ complex formation, and there is no evidence for a large pool of unbound $Ca_V\beta$ within the cell [15]. Notably, all of the studies in support of the decreased surface expression model involved investigation of L-type calcium channels, or the Ca_V1 family. In contrast, analysis of RGK-mediated inhibition of N-type, or $Ca_V2.1$ family, calcium channels consistently revealed that RGK proteins inhibit I_{Ca} without altering the density of channels at the membrane [103, 106, 111]. Thus, it is possible that RGK proteins use distinct means of regulating channels from different $Ca_V\alpha1$ families.

Yang and colleagues performed an elegant study of Rem-mediated VDCC regulation that has begun to reconcile these seemingly disparate models by suggesting that Rem uses a combination of mechanisms to inhibit I_{Ca} [17]. First, ectopic expression of Rem in HEK293 cells was found to decrease the expression of recombinant $Ca_V1.2$ channels at the cell surface [17]. Interestingly, however, Rem was shown to decrease the surface density of $Ca_V1.2$ channels by enhancing dynamin-dependent endocytosis of the channel rather than by preventing its forward trafficking to the membrane [17]. While the co-expression of dominant-negative dynamin with Rem normalized the surface density of $Ca_V1.2$, Rem-mediated I_{Ca} inhibition was still observed, suggesting that Rem is also capable of inhibiting calcium channels resident at the cell surface [17]. This study and others are beginning to suggest that RGK proteins use multiple

mechanisms to inhibit proper localization of calcium channels at the plasma membrane as well as to inhibit calcium channels already present at the membrane [17, 18]. In summary, studies from many laboratories using diverse experimental systems indicate that RGK proteins are intrinsic negative regulators of calcium current; however, the mechanisms for regulation of RGK proteins are much less characterized, particularly since cells that endogenously express RGK proteins are still electrically active. It also remains unclear whether the dominant physiological role for RGK proteins is to block calcium current or whether they may have additional roles in the regulation of calcium signaling or of other pathways altogether.

Regulation of RGK subfamily GTPases

Most Ras-related small GTPases function as molecular switches that are regulated by their nucleotide binding status, with nucleotide exchange facilitated by specific GEF and GAP regulatory proteins [112]. RGK subfamily proteins may be a novel exception, however, because as discussed earlier in this chapter, evidence for RGK control via the classical GTPase cycle is lacking [11]. Instead, studies from a number of systems indicate that RGK protein function may be modulated on a number of levels, through subcellular localization, post-translational modifications, and even transcriptional control. Further probing of the regulatory mechanisms for RGK proteins is critical to understanding how these proteins are controlled within the cell.

RGK regulation through subcellular localization

One layer of regulation of RGK protein function appears to be at the level of subcellular localization, as RGKs have been reported to localize to the plasma membrane, the cytosol, and the nucleus in various contexts [5, 16, 40, 41, 106, 109, 110, 113-117]. In particular, the C-terminus of RGK proteins, which is well conserved across the subfamily (**Figure 1.1**), plays an important role in the regulation of RGK subcellular distribution in part due to its interactions with other proteins [116-120] as well as with the phospholipid bilayer [106, 110]. Following its initial cloning, Rem2 was shown to have a punctate plasma membrane localization that was abolished upon deletion of the C-terminus [5], despite the lack of lipid modification of RGK proteins. Our laboratory later determined that the polybasic motif at the C-terminus of RGK proteins directs them to the plasma membrane through association with phosphatidyl inositol phospholipids (PIP lipids) [106, 110], and our studies suggest that this plasma membrane targeting is essential for calcium current modulation [110], as outlined previously. In addition to the polybasic motif, the C-terminal extension of RGK proteins also contains a nuclear localization sequence (NLS) that binds to importin proteins, a calmodulin binding site, and two serine residues that can be subject to phosphorylation [116]. One of these phospho-serine residues serves as a 14-3-3 binding site [118], while the other serine residue that is two amino acids upstream impedes 14-3-3 binding when phosphorylated [117]. The many overlapping regulatory regions within the RGK C-terminus complicate our understanding of its role; however, Mahalakshmi et al. showed for all four RGK

proteins that importins can bind to the NLS sequence at the C-terminus of RGK proteins to facilitate their nuclear transport [116, 117], and mass spectrometry studies conducted in our laboratory have also identified an association between Rad and importin proteins (data not shown). Work by Beguin and colleagues indicates that binding of 14-3-3 and calmodulin disrupts nuclear transport, likely by blocking the association of RGKs with importins [16, 109, 113]. In contrast, mutations that abolish 14-3-3 and calmodulin binding result in RGK protein accumulation in the nucleus [16, 109, 113]. Interestingly, 14-3-3 binding also interferes with PIP lipid binding [106]; hence, 14-3-3 binding to RGK proteins promotes cytosolic redistribution.

While plasma membrane targeting seems to play a crucial role in RGK-mediated calcium channel modulation [106, 110], the role of nuclear targeting of RGK proteins is not entirely clear. Beguin and colleagues argued that nuclear localization of RGK proteins constitutes a novel mechanism for calcium channel inhibition through sequestration of $Ca_V\beta$ [16, 109, 113]; however, it is plausible that RGK proteins may have a functional role in the nucleus, especially given recent reports that endogenous RGK proteins are localized predominantly in the nucleus [115, 117] and that Rad can bind to the transcription factors CCAAT-enhancer binding protein-delta (C/EBPδ) and RelA/p65 within the nucleus and regulate their binding to DNA [40, 41].

While many of the earlier studies of RGK protein subcellular distribution employed overexpression of wildtype and mutant proteins to probe the roles of

various binding partners on RGK localization [16, 109, 113, 116], recent studies have suggested that Rem2 subcellular redistribution may be stimulus-dependent [98, 114]. In response to N-methyl-D-aspartate (NMDA) receptor activation and calcium influx, Rem2 redistributes from a diffuse to a highly punctate pattern that colocalizes with calmodulin-dependent protein kinase II (CaMKII) in neurons [114]. A subsequent study demonstrated that Rem2 is a novel substrate for CaMKII phosphorylation, with CaMKII phosphorylation promoting nuclear redistribution of Rem2 [98]. Hence, redistribution of the RGK protein Rem2 from the cytoplasm to the nucleus appears to be a physiologically relevant event, but the function of Rem2 within the nucleus and the possibility that other RGK proteins may undergo stimulus-dependent changes in subcellular distribution require further investigation.

RGK regulation by post-translational modifications

While evidence for the regulation of RGK proteins by the canonical guanine nucleotide cycle is lacking, there is a growing body of literature suggesting that RGK proteins may instead be regulated by post-translational modifications, most notably phosphorylation. In particular, Rad phosphorylation at multiple distinct serine residues has been demonstrated by a variety of kinases including protein kinase A (PKA), protein kinase C (PKC), calmodulin-dependent protein kinase II (CaMKII), and casein kinase II [49]. Phosphorylation of RGK proteins has been reported to modulate their protein-protein interactions as well as their subcellular distribution [16, 49, 109, 113, 116-118, 121]. For instance, phosphorylation of N-

and C-terminal serine residues is required for RGK proteins to bind to 14-3-3 dimers [109, 113, 118, 121]. Interestingly, 14-3-3 binding seems to increase the half-life of RGK proteins and to modulate their subcellular localization, specifically by excluding them from the nucleus [16, 109, 113, 116, 117, 121]. Moreover, an additional C-terminal serine phosphorylation site was identified for all RGK proteins that blocks 14-3-3 binding [117]. Phosphorylation of Rad by PKC or casein kinase II was shown to reduce binding to calmodulin [49]. Furthermore, phosphorylation of serine residues within the C-terminal nuclear localization signal of RGK proteins was reported to block association with importins to regulate nuclear accumulation [116]. The effects of phosphorylation on binding to $Ca_V\beta$ subunits had not yet been explored and will be described in Chapter 4 of this dissertation.

Importantly, a number of recent studies have suggested that phosphorylation of RGK proteins at different serine residues may regulate their functions in both cytoskeletal reorganization and voltage-dependent calcium channel regulation. Phosphorylation of Ser261 and Ser289 in the Gem C-terminus was reported to regulate the cytoskeletal reorganization function of Gem separately from its role in calcium channel regulation [121]. Similarly, the phosphorylation of C-terminal serine residues within the nuclear localization signals that inhibited entry into the nucleus also blocked the effects of Gem on the cytoskeleton without impacting its ability to regulate calcium current [116]. The function of Rem2 in controlling dendritic complexity is also regulated by phosphorylation, as CaMKII phosphorylation of Rem2 triggered nuclear localization of Rem2 and was

required for its inhibition of dendritic arborization [98]. The physiological relevance of RGK phosphorylation is highlighted by the recent report that endogenous Rem2 is found in the nuclei of basal ganglia cells and is phosphorylated at multiple serine residues [115]. RGK phosphorylation has also recently been reported to afford regulation of calcium channel modulation. Rem phosphorylation by protein kinase D1 (PKD1) was shown to reverse Rem-mediated calcium channel blockade in heterologous expression systems and in primary cardiac myocytes [64]. Interestingly, PKA inhibition also partially relieved Rem-mediated calcium current inhibition [122], further suggesting that kinase cascades modulate RGK blockade of calcium current but that the nature of this regulation may be complex. These recent studies suggest that RGK phosphorylation is an important regulatory mechanism; however, the kinases that regulate RGK phosphorylation and the effects of phosphorylation on RGK function more broadly require more extensive study, particularly whether 14-3-3 binding to phosphorylated RGK proteins may block association with other binding partners or whether phosphorylated RGKs may show enhanced binding to certain effectors. It also remains unclear whether the same kinase cascades regulate each of the four RGK proteins or whether a diversity of regulatory pathways may exist.

While phosphorylation is the best-studied post-translational modification of RGK proteins, mass spectrometry analysis has demonstrated that Rad protein can also be ubiquitinated at Lys204 [123, 124]. However, the E3 ubiquitin ligase enzyme(s) responsible for catalysis of Rad ubiquitination and the physiological

relevance of this modification remain to be determined. The possibility of ubiquitin-mediated proteostatic control of Rad will be investigated in Chapter 3 of this dissertation.

Transcriptional regulation of RGK proteins

In contrast to the regulatory mechanisms reported for most Ras-related small GTPases, RGK proteins are unique in their ability to be regulated at the level of expression [3, 4, 6, 20, 26, 30-32, 34, 35, 37, 41, 43, 44, 46-74]. Gem was initially discovered as a gene up regulated in human T cells following mitogen stimulation [6] and in BCR-Abl-transformed B cells [125]. Subsequent studies have shown that Gem expression is also up regulated in the context of heart failure [50], as well as following stroke [63], sciatic nerve injury [66], spinal cord injury [68], peripheral nerve injury [73], and optic nerve crush [70]. Moreover, Gem is down regulated in hepatocellular carcinoma, with expression levels negatively correlated with the histological grade, the size of the tumor, and the invasive and proliferative properties of the cancer [37]. In contrast, high expression of Gem in bladder cancer was correlated with decreased survival [36]. Expression of Gem as well as Rem2 is induced in MIN6 cells, a pancreatic β-islet cell line, following glucose treatment [13, 126]. Insulin and potassium chloride treatment of MIN6 cells also induced Gem expression [126]. Rem2 is up regulated in developing neurons and in human embryonic stem cells [42, 43], as well as in endothelial cells of stage IV pancreatic disease [56]. Rem2 is also regulated at the transcriptional level by calcium influx through VDCCs [69]. Rem

expression is up regulated in cardiomyocytes following isoproterenol treatment [127] and down regulated in mouse cardiac muscle following lipopolysaccharide injection [4].

While all four RGK proteins have been shown to be under transcriptional control [3, 4, 6, 13], modulation of Rad expression has been described the most frequently, particularly in muscle. Rad was initially identified as a gene overexpressed in the skeletal muscle of type II diabetic individuals [3], although analysis of Rad expression in Pima Indians and the Zucker diabetic rat model did not find such a correlation [128]. Subsequent studies indicated that Rad expression in muscle was positively correlated with body mass index and body fat percentage and negatively correlated with resting metabolic rate [129]. Several independent studies have identified insulin as a stimulus for induction of Rad expression in muscle [47, 55, 57], and in the same vein, Rad expression was increased in pancreatic islets following exposure to type I diabetic serum [58, 65]. Rad expression also appears to be up regulated during muscle development and in response to muscle injury, as Rad levels are elevated in the progression of myoblasts to myotubes *in vitro* [128, 130], in regenerating limb muscle following amputation in the newt [46], in denervated mouse muscle [51, 61], in ALS muscle [61], in vascular smooth muscle following balloon injury [20] and stimulation with platelet-derived growth factor [62], in dissecting aorta [72], and in the myogenic progenitor cell population during skeletal muscle regeneration [54]. In the heart, Rad expression is up regulated following ischemic preconditioning [60] and down regulated in heart failure [131, 132]. Rad

levels are also altered in a number of other tissues [34, 48, 52, 53, 67, 74], which will be described in more detail later. Taken together, these studies indicate that RGK proteins, and Rad in particular, are regulated at the level of expression. Evidence suggests that much of this regulation occurs at the level of transcription; however, post-translational protein stability could provide an additional level of control that remains to be explored, especially given the observation that Rad protein is subject to ubiquitination [123, 124].

Physiological significance of the RGK subfamily protein Rad

While the functions of RGK proteins have been investigated in a variety of cell models, we are still working to understand the physiological roles of these proteins. RGK proteins are expressed in a number of excitable tissues where their regulation of VDCCs may be particularly relevant [11]. For instance, Rem is expressed in the heart, Rem2 is expressed in neurons, Gem is expressed in pancreatic β-cells, and Rad, the focus of this dissertation, is present in cardiac and skeletal muscle [11]. Rad expression has also been recently found in non-excitable cell types [34, 48, 52, 53, 67, 74], however, suggesting that its physiological significance extends well past its role in VDCC regulation.

Roles of Rad in the heart

Given its high expression in cardiac muscle [3, 128] and its role in the regulation of VDCCs [12], the function of Rad has been characterized most extensively in the heart. Rad expression is decreased in human heart failure and in cardiac

hypertrophy induced by pressure overload in mice [131, 132]. A novel single nucleotide polymorphism (SNP) resulting in a Q66P mutation in the human Rad protein was correlated with congestive heart failure [133]; however, mutation of this residue does not alter the ability of ectopic Rad expression to block calcium current [134], suggesting that this mutation may contribute to cardiomyopathy through an alternative mechanism than calcium channel modulation. Rad has also been reported to regulate apoptosis of cardiomyocytes through p38 protein kinase activation [135] and to regulate excitation-contraction coupling and β-adrenergic signaling in cardiac myocytes [86].

The first loss-of-function studies for Rad in heart were performed using the putative dominant negative mutant Rad S105N [84-86]. Overexpression of this mutant in guinea pig cardiomyocytes was reported to cause an increase in calcium current and a prolonged QT interval resulting in arrhythmias [85]. Another study found that transgenic mice overexpressing Rad S105N exhibited increased phosphorylation of the Ryanodine receptor, the channel by which calcium is released from the sarcoplasmic reticulum (SR) in response to calcium influx through VDCCs, and a subsequent increase in the frequency of inappropriate calcium release from the SR, termed calcium sparks, and of arrhythmias [84]. Furthermore, Wang et al. reported that overexpression of Rad S105N resulted in a comparable increase in I_{Ca} compared to Rad knock down [86]. However, other studies have suggested that the “dominant negative” mutations in RGK proteins are not effective [88], and the lack of solid evidence of GTP cycle regulation of Rad makes interpretation of these data difficult. The

generation of Rad$^{-/-}$ mice helped to circumvent this issue. Initial studies in these mice indicated that loss of Rad results in more severe cardiac hypertrophy following pressure overload [132] and more extensive cardiac fibrosis through enhanced extracellular matrix (ECM) deposition [41], but the impact of Rad loss on calcium channel dynamics had not been investigated in these earlier studies.

Over the past several years, the Andres and Satin laboratories have collaborated to further study the role of Rad GTPase in the heart through analysis of the cardiac phenotype of Rad$^{-/-}$ mice. I have contributed data to a number of these studies and am a co-author on several manuscripts, but this work will not appear in a chapter of this dissertation [104, 131, 136]. Briefly, we have shown that cardiac myocytes from Rad$^{-/-}$ mice have higher calcium current [104], suggesting that Rad is indeed an endogenous inhibitor of VDCCs. Rad$^{-/-}$ cardiomyocytes also exhibited elevated diastolic and twitch calcium levels, higher sarcoplasmic reticulum calcium load, and elevated sarco/endoplasmic reticulum Ca^{2+}-ATPase (SERCA2a) expression, and the Rad$^{-/-}$ cardiac phenotype closely resembled tonic β-adrenergic stimulation of the calcium channel complex [104, 136]. In keeping with this sympathomimetic phenotype, we went on to establish that Rad$^{-/-}$ mouse hearts are hypercontractile relative to wildtype hearts, and that this improved cardiac function is maintained in aging [136]. Notably, unlike the Rad S105N overexpression studies, we did not observe arrhythmias in Rad$^{-/-}$ mice. Finally, we have replicated the finding that Rad protein levels are significantly lower in human failing hearts [131]; however, while more work is needed, our data from Rad$^{-/-}$ mice suggest that the loss of Rad may be a compensatory

response to the need to increase cardiac output in this setting rather than a pathological consequence of heart failure. In summary, our work suggests that loss of Rad does not exacerbate cardiac hypertrophy or induce cardiac arrhythmias as may be expected with an increase in calcium current; instead, Rad deletion appears to generate a stable increase in cardiac function that renders protection upon cardiac insult [136], (unpublished data).

Emerging roles of Rad in non-excitable tissues

While Rad, as a putative inhibitor of VDCC function, has primarily been studied in excitable tissues, especially the heart where it is highly expressed, a number of recent reports suggest that there is value in exploring the function of Rad in non-excitable tissues. In addition to the changes in Rad expression in muscle described above, Rad levels are also altered in other systems that require further investigation. For instance, Rad expression is induced in the suprachiasmatic nucleus following stimulation with light [59, 71], in peripheral blood mononuclear cells following heat shock [48] or polychlorinated biphenyl (PCB) exposure [74], in cirrhotic livers relative to normal livers [52], in human placenta following hypoxia [53], and during erythropoiesis to confer erythroid survival [67]. In each of these cases, the mechanism for up regulation of Rad expression and the functional implications of this up regulation require further investigation.

Interestingly, modulation of Rad levels has also been reported in a diverse assortment of cancers. Rad silencing has been reported in breast [28], lung [24, 25, 30, 34, 137], ovarian [38], cervical [138], liver [26, 27], nasopharyngeal [32],

and esophageal cancer [35], as well as in glioblastoma [39]. In many of these cases, Rad silencing is correlated with aberrant methylation of its promoter region [32, 35, 38, 39, 138]. Notably, elevated Rad expression was also observed in some cancers, especially in highly invasive tumors and in drug-resistant tumors [28, 29, 33, 139]. Mechanistically, the frequent down regulation of Rad in cancer has been attributed to a novel role of Rad in inhibiting the Warburg effect [25, 27], suggesting a role for Rad in metabolism. Interestingly, Rad was found to repress glycolysis primarily through inhibition of glucose transporter translocation to the plasma membrane [24]. In the same vein, earlier studies also implicated Rad in the regulation of glucose uptake, as Rad overexpression inhibited glucose uptake in muscle and fat cells [140], and Rad silencing promoted glucose uptake in an ovarian cancer model [38]. The role of Rad in mediating these changes, however, remains unclear.

The ability of Rad to localize to the nucleus in addition to the cytosol and plasma membrane is well established [16, 29, 40, 117], and the nuclear localization of Rad was initially thought to provide a means of sequestration of Rad to inhibit its activities in cytoskeletal reorganization and/or VDCC control [16, 117]. However, recent studies suggest that Rad may play a direct role in the regulation of gene transcription. Following the observation that $Rad^{-/-}$ mice exhibited more severe cardiac fibrosis, Zhang et al. identified up regulation of connective tissue growth factor (CTGF) as a key factor in the observed phenotype, and further analysis indicated that Rad associates with CCAAT-enhancer binding protein-δ (C/EBP-δ) and inhibits its binding to the *CTGF* promoter [41]. Similarly, Hsiao et al. recently

reported a direct interaction between Rad and the p65/RelA subunit of nuclear factor kappa B (NFκB) that occurs in the nucleus and inhibits DNA binding of RelA [40]. Notably, overexpression of Rad decreased NFκB transcriptional activity, whereas Rad deletion resulted in up regulation of NFκB target genes [40]. Thus, it is plausible that Rad localization in the nucleus extends beyond a means of sequestering the protein to inhibit its regulation of VDCCs and the cytoskeleton; rather, Rad may actively bind to and activate or inhibit transcription factors and co-activators/co-repressors to influence gene expression.

Finally, similar to the reports of Rem2 regulating embryonic stem cell self-renewal and pluripotency [42, 43], Rad was also recently identified to have a potential role in embryonic stem cell differentiation [45] and to contribute to expression of stem factors enhancing self-renewal ability [139]. The involvement of Rad in regulation of stem cell maintenance and differentiation has also been extended to mesenchymal stem cells (MSCs), as Satija and colleagues recently reported that lithium priming of human MSCs toward the osteoblast lineage resulted in a significant up regulation of Rad expression, and that Rad silencing reversed the osteogenic effects of lithium [44]. The idea that RGK proteins, and Rad in particular, may influence MSC differentiation and osteogenesis will be explored in Chapter 5 of this dissertation. In preparation for Chapter 5, a brief introduction of bone biology and osteoblast differentiation will now be described.

Bone remodeling

Bone remodeling is a physiological process in which old or damaged bone is removed by osteoclasts and replaced by new bone formed by osteoblasts (**Figure 1.2**) [141]. This process occurs throughout life, with the entire skeleton of a child being replaced every four years and the entire adult skeleton being replaced every ten years [141]. The bone remodeling cycle can be broken into five stages: the resting state, resorption, reversal, formation, and mineralization [142].

In the resting state, the surface of the bone is covered with bone-lining cells, which are aged osteoblasts that no longer play a role in synthesis of bone matrix [143]. These bone-lining cells cover all non-metabolically active areas of the bone and thereby close it off to other cells, including osteoclasts [143]. The peeling back of the bone-lining cells stimulates and allows attachment of osteoclasts to the bone surface. Osteocytes, which comprise 90% of all bone cells, are also derived from old osteoblasts that have been incorporated into the mineralized bone [144]. Osteocytes sense mechanical force and bone strain and respond to these forces by secreting factors that regulate osteoclast and osteoblast generation, thereby initiating the remodeling process on the bone surface [144].

The bone remodeling cycle begins with osteoclast generation and recruitment to a particular site. Under physiological conditions, this site may be in need of repair, while under pathological conditions it may be randomly and

inappropriately targeted. Osteoclasts are giant, multinucleated cells derived from the hematopoietic lineage, and they have a specialized plasma membrane domain known as a ruffled border that attaches to the bone surface [145]. The osteoclast degrades mineralized extracellular matrix by secreting acid and lysosomal proteins, and the osteoclast then reabsorbs, packages, and secretes the minerals and proteins [145].

After osteoclastic resorption is complete, there is a reversal phase in which mononuclear cells migrate to the bone surface. These cells put down a layer of glycoprotein-rich material known as the cement line to which osteoblasts can adhere, and they provide necessary signals for osteoblast differentiation and migration in the bone formation phase [142]. In this phase, successive waves of osteoblasts adhere to the cement line and lay down bone until the resorbed bone is completely replaced [142]. During the final stage, the newly formed bone matrix becomes mineralized, and the bone then returns to its resting state with little cellular activity on the bone surface until a new remodeling cycle begins.

In normal bone remodeling, a balance between bone resorption mediated by osteoclasts and bone formation mediated by osteoblasts is tightly regulated and maintained in order to ensure that, in mature healthy bone, there are no major net changes in bone mass or mechanical strength after each remodeling cycle. Nonetheless, an imbalance between bone resorption and bone formation may occur under certain pathological conditions, such as osteoporosis, and this imbalance results in reduced bone density, or osteopenia [141]. Some of the

factors that can lead to dysregulation of the bone remodeling balance include aging, hormonal changes associated with menopause, changes in physical activity, medications, and secondary diseases [141]. Interestingly, many of these factors that are correlated with osteopenia are also associated with an increase in bone marrow adipose tissue, an idea that will be expanded in Chapter 5.

Osteoblast and osteoclast differentiation

As described above, the osteoblast is the cell type responsible for new bone formation through synthesis and secretion of collagen matrix and calcium salts [146]. Osteoblasts are derived from MSCs, which are pluripotent stem cells that can differentiate into a variety of tissues including adipocytes (fat), chondrocytes (cartilage), and myocytes (muscle) in addition to osteoblasts (bone) [146]. Differentiation of MSCs toward the osteoblast lineage is controlled by a variety of cytokine signaling pathways including the Hedgehogs, transforming growth factor-β (TGF-β), parathyroid hormone (PTH), Wnts, and bone morphogenetic proteins (BMPs) [146]. Although there are a variety of upstream signals that can initiate the process of osteoblast differentiation, they each converge on the activation of Runt-related transcription factor 2 (Runx2), which is considered the master transcription factor for the regulation of osteoblast differentiation [147]. Deletion of Runx2 in mice results in the complete absence of osteoblasts and a cartilaginous skeleton that lacks mineralized matrix [148]. Runx2 interacts with a number of co-regulatory proteins to positively or negatively regulate the expression of osteoblastic genes such as type I collagen, alkaline phosphatase,

osteocalcin, and osterix [149, 150]. Osterix is itself a transcription factor with a critical function in osteoblast differentiation, as Osterix$^{-/-}$ mice fail to develop osteoblasts [151]. The osteoblast differentiation process can be divided into the stages of proliferation of MSCs and osteo-chondrocyte precursors, maturation of these precursors into osteoblasts, and termination in which osteoblasts no longer function in bone formation and rather terminally differentiate into bone lining cells or osteocytes or undergo apoptosis [147]. Runx2 plays an early role in the differentiation of osteogenic precursors into immature osteoblasts, while Osterix promotes the maturation of these osteoblasts [147].

Osteoclasts are the cells responsible for bone resorption, or break down. Unlike osteoblasts, osteoclasts are multi-nucleated cells derived from the hematopoietic lineage, specifically from monocytes and macrophages near the bone surface [145]. Notably, differentiation of these macrophage precursors into osteoclasts requires two cytokines, receptor activator of nuclear factor-kappa B ligand (RANKL) and macrophage-colony stimulating factor (M-CSF), both of which are produced by osteoblasts [145, 152]. Hence, a direct regulatory linkage exists between osteoblasts and osteoclasts that is important for controlling bone homeostasis.

Bone morphogenetic protein signaling

The bone morphogenetic protein (BMP) signaling pathway is one of the pathways implicated in the regulation of osteoblast differentiation. BMPs are members of the transforming growth factor-β (TGF-β) superfamily that were

initially identified for their capacity to induce bone formation at ectopic sites in rats [153]. Since their discovery, the role of BMPs in bone homeostasis has been confirmed by their expression in skeletal tissues and their roles in skeletal development as well as in fracture healing [154]. Notably, conditional deletion of BMPs in mouse bone results in skeletal defects [154, 155], and inherited mutations in BMPs or their receptors are observed in skeletal disorders in humans [156]. BMPs are also utilized therapeutically in certain settings such as for the repair of open fractures of long bones and for spinal fusions [157].

BMP ligands bind as dimers to type-I and type-II serine/threonine receptor kinases, allowing receptor oligomerization. This oligomerization allows the constitutively active type-II BMP receptors to phosphorylate and thereby activate the type-I receptors (**Figure 1.3**). Type-I BMP receptor kinases activated by the type-II receptor kinases then phosphorylate the C-terminus of the receptor-associated Smads (R-Smads) 1 and 5 (**Figure 1.3**). Phosphorylated R-Smads can heterodimerize with the common-partner Smad (co-Smad) Smad4 and translocate into the nucleus (**Figure 1.3**), where they regulate the transcription of genes including Runx2 that are associated with bone development via interaction with various transcription factors and transcriptional co-activators or co-repressors. Meanwhile, C-terminally phosphorylated R-Smads in the nucleus are also subject to phosphorylation within the linker region by mitogen activated protein kinases (MAPKs) and glycogen synthase kinase-3 (GSK3) [158] (**Figure 1.4**). This linker phosphorylation allows R-Smad binding to E3 ubiquitin ligases such as Smurf1, which ubiquitinate the R-Smad proteins and target them for

degradation in the proteasome [158] (**Figure 1.4**). Smurf1 thus regulates osteoblast differentiation by providing negative feedback on BMP signaling.

Skeletal anatomy

Bone tissue in mammals is classified into two different types of bone tissue: cortical and trabecular bone. Cortical bone, sometimes also referred to as compact bone, forms the dense, outer shell (**Figure 1.5**) and is responsible for the majority of the weight of the skeleton (~80%). Important functions of the cortical bone include supporting the weight of the body, protecting vital organs such as the brain and bone marrow, storing calcium, and providing leverage for movement. Trabecular bone, also known as cancellous or spongy bone, is enclosed by the cortical bone and forms a less dense meshwork of bony plates and rods (**Figure 1.5**). Trabecular bone is primarily found at the ends of long bones near joints and within vertebrae and flat bones. Trabecular bone has a much higher surface area than cortical bone and is the primary site of bone remodeling associated with metabolism and maintenance of calcium homeostasis. Trabecular bone is often impacted more severely than cortical bone in the setting of osteoporosis.

The ends of long bones are known as the epiphyses. The proximal epiphysis is the end that is closest to the center of the body (for instance, the top end of the femur which forms part of the hip joint), and the distal epiphysis is that farthest from the center of the body (the lower end of the femur which forms part of the knee joint) (**Figure 1.5**). The majority of the histology presented in this

dissertation, as well as the trabecular bone μCT, utilizes the distal femur. The shaft of long bones, or the portion between the two epiphyses, is called the diaphysis. The diaphysis consists of a tube of cortical bone that encloses the medullary cavity (**Figure 1.5**). Cortical analyses in this dissertation are performed at the mid-diaphysis of the femur.

The medullary cavity is surrounded by a delicate membrane known as the endosteum (**Figure 1.5**), and the inner surface of the cortical bone is similarly called the endocortical surface. A fibrous membrane called the periosteum surrounds the outer surface of the bone and is the site of tendon and ligament attachment to bones, as well as for blood vessels, nerves, and lymphatic vessels (**Figure 1.5**). The outer surface of the cortical bone is thus referred to as the periosteal surface. The bone formation rates of cortical bone in this dissertation will be presented for both the periosteal and endocortical surfaces.

Scope of dissertation

In summary, Rad is a member of the RGK subfamily of Ras-related small GTPases. This unique family of G-proteins binds to guanine nucleotides despite unusual amino acid substitutions within regions associated with nucleotide binding and hydrolysis. Rad has established functions in the regulation of cytoskeletal remodeling and of voltage-dependent calcium channel modulation, but it is unclear whether these functions are regulated through nucleotide binding status, subcellular distribution, post-translational modifications, transcriptional regulation, or proteostatic control mechanisms. Rad expression has also been

reported in non-excitable cell types, and roles of Rad beyond its documented functions in regulating the cytoskeleton and calcium current are emerging. In this dissertation, I seek to advance our understanding of how Rad might be regulated, both in excitatory and non-excitatory cells. I will investigate the role of a novel Rad-interacting protein and an associated E3 ubiquitin ligase in the regulation of Rad protein levels in Chapter 3, followed by an examination of the role of Rad phosphorylation in the regulation of protein-protein interactions and calcium current regulation in Chapter 4. Finally, I will explore the role of Rad in the regulation of bone homeostasis and osteoblast function in Chapter 5 of this dissertation.

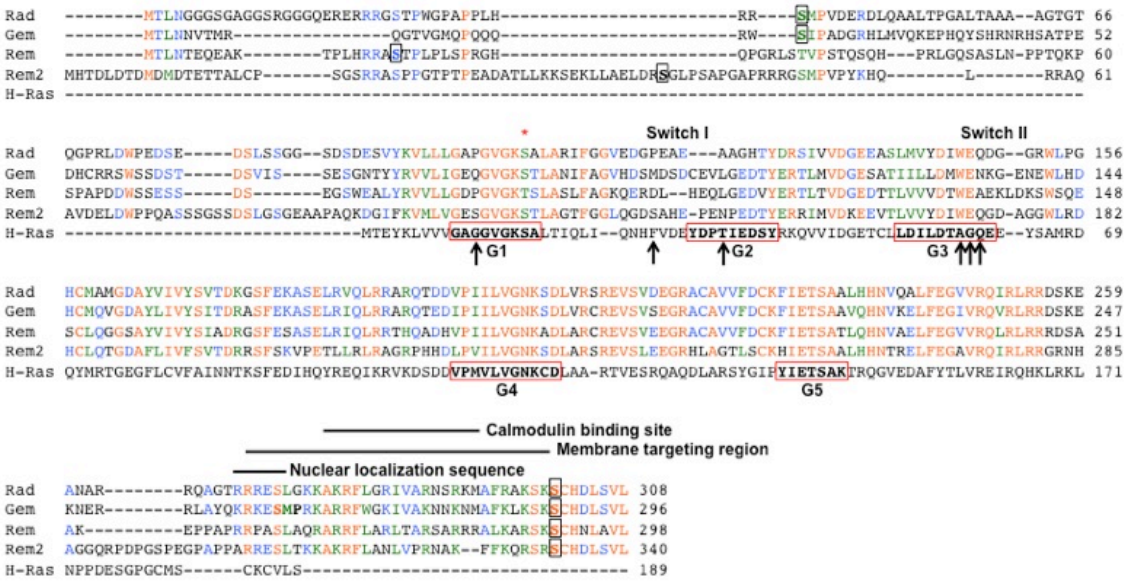

Figure 1.1: Sequence alignment of the RGK subfamily

The amino acid sequence of each of the four RGK subfamily proteins and H-Ras are aligned to illustrate regions of conservation and the lack thereof. The G1-G5 boxes of H-Ras, which are typically highly conserved among Ras-related GTPases, are enclosed in red boxes. Black arrows indicate residues in H-Ras important for nucleotide binding and hydrolysis that are absent in RGK proteins. Amino acid residues depicted in orange represent sequence identity across the RGK subfamily, those in green represent sequence similarity across the RGK subfamily, and those in blue represent sequence similarity among three of the four RGK proteins. The lack of conservation in the N-terminal extensions of RGK proteins is readily observed. The N- and C-terminal serine residues involved in phosphorylation-dependent 14-3-3 binding are enclosed in black boxes, and the site for calmodulin binding, the polybasic membrane targeting region, and the nuclear localization sequence within the conserved C-terminus of RGK proteins are also denoted.

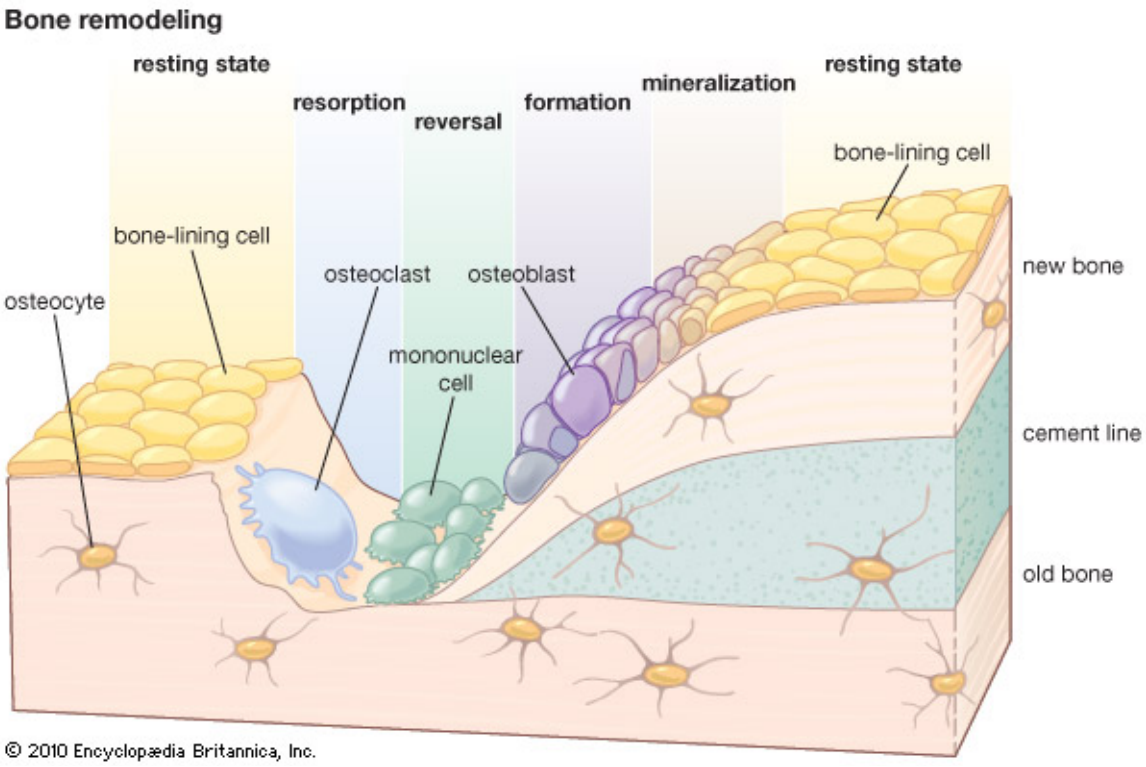

Figure 1.2: The bone remodeling cycle

Bone is a dynamic tissue that is constantly undergoing cycles of bone remodeling. The five stages of bone remodeling are the resting state, osteoclast-mediated bone resorption, reversal, osteoblast-mediated bone formation, and mineralization.

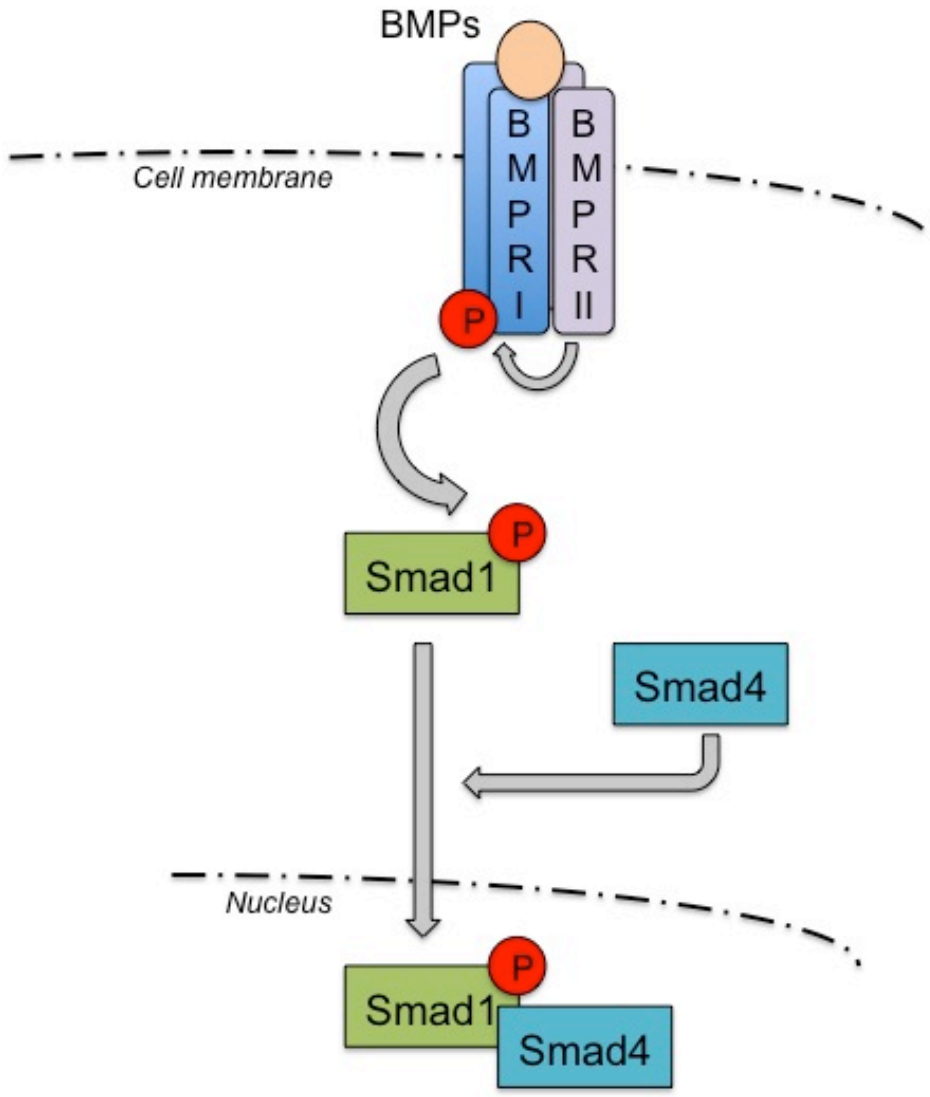

Figure 1.3: Bone morphogenetic protein signaling pathway

Bone morphogenetic protein (BMP) ligand binding to BMP type I and type II receptors facilitates their oligomerization. BMPRII phosphorylates and activates BMPRI, which then phosphorylates the C-terminus of receptor-associated Smad proteins such as Smad1. Phosphorylated Smad1 then heterodimerizes with Smad4, and this complex translocates into the nucleus where it regulates gene transcription.

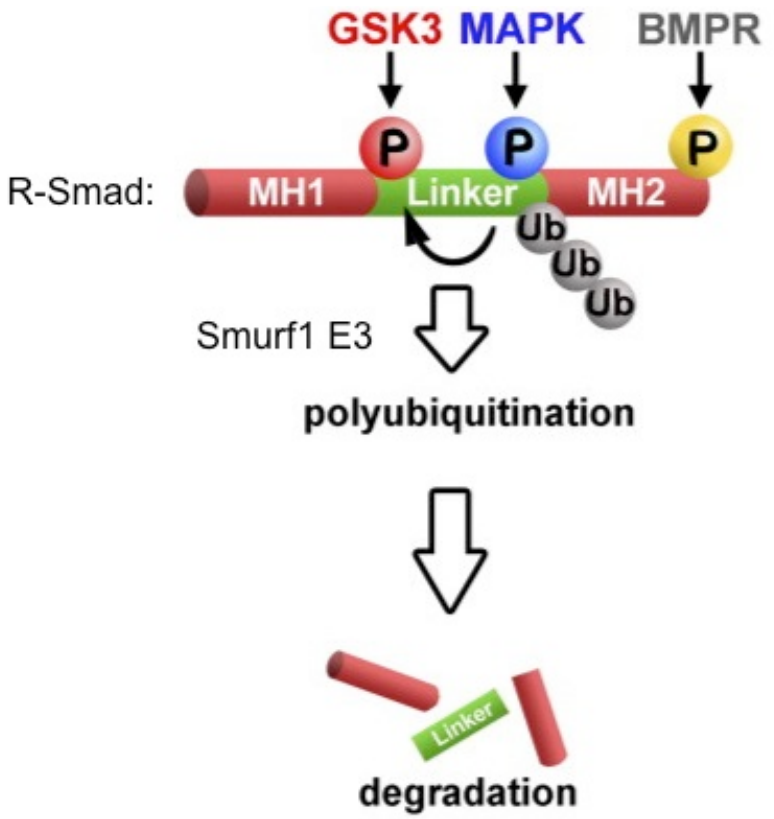

Figure 1.4: Smurf1-mediated ubiquitination of R-Smad proteins

Following C-terminal phosphorylation of R-Smads by the BMP receptor, dimerization with Smad4, and nuclear translocation, R-Smad proteins are subject to phosphorylation at two serine residues within their linker region by MAPKs and GSK3. Linker phosphorylation allows recruitment of the Smurf1 E3 ligase, polyubiquitination of R-Smads, and proteasomal degradation.

Modified from Fuentealba et al. 2007 [159]

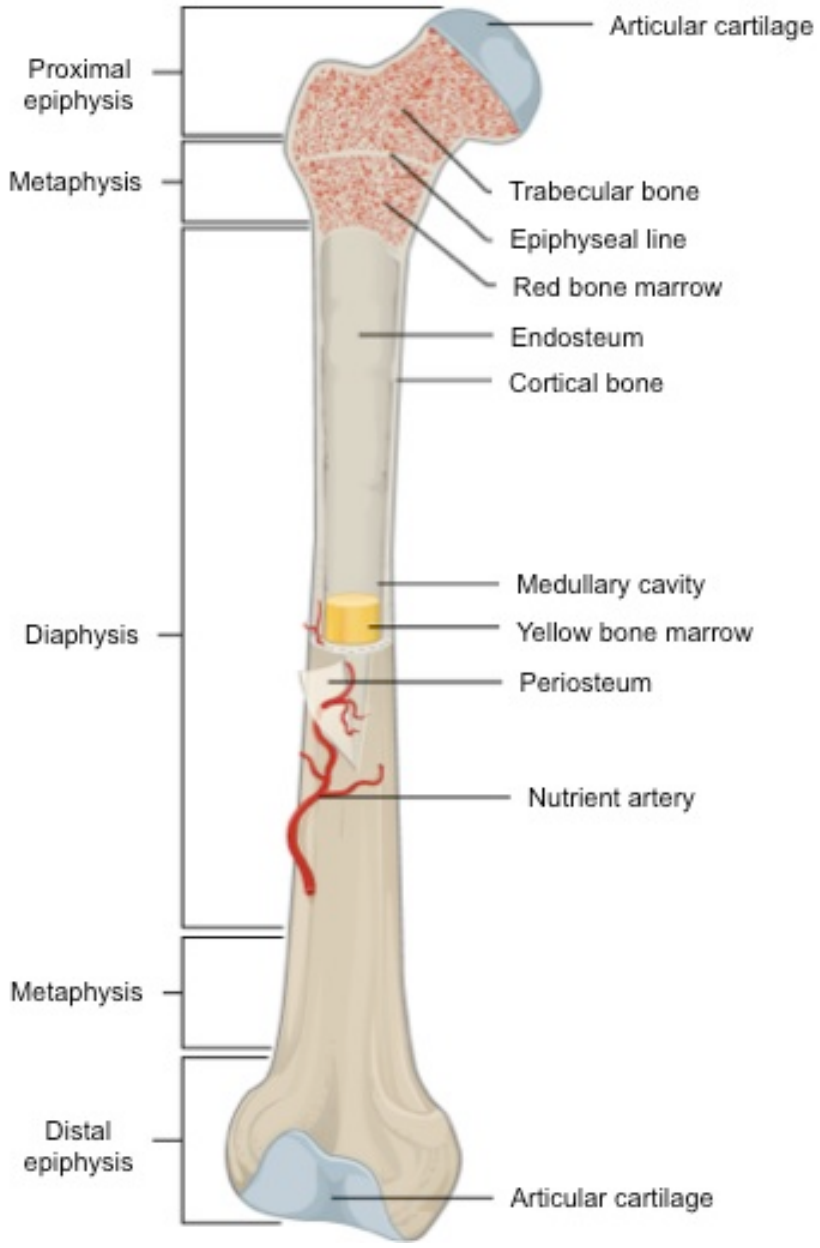

Figure 1.5: Long bone anatomy

This diagram of a long bone indicates the locations of important anatomical structures, such as cortical versus trabecular bone, diaphysis versus epiphysis, and periosteum versus endosteum.

Modified from OpenStax College, Anatomy and Physiology. OpenStax CNX. http://cnx.org/contents/14fb4ad7-39a1-4eee-ab6e-3ef2482e3e228.81.

Chapter 2

Materials and Methods

HEK293 cell culture and transfection

HEK293 cells were obtained from American Type Cell Culture (ATCC) and were cultured in DMEM supplemented with 10% fetal bovine serum (FBS), 100 units/mL penicillin, and 100 μg/mL streptomycin. The day prior to transfection, HEK293 cells were split into 6-well dishes at a density of $1x10^6$ cells/well. Cells were transfected using Transgin DNA Transfection Reagent (America Pharma Source, Gaithersburg, MD). For each well of a 6-well plate, a total of 2 μg of plasmid DNA and 2 μL of Transgin were added to 100 μL of Opti-Mem and incubated at room temperature for 20 minutes. HEK293 cells were incubated in 1 mL of Opti-MEM per well plus the 100 μL transfection reaction for 4-6 hours, after which the Opti-MEM was replaced with 2 mL of standard growth media per well. Cells were serum-starved for six hours prior to application of stimuli. Cells were harvested 48 hours after transfection for immunoprecipitation or Western blotting analysis, or split 24 hours after transfection at low density into 35-mm dishes for electrophysiology experiments.

Plasmids and reagents

Rat Enigma, mouse Enigma homolog 1 (ENH1), and human Cypher cDNA constructs were obtained from the DNASU plasmid repository and were subsequently subcloned into the p3XFLAG-CMV10 vector (Sigma) using the oligonucleotides in rows 1-6 of **Table 2.1**. An N-terminal truncation of Enigma lacking the PDZ domain (ΔPDZ) was generated using the 5' oligonucleotide in row 7 and the 3' oligonucleotide in row 2 of **Table 2.1**, and a C-terminal truncation of Enigma lacking the three LIM domains (ΔLIM1-3) was generated using the 5' oligonucleotide in row 1 and the 3' oligonucleotide in row 8 of **Table 2.1**.

pKH3-Rem WT, pKH3-Rad WT, pKH3-Rem2 WT (long isoform), and pKH3-Gem WT have been previously described [12, 13]. pKH3-Rad K204R was generated by site directed mutagenesis using the QuikChange II Site-Directed Mutagenesis Kit (Agilent) and the oligonucleotides in rows 9 and 10 of **Table 2.1**. pKH3-Rad S39A, S39D, and S301A were also generated by site directed mutagenesis by Dr. Hongge Jia.

pRK-Myc-Smurf1 and pRK-Myc-Smurf2 were gifts from Dr. Ying Zhang (Addgene plasmids #13676 and 13678). pCMV5B-Flag-Smurf1 WT, pCMV5B-Flag-Smurf1 C699A, pCMV5B-Flag-Smad3, and pCMV5B-Flag-Smad4 were gifts from Dr. Jeff Wrana (Addgene plasmids #11752, 11753, 11742, and 11743). pCMV5 Flag-Smad1 was a gift from Dr. Joan Massague (Addgene plasmid #14044). pRK-Myc-Ubiquitin was a gift from Dr. Tianyan Gao. The β2-

adrenergic receptor mammalian expression construct was a gift from Dr. John Kehrl (National Institute of Allergy and Infectious Diseases, National Institutes of Health). LNCX BMP-RII was a gift from Dr. Rik Derynck (Addgene plasmid #12641). pcDNA3.1-C/EBP α, β, and δ were gifts from Dr. Peter Johnson (Addgene plasmids #12550, 12557, and 12559).

GFP-$Ca_V1.2$ (rabbit) was a gift from Dr. Kurt Beam (University of Colorado Health and Sciences Center, Aurora, CO). HA-tagged $Ca_V1.2$ truncations (amino acids 1507-2171, 1507-1906, and 1906-2171) have been described previously [107]. $Ca_V\beta2a$ was subcloned into the PiggyBac system vector PB514B-1 to generate a dual expression vector for $Ca_V\beta2a$ and RFP. The sequences of all constructs were confirmed using ACGT, Inc. or Eurofins MWG Operon.

MG-132 (Selleckchem, Cat No. S2619) was used at a concentration of 10 μM for 16 hours. Recombinant BMP-2 protein (R&D Systems, Cat No. 355-BM-010) was used at a concentration of 100 ng/mL for 2 hours (HEK293 cells) or 7 days (primary osteoblasts), adding fresh growth media with BMP-2 every third day. H-89 (Calbiochem, Cat No. 371962) was used at a concentration of 1 mM. HEK293 cells were pre-treated with H-89 for 30 minutes prior to transfection, and H-89 was replenished in the media throughout the experiments, including during serum starvation, until the cells were lysed. Isoproterenol (Sigma, 1351005) was used at a concentration of 100 ng/mL for 15 minutes. Forskolin (Sigma, Cat No. F6886) was used at a concentration of 1 μM for the indicated amounts of time. Phorbol 12-myristate 13-acetate (PMA) (Sigma, Cat No. P1585) was used at a

concentration of 1 μM for the indicated amounts of time. Macrophage-colony stimulating factor (M-CSF, Sigma, Cat No. M9170) and Receptor activator of nuclear factor kappa-B ligand (RANKL, Sigma, Cat No. R0525) were used as described in the osteoclast differentiation subsection of this chapter.

Co-immunoprecipitations (Co-IPs)

For co-IPs in chapters 3 and 5 of this dissertation, HEK293 cells were washed with PBS and harvested in ice-cold lysis buffer (20 mM HEPES (pH 7.4), 50 mM KF, 50 mM β-glycerophosphate, 150 mM NaCl, 2 mM EGTA (pH 8.0), 0.5% Triton X-100, 10% glycerol, 1x protease inhibitor (Calbiochem)) 48 hours after transfection. Lysates were cleared by high-speed centrifugation at 4^{o}C, and protein concentrations were measured using BioRad Quick Start Bradford 1x Dye Reagent. For co-immunoprecipitations, 1 mg of protein was brought up to 500 μL total volume with lysis buffer, and 15 μL of Protein G Plus Agarose Suspension (Calbiochem) and 4 μg of anti-Flag M2 monoclonal antibody (Sigma) or anti-HA monoclonal antibody (Sigma) were added. Tubes were rotated at 4^{o}C for two hours, and the agarose beads were pelleted and washed once with 500 μL lysis buffer, twice with lysis buffer plus 150 mM NaCl, and twice more with lysis buffer. The bound fraction and the input were resolved on 10% SDS-PAGE gels, transferred to nitrocellulose, and subjected to Western blotting analysis.

For $Ca_V\beta$2a co-IPs in Chapter 4 of this dissertation, HEK293 cells were instead harvested in ice-cold Cavβ IP buffer (20 mM Tris (pH 7.5), 250 mM NaCl, 1%

Triton X-100, 10 mM $MgCl_2$, 1x protease inhibitor (Calbiochem)), and co-IPs were otherwise performed as described in the above paragraph. To probe for the effects of free calcium and of phosphorylation on the association between Rad and Cavβ2a, 2 mM EGTA (stock solution pH 8.0) or 50 mM β-glycerophosphate, respectively, were added to the Cavβ IP buffer and co-IPs were performed.

Western blotting

Membranes were blocked with casein in PBS-tween for one hour prior to incubation with primary antibodies (**Table 2.2**) for one hour at room temperature or overnight at 4°C. Membranes were then subjected to three 10-minute washes with PBS-tween and incubated with peroxidase-conjugated secondary antibodies (AffiniPure Goat Anti-Mouse IgG, Light Chain Specific, Jackson ImmunoResearch; Monoclonal Mouse Anti-Goat IgG, Light Chain Specific, Jackson ImmunoResearch; ECL Donkey Anti-Rabbit IgG, GE Healthcare) or peroxidase-conjugated streptavidin (Thermo Scientific) for one hour at room temperature (1:20,000 dilution). Signals were developed with Hyglo chemiluminescent reagent (Denville Scientific) and visualized on a ChemiDoc MP (Bio-Rad).

Animals

All animal procedures were reviewed and approved by the Institutional Animal Care and Use Committee at the University of Kentucky. Global Rad knockout ($Rad^{-/-}$) mice were obtained from Dr. C. Ronald Kahn and have been described

previously [132]. Global Enigma knockout (Enigma$^{-/-}$) mice (also known as LIM mineralization protein (LMP)$^{-/-}$ mice) were obtained from Dr. Scott Boden at Emory University and have been described previously [160].

Heart tissue homogenization

Four-week-old male Enigma$^{-/-}$ mice and WT littermate controls were sacrificed, and hearts were excised, dissected into ventricles and apex, and snap frozen in liquid nitrogen. The ventricles were pulverized under liquid nitrogen and homogenized in ice-cold lysis buffer (20 mM HEPES (pH 7.4), 50 mM KF, 50 mM β-glycerophosphate, 150 mM NaCl, 2 mM EGTA (pH 8.0), 0.5% Triton X-100, 10% glycerol, 1x protease inhibitor (Calbiochem)). Heart homogenates were centrifuged, and lysates were prepared at a concentration of 4 μg/μL, resolved on 10% SDS-PAGE gels, transferred to nitrocellulose, and subjected to Western blotting analysis. The apices were stored at -80^{o}C for RNA isolation.

RNA isolation

Samples for RNA isolation were first homogenized in TRIzol reagent. Mouse heart tissue, specifically the apex of the heart, was pulverized under liquid nitrogen and homogenized in 0.5 mL of TRIzol in a microcentrifuge tube using a polypropylene pestle, after which an additional 0.5 mL of TRIzol was added to the tube. For calvarial osteoblast cultures, 0.5 mL of TRIzol was added to each well of a 6-well plate, and the wells were scraped with a cell scraper and contents

were transferred into a microcentrifuge tube along with an additional 0.5 mL of TRIzol. Samples were kept on ice during this time.

For phase separation, 200 μL of chloroform was added to each tube. Samples were vortexed vigorously for 15 seconds, incubated at room temperature for 3 minutes, and then centrifuged at 11,500 rpm for 15 minutes at 4°C. The colorless upper aqueous phase, which contains RNA, was transferred to a fresh microcentrifuge tube. RNA was precipitated by adding 500 μL of isopropanol to each sample, inverting the tubes to mix, and incubating at room temperature for 10 minutes. The tubes were then centrifuged at 11,500 rpm for 10 minutes at 4°C. The supernatant was aspirated, and the pellet was washed with 1 mL of 75% ethanol. Samples were then vortexed and centrifuged at 6700 rpm for 5 minutes at 4°C twice, removing as much ethanol as possible after each spin. The RNA pellet was then air-dried for 10 minutes and dissolved in 100 μL of DEPC-treated water. DNase I and the appropriate buffer were then added to each sample, and the tubes were incubated at 37°C for one hour to allow digestion of DNA in the samples.

To precipitate RNA, 12 μL of 5M ammonium acetate, 1.2 μL of linear acrylamide, and 240 μL of 100% ethanol were added to each sample, and the tubes were incubated at -20°C overnight. The samples were then centrifuged at high speed for 20 minutes at 4°C, and the supernatant was aspirated before another 5-minute high-speed centrifugation at 4°C. The supernatant was carefully removed, and RNA pellets were air-dried for 5-10 minutes to evaporate additional

ethanol. The pellets were then re-suspended in 10 μL of nuclease-free water, and concentrations were recorded and RNA quality was assessed using a Nanodrop instrument (Thermo Scientific).

cDNA synthesis

Total RNA (1 μg) was used as a template for cDNA synthesis using the RT^2 First Strand kit (SABiosciences). Briefly, 1 μg of total RNA was brought up to a volume of 10 μL with nuclease-free water in a 0.2 mL tube. To each sample, 2 μL of Buffer GE was added to facilitate degradation of any contaminating genomic DNA, and samples were heated at 42°C for 5 minutes. Samples were then placed on ice, and the remaining kit components were added. The tubes were then incubated at 42°C for 15 minutes and 95°C for 5 minutes to allow cDNA synthesis to proceed.

Quantitative reverse transcriptase-polymerase chain reaction (qRT-PCR)

cDNA from WT and Enigma$^{-/-}$ heart tissue was diluted 1:50 in nuclease-free water and amplified via RT-PCR using Taqman probes from Life Technologies: *Gapdh* (Mm99999915_g1) and *Rrad* (Mm00451053_m1). Each RT-PCR reaction consisted of 10 μL of Taqman universal PCR master mix (Life Technologies, Cat No. 4304437), 1 μL of the appropriate Taqman primers, 7 μL of nuclease-free water, and 2 μL of diluted cDNA for a total of 20 μL per assay. RT-PCR was performed in triplicate for each sample and primer. Threshold values (C_T) for *Rrad* were normalized by subtraction from *Gapdh*. WT was then

subtracted from Enigma$^{-/-}$ to determine $\Delta\Delta C_T$ values, and fold changes were calculated as $2^{-\Delta\Delta CT}$.

Fetal ventricular cardiomyocyte isolation and culture

Timed pregnant females were obtained from Jackson Laboratories and sacrificed at embryonic day 18. The embryo sac was removed, and pups were extracted from the sac. Hearts were dissected from each pup and placed in PBS + 0.1 M $MgCl_2$. Atria were removed, and ventricles were cleared of blood and placed in a 15 mL tube with PBS + 0.1 M $MgCl_2$. The tubes were centrifuged, and ventricles were re-suspended in 1 mL of filtered 0.5 mg/mL type II collagenase in PBS + 0.1 M $MgCl_2$ and transferred into a culture dish. Hearts were mechanically torn apart using forceps, transferred back into a 15 mL tube, and brought up to 10 mL with filtered collagenase. The tube was then incubated at 37^{o}C for 10 minutes and centrifuged for 5 minutes. Cells were re-suspended in fresh filtered collagenase solution, and the process of mechanical disruption, incubation at 37^{o}C, and centrifugation was repeated. The cell pellet was then re-suspended in DMEM + 10% FBS and pre-plated in a 10-cm culture dish for 2 hours at 37^{o}C to remove contaminating fibroblasts. Cells were seeded in a 24-well plate onto laminin-coated cover slips and maintained in DMEM + 10% FBS for 48-72 hours. Cells were treated with vehicle, forskolin, or isoproterenol and harvested in ice-cold lysis buffer (20 mM HEPES (pH 7.4), 50 mM KF, 50 mM β-glycerophosphate, 150 mM NaCl, 2 mM EGTA (pH 8.0), 0.5% Triton X-100, 10% glycerol, 1x protease inhibitor (Calbiochem)) and subjected to Western blotting analysis.

Electrophysiology

HEK293 cells were transiently transfected with GFP-tagged $Ca_V1.2$, a PiggyBac dual promoter vector (PB514B-1) expressing $Ca_V\beta2a$ and RFP, HA-tagged empty vector or Rad WT, and Flag-tagged empty vector or Enigma. Cells were split at low density into 35-mm dishes 24 hours post-transfection, and recordings were made 6-24 hours later. The whole-cell configuration of the patch clamp technique was used to measure ionic current, selecting isolated GFP^+/RFP^+ spherical cells. Patch electrodes were pulled from glass capillary tubes to resistances of 1-2 MΩ, and the tips were flame-polished. The external bath solution contained 112.5 mM CsCl, 30 mM $BaCl_2$, 1 mM $MgCl_2$, 10 mM tetraethylammonium chloride, 5 mM glucose, and 5 mM HEPES (pH 7.4). The internal recording solution contained 110 mM K-gluconate, 40 mM CsCl, 1 mM $MgCl_2$, 5 mM Mg-ATP, 3 mM EGTA, and 10 mM HEPES (pH 7.35). Recordings were performed at room temperature, and only those cells with seal resistances exceeding 1 GΩ were used for recording. pCLAMP 10.0 (Axon Instruments) software was used to generate the voltage-clamp protocols and to acquire and analyze data.

Alizarin Red / Alcian Blue skeletal stain

Neonatal mice at one day of age were sacrificed and dissected to remove all the skin and organs. Scalding the specimens in a 70°C water bath facilitates this process. The specimens were fixed in 95% ethanol in 50 mL conical tubes for 24 hours at room temperature with gentle rocking. All following incubations were

also performed at room temperature with slow rocking for the indicated amounts of time. After fixation, the ethanol was replaced with Alcian Blue staining solution (0.03% Alcian Blue in 80% ethanol/20% acetic acid), and specimens were incubated in this solution for three days to allow staining of cartilage. Skeletons were washed with 95% ethanol for six hours and then incubated in 2% KOH for 24 hours. The specimens were then stained in Alizarin Red S solution (0.03% Alizarin Red S in 1% KOH) for 12 hours. Finally, the skeletons were cleared in a solution of 1% KOH/20% glycerol for 24 hours, incubated in a 1:1 solution of glycerol and 95% ethanol for 24 hours, and then analyzed and photographed.

Bone collection

The right femora were dissected from 4-month-old male and female WT and $Rad^{-/-}$ mice immediately after sacrifice, taking care to remove all soft tissue. For microcomputed tomography and bone histology, femora were fixed in a ten-fold volume of 10% neutral buffered formalin for three days with rocking and then transferred to 70% ethanol until analysis. For four-point bending analysis, bones were snap frozen in liquid nitrogen and stored at -80^{o}C in saline-soaked gauze prior to analysis.

Microcomputed tomography

Microcomputed tomography (μCT) was performed in collaboration with the μCT core facility at Rush University. Femora were scanned (Scanco Model 40; Scanco Medical AG, Basserdorf, Switzerland) in 70% ethanol at 55 kV and 145

mA, 0.3-second integration time with a 10 μm isotropic voxel size in plane and a 10 μm slice thickness. The overall femur length was recorded and used to guide the cortical and trabecular analyses. Specifically, the trabecular region of interest ranged from just proximal of the distal growth plate to 30% of the bone length as measured from the distal end. The trabecular output variables included total volume (TV), bone volume (BV), bone volume fraction (BV/TV), connectivity density (Conn.D), structural model index (SMI), trabecular number (Tb.N), trabecular thickness (Tb.Th), trabecular spacing (Tb.Sp), apparent density (Ap.Dens), material density (Mat.Dens), specific bone surface (BS/BV), and degree of anisotropy (DA). Trabecular analyses utilized a sigma value of 0.8, support of 1, and threshold at 270. Cortical data at the midshaft of the femur were also analyzed, including cortical bone area (Ct.Ar), total cross-sectional area (Tt.Ar), medullary area (Ma.Ar), cortical thickness (Ct.Th), and cortical area fraction (Ct.Ar/Tt.Ar). Cortical analyses used a sigma value of 1.5, support of 2, and threshold at 350.

Four-point bending analysis

Four-point bend testing was performed in collaboration with Dr. Matthew Allen at Indiana University School of Medicine to measure whole bone mechanical properties [161]. Because four-point bending produces pure bending between two loading points, fractures occur at the weakest location in the region [162], making it superior to three-point bending which uses a single loading point.

The anterior surface of each femur was placed on two lower supports with a span length of 9 mm and an upper span length of 3 mm. Each femur was loaded at a rate of 2 mm/min until failure occurred, and a force-displacement curve was generated and used to determine structural properties including ultimate force, stiffness, displacement, and energy absorption for each specimen. Derivation of apparent material properties utilized the cross-sectional moments of inertia and the distances from the centroid to the tensile surface using standard beam-bending equations for four-point bending. The 0.2% offset criterion was used to define yield points, and a custom MATLAB (Version 11) program was used for all mechanical analyses [163].

Preparation of femur sections for histology

Following fixation in 10% neutral buffered formalin as described above, femora were dehydrated through a graded series of ethanols for 4 hours at each step and cleared in xylenes for 4 hours. For plastic embedding, the specimens were incubated in unpolymerized methyl methacrylate for 4 hours, in unpolymerized methyl methacrylate containing 4% dibutyl phthalate as a softening agent for 7 days, and finally embedded in methyl methacrylate containing 4% dibutyl phthalate and 0.25% Perkadox 16 as a catalyst and allowed to polymerize at room temperature. A band saw was used to remove excess plastic from the blocks, and the blocks were then shaped with a dental model trimmer. A rotary microtome with a tungsten-carbide knife was used to cut thin sections (4-10 μm,

mostly trabecular bone), and a diamond wire saw was used to cut thick sections (80+ μm, mostly cortical bone).

All histological measurements were made using a semiautomatic analysis system (Bioquant OSTEO 7.20.10, Bioquant Image Analysis Co.) attached to a Nikon Optiphot 2 microscope with both visible and ultraviolet light sources.

Tartrate-resistant acid phosphatase stain

Three thin sections per animal were de-plasticized in acetone and stained for tartrate resistant acid phosphatase (TRAP) as previously described [164] in collaboration with Dr. Keith Condon and the Bone Histology core facility at Indiana University School of Medicine. Briefly, thin sections were incubated in 0.2 M acetate buffer (pH 5.0), rinsed, and incubated in a warmed acid phosphatase solution. Sections were then counterstained with Gill's Hematoxylin No. 3 and coverslipped with an aqueous mounting media after air-drying. TRAP staining was quantified as the percentage of the bone surface occupied by osteoclasts (% Oc.S/BS) using Bioquant OSTEO 7.20.10.

Calcein labeling and dynamic histomorphometry

To prepare the 0.6% calcein injection solution, 0.9 g NaCl was dissolved in 90 mL of distilled water, followed by 2.0 g $NaHCO_3$ and 0.6 g calcein. The calcein must be added slowly to avoid foaming of the solution. The pH of the calcein solution was adjusted to 7.4 using 1 N NaOH or 1 N HCl, and the volume was

brought up to 100 mL with distilled water. The solution was then filtered into a sterile glass vial and stored at 4^{o}C in the dark.

Mice were injected intraperitoneally with 30 mg/kg calcein (0.05 mL of 0.6% calcein for every 10 grams body weight) at 7 and 2 days prior to sacrifice. The minimum dose used was 0.15 mL regardless of weight to ensure visualization of the label in bone, and each dose was administered as two half-doses.

Thin sections for dynamic histomorphometry were kept in plastic and coverslipped using Eukitt mounting reagent to analyze trabecular bone formation rates. Thick sections were briefly cleared in xylenes and coverslipped with Eukitt mounting reagent to analyze cortical bone formation rates at the periosteal and endocortical surfaces. Slides were stored in the dark prior to analysis.

Fluorochrome labels were quantified using Bioquant OSTEO 7.20.10. First, the bone surfaces containing a single label (sLS), double labeling (dLS), and no label (noLS) were measured. The mineral apposition rate (MAR) was calculated as the average distance between the two labels divided by the time interval of five days. The percent mineralizing surface (MS/BS), or the percentage of the bone surface that is actively forming bone, was calculated as the sum of the double-labeled surface and half of the single-labeled surface divided by the total bone surface, or (dLS + ½ sLS)/(dLS + sLS + noLS) * 100%. Finally, the bone formation rate (BFR/BS) in $\mu m^3/\mu m^2$/year was calculated as the mineral apposition rate multiplied by the percent mineralizing surface and 365 days/year, or MAR * MS/BS (as a decimal) * 365.

In vitro osteoclast isolation and culture

Spleens were dissected from two-month-old mice and kept on ice in sterile PBS. Spleens were then transferred to sterile culture medium (α-MEM + 10% FBS + 100 units/mL penicillin and 100 μg/mL streptomycin). Spleens were crushed in culture medium using a 70-μm filter mesh, followed by pipetting to generate a single cell suspension. This suspension was centrifuged 5 minutes at 1500 rpm, and the cell pellet was re-suspended in pre-osteoclast culture medium (α-MEM + 10% FBS + 100 units/mL penicillin and 100 μg/mL streptomycin + 10 ng/mL macrophage colony stimulating factor (M-CSF)). Cells were plated in untreated Petri dishes in pre-osteoclast medium for 5 days, changing the medium every other day. Cells were washed three times with PBS and then incubated in PBS + 0.25 mM EDTA for 15 minutes at 37^{o}C. EDTA was inactivated through the addition of an equal volume of culture medium, and cells were detached using a cell scraper and transferred into conical tubes. Cell suspensions were centrifuged for 5 minutes at 1000 rpm, and the cells were re-suspended in a small volume of complete osteoclast culture medium (α-MEM + 10% FBS + 100 units/mL penicillin and 100 μg/mL streptomycin + 5 ng/mL M-CSF + 50 ng/mL receptor activator of nuclear factor kappa-B ligand (RANKL)). Cells were counted and seeded in 24 well plates at a density of 25,000 cells/well in complete osteoclast culture medium for 7 days, changing the media every other day, prior to osteoclast differentiation analysis.

Osteoclast differentiation assay

Osteoclast differentiation was assessed using a tartrate-resistant acid phosphatase (TRAP) staining kit (Takara, Cat No. MK300). Briefly, cells were fixed for five minutes at room temperature in the sodium citrate fixation solution supplied with the kit. Cells were then stained with the substrate solution for acid phosphatase + 0.1 volume sodium tartrate solution at 37^{o}C for 20 minutes. This solution was discarded, and cells were washed three times with sterile water to stop the reaction. Stained cells were analyzed using the Axiovert 100 microscope. The number of osteoclasts, defined as multinucleated (at least three nuclei) cells positive for TRAP staining, per well were counted.

Neonatal calvarial osteoblast isolation and culture

Calvariae, or skullcaps, were isolated from pooled litters of 3-day-old neonatal mice, taking care to remove all conjunctive tissues. Calvariae were washed with ice-cold PBS and transferred to pre-warmed, filtered digestion media (α-MEM + 1.5 mg/mL Type 2 Collagenase + 0.00625% Trypsin-EDTA). The calvariae were digested with rotation at 37^{o}C for 5 minutes, followed by 20 seconds of vigorous shaking. The suspended cells, primarily fibroblasts, were discarded, and the medium was replaced with 10 mL of fresh digestion media. The calvariae were digested with rotation at 37^{o}C, shaking vigorously for 20 seconds every 10 minutes for a total of 30 minutes. The cell suspension was transferred to a new tube on ice, taking care to avoid large bone pieces. Fresh digestion media was added to the calvariae, and they were digested at 37^{o}C with rotation once more,

again shaking vigorously for 20 seconds every 10 minutes for a total of 30 minutes. The cell suspension was again transferred to a new tube on ice, and the two suspensions were centrifuged at 1300 rpm for 3 minutes at 4^{o}C. The cell pellets were re-suspended in growth media (GM; α-MEM + 10% FBS + 100 units/mL penicillin and 100 μg/mL streptomycin) and plated in 10-cm dishes. After 72 hours, the cells were split into 6-well dishes at a density 15,000 cells/cm^2 and maintained in growth media for 72 hours. Upon confluence, cells were either maintained in growth media or switched to osteogenic media (OM; α-MEM + 10% FBS + 100 units/mL penicillin and 100 μg/mL streptomycin + 5 mM β-glycerophosphate + 100 μg/mL ascorbic acid) or adipogenic media (AM; α-MEM + 15% FBS, 5 μg/mL insulin, 50 μM indomethacin, 0.5 μM 3-isobutyl-1-methylxanthine (IBMX), and 1 μM dexamethasone). The media was changed every 2-3 days until endpoint assays were performed.

Alkaline phosphatase (ALP) stain

WT and Rad$^{-/-}$ primary calvarial osteoblasts were assayed for alkaline phosphatase activity on day 0 (upon confluence) and day 7 of culture in osteogenic media or adipogenic media using a premixed 5-bromo-4-chloro-3-indolyl phosphate (BCIP)/nitroblue tetrazolium (NBT) solution (Sigma, Cat No. B6404). A sodium citrate (pH 5.4) fixation solution was prepared by combining 45 mL of acetone, 10 mL of ethanol, 11.5 mL of 0.1 M citric acid monohydrate, and 33.5 mL of 0.1 M sodium citrate and was stored at -20^{o}C. Cell monolayers in 6-well dishes were incubated in 1 mL of sodium citrate fixation solution for 5

minutes and washed twice with distilled water. The monolayers were then incubated with the BCIP/NBT solution for 10 minutes at room temperature, washed four times with distilled water, and maintained in PBS for imaging. BCIP is a substrate for alkaline phosphatase, and dephosphorylation of BCIP generates an intermediate that dimerizes under alkaline conditions. Hydrogen ions released during this dimerization reaction result in reduction of NBT, generating a bluish-purple precipitate that is indicative of alkaline phosphatase activity in these cells.

Alizarin Red S (ARS) stain

WT and $Rad^{-/-}$ osteoblasts were assayed for calcium deposition on day 21 of culture in osteogenic media using Alizarin Red S (ARS). The working solution for this stain is 2% ARS, adjusted to pH 4.1-4.3 using NH_4OH. This solution must be filtered and stored in the dark and the pH checked prior to each use. Cell monolayers were washed with PBS and fixed with 10% neutral buffered formalin for at least 30 minutes. Cell monolayers were then incubated with the ARS working solution for 45 minutes at room temperature in the dark and then carefully washed four times with 1 mL of distilled water. The last wash was replaced with PBS, and the cell monolayers were imaged using the Axiovert 100 microscope.

To quantify the ARS staining, which is proportional to the amount of calcium deposition, the ARS was solubilized and the optical density was measured. ARS was solubilized from the osteoblast monolayers by adding 800 μL of 10% acetic

acid to each well and incubating for 30 minutes at room temperature with agitation. The cells were scraped, transferred into a tube, and vortexed for 30 seconds. Samples were then heated at 85^{o}C for 10 minutes, placed on ice for five minutes or until fully cooled, and centrifuged at high speed at 4^{o}C for 15 minutes. Five hundred microliters of the supernatant were transferred to a new tube and neutralized with 200 μL of 10% NH_4OH. Samples were mixed well, and the pH was tested to ensure it fell between 4.1-4.5. The absorbance at 405 nm was measured for each sample in triplicate by aliquoting 150 μL of each sample per well into an opaque-walled, transparent-bottomed 96-well plate. The absorbance is directly proportional to the amount of ARS staining in the sample.

Microarray analysis

Total RNA was isolated from confluent WT and Rad$^{-/-}$ calvarial osteoblast cultures using the standard TRIzol and chloroform method described above, and RNA quality was assessed using RNA 6000 Nano-LabChip (Agilent). The University of Kentucky Genomics Core Laboratory performed labeling of the RNA and hybridization to the chip. Total RNA (100 ng per sample) was labeled and hybridized onto the Affymetrix Clariom D mouse array. The arrays were hybridized for 16 hours at 45^{o}C and 60 rpm. The arrays were washed and stained on the Affymetrix Fluidics 450 station and scanned on the Affymetrix GeneChip7G scanner to quantify the signal intensity of hybridized probes. Data were analyzed using the Affymetrix Command Console software.

Semi-quantitative RT-PCR

For RT-PCR, cDNA from WT and Rad$^{-/-}$ osteoblast cultures was prepared from 1 μg of total RNA using the RT^2 First Strand Kit (Qiagen) as described above. RT-PCR reactions consisted of 12.5 μL of DreamTaq Green PCR Master Mix (2X) (Thermo Scientific), 2 μL of cDNA, 1 μL of the appropriate primers, and 9.5 μL of nuclease-free water. Primers for mouse matrix Gla protein (*MGP*) and 18S were obtained from Real Time Primers, and RT-PCR cycling parameters followed the manufacturer's instructions. PCR products were separated on 1% agarose gels, and band intensities were measured using ImageJ.

Oil Red O (ORO) stain

A stock solution of 0.3% Oil Red O (ORO) was prepared in isopropanol and stored in the dark. Oil Red O staining was performed on osteoblast monolayers after 14 days in culture to quantify adipogenesis. Cell monolayers were washed with PBS and fixed with 10% neutral buffered formalin for at least 30 minutes. During fixation, three parts of the ORO stock solution were combined with two parts distilled water and filtered to generate the working ORO solution. This working solution must be used within 30 minutes of its preparation. Cells were washed with distilled water and incubated in 60% isopropanol for 5 minutes at room temperature. The cell monolayers were then incubated in ORO working solution for 15 minutes at room temperature, after which they were washed with distilled water four times. Nuclei were stained purple by incubating the monolayers with Harris Hematoxylin solution for one minute at room temperature

and washing four times with distilled water. Cell monolayers were kept in PBS for imaging on the Axiovert 100 microscope. The number of ORO-positive cells per 20X field were quantified.

Echo-MRI

The body composition of live, unanesthetized WT and $Rad^{-/-}$ mice was measured using an EchoMRI-100 whole body composition analyzer (Echo Medical System, Houston, TX).

Von Kossa / MacNeal's tetrachrome stain

Three thin sections per animal were de-plasticized in acetone and stained using a modification of the Von Kossa / MacNeal's (VKM) tetrachrome protocol [165] in collaboration with the Bone Histology core facility at Indiana University School of Medicine. Briefly, mineralized bone was stained using the Von Kossa silver method and unmineralized tissue was counterstained with MacNeal's tetrachrome. Slides were blinded, three random fields per section were imaged at the distal femur just proximal to the growth plate, and adipocyte number and size were quantified using ImageJ software.

Statistics

Statistical analysis was performed using Student's *t* test, with $p<0.05$ considered significant, and all data are reported as mean +/- SEM.

Table 2.1: Primers

Oligo Name	Sequence
1. Enigma 5' HindIII -> Flag	AATTAAGCTTATGGATTCCTTCAAGGT
2. Enigma 3' NotI -> Flag	AATTGCGGCCGCTCATACGTGGGAAA
3. ENH1 5' HindIII -> Flag	AATTAAGCTTATGAGCAACTACAGTG
4. ENH1 3' NotI -> Flag	AATTGCGGCCGCTCAAAAATTCACAG
5. Cypher 5' HindIII -> Flag	AATTAAGCTTATGTCTTACAGTGTGAC
6. Cypher 3' NotI -> Flag	AATTGCGGCCGCTCACAAGTTGATGG
7. Enigma ΔPDZ 5' HindIII -> Flag	AATTAAGCTTATGCACATGAAGCCC
8. Enigma ΔLIM1-3 3' NotI -> Flag	AATTGCGGCCGCTCATACAGGCGTCT
9. Rad K204R Sense	CTCGTGGGCAACAGGAGTGACCTGGTG
10. Rad K204R Antisense	CACCAGGTCACTCCTGTTGCCCACGAG

Table 2.2: Primary antibodies

Antibody	Species	Company and Catalog Number	Dilution
C/EBP alpha	Rabbit	Cell Signaling, 8178	1:1000
C/EBP beta	Rabbit	Cell Signaling, 3087	1:1000
C/EBP delta	Rabbit	Cell Signaling, 2318	1:1000
FLAG	Mouse	Sigma, F1804	1:2000
Gapdh	Rabbit	Cell Signaling, 2118	1:1000
GST	Rabbit	Santa Cruz, sc-459	1:1000
HA	Mouse	Sigma, H9658	1:2000
Myc	Mouse	Sigma, M4439	1:2000
Phospho-Rad S39	Rabbit	Custom antibody	1:1000
Rad	Goat	Abcam, ab136865	1:1000
Smad1	Rabbit	Cell Signaling, 6944	1:1000

Chapter 3

Rad levels are regulated through a novel interaction with Enigma and the associated E3 ligase Smurf1

Introduction

Ras-related GTPases function as guanine nucleotide-dependent switches that cycle between an active guanosine triphosphate (GTP)-bound state and an inactive guanosine diphosphate (GDP)-bound state [2]. This classical regulatory cascade is facilitated by the activities of guanine nucleotide exchange factors (GEFs), which promote GDP release and GTP loading, and GTPase activating proteins (GAPs), which catalyze GTP hydrolysis and promote inactivation [2]. Unlike most other small GTPases, the nucleotide dependence of Rad and the other RGK (Rad, Rem, Rem2, Gem/Kir) subfamily protein function has not been established, and they instead share the unique property of regulation at the level of expression [11]. Briefly, Rad levels are significantly decreased in human heart failure [131, 132] and in a variety of human cancers [24-28, 30, 32, 34, 38, 39], while Rad expression is up regulated in developing and regenerating muscle [20, 46, 51, 54] and during osteoblast differentiation [44]. Although most of these alterations in Rad expression have been attributed to transcriptional changes, it

is unclear whether Rad protein levels may also be regulated post-translationally. Specifically, Rad protein turnover presents a potential, as of yet unexplored regulatory mechanism in light of recent mass spectrometry studies that have revealed that Rad protein is subject to modification by ubiquitination [123, 124]. In this chapter, I will describe the association of RGK proteins with a scaffolding protein known to interact with E3 ubiquitin ligases and demonstrate that Rad protein is subject to ubiquitination and degradation following ectopic expression of one of these E3 ubiquitin ligases.

Plasma membrane localization of RGK proteins is essential for their function in voltage-dependent calcium channel (VDCC) inhibition [110], and data suggest that the C-terminus of RGK proteins is required for calcium channel blockade and for proper localization to the plasma membrane, at least in part through binding to phosphatidyl inositol phospholipids [12, 106]. Moreover, the independent observations by our laboratory and the Colecraft laboratory that RGKs can bind directly to the $Ca_V1.2$ pore-forming subunit of the calcium channel suggest another means of localization of these GTPases at the cell membrane [18, 107]. We were interested in defining other potential regulatory partners for RGK proteins, and for Rad in particular, and we began looking for candidate binding partners that are expressed in the heart and that might link RGK proteins to the plasma membrane and/or the calcium channel complex.

A recent network map of 14,000 protein-protein interactions identified Enigma (also known as *PDLIM7* or LIM mineralization protein (LMP)) as a novel Gem-binding protein [166]. Enigma contains an N-terminal PDZ (Postsynaptic density 95, discs large, and zonula occludens-1) domain and three C-terminal LIM (Lin11, Isl-1, and Mec-3) domains. Proteins containing PDZ and LIM domains play important roles as scaffolding proteins that allow the formation of multi-protein complexes to provide spatial and temporal regulation of signaling [167]. Both PDZ and LIM domains mediate protein-protein interactions. PDZ domains recognize and bind to short motifs usually found at the C-terminus of other proteins [168]. For instance, class I PDZ binding motifs are found at the C-terminus of proteins whose last three amino acid residues are S/T-X-Φ, where X is any amino acid and Φ is a hydrophobic residue [168]. It should be noted that Rad, Gem, and Rem2 end in class I PDZ binding motifs (-SVL), while Rem does not (-AVL). LIM domains consist of two adjacent zinc finger domains separated by a short hydrophobic linker, and a specific recognition motif has not been identified for these domains [169]. There are ten genes in the mammalian genome that encode proteins containing both PDZ and LIM domains [167]. Of these, the Enigma subfamily of PDZ-LIM proteins consists of three members, each of which contains an N-terminal PDZ domain and three C-terminal LIM domains [170]: Enigma (LIM mineralization protein (LMP), *PDLIM7*) [171], Enigma homolog (ENH, *PDLIM5*) [172], and Cypher/Z-band associated protein (ZASP, *PDLIM6*) [173]. These proteins are highly homologous in sequence to

one another, with the main differences lying in the region between the PDZ and LIM domains.

The potential for an interaction between RGK proteins and Enigma was of interest for several reasons. First, each of the Enigma subfamily proteins is expressed in the heart [173-175], and ENH and Cypher have been reported to bind to and regulate voltage-dependent calcium channels [176-179]. Moreover, deletion of Cypher or ENH in mice results in dilated cardiomyopathy [180, 181], Cypher and ENH play roles during cardiac development [182], and Enigma-null ($Enigma^{-/-}$) mice exhibit cardiac structural and functional abnormalities [183]; thus, Enigma subfamily proteins appear to have important roles in the heart and in VDCC regulation. In addition to its potential role in the heart, Enigma also binds to and alters the activity of several different E3 ubiquitin ligases, including Smad ubiquitin regulatory factor 1 (Smurf1) [184], murine double minute 2 (MDM2) [185], and Cbl-c [186]. It remains unclear whether Enigma directly regulates the activity of these proteins or whether Enigma, through its multiple protein-protein interaction domains, may act as a scaffolding protein to regulate ubiquitin ligase activity by directing substrate specificity via proximity. Based on the properties of PDZ-LIM family proteins described above and the report of a putative interaction between Gem and Enigma [166], the work in this chapter aims to confirm the Gem interaction and ask whether the association with Enigma is shared by the other RGK subfamily proteins, particularly Rad, and whether the E3 ubiquitin ligases reported to bind to Enigma might regulate Rad protein stability.

Of the E3 ubiquitin ligases that bind to Enigma, I chose to focus on Smurf1 because of its established role in the regulation of osteoblast differentiation [158, 187] given the report of Rad up regulation during osteogenic differentiation of mesenchymal stem cells (MSCs) [44] and the bone density phenotype of $Rad^{-/-}$ mice that will be described in detail in Chapter 5. Briefly, Smurf1 regulates osteoblast differentiation by providing negative feedback on bone morphogenetic protein (BMP) signaling through polyubiquitination of Smad proteins, thereby targeting them for degradation in the proteasome [158]. Enigma, or LIM mineralization protein (LMP) in the bone literature, has an established role in the regulation of osteoblast differentiation that is thought to occur through its regulation of Smurf1 [184, 188, 189], and $Enigma^{-/-}$ mice have documented deficits in bone density as a result [160]. As mentioned previously, Rad levels are up regulated when MSCs are primed for osteoblast differentiation using lithium [44]. Notably, Satija et al. have found that RNAi-mediated Rad silencing impaired lithium-dependent osteogenic priming [44], suggesting that the loss of Rad may result in a similar phenotype to increased Smurf1 activity. This chapter will describe studies defining the interaction of RGK proteins with Enigma and provide evidence that Rad is subject to ubiquitination and that Rad protein levels are reduced following ectopic expression of the Smurf1 E3 ligase and in response to prolonged BMP signaling. Taken together, these studies suggest that ubiquitination may serve as a novel regulatory mechanism to permit dynamic control of Rad, and perhaps other RGK, protein levels.

Results

RGK subfamily proteins co-immunoprecipitate with Enigma

To determine whether Gem and other RGK proteins associate with Enigma [166], HEK293 cells were transfected with HA-tagged RGK proteins (Rad, Rem, Rem2 and Gem) and Flag-tagged empty vector (EV), Enigma, ENH1, or Cypher, and interactions between these proteins were assessed by anti-Flag co-immunoprecipitations. While each of the RGK proteins co-immunoprecipitated with Enigma, no interaction was detected between RGK proteins and either ENH1 or Cypher (**Figure 3.1**). Thus, Enigma serves as a common interacting partner for all members of the RGK subfamily, joining calmodulin, 14-3-3, and $Ca_V\beta$ [12, 14, 16, 109, 118-120]. As Enigma has been shown to have a role in heart development [183], and a focus of our laboratory is to examine the physiological role of Rad signaling in the heart, further studies were directed at examining whether Enigma plays a role in the control of Rad GTPase.

Rad association with Enigma does not require the PDZ domain

I next sought to determine which of the protein-protein interaction domain(s) of Enigma were required for interaction with Rad. Given that the C-termini of Rad, Gem, and Rem2 consist of a putative PDZ-binding motif and that Rem, the only RGK protein without a PDZ-binding motif, consistently displayed the weakest interaction with Enigma (**Figure 3.1**), I hypothesized that the PDZ domain might mediate, or at least enhance, the interaction between Rad and Enigma.

Truncations of Enigma were generated to lack either the N-terminal PDZ domain (ΔPDZ) or the three C-terminal LIM domains (ΔLIM1-3) to determine which domain in Enigma is required for the interaction with Rad (**Figure 3.2A**). Co-immunoprecipitation analyses using these truncations revealed that the interaction between Enigma and Rad was maintained when the PDZ domain was removed; however, deletion of the three LIM domains completely abolished the interaction between these two proteins (**Figure 3.2B**). Therefore, Rad likely interacts with Enigma through its LIM domain(s), whereas the PDZ domain is dispensable for Rad-Enigma complex formation.

Rad protein levels are elevated in the hearts of Enigma$^{-/-}$ mice

Unlike ENH1 and Cypher [178, 179], Enigma has not been studied in the regulation of calcium channels. However, Enigma has an established role in E3 ubiquitin ligase regulation that sets it apart from the other members of the PDZ-LIM scaffold family [184-186]. Studies by our lab and others have reported that Rad protein levels are decreased in human heart failure [131, 132], but the mechanism underlying the down regulation of Rad expression is unclear. Thus, I next asked whether the interaction between Rad and Enigma might serve to modulate Rad levels. Hearts from Enigma$^{-/-}$ mice and WT littermates were homogenized and subjected to Western blotting analysis to probe the impact of Enigma deletion on Rad protein levels. Enigma$^{-/-}$ hearts exhibited significantly higher levels of Rad protein than WT controls (**Figure 3.3A**). RNA was extracted from the apices of these hearts and quantitative RT-PCR analysis indicated a

modest increase in Rad mRNA levels in Enigma$^{-/-}$ hearts that did not reach statistical significance compared to WT hearts (**Figure 3.3B**). These data, while preliminary, suggest that Enigma deletion may result in an increase in Rad expression through post-transcriptional mechanisms, and we next investigated the potential contribution of the E3 ubiquitin ligases bound to Enigma in regulating Rad protein levels.

Smurf1 overexpression results in decreased Rad levels

Smad ubiquitin regulatory factor 1 (Smurf1) is one of the E3 ubiquitin ligases that binds to Enigma [184]. Given the observation that Enigma deletion imparts a significant increase in Rad protein, but not mRNA, levels in the heart, I next assessed the ability of Smurf1 to regulate Rad post-translationally. Transfection of HEK293 cells with Smurf1, but not the related E3 ligase Smurf2 which does not bind to Enigma, resulted in a significant reduction in Rad protein levels (**Figure 3.4A**). Ectopic expression of Enigma was not required for this down regulation of Rad; however, we cannot rule out the possibility that endogenous Enigma in HEK293 cells may act as a scaffold for Rad and Smurf1. To determine whether Rad is ubiquitinated following Smurf1 overexpression, HEK293 cells were transfected with Myc-tagged ubiquitin along with HA-tagged Rad and either Flag-tagged EV or Smurf1. Cells were treated with MG-132 prior to lysis to inhibit proteasomal degradation, and N-ethylmaleimide was added to the lysis buffer to block cellular deubiquitylating enzyme activity. In support of a role for Smurf1 in the proteostatic regulation of Rad function, Rad ubiquitination was

increased in the context of Smurf1 overexpression (**Figure 3.4B**). Moreover, treatment of these cells with the proteasome inhibitor MG-132 maintained Rad levels in the presence of Smurf1 overexpression (**Figure 3.4B**). This observation suggests that the E3 ubiquitin ligase activity of Smurf1 followed by proteasomal degradation is responsible for the decline in Rad levels observed upon Smurf1 overexpression. Notably, Smurf1 overexpression resulted in a decrease in the expression of the other RGK proteins Rem and Gem, but not of the unrelated Rin GTPase, suggesting that Smurf1 regulation may be a common feature across the RGK subfamily (**Figure 3.5**).

Rad Lys204 is required for Smurf1-mediated turnover

In keeping with the notion that ectopic Smurf1 expression promotes polyubiquitination and targeting of Rad for proteasomal degradation, overexpression of the catalytically inactive Smurf1 C699A mutant failed to alter Rad protein levels [190] (**Figure 3.6**). Previous mass spectrometry analysis indicates that Rad protein can be ubiquitinated at lysine-204 (Lys204) [123, 124]. To test whether Lys204 is required for Smurf1-mediated Rad regulation, site directed mutagenesis was performed to change this lysine to arginine (K204R) to prevent site-selective ubiquitination. Importantly, Rad K204R was insensitive to Smurf1 overexpression, suggesting that ubiquitination of Rad at this residue is required for Smurf1-mediated turnover of the protein (**Figure 3.6**). Taken together, these data suggest that Smurf1 ubiquitinates Rad at Lys204, targeting it for proteasomal degradation.

Rad co-immunoprecipitates with receptor-associated Smad (R-Smad) proteins

The studies described above suggest that Rad is a substrate for Smurf1, like the receptor-associated Smad (R-Smad) proteins in the BMP signaling pathway, Smad1 and Smad5 [190]. Given the regulation of Rad and Smad proteins by Smurf1-mediated ubiquitination as well as the recent reports of Rad binding to transcription factors [40, 41], co-immunoprecipitation experiments were performed to probe for a potential interaction between Rad and Smad proteins. HEK293 cells were transfected with HA-Rad WT and either Flag-tagged Smad1, Smad3, Smad4, Enigma as a positive control, or EV as a negative control. Smad1 is an R-Smad in the BMP signaling pathway and is targeted by Smurf1 [190], Smad3 is an R-Smad in the transforming growth factor β (TGFβ) signaling pathway and is targeted by the Smurf2 and ROC1 E3 ubiquitin ligases [191, 192], and Smad4 is the common Smad partner (co-Smad) that dimerizes with phosphorylated R-Smads to facilitate nuclear translocation and transcriptional activation and is not subject to Smurf-mediated turnover [193]. Co-immunoprecipitation analyses suggested that Rad forms a complex with Smad1 as well as, unexpectedly, Smad3 (**Figure 3.7).** Thus, the data suggest that Rad associates with R-Smads from both the BMP and TGFβ pathways, but not with the co-Smad, Smad4.

BMP-2 treatment decreases Rad levels

BMP receptor activation results in increased downstream Smurf1 activity toward R-Smad proteins [158], whether through activation of the Smurf1 enzyme or generation of a recognizable substrate in phosphorylated R-Smad proteins. For this reason, I next examined whether BMP-2 signaling might control Rad levels. HEK293 cells were transfected with HA-Rad WT and treated with vehicle or BMP-2 for two hours and probed for changes in Rad levels. Western blotting analysis indicated that BMP-2 treatment results in a decrease in Rad protein levels (**Figure 3.8A**). Since Enigma has been reported to inhibit Smurf1-mediated ubiquitination of Smad proteins [184], I next asked whether Enigma overexpression might alter the effects of BMP-2 signaling on Rad protein levels. Notably, the previously observed decrease in Rad protein levels following BMP-2 treatment was rescued when Enigma was overexpressed (**Figure 3.8A**).

In addition to the change seen by our laboratory and others in Rad protein levels during human heart failure [131, 132], we and others have also recently observed changes in Rad expression during MSC differentiation toward the osteoblast [44] and adipocyte lineages (see Chapter 5). Since BMP/Smad signaling plays a central role in the regulation of MSC differentiation toward the osteoblast lineage [153, 155, 194], and since Enigma has been recently implicated in the regulation of this process as well [184], I next assessed the impact of BMP-2 signaling on endogenous Rad levels in wildtype primary calvarial pre-osteoblasts. Interestingly, treatment of these cells with BMP-2 for one week resulted in a

marked reduction in Rad protein levels (**Figure 3.8B**). As confirmation that Smurf1 activity is detectable at this time point and at this dosage of BMP-2, Smad1 levels were also found to be decreased (**Figure 3.8B**). These data are preliminary, but they suggest that Smurf1 activation may be a physiological means of regulating Rad protein levels that warrants further investigation both in osteoblasts and cardiac myocytes.

Discussion

RGK GTPases comprise a unique subfamily of Ras-related GTPases in many ways, especially in the means by which these G-proteins are regulated. Unlike the majority of small GTPases, Rad and the other related RGK proteins do not appear to be predominantly controlled via the canonical GTP/GDP cycle, and attempts to identify GEF and GAP regulatory proteins have to date been largely unsuccessful [11]. Instead, regulation of RGK proteins via phosphorylation [64, 98] and expression levels [11] has been reported. We and others have reported that Rad levels are significantly lower in human failing hearts compared to healthy controls [102, 131], but the mechanism of Rad down regulation is unknown. In many cases, Rad down regulation has been attributed to transcriptional changes, but the potential for post-translational control of Rad levels has not been explored, despite the observation that Rad protein is subject to ubiquitination [123, 124].

The studies described in this chapter have identified a novel interaction between Rad GTPase and Enigma, a scaffolding protein containing an N-terminal PDZ

domain and 3 C-terminal LIM domains that can bind to and regulate the activity of E3 ubiquitin ligases [184-186]. Deletion of Enigma results in an increase in Rad protein, but not mRNA, levels in mouse heart tissue, and overexpression of Smurf1, an E3 ubiquitin ligase that binds to Enigma, results in ubiquitination of Rad protein at Lys204 and proteasomal degradation. While further studies are necessary and will be discussed below, we propose a working model in which Enigma acts as a scaffold to bring Smurf1 and its substrate Rad into close proximity to promote Rad ubiquitination and turnover (**Figure 3.9A**). According to this model, deletion of Enigma would result in less efficient ubiquitination of Rad by Smurf1 (**Figure 3.9B**), and resting Rad levels would therefore increase as we observed in **Figure 3.3** due to a loss of cellular proteostatic control. While the observation that Enigma overexpression rescued the BMP-mediated decline in Rad levels (**Figure 3.8A**) seems at the surface to be at odds with such a model, this finding could also be explained if Enigma is required to scaffold Rad and Smurf1. Overexpression of the scaffold may result in cases where Rad is sequestered away from limiting amounts of endogenous Smurf1; thus, paradoxically Enigma overexpression would result in Rad protection from Smurf1-dependent turnover (**Figure 3.9C**). We acknowledge that further studies are necessary to confirm our proposed model, some of which will be described in the following paragraphs.

First, the co-immunoprecipitation analyses in **Figure 3.1** indicate that RGK proteins associate with Enigma, but we cannot conclude whether this interaction is direct or indirect. Binding studies using purified recombinant proteins are

required to probe for direct binding of Rad to Enigma. If the interaction is direct, identification of a minimal domain or region of Enigma necessary for Rad binding, beyond the preliminary analysis performed in **Figure 3.2**, would be useful to test the requirement of Enigma binding for Rad turnover. The Smurf1 overexpression studies in HEK293 cells in **Figures 3.4** and **3.6** indicate that Rad is subject to ubiquitination at Lys204 and proteasome-dependent turnover, but the role of Enigma in this process requires further investigation that would be assisted by such additional insights into the Rad-Enigma interaction. For instance, overexpression of the minimal domain of Enigma required for Rad binding would likely out-compete Rad binding to endogenous, full-length Enigma scaffolds and would thus be expected to block Smurf1-mediated Rad turnover if Enigma scaffolding is indeed a requirement. Enigma knock down or overexpression of an Enigma construct lacking the Rad-binding region would be expected to have the same effect. The regions of Enigma and Smurf1 required for their binding interaction have been modeled [188] and could be exploited in a similar manner. The nature of the ubiquitin linkage on Rad also warrants further investigation.

Moreover, while the data in **Figure 3.3** indicating a significant increase in Rad protein, but not mRNA, levels in Enigma$^{-/-}$ hearts is consistent with the model presented above, the requirement for Smurf1 and for proteasomal turnover in general has not directly been tested. Primary calvarial osteoblasts present a cell system that expresses endogenous Rad and can be manipulated more readily than cardiac myocytes. Rad levels should be probed in WT and Enigma$^{-/-}$ calvarial osteoblast cultures to determine whether the increase in Rad levels is

also observed in this cell type. If so, overexpression of Enigma and Smurf1 may be expected to rescue this phenotype, and a pulse-chase experiment could be utilized to examine Rad turnover in these cells. To confirm that the increase in Rad protein in Enigma$^{-/-}$ cells is indeed the result of hampered protein turnover, primary calvarial osteoblasts from WT and Enigma$^{-/-}$ mice could be treated with vehicle or MG-132 prior to probing Rad protein levels by Western blotting. If the increase in Rad levels in cells lacking Enigma is due to a decrease in proteasomal degradation of Rad protein, then we would expect a more robust elevation in Rad levels in WT cells following proteasomal inhibition than in Enigma$^{-/-}$ cells. Finally, probing Rad levels in tissues from Smurf1$^{-/-}$ mice would be expected to show a significant increase in Rad protein, but not mRNA levels.

Furthermore, the observation that prolonged BMP-2 signaling results in decreased Rad levels in **Figure 3.8** requires further studies to confirm the role of Smurf1 in this process. To test for a direct role of Smurf1 in the down regulation of Rad, Smurf1 knock down could be performed in HEK293 cells or primary osteoblasts with the expectation that BMP treatment would no longer result in lower Rad or Smad1 expression. We observed that Enigma overexpression rescued the BMP-mediated decrease in Rad levels in HEK293 cells, but interpretation of this experiment is difficult as discussed previously. It would be worthwhile to ask whether Enigma knock down in HEK293 cells might also rescue Rad levels in the context of Smurf1 overexpression or BMP-2 treatment. In the same vein, BMP-2 treatment of WT calvarial osteoblasts in **Figure 3.8B** should be repeated in Enigma$^{-/-}$ osteoblasts with the expectation that BMP-2

would no longer promote a decrease in Rad levels, but perhaps that the decrease in Smad1 would be maintained since Enigma is not thought to associate with Smad proteins. To confirm that the BMP-2 mediated down regulation of Rad results from altered proteostatic control, HEK293 cells or primary osteoblasts should be treated with MG-132 in combination with BMP-2 to determine whether Rad levels are rescued, and analysis of Rad mRNA expression in BMP-treated cells should also be performed.

The potential significance of the interaction between Rad and Smad proteins identified in **Figure 3.7** is intriguing, especially in light of the recent reports of Rad binding to and regulating the DNA binding of other transcription factors [40, 41]. The observation that Rad associates with R-Smads but not with Smad4 suggests two potential models. First, Rad may associate with the R-Smad proteins in a manner that displaces Smad4, thereby inhibiting Smad dimerization and downstream transcriptional activation. Alternatively, Rad may associate with the R-Smad/Smad4 complex through a direct association with the R-Smad, but we could not identify an interaction between Rad and Smad4 because of limiting endogenous R-Smad levels. In this case, co-overexpression of the R-Smad (1 or 3) along with Rad and Smad4 would be expected to allow co-immunoprecipitation of Rad and Smad4 that was not observed in our studies. The potential impact of Rad on BMP/Smad signaling needs to be investigated further. Preliminary studies suggest no change in BMP-responsive luciferase activity in $Rad^{-/-}$ osteoblasts compared to WT, and both genotypes were comparably responsive to BMP-2 stimulation in this assay (data not shown). We

also fail to see a significant change in total Smad levels in $Rad^{-/-}$ hearts compared to WT (data not shown). Zhang and colleagues did, however, find an increase in Smad3 expression in cardiac myocytes after infection with Rad adenovirus, along with a trend towards increased transcription from a Smad reporter construct [41]. Hence, the significance of the Rad-Smad interaction remains unclear.

While the work presented in this chapter identifies Smurf1 as a novel regulator of Rad protein levels, Smurf1 may not be the only E3 ubiquitin ligase that regulates Rad stability. Enigma has also been shown to bind c-Cbl and MDM2 and to regulate their E3 ubiquitin ligase activities [185, 186]; thus, future studies investigating the ability of these E3 ligases to target Rad are worthwhile. Studies determining the specificity of the Enigma interaction and Smurf1 regulation to Rad are also of interest. Each of the RGK proteins co-immunoprecipitates with Enigma and is down regulated by Smurf1 (**Figures 3.1** and **3.5**), but it remains unclear whether each of the RGKs binds to Enigma with the same affinity. To date Rad is the only RGK protein for which ubiquitin modification has been identified, but further studies are necessary to determine whether modulation of the other RGK proteins by Smurf1 is ubiquitin-dependent and which lysine residue(s) are required. It is also unclear whether interactions with Enigma have additional functions beyond scaffolding RGKs to an E3 ubiquitin ligase enzyme. The reason for the specificity of RGKs for Enigma, and not the other PDZ-LIM family scaffolds that were investigated, also requires further assessment.

In the next chapter, we will also see that Enigma alters Rad phosphorylation status; hence, while we have uncovered a novel interaction between Rad and Enigma that likely plays an important regulatory role, there is much that remains to be determined.

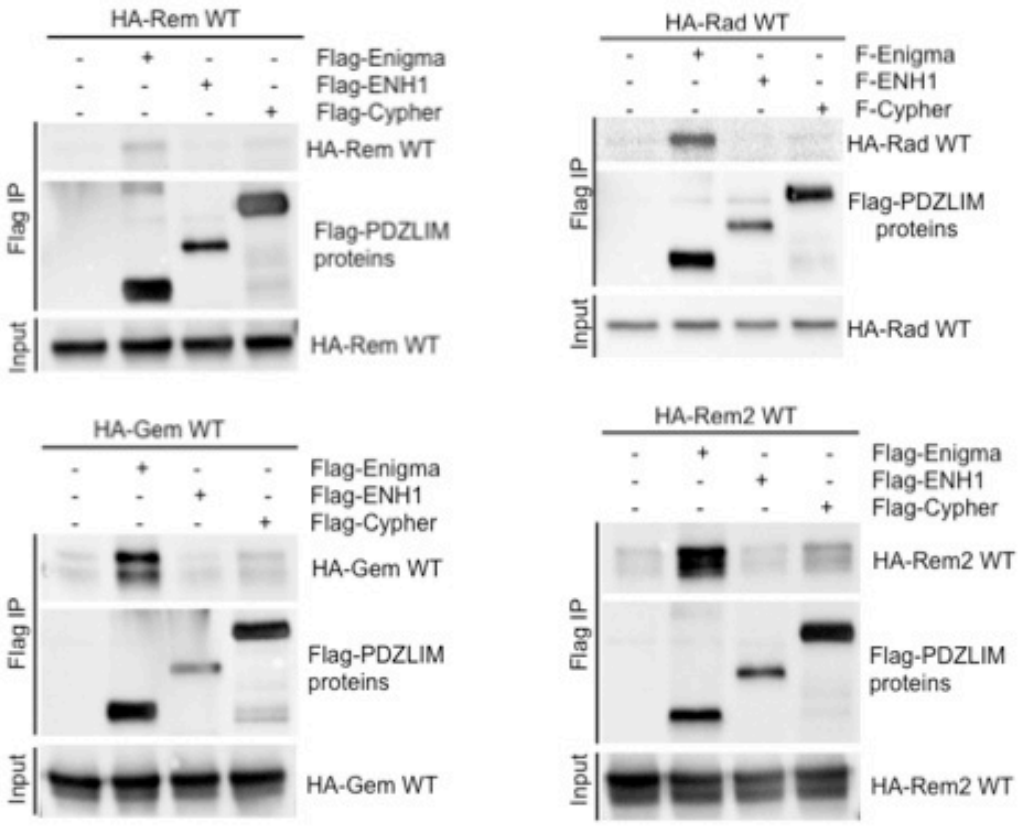

Figure 3.1: RGK subfamily proteins co-immunoprecipitate with Enigma

HEK293 cells were transfected with HA-tagged RGK proteins (Rem, Rad, Gem, or Rem2) and either Flag-tagged Enigma, ENH1, Cypher, or empty vector. Immunoprecipitation with anti-Flag antibody and Western blotting with biotinylated anti-HA antibody indicates that each of the RGK proteins interacts with Enigma, but not ENH1 or Cypher. Immunoprecipitates were probed with anti-Flag antibody to confirm expression and pull down of PDZ-LIM proteins, and whole lysates were probed with anti-HA antibody to confirm equal loading of HA-Rad. Results are representative of three independent experiments.

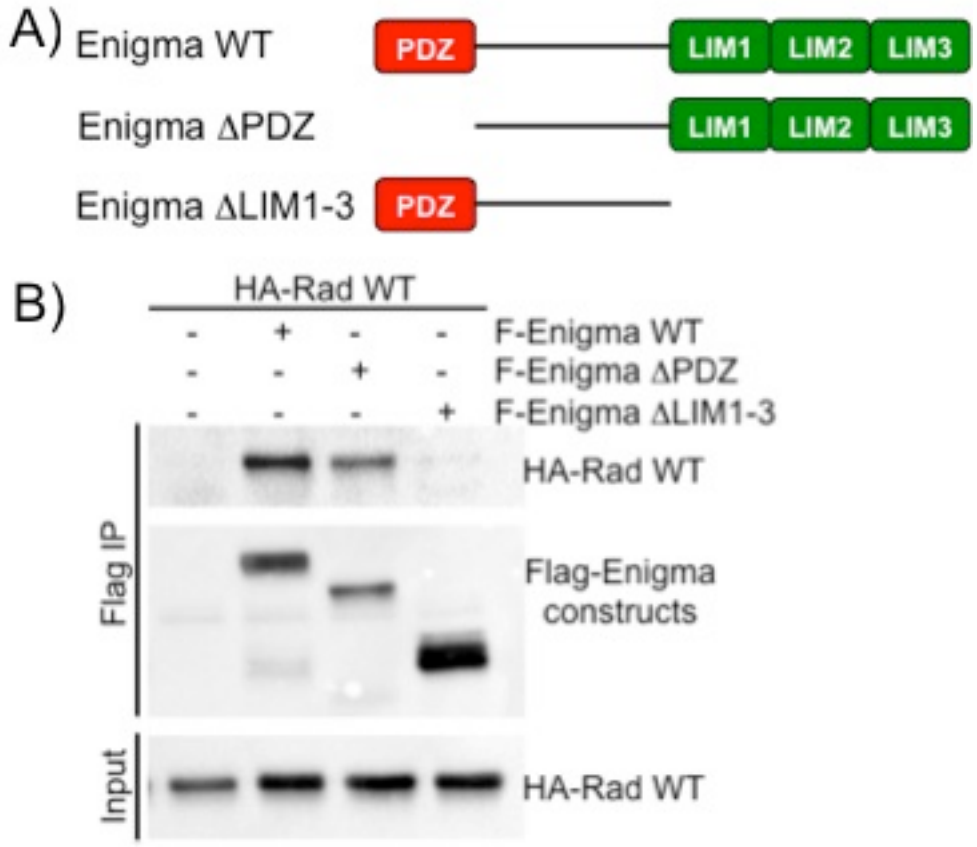

Figure 3.2: Rad interaction with Enigma is independent of the PDZ domain

Panel A) Schematic showing the domain structure of Enigma and of the truncation mutants generated for domain binding analysis.

Panel B) HA-Rad co-immunoprecipitates with Flag-Enigma WT and the ΔPDZ mutant but not with the ΔLIM1-3 mutant, suggesting that Rad may interact with Enigma through one or more of the LIM domains. Results are representative of three independent experiments.

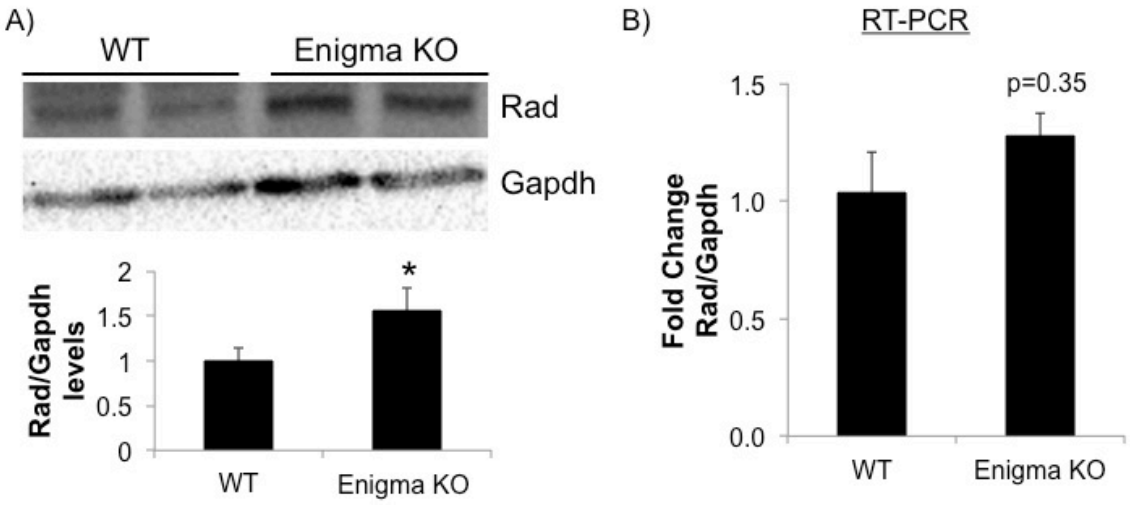

Figure 3.3: Rad protein levels are elevated in the hearts of Enigma$^{-/-}$ mice

Panel A) Rad protein levels normalized to Gapdh are higher in hearts from 4-week-old male Enigma$^{-/-}$ mice compared to WT littermate controls. N=4 mice per genotype, * $p<0.05$ by Student's *t* test.

Panel B) Rad mRNA levels normalized to Gapdh are not significantly different in hearts from 4-week-old male Enigma$^{-/-}$ mice compared to WT littermate controls. N=3 mice per genotype.

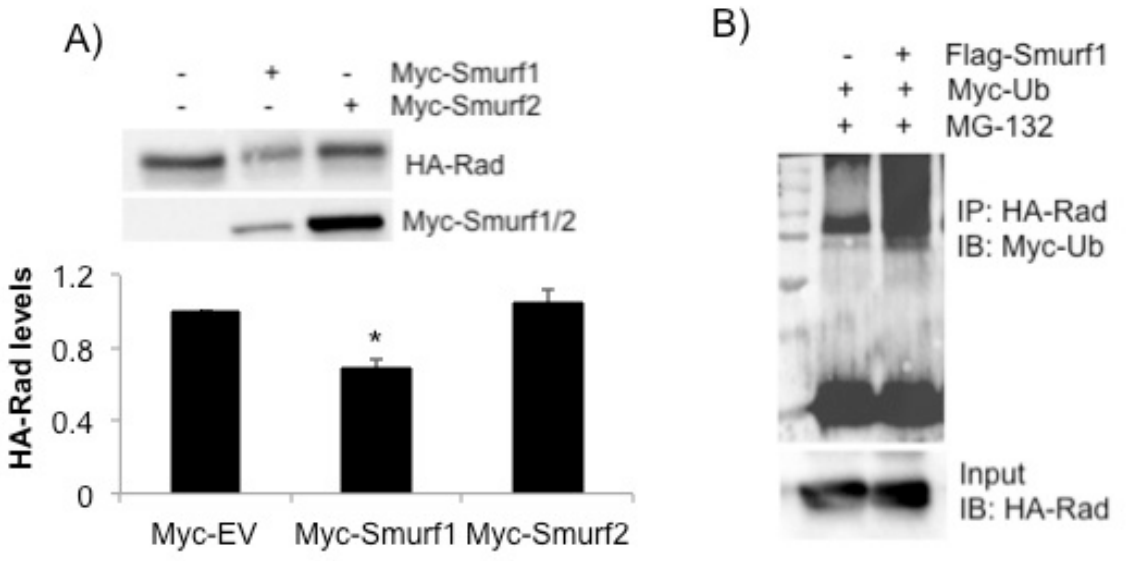

Figure 3.4: Smurf1 overexpression results in Rad ubiquitination and turnover

Panel A) HEK293 cells were transfected with HA-tagged Rad and Myc-tagged EV, Smurf1, or Smurf2. Overexpression of Smurf1, but not Smurf2, in HEK293 cells results in a significant decrease in HA-Rad levels. * $p<0.05$ compared to Myc-EV by Student's *t* test.

Panel B) HEK293 cells were transfected with HA-tagged Rad, Flag-tagged EV or Smurf1, and Myc-tagged ubiquitin. Treatment of HEK293 cells with 10 μm MG-132 for 16 hours prior to lysis protects Rad from Smurf1-mediated down-regulation. Immunoprecipitation of HA-Rad WT and immunoblotting with anti-Myc antibody demonstrates ubiquitination of Rad protein when Smurf1 is overexpressed.

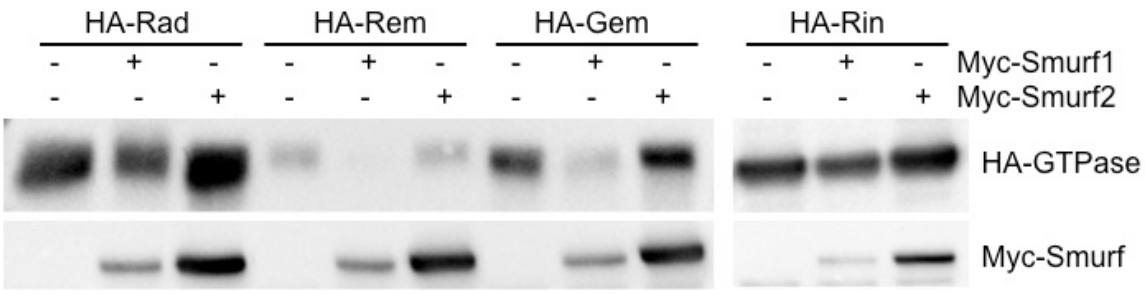

Figure 3.5: **Smurf1 overexpression results in lower levels of RGK proteins**

Overexpression of Myc-Smurf1, but not Smurf2, in HEK293 cells results in a decrease in the levels of other HA-tagged RGK proteins, Rem and Gem, in addition to Rad. Another small GTPase, Rin, was used as a negative control and does not appear to be modulated by Smurf1 overexpression.

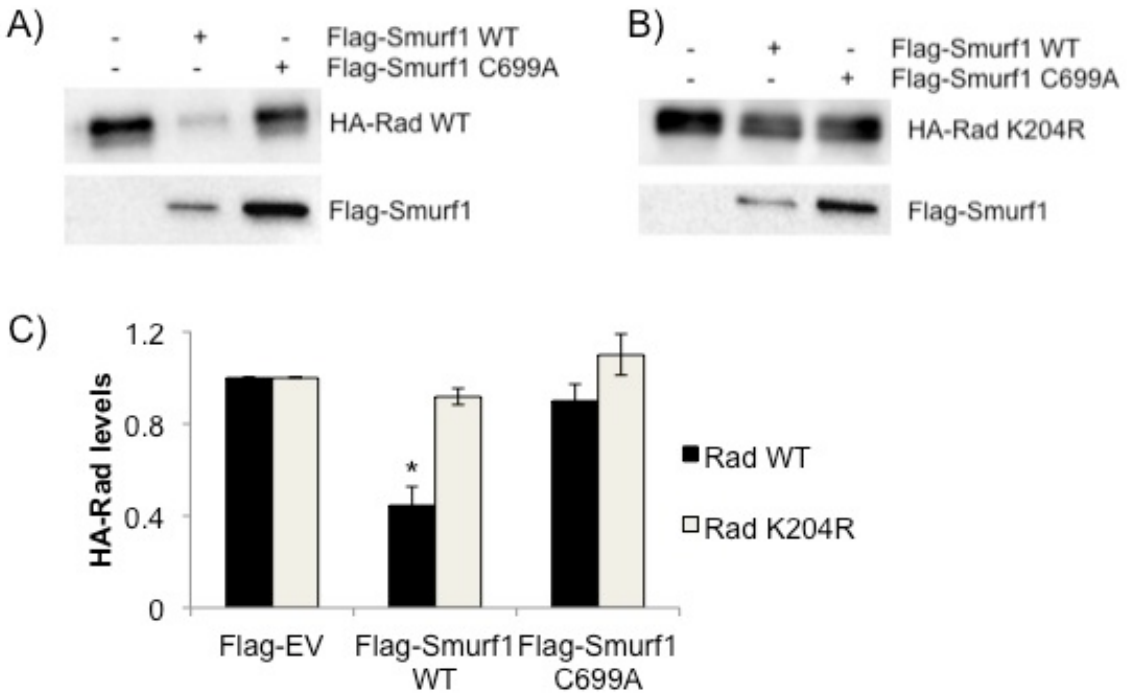

Figure 3.6: Smurf1-mediated Rad turnover requires Lys204

Panel A) Overexpression of Flag-Smurf1 WT, but not the catalytically inactive mutant C699A, results in a decrease in Rad protein levels.

Panel B) Mutation of the proposed ubiquitination site Lys204 to arginine results in protection of Rad from Smurf1-mediated turnover.

Panel C) Quantitation of the results of three independent experiments. * $p<0.05$ compared to Flag-EV by Student's *t* test.

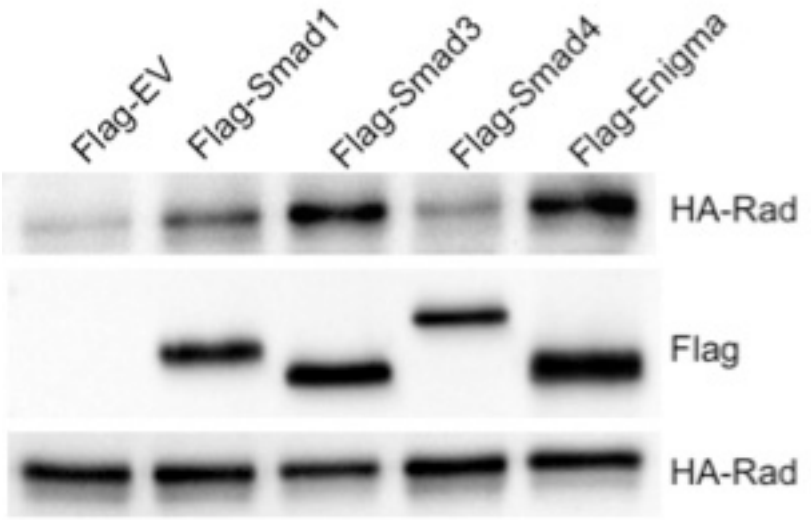

Figure 3.7: Rad co-immunoprecipitates with Smad1 and Smad3

HEK293 cells were transfected with HA-tagged Rad WT and Flag-tagged empty vector, Smad1, Smad3, Smad4, or Enigma (positive control). Co-immunoprecipitation analysis indicated that Rad associates with the receptor-associated Smads (Smad1 and 3), but not the co-Smad4 protein.

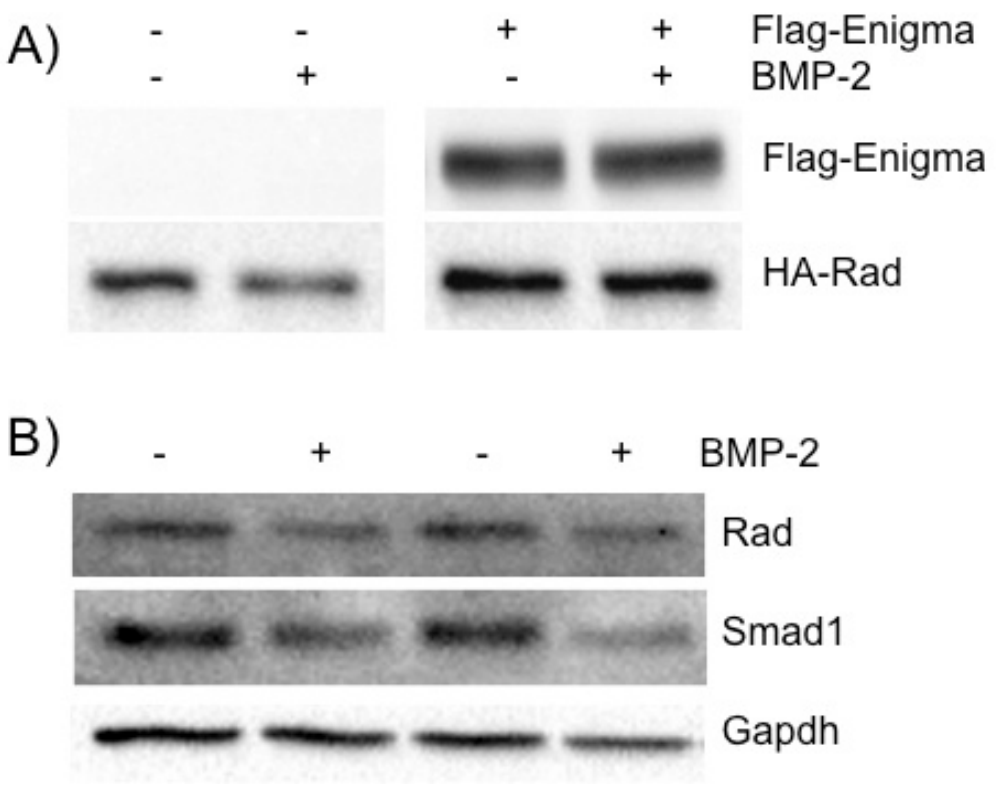

Figure 3.8: Bone morphogenetic protein stimulation results in decreased Rad levels

Panel A) HEK293 cells were transfected with HA-tagged Rad WT and Flag-tagged empty vector (left) or Enigma (right). Cells were serum-starved prior to stimulation with 100 ng/mL BMP-2 for one hour. BMP-2 treatment resulted in a decrease in Rad levels that was rescued when Enigma was overexpressed.

Panel B) Primary mouse calvarial osteoblasts were stimulated with 100 ng/mL BMP-2 or vehicle for one week, refreshing media every other day prior to harvest. Western blotting analysis indicated that Rad and Smad1 levels are decreased after prolonged BMP-2 stimulation. Results of two independent isolations are shown.

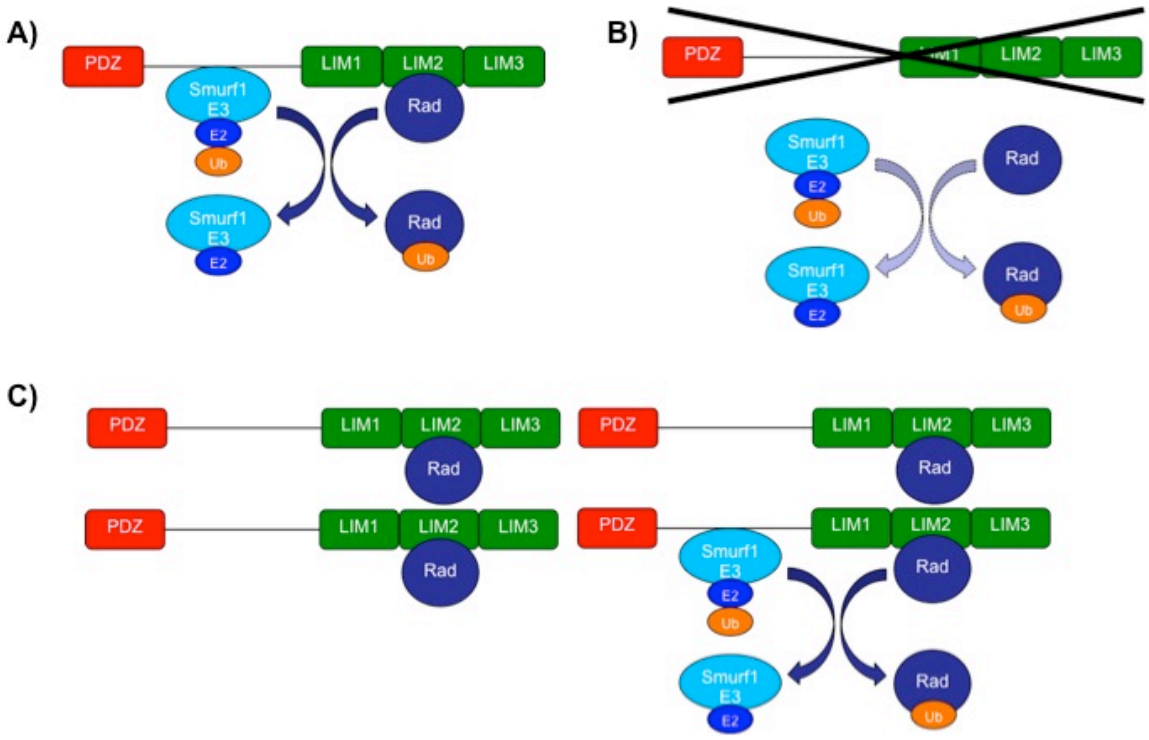

Figure 3.9: Proposed model in which Enigma serves as a scaffold for Smurf1 and Rad GTPase

Panel A) Proposed model in which Enigma serves as a scaffold to facilitate Smurf1-mediated Rad ubiquitination and turnover

Panel B) This model would suggest that Enigma deletion would result in uncoupling of Smurf1 and Rad, and thus less efficient Rad ubiquitination.

Panel C) This model may also suggest that Enigma overexpression may sequester overexpressed Rad away from limiting amounts of endogenous Smurf1, thus resulting in less efficient Rad ubiquitination and turnover.

Chapter 4

Regulation of Rad phosphorylation by β-adrenergic signaling

Introduction

RGK (Rad, Rem, Rem2, and Gem/Kir) proteins, and Rad in particular, have established roles in voltage-dependent calcium channel (VDCC) control [11, 12], cytoskeletal remodeling [19], cardiac contractility [104, 136], and more recently, tumorigenesis [24-28, 30, 32, 34, 38, 39] and stem cell differentiation [44, 45]. As detailed in Chapter 3, an outstanding issue in the RGK field that is central to this thesis is how these proteins are regulated, since evidence for nucleotide-dependent control is lacking [11]. In addition to regulation at the level of expression, whether by transcriptional or post-transcriptional mechanisms explored in Chapter 3, phosphorylation also represents a novel means of regulation for RGK subfamily G-proteins [49, 64, 98, 116, 118, 121]. Early *in vitro* studies revealed that Rad protein is phosphorylated at multiple serine (Ser) residues by a variety of kinases including protein kinase A (PKA), protein kinase C (PKC), calmodulin-dependent protein kinase II (CaMKII), and casein kinase II [49]. Previous studies in our laboratory and others have shown that RGK proteins are subject to phosphorylation-dependent 14-3-3 binding [109, 113, 118], and studies across the RGK family indicate that phosphorylation can regulate the subcellular localization [16, 109, 113] and the biological functions of

these proteins [64, 98, 121]. Some issues that remain unclear, however, are the nature of the upstream pathways that mediate RGK phosphorylation and the interplay of complex phosphorylation at multiple residues in RGK proteins, some of which are conserved across the family and others of which are unique.

The only report to date of RGK phosphorylation impacting VDCC regulation is the recent finding that Rem phosphorylation at Ser18 by protein kinase D1 (PKD1) in the α_1-adrenergic signaling cascade inhibited Rem-mediated blockade of calcium channel current [64]. The α_1-adrenergic receptor is a G-protein coupled receptor (GPCR) that signals through G_q to activate phospholipase C, which cleaves phosphatidyl inositol 4,5-bisphosphate (PIP_2) lipids to generate the second messenger molecules inositol 1,4,5-trisphosphate (IP_3) and diacylglycerol (DAG) [195]. IP_3 binds to receptors on the endoplasmic reticulum to induce intracellular calcium release, while DAG activates PKC, PKD1, and downstream signaling [195]. In addition to activation of the α_1-adrenergic receptor with phenylephrine, PKC can be activated downstream using phorbol esters such as phorbol 12-myristate 13-acetate (PMA). Jhun and colleagues showed convincingly that activation of this pathway, and specifically of PKD1, resulted in Rem phosphorylation and reversal of Rem-mediated calcium channel inhibition, while the Rem S18A point mutant was resistant to these treatments [64]. Notably, phosphorylated Ser18 is the N-terminal binding site for 14-3-3 within Rem [118]; however, the contribution of 14-3-3 binding to the reversal of channel block with Rem Ser18 phosphorylation is unclear.

While a role for Rem Ser18 phosphorylation in VDCC regulation has been documented [64], the impact of phosphorylation on the VDCC regulatory function of other RGK proteins remains to be tested. Notably, the N-terminal extensions of RGK proteins are not well conserved across the family (see **Figure 1.1**), and we hypothesized that different kinase cascades could be involved in the regulation of distinct RGK proteins. In this vein, intersections between Rad and the β-adrenergic signaling pathway have been reported in the literature [86, 104, 131]. Briefly, β-adrenergic receptors are also GPCRs, but they signal through G_s to activate adenylyl cyclase, which converts adenosine triphosphate (ATP) to cyclic adenosine monophosphate (cAMP) to activate PKA and downstream signaling [196]. Experimentally, activation of the β-adrenergic receptor can be achieved using isoproterenol (ISO), and stimulation of cells with forskolin serves to activate adenylyl cyclase and PKA downstream of the receptor. The first connection between Rad and β-adrenergic signaling in the literature was a report that overexpression of Rad in cardiac myocytes rendered the cells unresponsive to β-adrenergic stimulation of the calcium channel, as treatment with the general β-adrenergic agonist isoproterenol failed to elicit an increase in calcium current or calcium transients [86]. Additionally, we have reported that $Rad^{-/-}$ cardiac myocytes and whole hearts exhibit a phenotype that mirrors constitutive β–adrenergic activation [104, 131].

Interestingly, β-adrenergic agonism is known to result in phosphorylation of the L-type calcium channel complex as well as an increase in calcium current (I_{Ca}) in

cardiac myocytes [197, 198] . Traditionally, these two downstream events were thought to be linked; that is, phosphorylation of the calcium channel $Ca_V1.2$ and $Ca_V\beta2a$ subunits was thought to induce a conformational change that allowed for an increase in calcium current. Notably, however, a number of recent studies have indicated that the mechanism underlying the β-adrenergic increase in I_{Ca} may not be this simple [199-201]. Ser1928 phosphorylation within the C-terminus of $Ca_V1.2$ was the main event thought to afford increased I_{Ca} following β-adrenergic stimulation, and this residue was also the first to be excluded, as calcium current in cardiac myocytes from $Ca_V1.2$ S1928A mutant mice retained responsiveness to β-adrenergic stimulation [199]. Ganesan et al. demonstrated that the C-terminus of $Ca_V1.2$, but not Ser1928, was necessary for β-adrenergic stimulation of the channel [200]; this observation is intriguing, as RGK proteins associate with the C-terminus of $Ca_V1.2$ [107]. Subsequently, deletion of the C-terminal phosphorylation sites in the $Ca_V\beta2a$ subunit and mutations of the phosphorylation sites Ser1512 and Ser1570 in $Ca_V1.2$ did not abolish responsiveness to β-adrenergic stimulation [201]. These findings called into question the basic mechanism for elevated calcium current downstream of β-adrenergic receptor activation. This new uncertainty in the mechanism for β-adrenergic increases in I_{Ca}, coupled with the $Rad^{-/-}$ phenotype of tonic β-adrenergic drive in the absence of stimulus, led to an intriguing but provocative model in which Rad may function as a brake on a subset of calcium channels that can be reversed following β–adrenergic stimulation through Rad

phosphorylation to allow an acute rise in I_{Ca}. In other words, Rad phosphorylation would be equivalent to loss of Rad function with respect to calcium current.

The physiological significance of Rad phosphorylation and the stimuli mediating phosphorylation of N-terminal serine residues in Rad have not been studied. In this chapter, the role of Rad phosphorylation at Ser39, the N-terminal 14-3-3 binding site, will be interrogated. Specifically, the hypothesis that β–adrenergic signaling promotes Rad phosphorylation and subsequent reversal of calcium channel inhibition will be tested. While the data presented here are still preliminary, I have included them in this dissertation in order to document the progress we have made so far in understanding the regulatory role of Rad Ser39 phosphorylation as well as to highlight areas for future study.

Results

Generation of an antibody to detect Rad phosphorylation at Ser39

In order to characterize the stimuli that may induce Rad phosphorylation, an antibody was raised against a peptide corresponding to Rad phosphorylated at Ser39. This residue is equivalent to Rem Ser18 in terms of 14-3-3 binding [118]. The Rad anti-phospho-Ser39 (Rad pSer39) antibody was tested to confirm its specificity for phosphorylated Ser39 relative to other serine residues in the Rad protein, as well as its specificity for Rad relative to other RGK subfamily proteins (**Figure 4.1**). Western blotting analysis indicates that the antibody recognizes Rad phosphorylated at Ser39, as the S39A phosphorylation deficient mutation

was not recognized (**Figure 4.1**). Mutation of Ser272 and Ser301 to alanine also reduced immunoreactivity with the Rad pSer39 antibody (**Figure 4.1**), suggesting the possibility of Ser272 and/or Ser301 phosphorylation cross-reactivity, or perhaps of coordinated phosphorylation of these more C-terminal residues and Ser39. The latter is almost certainly true in the case of Ser301, as 14-3-3 dimers bind to phosphorylated Ser39 and Ser301 in Rad protein; hence, Rad S301A has diminished binding to 14-3-3, rendering Rad phosphorylation at Ser39 less protected from phosphatase activity in the S301A mutant compared to wildtype Rad. The Rad pSer39 antibody was specific to Rad, as it did not detect Rem, the long isoform of Rem2 (Rem2L), or Gem (**Figure 4.1**). Finally, this analysis suggested that under conditions of serum starvation, there remains a basal level of Rad Ser39 phosphorylation in HEK293 cells (**Figure 4.1**).

β-adrenergic stimulation results in phosphorylation of Rad

The Rad pSer39 antibody was next used to examine the stimuli capable of regulating Rad phosphorylation. HEK293 cells were transfected with HA-tagged Rad WT and serum starved prior to stimulation with various agonists. As seen in **Figure 4.1**, treatment with isoproterenol, a β-adrenergic agonist, appears to increase Rad Ser39 phosphorylation in HEK293 cells. Activation of the α-adrenergic kinase PKC using the phorbol ester PMA failed to induce phosphorylation of Rad (**Figure 4.2**) at concentrations that successfully resulted in Rem phosphorylation in prior studies in our laboratory (data not shown). Notably, robust and time-dependent phosphorylation of Rad at Ser39 in HEK293

cells was observed following treatment with forskolin (**Figure 4.2**), which activates adenylyl cyclase downstream of the β-adrenergic receptor and thereby increases intracellular cAMP levels and triggers PKA activation. Preliminary studies suggest that these effects of isoproterenol and forskolin are also observed in cardiac myocytes, as stimulation of wildtype fetal ventricular myocytes with either of these agonists induced a robust increase in Rad Ser39 phosphorylation (**Figure 4.3**). This experiment needs to be repeated with better quality total Rad immunoblotting as well as with a loading control so that quantification and statistical analysis can be performed. Furthermore, preliminary studies suggest that Rad Ser39 phosphorylation is also elevated in hypertensive human hearts (**Figure 4.4**), a condition associated with up regulation of β-adrenergic signaling, but we acknowledge the need for a loading control in these studies. Together, these data suggest that Rad Ser39 phosphorylation may be accomplished downstream of the β- rather than α-adrenergic signaling pathway.

Rad phosphorylation at Ser39 may weaken its association with $Ca_V\beta$2a

The impact of Rad phosphorylation at Ser39 on its interaction with the $Ca_V\beta$2a subunit of the L-type calcium channel complex was next assessed by a series of co-immunoprecipitation experiments. First, Rad Ser39 was mutated to alanine (S39A) so that this residue could not be phosphorylated or to aspartate (S39D) to mimic the size and charge of a phosphorylated serine at this position using site directed mutagenesis. The S39A mutation thus results in a phosphodeficient Rad protein with a reduced ability to bind 14-3-3 dimers [16], while the S39D mutation

generates a phosphomimetic protein that we hypothesized might display stimulus-independent 14-3-3 association. HEK293 cells were co-transfected with HA-tagged Rad WT, S39A, or S39D and Flag-tagged $Ca_V\beta 2a$ or empty vector as a control. Cell lysates were subjected to Flag immunoprecipitation, and co-immunoprecipitated HA-tagged Rad proteins were detected by Western blotting. Mutation of Ser39 to alanine had no effect on Rad binding to the $Ca_V\beta 2a$ subunit of the calcium channel; however, the phosphomimetic S39D mutation resulted in a reduction in $Ca_V\beta 2a$ association by ~50% (**Figure 4.5**), suggesting that phosphorylation of this residue may promote dissociation of Rad from the calcium channel complex, perhaps due to enhanced 14-3-3 binding.

To probe the role of phosphorylation in regulation of the Rad-$Ca_V\beta$ association further, co-immunoprecipitation of Rad and $Ca_V\beta 2a$ was assessed in the presence and absence of phosphatase inhibitor in the cell lysis buffer. The lysis buffer used in the co-immunoprecipitations in **Figure 4.5** lacked both EGTA, which chelates calcium ions, and β-glycerophosphate, a phosphatase inhibitor. In preliminary experiments, addition of EGTA to the lysis buffer had no effect on the Rad-$Ca_V\beta 2a$ association; however, phosphatase inhibition using β-glycerophosphate appears to reduce Rad association with $Ca_V\beta 2a$ (**Figure 4.6**), further suggesting that Rad phosphorylation may reduce its association with the calcium channel complex either directly or through displacement by 14-3-3 binding.

To probe for a role of PKA in modulating the interaction between Rad and $Ca_V\beta 2a$, HEK293 cells were pre-treated with H-89 to block PKA activity prior to and during transfection with HA-tagged Rad WT and Flag-tagged $Ca_V\beta 2a$ or empty vector. In the setting of PKA inhibition, which decreases Rad phosphorylation, Rad association with $Ca_V\beta 2a$ is enhanced (**Figure 4.7**). Taken together, the three different co-immunoprecipitation based experiments shown here suggest that Rad phosphorylation at Ser39 may be inversely related to its relative association with $Ca_V\beta 2a$ and that further studies are warranted to confirm this notion.

Rad phosphorylation at Ser39 promotes 14-3-3 association

The impact of Rad phosphorylation at Ser39 on 14-3-3 association was also probed by co-immunoprecipitation. First, HEK293 cells were transfected with HA-tagged Rad WT, S39A, S39D, or empty vector as a control along with GST-tagged 14-3-3. Cell lysates were subjected to immunoprecipitation with anti-HA antibody, and co-immunoprecipitated GST-14-3-3 was detected by Western blotting. Mutation of Ser39 to alanine a in a reduction in Rad association with 14-3-3 as has been reported [16], while the S39D mutant associated with 14-3-3 more strongly than WT (**Figure 4.8**). Similarly, stimulation of the cells with forskolin prior to harvest and immunoprecipitation resulted in an increase in Rad WT association with 14-3-3 but had no effect on S39A or S39D association with 14-3-3 (**Figure 4.8**), representing the first report of RGK association with 14-3-3 in response to a stimulus. These results suggest that Rad Ser39 phosphorylation

promotes 14-3-3 association. Coupled with the observation that phosphorylated Rad seems to have a reduced interaction with $Ca_V\beta 2a$ (**Figures 4.5**, **4.6**, and **4.7**) suggests a potential mechanism in which 14-3-3 binding may displace phosphorylated Rad from the calcium channel complex.

Enigma overexpression promotes Rad Ser39 phosphorylation

Given the established association between Rad and Enigma (see Chapter 3) and a literature indicating that Enigma and related proteins bind to a variety of kinases through their C-terminal LIM domains [172, 176-179], I next asked whether Enigma might modulate Rad phosphorylation. Interestingly, overexpression of Enigma alone was sufficient to increase Rad Ser39 phosphorylation without any additional stimulus (**Figure 4.9**). In fact, Enigma overexpression resulted in Rad Ser39 phosphorylation nearly as robust as that observed following stimulation with isoproterenol, a β-adrenergic receptor agonist (**Figure 4.9**).

Enigma associates with $Ca_V1.2$

The Enigma subfamily proteins Enigma homolog protein (ENH) and Cypher have been reported to bind to and regulate voltage-dependent calcium channels [176-179], but the potential interaction between Enigma and $Ca_V1.2$ has not been previously examined. HEK293 cells were transfected with an HA-tagged $Ca_V1.2$ C-terminal construct comprising amino acids 1507-2171 along with Flag-tagged EV or Enigma. Co-immunoprecipitation analysis revealed a novel interaction

between Enigma and the $Ca_V1.2$ C-terminus (**Figure 4.10A**). Further investigation of the Enigma-$Ca_V1.2$ association by co-immunoprecipitation narrowed down the region of $Ca_V1.2$ required for Enigma binding to amino acids 1507-1906 and suggested that the PDZ domain of Enigma is not required for the interaction with $Ca_V1.2$ (**Figure 4.10B**). Thus, Enigma, like ENH and Cypher, associates with the calcium channel $Ca_V\alpha1$ subunit, and we hypothesized that Enigma may therefore contribute to the regulation of Rad-mediated VDCC control.

Enigma overexpression does not alleviate Rad-mediated calcium channel inhibition

Since Rem phosphorylation at Ser18 was reported to reverse its calcium channel inhibitory activity [64], Enigma overexpression was used as a means of enhancing Rad Ser39 phosphorylation (**Figure 4.9**) to ask whether Rad-mediated calcium current blockade may be altered by increased Rad Ser39 phosphorylation. To this end, HEK293 cells were transfected with GFP-tagged $Ca_V1.2$ (calcium channel α subunit), a dual expression vector for RFP and $Ca_V\beta2a$ (allowing transfected cells to be readily identified), and either HA- and Flag-tagged empty vectors as a control to establish basal calcium current, HA-tagged wildtype Rad and empty vector to reproduce published work that Rad overexpression blocks calcium current [12], or HA-Rad WT and Flag-Enigma to ask whether Enigma overexpression and increased Rad Ser39 phosphorylation would alter Rad-dependent current block. While Rad overexpression resulted in

a complete block of calcium current, co-overexpression of Enigma failed to reverse channel inhibition (**Figure 4.11**) despite the observed increase in Rad Ser39 phosphorylation. Thus, further studies of the role of Enigma in the regulation of Rad-mediated VDCC control, as well as more direct analysis of the impact of Rad phosphorylation on VDCC regulation, are needed.

Discussion

In addition to their regulation through expression levels, RGK subfamily proteins have long been known to be subject to complex phosphorylation [49], and more recently Rem Ser18 phosphorylation was shown to regulate Rem-dependent calcium current blockade *in vitro* [64]. The idea that phosphorylation of RGK proteins could provide an acute increase in calcium current in response to an upstream stimulus is intriguing. Given the linkage between Rad and β-adrenergic signaling in the literature [86, 104, 131] and the absence of a mechanism to explain the acute rise in calcium current following β-adrenergic receptor stimulation [199-201], the studies in this chapter aimed to explore the contribution of the β–adrenergic signaling cascade to Rad phosphorylation at Ser39 as well as the significance of Rad phosphorylation to protein-protein interactions and calcium current regulation. While many of the results are still preliminary, the data in this chapter suggest that β-adrenergic agonism results in Rad Ser39 phosphorylation and that phosphorylation at this site promotes 14-3-3 binding while potentially weakening the association between Rad and the calcium channel $Ca_V\beta$2a subunit. We also find that Enigma overexpression promotes

Rad Ser39 phosphorylation but is not sufficient to alter Rad-mediated VDCC blockade; however, we do establish a novel interaction between Enigma and the $Ca_V1.2$ C-terminus that suggests that further study of the role of Enigma in the regulation of Rad and VDCCs is warranted.

While Rem is subject to phosphorylation downstream of α-adrenergic signaling and PKD1 activation [64], Rad phosphorylation is more robust following stimulation of the β-adrenergic receptor, likely via PKA-dependent signaling, as shown in **Figures 4.1-4.3**. This specificity of signaling is not surprising, as there is an overall lack of sequence conservation in the N-terminal regions of RGK subfamily GTPases where these serine residues are found that suggests differential kinase control. For instance, the PKD1 consensus motif (L-X-R-X-X-S*) [202] is present in the sequence preceding Rem Ser18 but is not found upstream of Rad Ser39, as the important -5 position leucine is instead located at the -4 position in the Rad sequence (**Figure 4.12**). Notably, this idea of differential regulation of RGK subfamily proteins may extend to Gem and Rem2 as well, as the degree of conservation in the sequences surrounding the N-terminal 14-3-3 binding sites of these two RGKs are even more divergent than Rem and Rad (**Figure 4.12**).

A series of co-immunoprecipitation experiments in **Figures 4.5**-**4.8** suggested that Rad Ser39 phosphorylation may disrupt the interaction between Rad and $Ca_V\beta2a$ while enhancing the interaction between Rad and 14-3-3. The model that logically extends from these data is that upon phosphorylation, 14-3-3

binding displaces Rad from $Ca_V\beta$2a and the calcium channel complex (**Figure 4.13**). Consistent with such a model, 14-3-3 binding has been reported to modulate the subcellular distribution of RGK proteins [16, 109, 113]. This notion is complicated, however, by the many functions of the C-terminus of RGK proteins. 14-3-3 dimers bind to N- and C-terminal phospho-serine residues in RGK proteins (Ser39 and Ser301 in Rad), and 14-3-3 binding to the phospho-Ser301 residue impedes importin binding and nuclear trafficking [116, 117]. 14-3-3 binding also interferes with PIP lipid binding and likely with plasma membrane targeting of RGKs as a result [106]. Hence, it is difficult to distinguish whether 14-3-3 binding might have a direct or indirect role.

In contrast to our proposed model, Jhun and colleagues suggested a different mechanism after demonstrating that Rem Ser18 phosphorylation reversed VDCC blockade. Jhun et al. instead proposed that overexpressed Rem binds to and sequesters VDCCs in the endoplasmic reticulum, with phosphorylation of Rem at Ser18 releasing VDCCs to traffic appropriately to the plasma membrane, thereby increasing calcium current [64]. This model set forth by Jhun et al., although untested, is reminiscent of reports in which RGK proteins inhibit calcium current by binding to and sequestering $Ca_V\beta$ subunits away from the $Ca_V\alpha$1 pore-forming subunit to interfere with trafficking of the channel complex to the plasma membrane [14, 16, 64, 90, 109]. In contrast to these reports, studies in our laboratory and others suggest that RGK proteins can act as inhibitors of calcium channels resident at the plasma membrane [12, 13, 15, 103, 106, 110, 111]. We have also shown that RGK proteins lacking the C-terminal region that directs

membrane association fail to block calcium current and that addition of a membrane-targeting sequence to truncated RGK proteins restores VDCC current inhibition [110]. Furthermore, the affinity of $Ca_V\beta$ subunits for $Ca_V1.2$ far exceeds that for RGK proteins [15], and the RGK and $Ca_V1.2$ binding sites on $Ca_V\beta$ are distinct [15]. Indeed, we have demonstrated that $Ca_V\beta2a$ can simultaneously associate with both $Ca_V1.2$ and RGK proteins [15]. Coalesced, these data oppose the idea that Rad blocks calcium current through sequestration of $Ca_V\beta$ and dysregulation of VDCC trafficking.

To test the model we propose in **Figure 4.13** and ask whether 14-3-3 binding is necessary for the decrease in association with $Ca_V\beta2a$ following phosphorylation of Rad, the co-immunoprecipitation experiments in this chapter could be repeated using the Rad S301A mutant that is null for 14-3-3 binding. In particular, a dual Rad S39D/S301A mutant could be probed for $Ca_V\beta2a$ association, with the expectation that the phosphomimetic mutation at Ser39 would no longer result in dissociation of Rad from $Ca_V\beta2a$ when combined with the S301A mutation if 14-3-3 binding is necessary to displace Rad from the calcium channel. Alternatively, this mutant would be indistinguishable from the Rad S39D single point mutant if, instead, Rad Ser39 phosphorylation disrupts association with $Ca_V\beta2a$ through a conformational change in Rad protein without the necessity of 14-3-3 binding.

The data in the previous chapter identified a novel interaction between Rad and Enigma that may modulate Rad ubiquitination and turnover, and in the present chapter the interaction with Enigma is also shown to enhance Rad phosphorylation (**Figure 4.9**). Enigma and the related proteins ENH and Cypher bind to a variety of kinases including PKA, PKC, and PKD1 [172, 176-179]; hence, it follows that Enigma could serve as a scaffold for kinase recruitment to promote Rad phosphorylation. Alternatively, we cannot exclude a model in which Enigma overexpression may result in more Rad phosphorylation at Ser39 through binding to and protecting this phosphorylated residue from phosphatase activity. This alternative model could be tested by asking whether Rad S39A associates with Enigma as well as wildtype Rad, with the expectation that this phosphorylation-deficient mutant would exhibit weaker association with Enigma if Enigma promotes Rad phosphorylation through protection of the phospho-serine residue. A second means of testing this alternative model could utilize phosphatase treatment to determine whether Enigma overexpression is indeed protective of Rad Ser39 phosphorylation. Finally, identification of the subdomain of Enigma required for interaction with Rad, as was proposed in Chapter 3, would allow us to determine whether the Rad-Enigma association is necessary for the increase in Rad phosphorylation that is observed. We could also then overexpress the minimal Rad binding region of Enigma to differentiate between the two models described above. Namely, if Enigma acts as a scaffold for Rad and its kinase, overexpression of the minimal Rad binding domain of Enigma should abolish the increase in phosphorylation observed with Enigma

overexpression. Conversely, if Enigma increases Rad phosphorylation via protection of this phospho-serine residue from phosphatase activity, then the minimal binding domain should still be effective in increasing Rad phosphorylation.

A novel interaction between Enigma and $Ca_V1.2$ is reported in **Figure 4.10**. The related PDZ/LIM proteins ENH1 and Cypher have been reported to bind to calcium channel $Ca_V\alpha1$ subunits, although there has been debate as to which domain of these proteins is required for calcium channel association, and the region of the $Ca_V\alpha1$ subunit that associates with these proteins has never been analyzed [176-179]. Here, Enigma is demonstrated to associate with the C-terminal region of $Ca_V1.2$, specifically the region between amino acids 1507-1906, in a PDZ-independent fashion. The association between Enigma and the calcium channel suggested that Enigma likely has a regulatory role in the function of Rad in VDCC control.

Having observed that Enigma overexpression promotes Rad Ser39 phosphorylation, Enigma overexpression was used as a “stimulus” to probe for the role of Rad phosphorylation on its ability to block calcium current. Unlike Rem Ser18 phosphorylation [64], inducing Rad Ser39 phosphorylation through Enigma overexpression had no effect on calcium current (**Figure 4.11**). On one level, these data suggest that Rad phosphorylation may not regulate its calcium channel inhibitory activity; however, there are caveats to such a conclusion. First, the electrophysiology experiment described here required transfection of four

plasmids: GFP-$Ca_V1.2$, RFP/$Ca_V\beta2a$, EV or Rad, and EV or Enigma. Since each recording represents an individual cell, this analysis assumed that each cell expressed all four plasmids. While selecting for GFP^+/RFP^+ cells ensured that every cell that was recorded should have contained a functional calcium channel complex, it cannot be known for certain that every cell expressed both Enigma and Rad, potentially confounding the results. To ask more directly whether Rad Ser39 phosphorylation modulates its calcium channel inhibition, further electrophysiology experiments should probe whether Rad S39D/E mutants are as effective as Rad WT at inhibiting calcium current. Similarly, stimulation with isoproterenol or forskolin or transfection of constitutively active PKA could provide additional means of testing this hypothesis. Second, it is possible that phosphorylation of Rad at a different residue, or at multiple residues, may afford regulation of calcium current. Rad is subject to complex phosphorylation at a number of sites including threonine-2 (Thr2), Ser26, Thr27, Ser39, Thr52, Ser79, Ser105, Ser214, Ser257, Ser273, Ser290, Ser299, and Ser301 [49, 203-209]; thus, interrogation of the role of phosphorylation of one residue in the regulation of Rad is likely a gross over-simplification of the potential for kinase regulation *in vivo*. While use of the RadpSer39 antibody suggested that β-adrenergic stimulation and Enigma overexpression promote Rad phosphorylation at Ser39, it is unclear whether these conditions alter phosphorylation of additional sites in the Rad protein. Moreover, Ser39 was chosen for analysis as the N-terminal 14-3-3 binding site within Rad and thus as the analogous residue to Rem Ser18 reported in the study by Jhun et al [64]. However, Jhun and colleagues only

speculated but did not establish that 14-3-3 binding was important for the modulation of Rem-mediated channel block following Ser18 phosphorylation [64]. While Rad Ser39 is analogous to Rem Ser18 with respect to 14-3-3 binding, an alignment of the amino acid sequences of Rem and Rad indicates that Rad Ser26 corresponds more directly to Rem Ser18. An alternative hypothesis, then, is that while β-adrenergic stimulation may regulate Rad Ser39 phosphorylation and 14-3-3 binding, Rad phosphorylation at Ser26 could afford regulation of calcium channel blockade in a manner similar to Rem Ser18 phosphorylation and in a manner that does not require 14-3-3 binding. In this case, the stimuli responsible for regulating Rad phosphorylation at Ser26, and potentially at other residues, would require further investigation. Electrophysiology experiments probing the ability of additional phosphomimetic Rad mutants to inhibit calcium current may provide further insight as well. Finally, the potent calcium channel blockade established upon Rad overexpression also makes this experiment difficult to interpret. It is plausible that even in a setting in which phosphorylated Rad is displaced from the calcium channel and no longer an effective inhibitor of current, the degree of Rad overexpression is sufficient that another Rad protein quickly takes its place and blocks calcium current.

In summary, the studies in this chapter provide preliminary evidence that β-adrenergic signaling may regulate Rad Ser39 phosphorylation and that this phosphorylation event may modulate Rad interactions with $Ca_V\beta 2a$ and 14-3-3. The experiments in this chapter should be repeated more rigorously to confirm these conclusions. The functional significance of Rad phosphorylation at Ser39

and other residues and the role of Rad in β-adrenergic signaling remain unclear and require further study. Data from our laboratory suggest that deletion of Rad in cardiac myocytes results in a phenotype that mirrors β-adrenergic agonism of the calcium channel in the absence of stimulus [104, 131]. Rad deletion also renders cardiac myocytes nearly insensitive to further β-adrenergic stimulation of the calcium channel [104], suggesting that Rad plays a functional role in this pathway. Although $Ca_V1.2$ and $Ca_V\beta2a$ are phosphorylated downstream of β-adrenergic activation, calcium channel phosphorylation appears to be dispensable for the increase in calcium current that is triggered through this pathway [199-201]; hence the potential role of Rad phosphorylation, re-localization, or turnover in response to β-adrenergic signaling remains a possible hypothesis for the increase in calcium current downstream of β-adrenergic signaling.

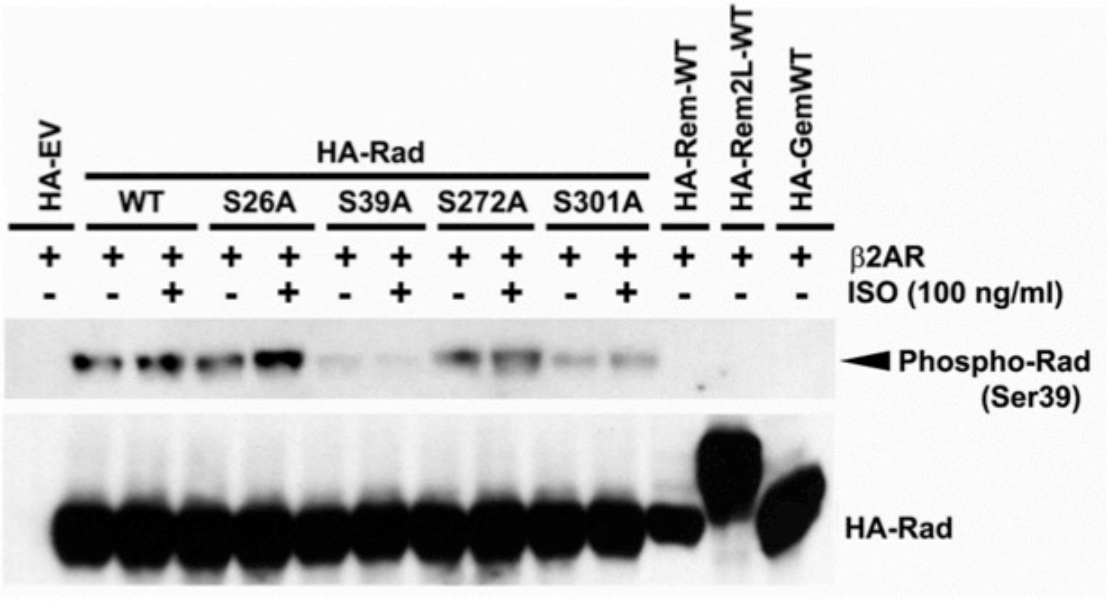

Figure 4.1: Rad phospho-Ser39 antibody validation

HEK293 cells were transfected with HA-tagged empty vector (EV) or Rad WT, S26A, S39A, S272A, or S301A mutants in order to validate the specificity of the rabbit antibody raised against Rad phospho-serine 39 in collaboration with 21st Century Bio. Cells were also transfected with the β2 adrenergic receptor (β2AR) and stimulated with isoproterenol (ISO, 100 ng/mL) as an agonist to promote Rad phosphorylation. In the last three lanes, HEK293 cells were transfected with HA-tagged Rem, Rem2L (long isoform), and Gem in order to validate that the antibody does not cross-react with other RGK subfamily proteins.

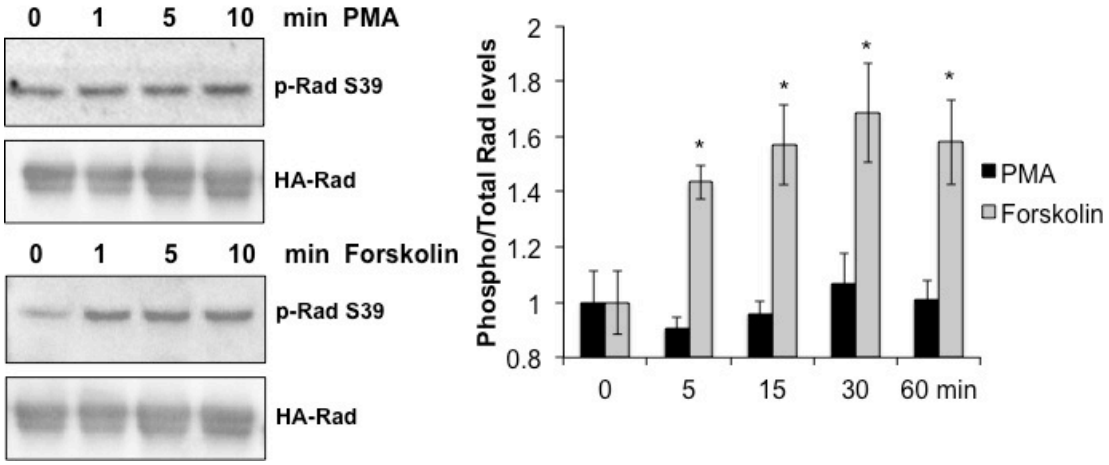

Figure 4.2: Forskolin treatment increases Rad Ser39 phosphorylation in HEK293 cells

HEK293 cells transfected with HA-tagged Rad were starved prior to stimulation with 1 μM phorbol 12-myristate 13-acetate (PMA) to activate PKC in the α-AR pathway or 1 μM forskolin to activate PKA in the β-AR pathway. Unlike Rem, Rad is phosphorylated downstream of PKA, not PKC. Results are representative of three independent experiments. * $p<0.05$ relative to unstimulated by Student's *t* test.

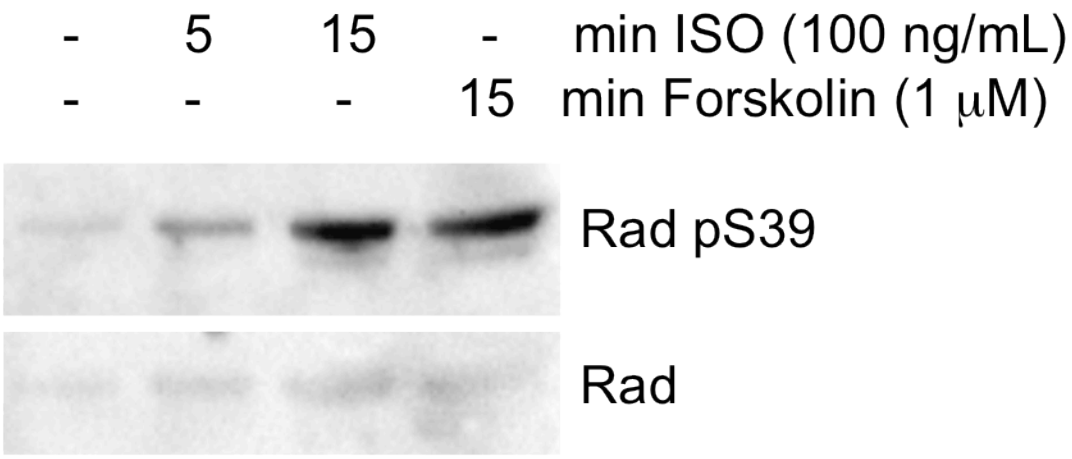

Figure 4.3: β-adrenergic stimulation of fetal ventricular cardiomyocytes induces Rad Ser39 phosphorylation

Ventricular cardiomyocytes were isolated from fetal wildtype mice at embryonic day 18 and stimulated with vehicle, isoproterenol (100 ng/mL), or forskolin (1 μM) for the indicated amounts of time. Western blotting analysis suggests that treatment with either of these activators of the β-adrenergic signaling cascades may result in an increase in Rad Ser39 phosphorylation.

.

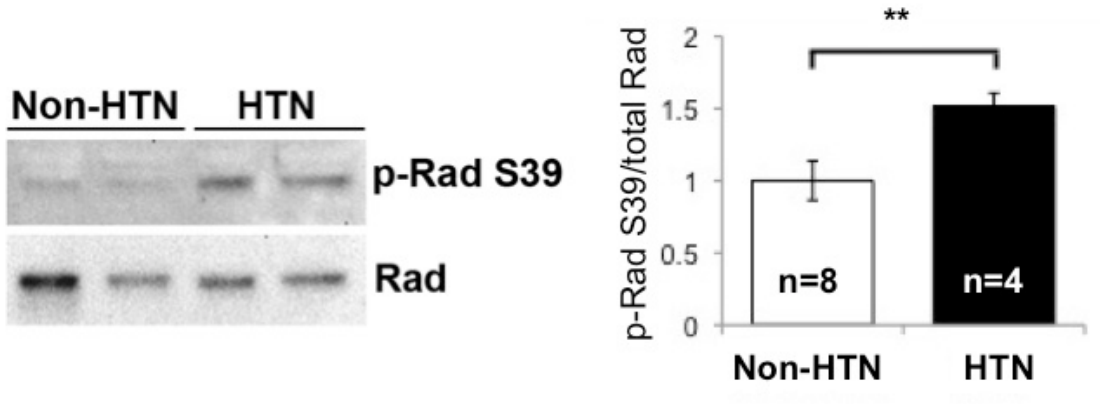

Figure 4.4: Rad Ser39 phosphorylation is elevated in human heart samples from patients with a history of hypertension

Human heart samples were homogenized, and Rad phosphorylation levels were assessed by Western blotting and normalized to total Rad levels. Samples from patients with a history of hypertension (HTN) exhibited significantly higher levels of Rad Ser39 phosphorylation/total Rad relative to non-hypertensive (non-HTN) controls. ** $p<0.01$ relative to non-HTN by Student's *t* test.

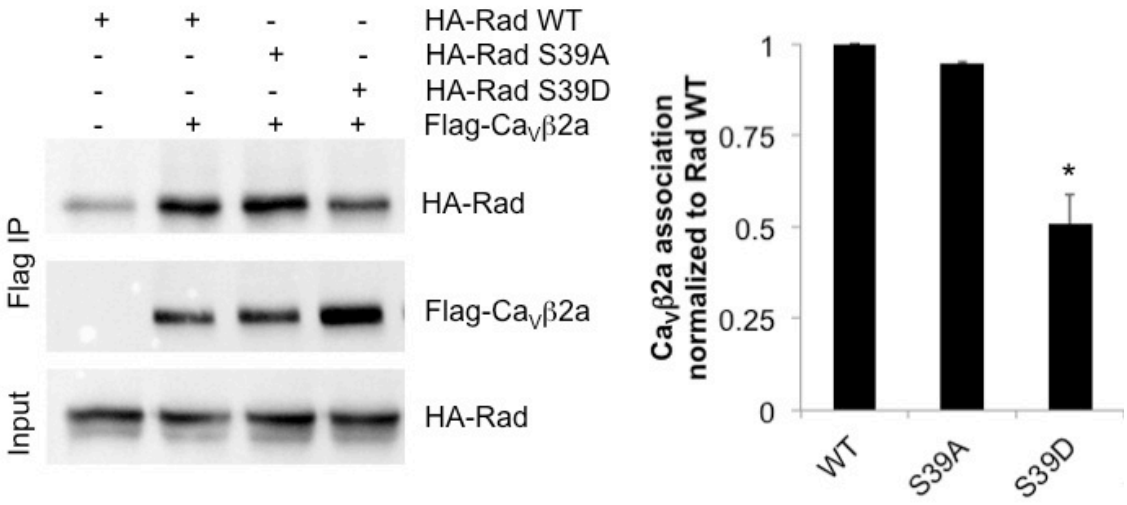

Figure 4.5: Phosphomimetic mutation of Rad at Ser39 decreases its association with $Ca_V\beta 2a$

HEK293 cells were transfected with Flag-tagged $Ca_V\beta 2a$ along with HA-tagged Rad WT, S39A, or S39D. Co-immunoprecipitation analysis suggests that the phosphomimetic S39D mutation results in weaker association with $Ca_V\beta 2a$. Results are representative of three independent experiments, * $p<0.05$ compared to Rad WT by Student's *t* test.

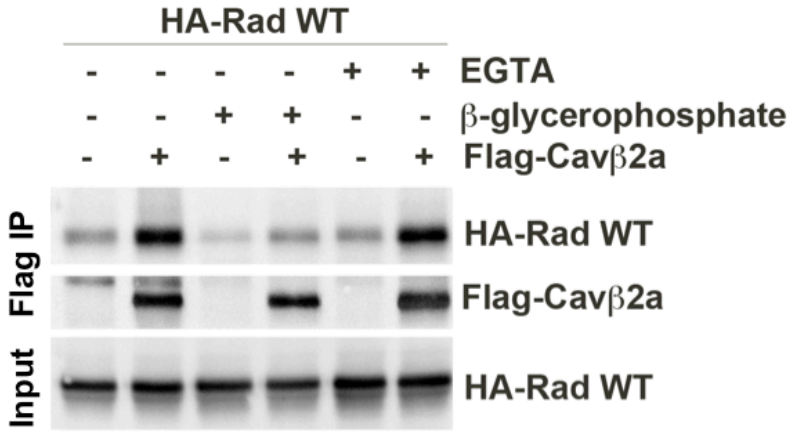

Figure 4.6: Phosphatase inhibition may decrease the interaction between Rad and $Ca_V\beta 2a$

HEK293 cells were transfected with Flag-tagged $Ca_V\beta 2a$ along with HA-tagged Rad WT. Co-immunoprecipitation was performed with standard IP buffer or with the addition of 50 mM β-glycerophosphate to inhibit phosphatases or 2 mM EGTA to chelate calcium. Addition of β-glycerophosphate appears to result in loss of association between Rad and $Ca_V\beta 2a$.

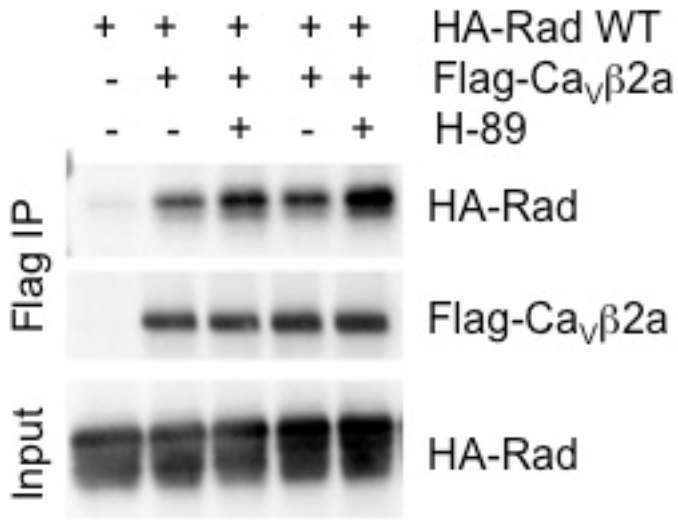

Figure 4.7: Inhibition of PKA may enhance Rad interaction with $Ca_V\beta$2a

HEK293 cells were transfected with HA-tagged Rad and Flag-tagged EV (lane 1) or $Ca_V\beta$2a (lanes 2-5) and subjected to immunoprecipitation with an anti-Flag antibody. Pre-treatment with the PKA inhibitor H-89 appears to result in an increase in the association between Rad and $Ca_V\beta$2a. Results of two independent experiments are shown here.

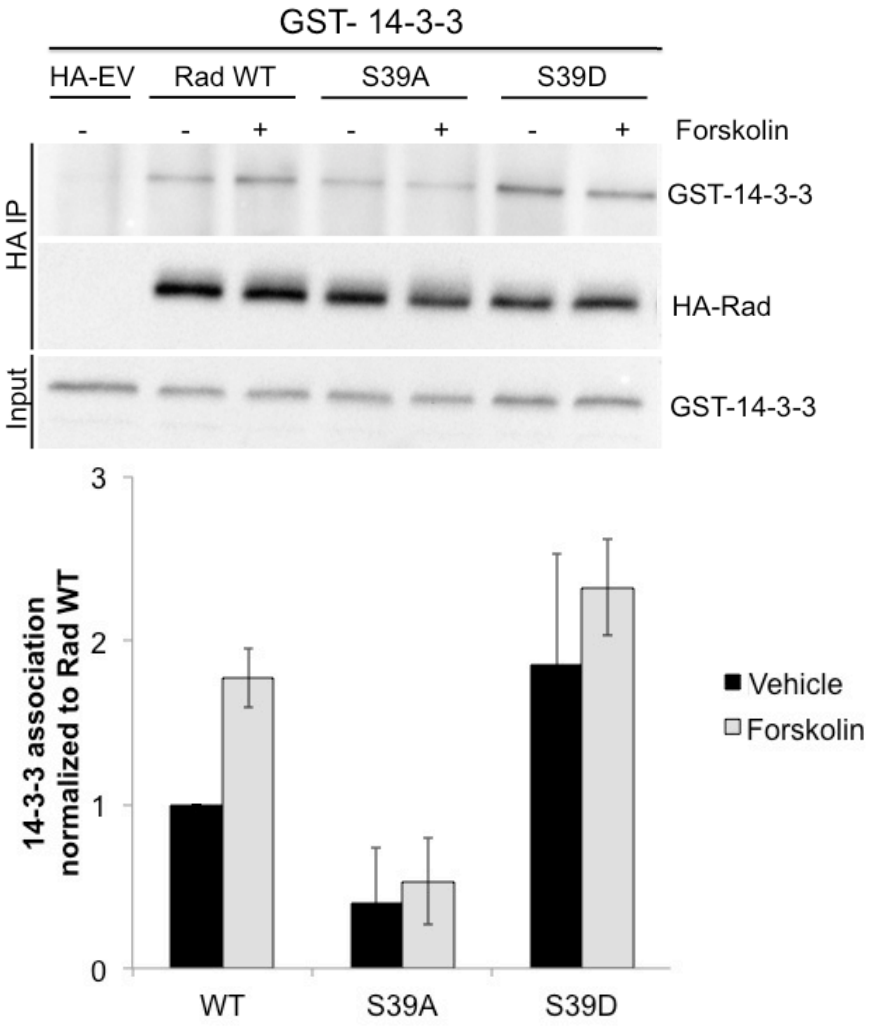

Figure 4.8: Rad phosphorylation at Ser39 promotes 14-3-3 association

HEK293 cells were transfected with GST-tagged 14-3-3 and HA-tagged empty vector (EV) or HA-tagged Rad WT, S39A, or S39D. Cells were starved in serum-free media and treated with 1 μM forskolin or vehicle prior to harvest. Co-immunoprecipitation analysis suggests that forskolin stimulation to induce phosphorylation of Rad WT at Ser39 or phosphomimetic mutation of Ser39 to aspartic acid strengthens the association between Rad and 14-3-3. Results are representative of three independent experiments.

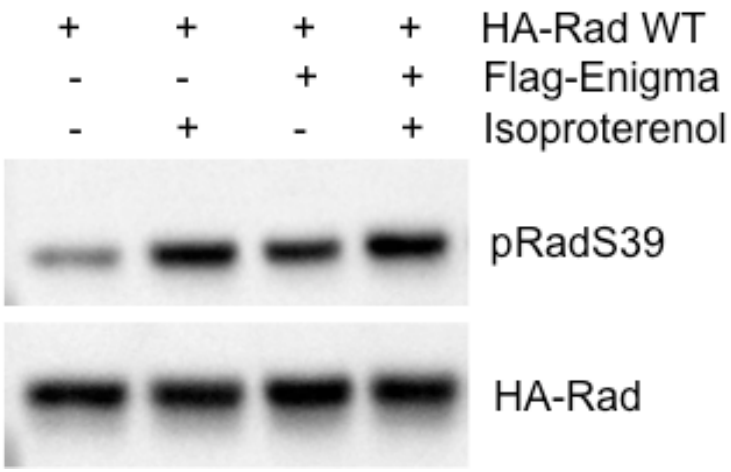

Figure 4.9: Enigma overexpression increases Rad Ser39 phosphorylation

HEK293 cells were transfected with HA-tagged Rad WT and Flag-tagged empty vector or Enigma. 48 hours after transfection, cells were serum-starved and treated with 100 ng/mL isoproterenol or vehicle for 15 minutes. Western blotting analysis indicates that Enigma overexpression is sufficient to increase Rad Ser39 phosphorylation without an additional stimulus. Results are representative of three independent experiments.

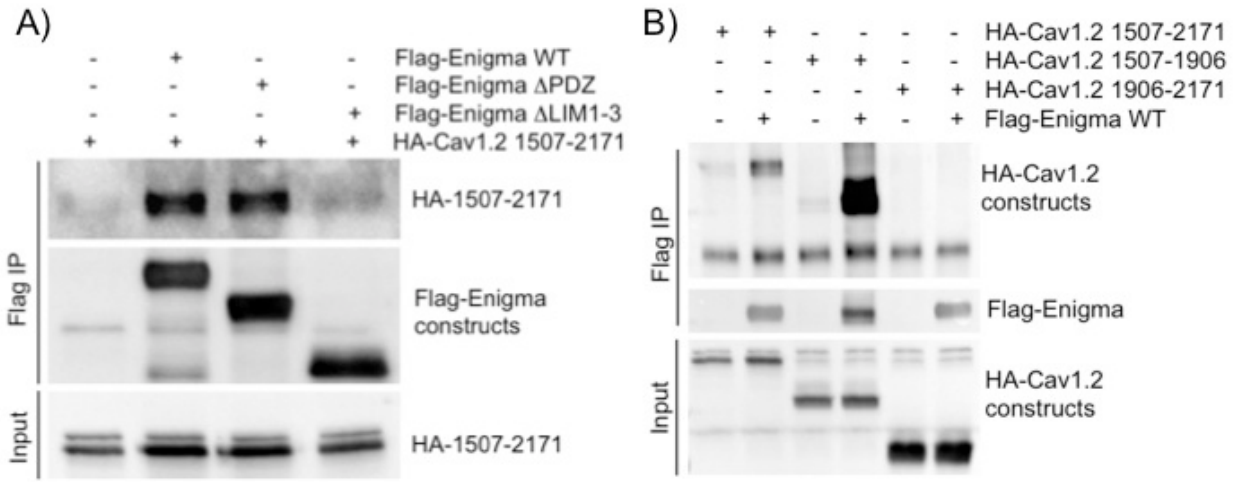

Figure 4.10: Enigma associates with the C-terminus of $Ca_V1.2$

Panel A) HEK293 cells were transfected with HA-tagged $Ca_V1.2$ C-terminus (amino acids 1507-2171) and either Flag-tagged Enigma WT, ΔPDZ, ΔLIM1-3, or empty vector. Immunoprecipitation with anti-Flag antibody and Western blotting with biotinylated anti-HA antibody indicate that the $Ca_V1.2$ C-terminus forms a complex with Enigma that does not require the PDZ domain.

Panel B) HEK293 cells were transfected with HA-tagged $Ca_V1.2$ C-terminus constructs (amino acids 1507-2171, 1507-1906, or 1906-2171) and Flag-tagged Enigma or empty vector and subjected to immunoprecipitation with anti-Flag antibody. Western blotting with biotinylated anti-HA antibody indicates that the interaction between the $Ca_V1.2$ C-terminus and Enigma requires amino acids 1507-1906. Results are representative of three independent experiments.

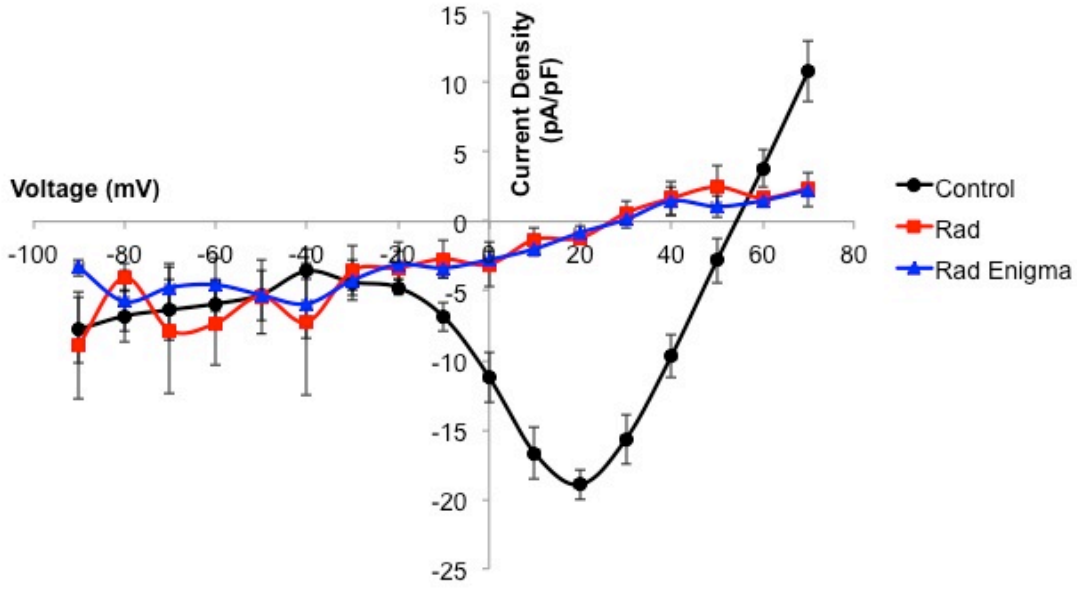

Figure 4.11: Enigma overexpression does not alleviate Rad-mediated calcium channel blockade

HEK293 cells were transfected with full-length rabbit GFP-tagged $Ca_V1.2$, a dual expression vector containing RFP and $Ca_V\beta2a$, HA-tagged empty vector or Rad WT, and Flag-tagged empty vector or Enigma. Cells expressing the calcium channel complex alone had detectable inward calcium current that was completely blocked by Rad overexpression. Overexpression of Enigma with Rad did not rescue calcium channel blockade. N=3-8 cells per group.

Figure 4.12: Alignment of N-terminal 14-3-3 binding sites across the RGK subfamily

The lack of conservation in the amino acid sequences surrounding the N-terminal 14-3-3 binding sites across the RGK subfamily suggests that distinct upstream stimuli and kinases may mediate phosphorylation of the different GTPases in the family.

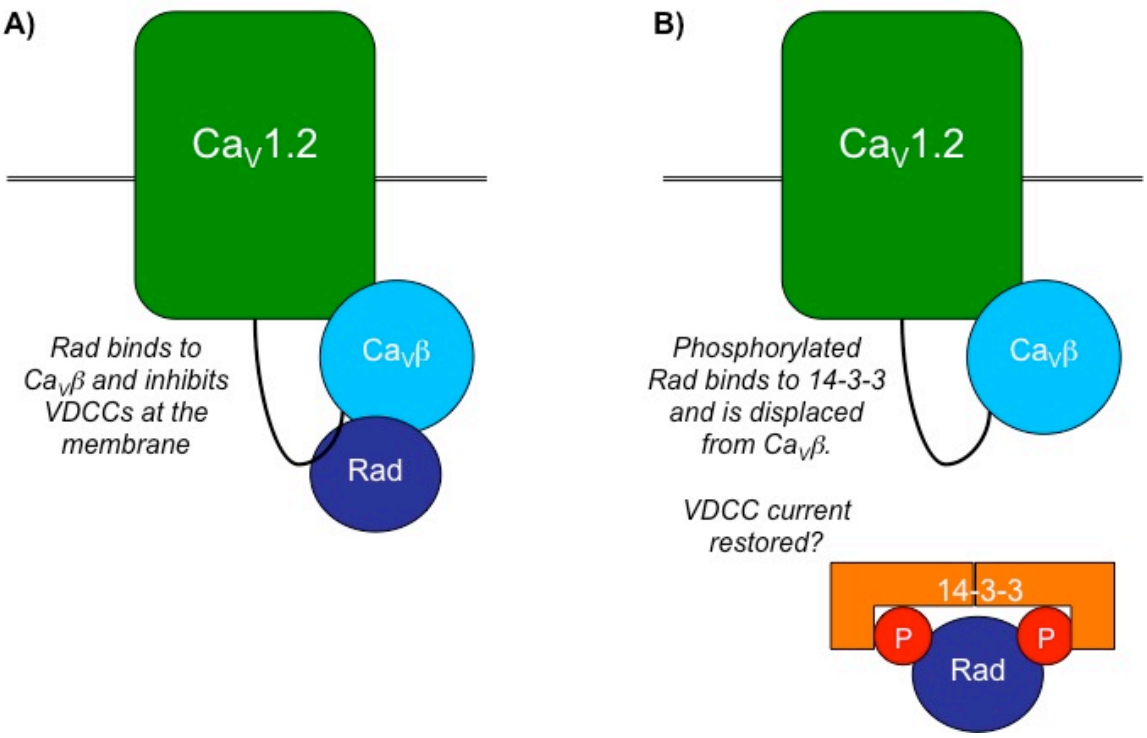

Figure 4.13: Proposed model in which phosphorylated Rad is displaced from the calcium channel complex via 14-3-3 binding

Panel A) In its non-phosphorylated state, Rad binds to the C-terminus of $Ca_V1.2$ and to the accessory $Ca_V\beta$ subunit of calcium channels resident at the plasma membrane and blocks calcium current.

Panel B) Upon phosphorylation at Ser39 (and Ser301, the other 14-3-3 binding site), 14-3-3 dimers bind to phosphorylated Rad, potentially displacing it from the calcium channel complex. Further studies are needed to determine whether Rad Ser39 phosphorylation can reverse calcium channel blockade.

Chapter 5

Rad GTPase is essential for the regulation of bone density and bone marrow adiposity in mice

Introduction

While frequently studied in the context of calcium channel modulation in excitable cells, the recent surge in reports of Rad expression changes in non-excitable cell types suggests that our analysis of the physiological functions of Rad should be expanded. Specifically, RGK (Rad, Rem, Rem2, and Gem/Kir) subfamily proteins have recently been implicated in the regulation of cell differentiation [42-45]. Rem2, an RGK family protein that is primarily expressed in the nervous system, is highly expressed in embryonic stem cells and plays a key role in ectoderm differentiation and neuronal development [42, 43]. Similarly, gene co-regulation mapping studies have suggested a likely role for Rad in embryonic stem cell differentiation [45]. Importantly for the work in this chapter, Satija and colleagues reported that lithium treatment of human mesenchymal stem cells (MSCs) to enhance osteogenic differentiation elicited a robust increase in Rad expression [44]. Notably, siRNA-mediated Rad silencing reversed the osteogenic priming effect of lithium [44]; hence, Rad may play a role in the regulation of osteogenesis that requires further investigation.

Although it is often erroneously thought of as a static support structure, the skeleton is a living, highly dynamic tissue with a number of important functions in the body [141]. Best known for its roles in supporting the weight of the body and in facilitating movement, the skeleton also provides protection for vital organs including the brain, bone marrow, and spinal cord. Moreover, the bone marrow is the site of blood cell production and is also the site for storage of a fat depot known as bone marrow adipose tissue (BMAT) [210]. Finally, the skeleton plays a crucial role in overall mineral homeostasis in the body, acting as a storage reservoir for calcium and phosphate. Remodeling of the bone tissue allows mobilization of these minerals as needed by the body [141]. Calcium homeostasis is critical to overall health, as the body uses calcium for muscle and heart contraction, neurotransmission, hormone secretion, and blood clotting [100].

Osteoporosis is a disease of low bone mass and deterioration of bone tissue leading to structural fragility and increased risk of fractures [211]. According to the National Osteoporosis Foundation, 54 million adults age 50 and over in the United States are affected by osteoporosis and low bone mass, amounting to over half of the total US adult population in that age category [211]. Interestingly, many conditions that can induce bone loss, such as estrogen insufficiency, anorexia, disuse, and hind limb unloading, are accompanied by increased bone marrow adipose tissue (BMAT) [212, 213]. In patients with osteoporosis, bone marrow adiposity is significantly increased, and bone formation rates are inversely related to BMAT levels [214, 215]. BMAT has gained recent interest as

a distinct fat depot that appears to have roles regulating bone homeostasis, hematopoiesis, and metabolism, and it is well established that adipokines and free fatty acids released by adipocytes can modulate bone remodeling and hematopoiesis [210]. BMAT constitutes 70% of the adult bone marrow volume on average and represents about 10% of total body adipose in humans [216], yet its origin and physiological functions remain to be fully characterized.

Mesenchymal stem cells (MSCs) present in the bone marrow are the precursors for osteoblasts, chondrocytes, and white and brown adipocytes [146]. One mechanism that has been proposed to explain the often-inverse relationship between bone density and bone marrow adiposity is a shift in mesenchymal progenitors toward more adipogenic differentiation at the expense of osteoblast formation, but much remains to be determined [217]. The transcriptional programs that drive MSCs to adopt these two cell fates are well characterized, with CCAAT-enhancer binding protein- α (C/EBP-α) and peroxisome proliferator-activated receptor γ2 (PPARγ2) initiating expression of genes associated with mature adipocytes [218], and Runt-related transcription factor 2 (Runx2) and the downstream osteoblast-specific transcription factor osterix/Sp7 required for osteogenic differentiation [151, 219]. However, there is some debate as to whether bone marrow adipocytes are derived from the same precursors as gonadal and intramuscular adipose. Unexpectedly, and in contrast to white and brown adipocytes, bone marrow adipocytes were recently found to express osterix/Sp7 [220], suggesting that MSCs directed toward an osteogenic fate may be re-allocated toward an adipogenic one. Similarly, lineage tracing studies

performed in mT/mG mice expressing a floxed, membrane-targeted tdTomato cassette (mT) upstream of an eGFP cassette (mG), which allows excision of mT and expression of membrane-targeted green fluorescent protein (GFP) when Cre-recombinase is expressed, demonstrated that bone marrow adipocytes traced in Osterix-cre:mT/mG mice [221]. Hence, while more studies are necessary, bone marrow adipocytes are unique in their expression of the osteoblast-specific transcription factor Osterix and thus may not follow the traditional adipogenic differentiation pathway.

In addition to the report of increased Rad expression during the osteogenic differentiation of MSCs [44], the interaction between Rad and Enigma that was demonstrated in Chapter 3 also points to a potential role for Rad in osteogenesis. Enigma is also referred to as LIM mineralization protein (LMP) in the bone literature [222] and has an established function in bone mineralization as its name suggests. Multiple studies have demonstrated that Enigma/LMP overexpression induces mineralization of calvarial cells *in vitro* and bone formation *in vivo* [223-229]. Similarly, loss of Enigma/LMP expression prevents *in vitro* osteoblast differentiation [223] and periodontal ligament cell mineralization [230], and $LMP^{-/-}$ mice have lower bone density compared to WT [160]. The osteoinductive effects of Enigma/LMP are thought to involve both the regulation of bone morphogenetic protein (BMP) expression [231-233] as well as regulation of BMP responsiveness through modulation of Smad ubiquitin regulatory factor 1 (Smurf1) E3 ubiquitin ligase activity [184, 188].

Given the importance of the balance between osteogenesis and adipogenesis in human disease, coupled with the report of Rad up regulation during osteogenic priming of MSCs [44] and our observation of a novel interaction between Rad and Enigma/LMP (see Chapter 3), the goal of the work in this chapter is to characterize the effects of Rad deletion on bone homeostasis and bone marrow adiposity *in vivo* and on osteoblast function *in vitro* using global Rad-knockout ($Rad^{-/-}$) mice. I will test the hypothesis that genetic deletion of Rad results in low bone mass through a decrease in bone formation by osteoblasts and ultimately postulate that Rad might be one of the elusive upstream regulators of the switch between osteogenesis and adipogenesis.

Results

$Rad^{-/-}$ mice are small and weigh less than WT

Because of a routine observation during maintenance of the $Rad^{-/-}$ mouse line that these mice tended to appear smaller in size than WT counterparts, the weights and lengths of these mice were quantified. At four months of age, both male and female $Rad^{-/-}$ mice weighed significantly less than WT (**Table 5.1**). The lengths of male mice were measured at four months of age, and $Rad^{-/-}$ mice were shorter in length than WT (**Table 5.1**). Lengths and weights were also quantified at neonatal day one, and again $Rad^{-/-}$ mice weighed significantly less and were shorter than WT (**Table 5.1**).

No gross skeletal abnormalities in the absence of Rad

To assess skeletal development at a gross level, skeletons were isolated from one-day-old WT and $Rad^{-/-}$ neonates and sequentially stained with Alcian blue and Alizarin Red S, which mark cartilage in blue and bone in reddish-purple, respectively. This analysis indicated no gross abnormalities in $Rad^{-/-}$ skeletal development (**Figure 5.1**).

Lower trabecular and cortical bone density in $Rad^{-/-}$ mouse femora

To explore the impact of Rad deletion on bone density, WT and $Rad^{-/-}$ femora from both male and female mice were analyzed by microcomputed tomography (μCT) in collaboration with the μCT Core Laboratory at Rush University. $Rad^{-/-}$ femora from female mice exhibited a significantly lower trabecular bone volume fraction and trabecular number, with a parallel increase in trabecular spacing relative to WT controls (**Figure 5.2 and Table 5.2**). A similar trend was observed in male $Rad^{-/-}$ femora (**Figure 5.2**). Trabecular thickness was not significantly different from WT. $Rad^{-/-}$ femora also exhibited a significantly lower cortical bone area and thickness than WT, whereas the medullary area was significantly higher when compared to WT controls (**Figure 5.2 and Table 5.2**). Taken together, these data suggest that Rad GTPase contributes to the maintenance of normal bone density.

Rad$^{-/-}$ femora have altered mechanical properties

To determine whether the decrease in bone density in Rad$^{-/-}$ femora changed the mechanical properties of these bones, four-point bending analysis was performed by our collaborators at Indiana University School of Medicine. Rad$^{-/-}$ femora displayed a significant mechanical phenotype, including a significantly lower cortical bone ultimate force, stiffness, work to yield, ultimate stress, and elastic modulus compared to femora from WT controls (**Figure 5.3 and Table 5.3**). Total displacement, toughness, and total strain were all significantly higher in the absence of Rad (**Table 5.3**). These data indicate that Rad loss results in a unique mechanical phenotype characterized by weaker and more elastic bones, which is consistent with the lower bone density evident from μCT analysis.

Rad deletion enhances osteoclast differentiation *in vitro*

A decrease in bone density and strength could occur via an increase in bone resorption by osteoclasts, a decrease in bone formation by osteoblasts, or a combination of the two. To determine the impact of Rad deletion on osteoclast differentiation, mononuclear cells were isolated from the spleens of WT and Rad$^{-/-}$ mice and treated with M-CSF and RANKL to stimulate their differentiation toward multinucleated osteoclasts. Staining for tartrate-resistant acid phosphatase (TRAP) and counting TRAP^{+} multinucleated cells (MNCs) indicated that loss of Rad significantly enhanced osteoclast differentiation *in vitro* (**Figure 5.4**).

Osteoclast surface is not higher in Rad$^{-/-}$ femora *in vivo*

To examine whether the lower bone density of Rad$^{-/-}$ femora resulted from an increase in osteoclast numbers *in vivo*, we performed TRAP staining at the distal femur of 4-month-old animals. Osteoclast surface was unchanged in male Rad$^{-/-}$ animals, and a small but significant decrease in osteoclast surface was observed in the distal femora of female Rad$^{-/-}$ mice compared to WT (**Figure 5.5**). These data suggest that, despite the increase in *in vitro* osteoclastogenesis that was observed in **Figure 5.4**, the low bone density phenotype of Rad$^{-/-}$ mice is not likely to arise solely from increased osteoclast numbers.

Lower bone formation rate in Rad$^{-/-}$ femora

The reduction in osteoclast surface in Rad$^{-/-}$ femora, coupled with the report of a role for Rad in osteogenic priming of MSCs [44], suggested that altered osteoblast function might also contribute to the lower bone density observed in Rad$^{-/-}$ mice. To test this notion, dynamic histomorphometry was used to determine the rate of bone formation in WT and Rad$^{-/-}$ femora *in vivo*. In trabecular bone at the distal femur, a significantly lower mineral apposition rate (MAR) but a higher percent mineralizing surface (MS/BS) was observed in Rad$^{-/-}$ femora compared to WT controls (**Figure 5.6** and **Table 5.4**). The latter observation may arise in part due to the significant decrease in total trabecular bone surface at the distal femora of Rad$^{-/-}$ mice compared to WT (**Figure 5.6A**). Normalization of MAR and MS/BS results in a downward trend in bone formation

rate (BFR/BS) in trabecular bone of Rad$^{-/-}$ animals compared to WT (**Figure 5.6B** and **Table 5.4)**.

These parameters were also measured in cortical bone. Consistent with the μCT data, histology indicated a significantly lower cortical bone area at the mid-diaphysis of Rad$^{-/-}$ femora compared to WT (**Table 5.4**). The mineralizing surface (MS/BS) and bone formation rate (BFR/BS) at the periosteal surface of Rad$^{-/-}$ femur diaphyses were significantly lower than in WT, and the periosteal mineral apposition rate (MAR) also trended downward in Rad$^{-/-}$ femora (**Figure 5.6B** and **Table 5.4**). These same measures at the endocortical surface of the femur diaphysis trended downward in Rad$^{-/-}$ animals but did not reach significance (**Table 5.4**). Overall, these data suggest that a decrease in osteoblast function may contribute to the lower bone mass observed in Rad$^{-/-}$ mice.

Rad$^{-/-}$ calvarial osteoblast function is blunted *in vitro*

To characterize the contribution of Rad GTPase signaling to osteoblast differentiation and function *in vitro*, the phenotype of osteoblasts derived from neonatal WT and Rad$^{-/-}$ calvariae was examined. Immunoblot analysis confirmed Rad expression in this cell population (**Figure 5.7A**). Consistent with the *in vivo* decrease in bone formation, osteoblast differentiation was impaired in Rad$^{-/-}$ calvarial cells as shown by a reduction in alkaline phosphatase activity, an enzymatic marker of osteoblast maturation (**Figure 5.7B**), and a significant decrease in mineralization as indicated Alizarin Red S staining (**Figure 5.7C**)

following osteogenic induction. Together these data indicate that osteoblast development and/or function is diminished in the absence of Rad.

Higher expression of matrix Gla protein in Rad$^{-/-}$ calvarial osteoblasts

To examine the molecular mechanisms underlying the decrease in osteoblast function upon Rad loss, microarray analysis was performed to compare the gene expression profile of naïve calvarial osteoblasts from WT and Rad$^{-/-}$ mice. Surprisingly, Rad deficiency had no effect on the expression of the canonical osteoblast marker genes Runt-related transcription factor 2 (*Runx2*), osteocalcin (*Bglap*), or type I collagen (*Col1a1*) (**Figure 5.8A**). Expression of the osteogenic transcription factor osterix (*Sp7*) and of alkaline phosphatase (*Alpl*) trended downwards but did not reach significance (**Figure 5.8A**)**.** Instead, the profiling data indicated that matrix Gla protein (*Mgp*), a 15-kDa secreted protein that was initially isolated and identified from demineralized bovine bone and has since been found to inhibit bone mineralization [234-236], was markedly increased in Rad$^{-/-}$ calvarial osteoblasts compared to WT (+11.28-fold) (**Figure 5.8A**). This increase in matrix Gla protein (MGP) expression in Rad$^{-/-}$ osteoblasts was confirmed by RT-PCR (**Figure 5.8B**) and suggests a novel means by which Rad loss may result in a decrease in osteoblast activity and therefore overall bone density.

Rad$^{-/-}$ calvarial osteoblasts show a striking adipogenic phenotype

During the course of culturing primary calvarial cells, a dramatic increase in the number of cells that appeared to have lipid droplets was observed in the Rad$^{-/-}$ osteoblast preparations after 10-14 days in culture when compared to WT osteoblasts. This observation, coupled with published work indicating that MGP not only inhibits mineralization but that its secretion increases ~30-fold during the *in vitro* differentiation of human pre-adipocytes [237], suggested that lower osteogenesis following Rad deletion might be linked to increased adipogenic differentiation. To test this possibility, WT and Rad$^{-/-}$ calvarial osteoblast monolayers were stained with Oil Red O (ORO) on day 14 to confirm that these structures were lipid droplets. Consistent with a potential role for Rad in inhibiting adipogenesis, the number of ORO-positive cells was significantly higher in Rad$^{-/-}$ calvarial cultures compared to WT (**Figure 5.9**).

Adipogenic induction of WT osteoblasts causes a decline in endogenous Rad levels

Rad gene expression is increased following lithium stimulation of mesenchymal stem cells, which enhances osteogenic differentiation, and Rad silencing has been shown to attenuate osteogenic priming [44]. These data prompted examination of Rad expression in primary calvarial cells upon adipogenic differentiation. Treatment of WT calvarial osteoblasts with adipogenic media for one week resulted in a dramatic loss of endogenous Rad protein (**Figure 5.10**). Together with the data from Satija and colleagues [44], this observation suggests

that dynamic control of Rad may play a role in directing differentiation toward the osteogenic versus adipogenic lineages. In addition to Rad down regulation, adipogenic treatment of WT calvarial cells generated a phenotype that resembled that of $Rad^{-/-}$ osteoblasts without adipogenic induction. Specifically, treatment with adipogenic media for one week resulted in the accumulation of ORO^{+} lipid droplets in WT calvarial cultures, a reduction in alkaline phosphatase staining, and a significant rise in MGP gene expression (**Figure 5.11**).

Increased bone marrow adiposity at the distal femora of $Rad^{-/-}$ mice

The significant increase in adipogenesis observed in primary $Rad^{-/-}$ calvarial osteoblast cultures under normal growth conditions suggested that Rad deficiency might alter the *in vivo* balance of osteoblasts and adipocytes in the bone marrow compartment. Von Kossa/MacNeal's tetrachrome staining of WT and $Rad^{-/-}$ distal femora was performed to evaluate the overall cell distribution and revealed a significant increase in BMAT at the $Rad^{-/-}$ distal femur compared to WT (**Figure 5.12**). Rad deletion resulted in significantly higher adipocyte numbers as well as significantly larger adipocyte size compared to WT (**Figure 5.1**). Notably, reexamination of TRAP-stained distal femora (**Figure 5.4**) was consistent, with unstained round structures resembling adipocytes frequently observed in $Rad^{-/-}$ femora.

Total body fat percentage is unchanged in Rad$^{-/-}$ mice

To determine whether Rad loss results in a global alteration in adipogenesis, 4-month-old WT and Rad$^{-/-}$ mice were weighed and subjected to EchoMRI body composition analysis. These analyses showed that although Rad$^{-/-}$ mice weigh less than WT littermates (**Table 5.1** and **Figure 5.13**), there is no significant change in body fat percentage upon Rad deletion (**Figure 5.13**); thus, the increase in adipogenesis in Rad$^{-/-}$ mice appears to be specific to BMAT.

Rad associates with C/EBP proteins

CCAAT-enhancer binding proteins (C/EBPs) play an important role in adipocyte differentiation, with induction of C/EBP-β and -δ observed early in adipogenesis and induction of C/EBP-α necessary for terminal adipocyte differentiation [238-240]. Rad has been reported to bind to C/EBP-δ and to impede its DNA binding and its function as a transcription factor in heart tissue [41], and a similar regulatory mechanism in osteoblast progenitors could explain the increase in adipogenesis observed in the absence of Rad. Co-immunoprecipitation studies in HEK293 cells corroborate the finding that Rad interacts with C/EBP-δ, and notably, we also observe co-immunoprecipitation of Rad and the C/EBP-α and β isoforms (**Figure 5.14**), suggesting that regulation of C/EBP activity is an area that should be pursued as a potential mechanism for the increased adipogenesis and decreased osteogenesis in Rad$^{-/-}$ bone marrow.

Discussion

Bone is a dynamic tissue that undergoes continuous remodeling throughout life in response to changing demands on the skeleton and in order to maintain mineral homeostasis. Dysregulation of the bone remodeling process is one characteristic of age-related osteoporosis. In addition to low bone mass, osteoporosis is often characterized by an increase in bone marrow adiposity [214]. Osteoblasts and adipocytes share a common mesenchymal stem cell precursor [146], but the mechanisms by which these precursors are marked for an adipogenic versus an osteogenic cell fate have not been fully elucidated, and the literature also suggests potential differences in the origin of bone marrow adipocytes compared to white and brown adipocytes [216]. The data in this chapter represent the first analysis of the bone physiology of $Rad^{-/-}$ mice and demonstrate that Rad GTPase plays an important, previously uncharacterized role in the regulation of bone homeostasis in mice. Deletion of Rad in mice results in low bone density owing in part to a lower rate of bone formation *in vivo* and lower osteoblast function *in vitro.* A concomitant increase in BMAT is also observed within $Rad^{-/-}$ femora without obvious expansion of peripheral adipose tissue, and adipocytes spontaneously arise in primary cultures from $Rad^{-/-}$ calvaria. The work in this chapter suggests that Rad may alter osteogenic versus adipogenic lineage commitment, potentially via regulation of matrix Gla protein expression. Endogenous Rad levels are decreased following adipogenic treatment of calvarial cells, complementing the previously reported increase in Rad expression during osteogenesis. These observations implicate Rad

GTPase as a regulatory protein whose levels can be dynamically modulated to control the shift between osteogenesis and adipogenesis, and as such, studies into the mechanism of Rad action and regulation may present potential targets for osteoporosis research.

Following the report of a requirement for Rad function in lithium-mediated osteogenic priming of MSCs [44], we hypothesized that global $Rad^{-/-}$ mice would have lower bone density than WT controls, which was confirmed by μCT analysis in **Figure 5.2** and **Table 5.2**. Further evaluation of these bones to examine their mechanical properties in **Figure 5.3** and **Table 5.3** revealed that while $Rad^{-/-}$ femora have significantly lower strength and stiffness, which would typically render them more susceptible to fracture, they also have significantly longer displacement than femora from WT controls. Hence, $Rad^{-/-}$ femora are simultaneously weaker and more elastic, bending under smaller loads than WT but not overtly fracturing. Both collagen and water provide plasticity to bone, and the contribution of these variables to the $Rad^{-/-}$ mechanical phenotype could be explored in the future.

Bone dynamics are controlled by the coordinated actions of osteoclasts and osteoblasts, and I sought to define the cell type(s) responsible for the lower bone density in $Rad^{-/-}$ mice. Despite the observation of an increase in osteoclast differentiation in $Rad^{-/-}$ cells *in vitro* in **Figure 5.4**, the *in vivo* result in **Figure 5.5** Indicates that osteoclast number is not increased in the absence of Rad in 4-month-old animals. This observation suggests that an increase in osteoclasts

may not be the primary source of the low bone mass seen in $Rad^{-/-}$ animals. Further studies should investigate the serum and/or urine levels of bone resorption markers such as carboxy-terminal collagen crosslinks (CTX-I) or deoxypyridinoline (DPD) to determine whether osteoclast activity is altered in these mice. In addition, investigation of the bone density and osteoclast surface area of WT and $Rad^{-/-}$ femora from younger and older mice will also better inform the phenotype that we have observed.

Analysis of osteoblast function *in vivo* and *in vitro* suggested that bone formation is impaired in $Rad^{-/-}$ mice. The bone formation rate was significantly lower at the periosteal surface of cortical bone and trended downwards at the endocortical surface as well as in trabecular bone (**Figure 5.6** and **Table 5.4**), indicating that Rad loss might result in decreased osteoblast differentiation and/or function. *In vitro* calvarial osteoblast assays corroborated this notion, as our studies in **Figure 5.7** indicated lower alkaline phosphatase activity and decreased mineralization in $Rad^{-/-}$ calvarial cells following osteogenic induction compared to WT. Further studies will be important to determine whether the loss of Rad impacts osteoblast differentiation, function, or both. Specifically, isolation of WT and $Rad^{-/-}$ MSCs for analysis of their differentiation potential toward the osteogenic and adipogenic lineages will be informative.

Surprisingly, we did not see a change in the expression of canonical osteoblast marker genes in $Rad^{-/-}$ calvarial cells in **Figure 5.8**, as would be expected if osteoblast development were hindered in the absence of Rad. In part this might

arise from our study design, using freshly isolated calvarial cells prior to osteogenic induction. It will be important to determine whether Rad deletion hinders this gene expression program following osteogenic induction. Our microarray analysis did, however, reveal a robust increase in matrix Gla protein expression in $Rad^{-/-}$ calvarial cells compared to WT (**Figure 5.8**). MGP up-regulation may provide a novel mechanism for the decrease in osteogenesis as well as the increase in adipogenesis observed upon Rad deletion. MGP has been shown to prevent mineralization in the osteoblast-like cell line MC3T3-E1 [235, 236]. In keeping with its role as an inhibitor of mineralization, transgenic mice overexpressing MGP in osteoblasts have low bone density [241], and $MGP^{-/-}$ mice exhibit profound calcification of the aorta and other arteries, as well as inappropriate calcification of cartilaginous structures like the growth plate and the tracheal rings [242, 243]. Interestingly, not only does MGP inhibit mineralization, but its secretion is robustly increased during adipocyte differentiation, second only to the body fat regulatory hormone leptin [237], and we observed induction of MGP gene expression following adipogenic differentiation of WT cells in **Figure 5.11**. Thus, the elevation in MGP gene expression in $Rad^{-/-}$ osteoblasts is likely important to the overall phenotype of increased adipogenesis at the expense of osteogenesis.

While calvarial cells were isolated from WT and $Rad^{-/-}$ mice with the purpose of examining osteoblast differentiation and activity, the finding of spontaneous adipogenesis in the absence of Rad in **Figure 5.9** was unexpected and exciting. Moreover, the observations that endogenous Rad expression decreases during

adipogenesis of WT calvarial cells in **Figure 5.10** and that adipogenic induction of WT cells phenocopies $Rad^{-/-}$ cells in **Figure 5.11** indicate that Rad may be a physiological regulator of the adipogenesis process. Specifically, our finding that Rad levels decrease during adipogenesis complements the report by Satija and colleagues that Rad expression is increased during osteogenic priming [44]. The observation that Rad deletion increases bone marrow adiposity but not total body fat percentage in **Figures 5.12** and **5.13** is equally intriguing, as recent studies have hinted at differences in the origins of BMAT and peripheral adipose depots [216]. The increase in BMAT, but not of peripheral fat, in $Rad^{-/-}$ animals suggests that Rad function may serve as a novel regulator of BMAT development and regulation. This possibility is supported by a study showing that Rad protein levels in human skeletal muscle are correlated with measures of obesity and resting metabolic rate [129]. Taken together, these studies lead to the hypothesis that Rad levels may be dynamically regulated at the level of expression to modulate cell fate of MSCs or potentially even redirection of osteoprogenitors toward an adipogenic differentiation course. We hypothesize that higher Rad expression promotes osteogenesis and that lower Rad expression promotes adipogenesis, and more specifically, BMAT production.

Finally, while preliminary, our finding of an interaction between Rad and C/EBP-α, β, and δ in **Figure 5.14** suggests a potential mechanism for the increase in adipogenesis observed in the absence of Rad. C/EBPs are critical for adipocyte differentiation [239], and Rad binding to C/EBP-δ in cardiac myocytes has been shown to decrease its DNA binding and transcriptional activity [41]. Moreover,

preliminary studies suggest that C/EBP protein expression may be higher in $Rad^{-/-}$ calvarial cells than WT (data not shown), suggesting that Rad may regulate the stability of C/EBP proteins as well. Future studies should probe for changes in C/EBP promoter occupancy or transcriptional activity in $Rad^{-/-}$ calvarial cells and following ectopic Rad expression. A reasonable hypothesis that stems from these data is that Rad function may be required for osteogenic differentiation of MSCs during adult bone homeostasis via inhibition of C/EBP family proteins, with the lack of Rad function promoting adipogenesis through enhanced C/EBP-dependent transcription.

Unraveling the pathways that regulate the bifurcation between osteogenic and adipogenic differentiation is critical to understanding the disease progression of osteoporosis and identifying new therapies, as a shift in this balance favoring adipogenesis at the expense of osteogenesis may contribute to the increase in BMAT that accompanies low bone density in osteoporotic patients. The data in this chapter suggest that Rad may represent a promising target in regulating this balance.

Table 5.1: Mouse weights and lengths

Age	Genotype	Gender	Weight (g)	Length (cm)
4 months	Wildtype	Male	35.9 +/- 0.4	18.4 +/- 0.1
		Female	26.5 +/- 0.9	
	RadKO	Male	32.1 +/- 0.7 ***	17.0 +/- 0.1 ***
		Female	22.2 +/- 0.4 **	
1 day	Wildtype		2.67 +/- 0.06	5.66 +/- 0.06
	RadKO		2.16 +/- 0.11 ***	5.08 +/- 0.07 ***

** $p<0.01$, *** $p<0.001$ compared to WT using Student's *t* test

Table 5.2: Trabecular and cortical geometry of 4-month-old mouse femora from μCT analysis

Distal Femur	**Wildtype (N=5)**	**RadKO (N=5)**
TV (mm^3)	3.26 +/- 0.18	4.65 +/- 0.06 ***
BV (mm^3)	0.32 +/- 0.04	0.22 +/- 0.04
BV/TV (%)	9.60 +/- 0.88	4.81 +/- 0.80 **
Conn.D	109.3 +/- 8.8	27.1 +/- 6.2 ***
SMI	2.43 +/- 0.09	3.20 +/- 0.08 ***
Tb.Th (mm)	0.045 +/- 0.002	0.047 +/- 0.002
Tb.N (1/mm)	3.49 +/- 0.12	2.72 +/- 0.11 **
Tb.Sp (mm)	0.29 +/- 0.01	0.37 +/- 0.02 **
Ap.Dens	278.6 +/- 9.7	204.5 +/- 11.3 **
BS/BV	61.3 +/- 2.2	63.4 +/- 3.3
DA	1.34 +/- 0.04	1.35 +/- 0.03
Femoral Midshaft	**Wildtype (N=5)**	**RadKO (N=5)**
Ct.Ar (mm^2)	0.96 +/- 0.02	0.79 +/- 0.02 ***
Tt.Ar (mm^2)	1.45 +/- 0.01	1.81 +/- 0.03 ***
Ma.Ar (mm^2)	0.49 +/- 0.01	1.02 +/- 0.02 ***
Ct.Th (mm)	0.26 +/- 0.01	0.18 +/- 0.01 ***
Ct.Ar/Tt.Ar (%)	66.3 +/- 0.8	43.7 +/- 0.6 ***
Ct.Po (%)	7.9 +/- 0.5	11.2 +/- 0.5 ***

** $p<0.01$, *** $p<0.001$ compared to WT using Student's *t* test

Table 5.3: Whole bone structural and estimated material mechanical properties from femoral four-point bending

Femur	Wildtype (N=13)	RadKO (N=15)
Yield Force (N)	24.5 +/- 1.2	8.0 +/- 0.4 ***
Ultimate Force (N)	28.9 +/- 1.6	17.5 +/- 0.7 ***
Displacement to Yield (mm)	186.9 +/- 4.2	104.0 +/- 5.8 ***
Postyield Displacement (mm)	165.9 +/- 18.4	810.3 +/- 87.6 ***
Total Displacement (mm)	352.8 +/- 18.5	914.3 +/- 88.1 ***
Stiffness (N/mm)	195.7 +/- 8.0	127.2 +/- 5.4 ***
Work to Yield (mJ)	2.52 +/- 0.16	0.51 +/- 0.05 ***
Postyield Work (mJ)	4.46 +/- 0.49	10.17 +/- 0.75 ***
Total Work (mJ)	6.98 +/- 0.52	10.68 +/- 0.75 ***
Yield Stress (MPa)	258.7 +/- 13.5	74.8 +/- 4.9 ***
Ultimate Stress (MPa)	301.6 +/- 12.3	160.6 +/- 4.5 ***
Strain to Yield (mε)	20380.8 +/- 935.8	11527.4 +/- 533.2 ***
Total Strain (mε)	38517.2 +/- 2681.7	101673.0 +/- 9722.0 ***
Elastic Modulus (GPa)	14.2 +/- 0.6	7.7 +/- 0.2 ***
Resilience (MPa)	2.9 +/- 0.3	0.5 +/- 0.1 ***
Toughness (MPa)	8.3 +/- 0.9	10.8 +/- 0.7 *

* $p<0.05$, *** $p<0.001$ compared to WT using Student's *t* test

Table 5.4: Histomorphometry

Distal Femur	**Wildtype (N=5)**	**RadKO (N=5)**
Trabecular MAR (μm/day)	3.51 +/- 0.26	2.52 +/- 0.18 *
Trabecular MS/BS (%)	36.6 +/- 1.4	45.2 +/- 0.6 **
Trabecular BFR/BS ($\mu m^3/\mu m^2$/year)	470.0 +/- 41.7	417.0 +/- 36.0
Femur Diaphysis	**Wildtype (N=5)**	**RadKO (N=5)**
Ct.Ar (mm)	0.92 +/- 0.02	0.74 +/- 0.01 ***
Periosteal MAR (μm/day)	1.01 +/- 0.07	0.78 +/- 0.08
Periosteal MS/BS (%)	55.0 +/- 4.8	39.5 +/- 2.3 *
Periosteal BFR/BS ($\mu m^3/\mu m^2$/year)	204.8 +/- 28.7	114.3 +/- 17.1 *
Endocortical MAR (μm/day)	1.08 +/- 0.09	0.93 +/- 0.06
Endocortical MS/BS (%)	76.0 +/- 4.0	69.0 +/- 4.7
Endocortical BFR/BS ($\mu m^3/\mu m^2$/year)	299.1 +/- 32.8	237.5 +/- 30.4

* $p<0.05$, ** $p<0.01$, *** $p<0.001$ compared to WT using Student's *t* test

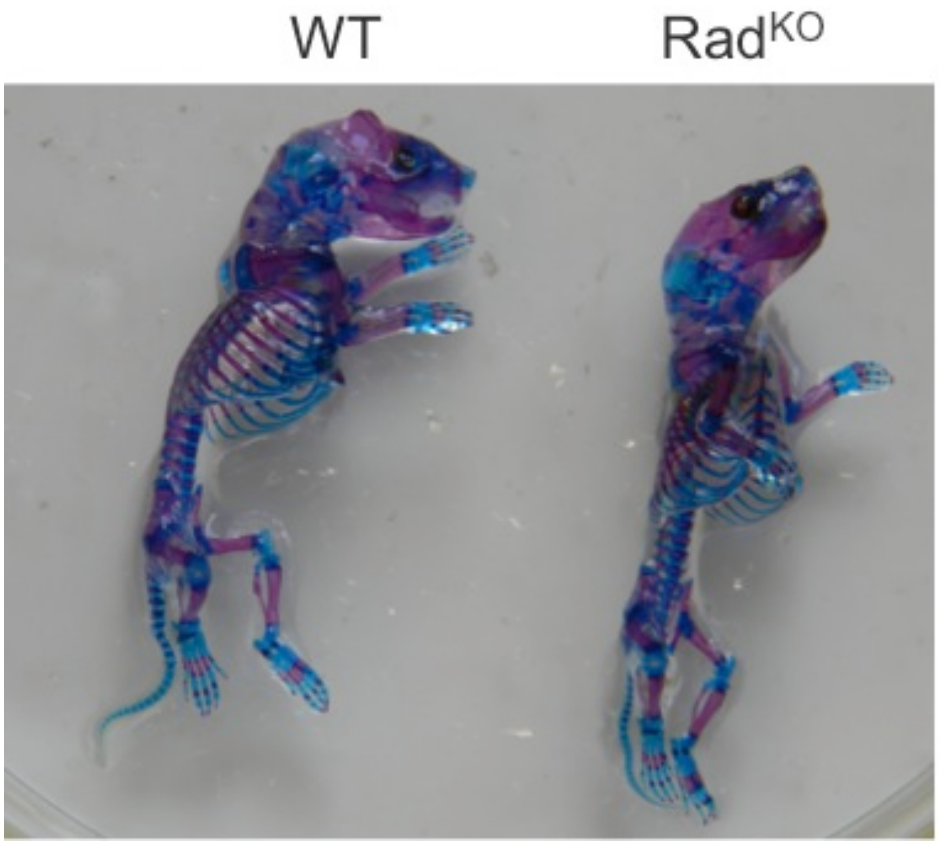

Figure 5.1: No gross alterations in skeletal development in Rad$^{-/-}$ mice

Skeletons of one-day-old mouse pups were isolated from surrounding tissue and stained with Alcian Blue (cartilage, blue) and Alizarin Red S (bone, purple). RadKO skeletons appeared smaller than WT, but no profound differences in skeletal development were observed.

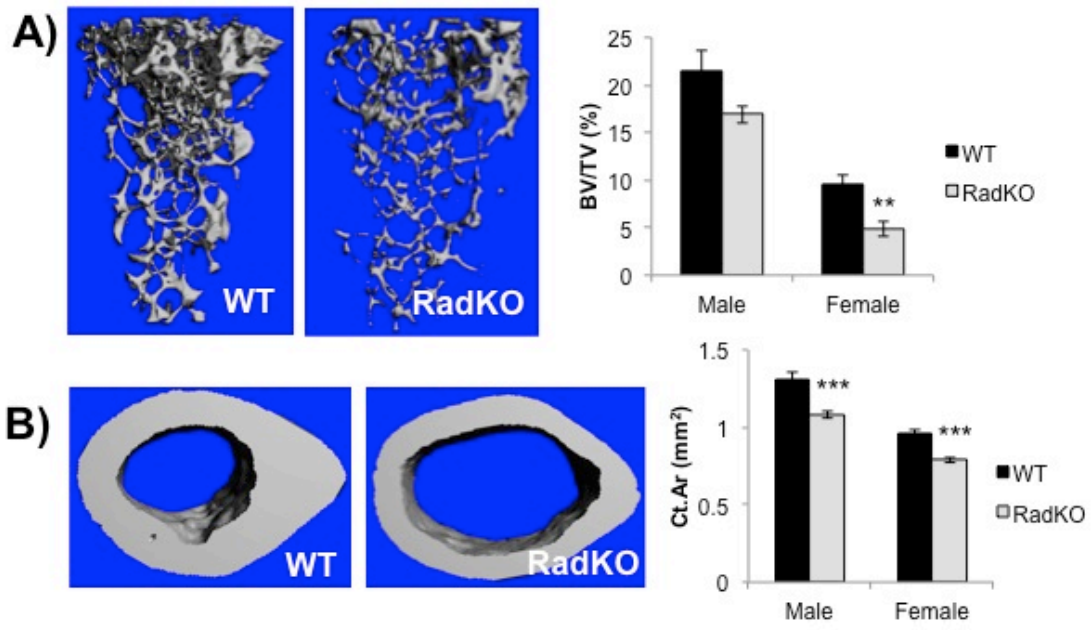

Figure 5.2: Lower trabecular and cortical bone density in Rad$^{-/-}$ mouse femora

Panel A) Representative images from μCT analysis of trabecular bone at the distal femora of WT and RadKO mice with accompanying quantification of the trabecular bone volume fraction (BV/TV).

Panel B) Representative images from μCT analysis of cortical bone at the mid-diaphysis of WT and RadKO mouse femora with corresponding quantification of the cortical bone area (Ct.Ar). N=5-15 mice per group, 4 months of age. **p<0.01, ***p<0.001 compared to WT by Student's *t* test.

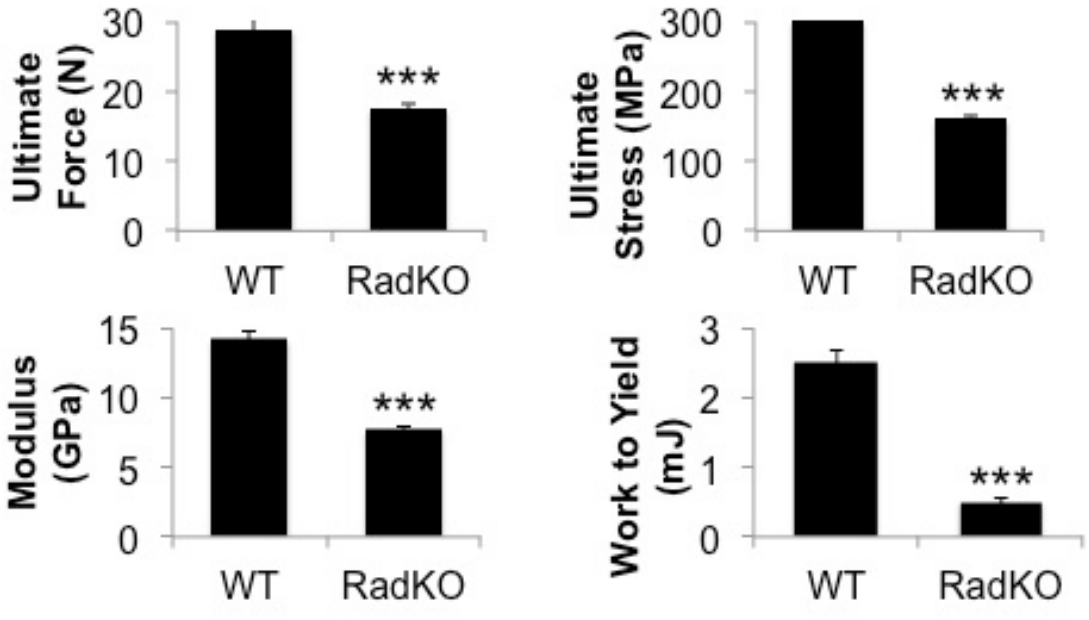

Figure 5.3: Rad deletion results in altered mechanical properties

Quantification of mechanical properties obtained from four-point bending analysis of WT and RadKO mouse femora. N=13-15 mice per genotype, male, 4 months of age. ***p<0.001 compared to WT by Student's *t* test.

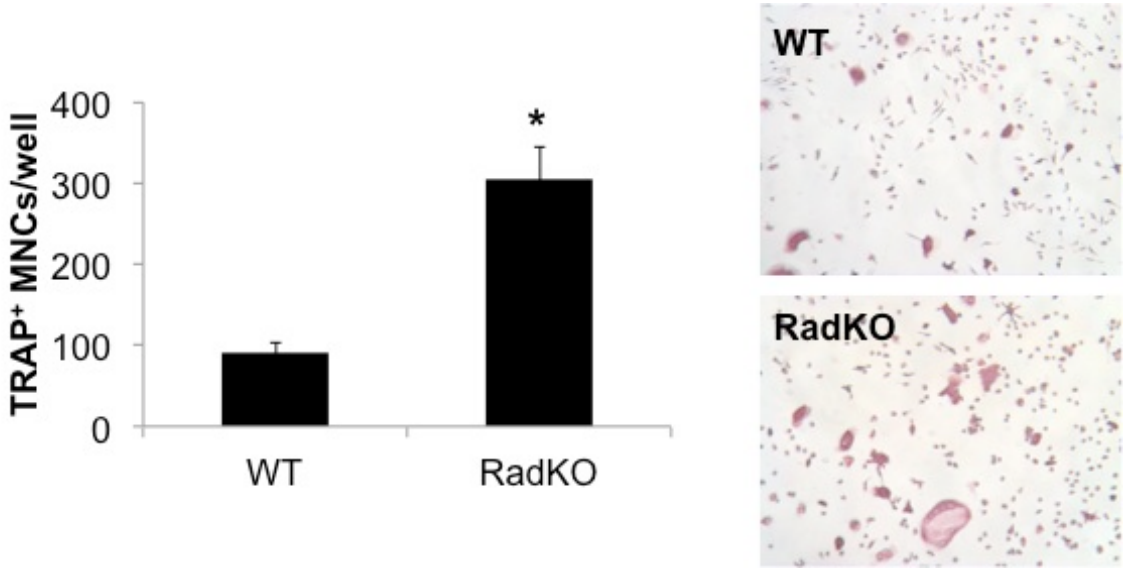

Figure 5.4: *In vitro* osteoclast differentiation is enhanced in the absence of Rad

Representative images and quantification of tartrate-resistant acid phosphatase (TRAP) stained osteoclasts derived from spleen. The number of TRAP-positive multinucleated cells (MNCs, at least three nuclei) was counted in each well of a 24-well plate. N=3 animals per genotype, male, 2 months of age. *$p<0.05$ compared to WT by Student's *t* test

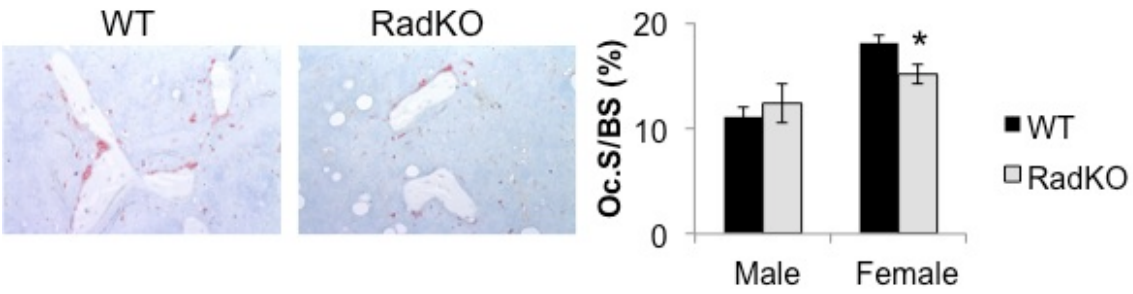

Figure 5.5: Osteoclast surface is not higher in the absence of Rad

Tartrate-resistant acid phosphatase (TRAP) staining of WT and RadKO distal femur thin sections and corresponding quantification of the percentage of the bone surface occupied by osteoclasts (Oc.S/BS). N=5 mice per group, 4 months of age. * $p<0.05$ by Student's *t* test.

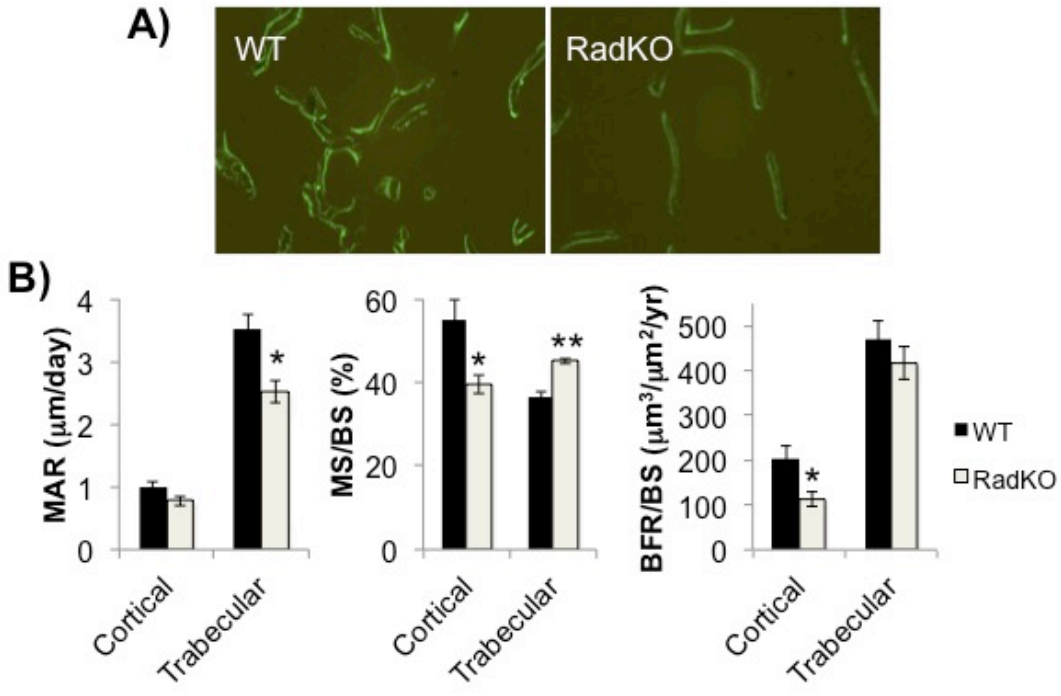

Figure 5.6: Lower bone formation rate in Rad$^{-/-}$ femora

Panel A) Representative images of calcein double labeling in distal femur trabecular bone of WT and RadKO mice (10X).

Panel B) Mineral apposition rate (MAR), mineralizing surface/bone surface (MS/BS), and bone formation rate/bone surface (BFR/BS) in the cortical bone (periosteal surface) and trabecular bone of WT and RadKO mice. N=5 mice per genotype, female, 4 months of age. * $p<0.05$, ** $p<0.01$ compared to WT by Student's *t* test.

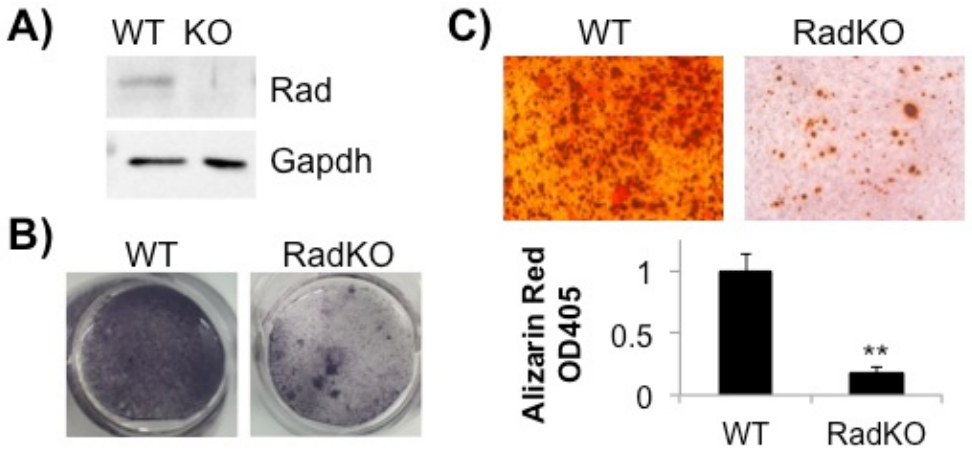

Figure 5.7: Rad$^{-/-}$ osteoblast activity is depressed *in vitro*

Panel A) Representative immunoblot of WT and RadKO calvarial osteoblast lysates confirms Rad expression in these cells. N=3 isolations per genotype.

Panel B) Representative images of WT and RadKO primary calvarial osteoblasts stained for alkaline phosphatase activity after 7 days in osteogenic media. N=4 isolations per genotype.

Panel C) Representative images of Alizarin Red S staining of WT and RadKO primary osteoblast monolayers following 21 days in mineralizing conditions. Staining was quantified by solubilization of the stain in acetic acid, neutralization, and optical density measurement at 405 nm. N=3-5 isolations per genotype. **p<0.01 compared to WT by Student's *t* test.

A)

Gene	Fold Change (RadKO vs. WT)	ANOVA p-value
Runx2	+1.04	0.813
Bglap	1.00	0.993
Sp7	-1.39	0.169
Col1a1	1.00	0.406
Alpl	-1.35	0.068
MGP	**+11.28**	**0.007**

B)

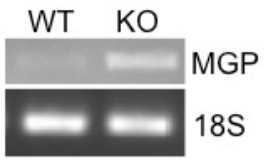

Figure 5.8: Higher expression of matrix Gla protein in Rad$^{-/-}$ osteoblasts

Panel A) Osteoblast marker gene expression from microarray analysis of WT and RadKO primary osteoblasts. N=2 isolations per genotype.

Panel B) RT-PCR analysis of MGP expression confirms its expression is elevated in RadKO osteoblasts compared to WT. N=3 isolations per genotype.

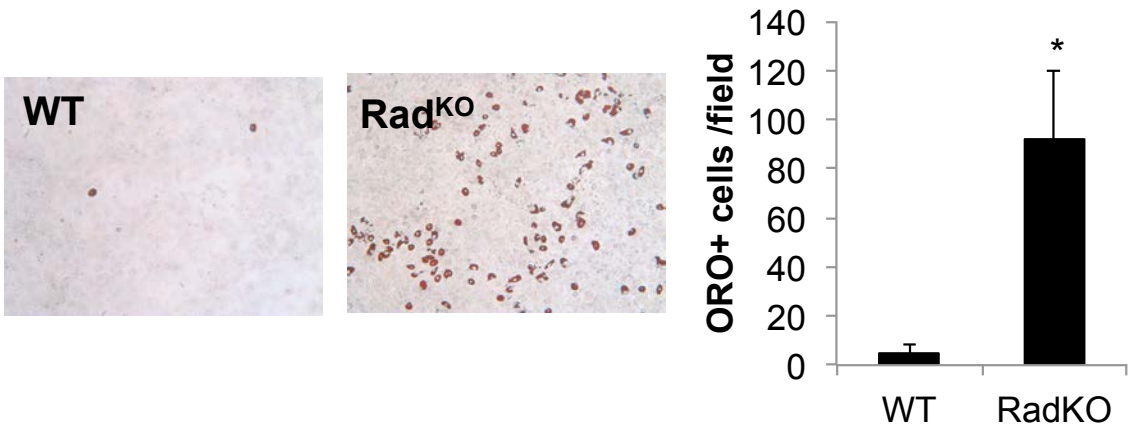

Figure 5.9: Loss of Rad results in spontaneous adipogenesis of calvarial osteoblasts *in vitro*

Representative images of wildtype and RadKO primary calvarial osteoblasts stained with Oil Red O (ORO) after 14 days in mineralizing conditions. The number of ORO-positive cells was counted for 3 random fields per isolation. N=3-4 isolations per genotype. * $p<0.05$ by Student's *t* test.

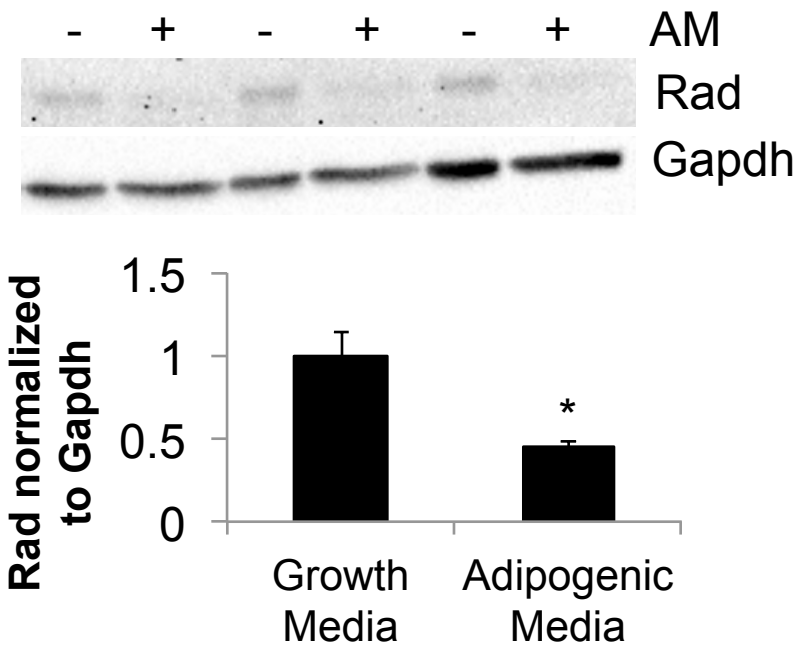

Figure 5.10: Adipogenic induction of WT osteoblasts results in a reduction in endogenous Rad levels

WT osteoblasts were maintained in growth media or adipogenic media (AM) for 7 days and harvested for Western blotting analysis of Rad and Gapdh levels. Quantification of Rad levels normalized to Gapdh is shown. N=3 isolations. * $p<0.05$ by Student's *t* test.

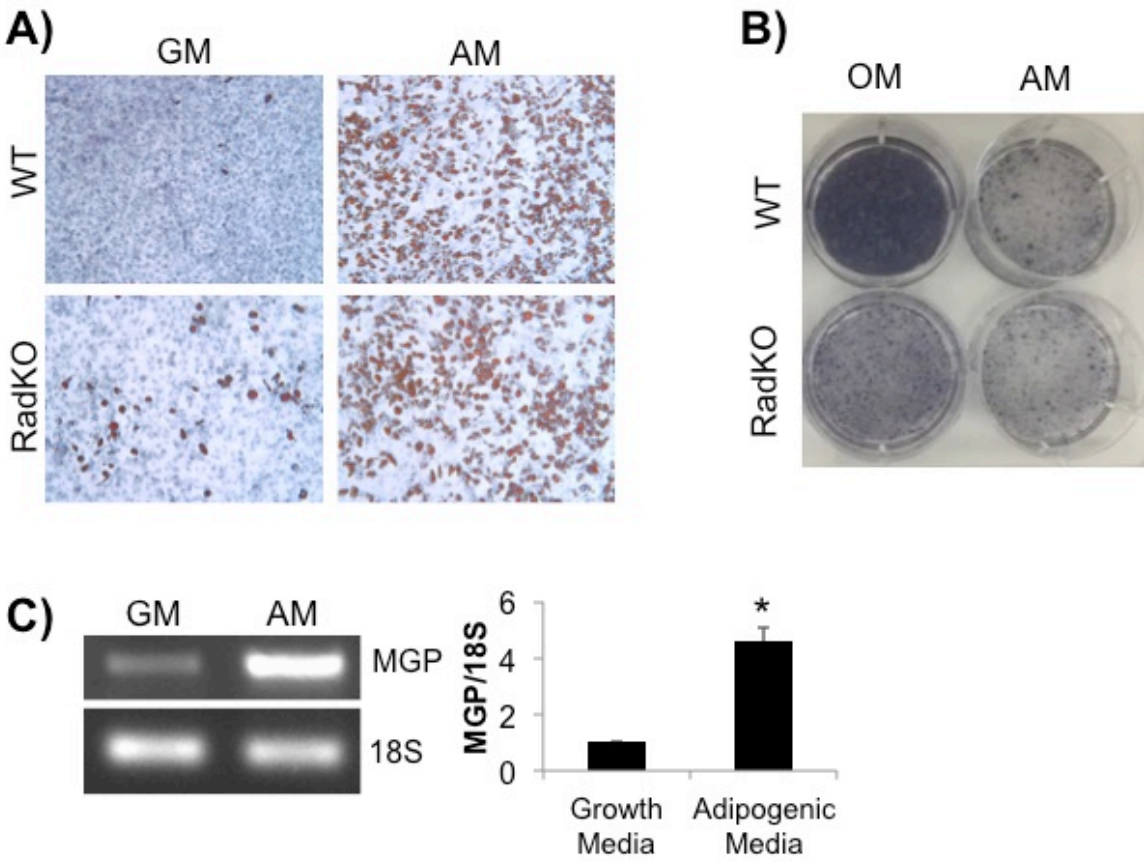

Figure 5.11: Adipogenic induction of WT cells results in a phenotype similar to Rad deletion

Panel A) Representative images of Oil Red O staining in WT and RadKO primary osteoblast monolayers following 14 days in growth (GM) or adipogenic (AM) media. Adipogenic treatment of WT and RadKO cells resulted in a marked increase in ORO^{+} cells. N=3 isolations per genotype.

Panel B) Representative images of alkaline phosphatase activity in WT and RadKO primary osteoblast monolayers following 7 days in osteogenic (OM) or adipogenic (AM) media. Adipogenic treatment of WT cells reduced alkaline

phosphatase activity to a level comparable to RadKO basally. N=3 isolations per genotype.

Panel C) RT-PCR analysis of MGP expression levels normalized to 18S RNA. RNA was isolated from WT primary osteoblasts after 3 days in growth (GM) or adipogenic (AM) media. N=3 isolations. * $p<0.05$ by Student's *t* test.

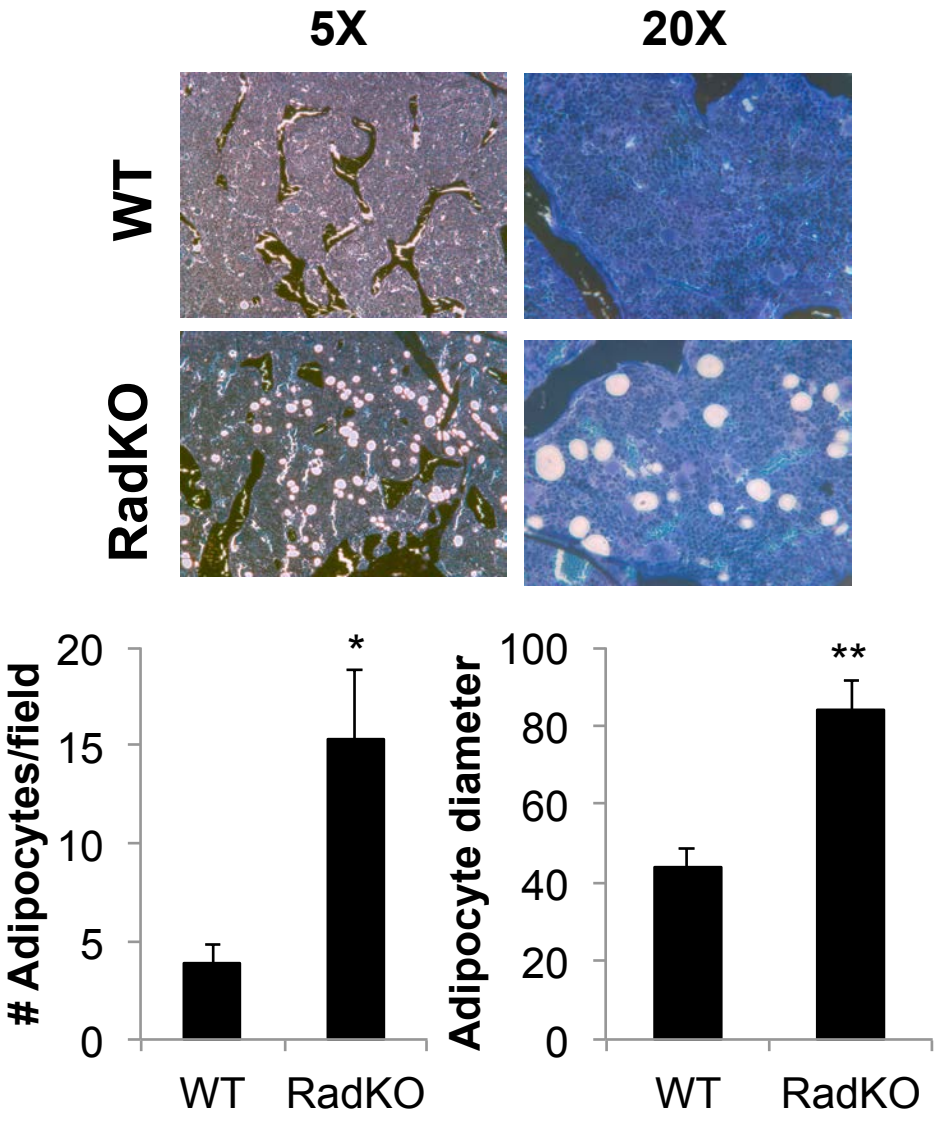

Figure 5.12: Higher bone marrow adiposity at the distal femur of Rad$^{-/-}$ mice

Representative images of Von Kossa/MacNeal's staining of thin sections from WT and RadKO femora at 5X and 20X magnification. Number of adipocytes per 20x field and the average adipocyte diameter in pixels were quantified. N=5 mice per genotype, female, 4 months of age. * $p<0.05$, ** $p<0.01$ by Student's *t* test.

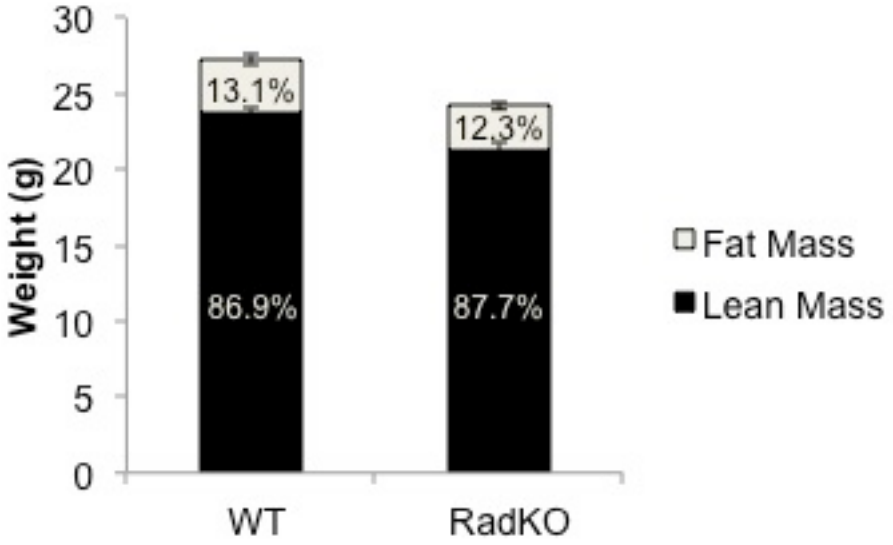

Figure 5.13: No change in global adiposity in Rad$^{-/-}$ mice

Echo-MRI analysis of body composition of WT and RadKO mice indicates no significant difference in lean or fat mass percentage. N=21 WT, 11 RadKO mice, 4 months of age, female.

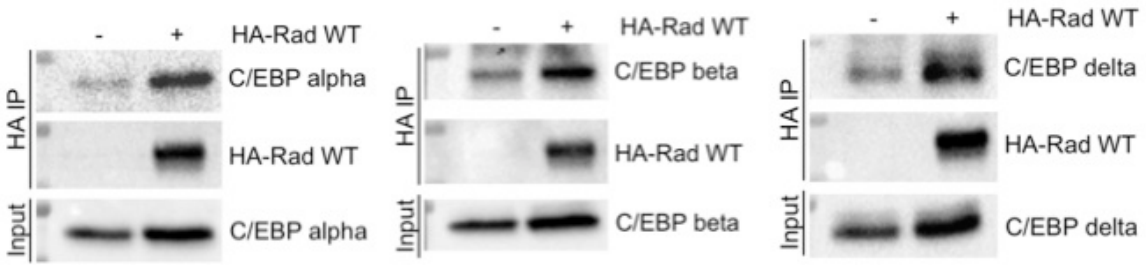

Figure 5.14: Rad interacts with C/EBP proteins

HEK293 cells were transfected with C/EBP α, β, or δ along with HA-tagged Rad WT or empty vector as a control. Immunoprecipitation with anti-HA antibody and Western blotting with the appropriate C/EBP isoform antibodies indicates that each of these three C/EBP isoforms can associate with Rad. Results are representative of 2-3 independent experiments.

Chapter 6

Discussion

The studies described in this dissertation were performed with two main objectives. The first goal was to identify potential mechanisms for the regulation of RGK (Rad, Rem, Rem2, Gem/Kir) subfamily proteins with a particular focus on Rad, given that these proteins act as intrinsic negative regulators of calcium current yet are highly expressed in excitable cell types such as cardiomyocytes and given the unusual characteristics of this subfamily compared to other Ras-related small GTPases. The second goal was to explore potential roles of Rad beyond voltage-dependent calcium channel (VDCC) regulation in light of the increasing number of reports that have found expression of this small GTPase in non-excitable cell types.

Identification of Rad/RGK subfamily regulatory mechanisms: ubiquitination and phosphorylation

The results described herein demonstrate that Rad associates with Enigma, a putative scaffolding protein with a PDZ domain and three LIM domains. This Rad-Enigma interaction likely plays a regulatory function, as Enigma is known to associate with E3 ubiquitin ligases including Smad ubiquitin regulatory factor 1 (Smurf1) as well as with protein kinases. Notably, ectopic Smurf1 expression

resulted in ubiquitination and turnover of Rad protein (**Figure 3.4**), and Enigma overexpression resulted in an increase in Rad phosphorylation at Ser39 (**Figure 4.10**), suggesting that this protein complex indeed plays a role in regulating post-translational modifications of the Rad protein. Two related and interesting questions that remain to be answered, then, are which of these proteins form a larger complex, and whether the processes of Rad phosphorylation and ubiquitination may be linked. Our studies established that Enigma associates with Rad and $Ca_V1.2$ through the LIM domains (**Figure 3.2** and **4.10**), raising the possibility of steric clash. Likewise, it is unclear whether E3 ubiquitin ligases, kinases, and RGK proteins may simultaneously bind to Enigma or whether binding of some of these components to Enigma may block association of others. Furthermore, the idea of sequential control of phosphorylation and ubiquitination requires further exploration; perhaps Rad phosphorylation is a prerequisite for ubiquitination (**Figure 6.1A**). This idea could be tested by asking whether the Rad S39A mutant, or potentially other phospho-site mutants, is subject to Smurf1-mediated degradation. Alternatively, phosphorylation of Rad could inhibit ubiquitination and turnover, since 14-3-3 dimers may impede the availability of Rad Lys204 as a substrate for E3 ubiquitin ligases (**Figure 6.1B**). Analysis of ubiquitination and Smurf1-mediated turnover of Rad S39D/E and other phosphomimetic Rad mutants could help to answer this question.

Although Enigma overexpression had no effect on the calcium channel inhibitory property of Rad despite increasing Rad Ser39 phosphorylation, the interaction between Enigma and $Ca_V1.2$ is likely not coincidental. A different but attractive

hypothesis moving forward is that Enigma may act as a scaffold that tethers Rad to the calcium channel, thereby enhancing its ability to block calcium current, potentially while also regulating turnover of Rad to fine tune calcium current. It is worth noting, however, that pilot echocardiography studies suggest that Enigma$^{-/-}$ mice do not display the Rad$^{-/-}$ cardiac phenotype and thus that Enigma is not essential for Rad function at the level of heart function (data not shown). Future studies of the role of Enigma in regulating Rad and its control of calcium current are needed, particularly Enigma knock down experiments in HEK293 cells to determine whether Rad overexpression still abolishes calcium current. Likewise, overexpression of Rad in Enigma$^{-/-}$ cardiac myocytes should be performed to determine whether Enigma is required for Rad-mediated inhibition of endogenous VDCCs. Given the roles of Enigma in interacting with Rad and the Smurf1 E3 ligase and potentially thereby controlling Rad ubiquitination and turnover (Chapter 3), promoting Rad phosphorylation (**Figure 4.9**), and interacting with the calcium channel (**Figure 4.10**), the role of Enigma in Rad regulation is likely complicated. It is conceivable that Enigma may help to localize Rad to the calcium channel while also scaffolding E3 ubiquitin ligases and kinases that might control Rad and calcium channel function.

The findings of an interaction with Enigma and of down regulation in the context of ectopic Smurf1 expression were not only demonstrated for Rad, but were found to be consistent across the RGK subfamily of GTPases (**Figures 3.1** and **3.5**). These observations suggest that Smurf1 may contribute to proteostatic regulation of each of the four RGK proteins. The subsequent studies performed

with Rad warrant repetition with the other RGK subfamily proteins, namely determining whether proteasome inhibition abolishes the Smurf1-mediated decline in RGK expression and whether Smurf1 overexpression results in an increase in ubiquitination of the other RGKs. While ubiquitination had been established as a post-translational modification of Rad protein [123, 124], the same has not yet been reported for Gem, Rem, or Rem2. Hence, should these proposed studies indicate that the other RGKs are indeed subject to Smurf1-mediated ubiquitination, the lysine residue(s) that are involved would require elucidation through mass spectrometry analysis or targeted mutagenesis of candidate lysine residues.

The contribution of the interaction between RGKs and Enigma to RGK-mediated cytoskeletal modulation is another interesting avenue for future investigation. Early work investigating the role of Rad indicated that Rad associates with the actin cytoskeleton through an interaction with the actin-binding protein β-tropomyosin [244]. Interestingly, Enigma has also been reported to localize to the actin cytoskeleton and to bind directly to β-tropomyosin through its PDZ domain, and a role has been proposed for Enigma as an adaptor protein to guide LIM domain-binding proteins to muscle cell actin filaments [245]. Notably, the PDZ domains of PDZ-LIM family proteins are highly conserved, and several of these related proteins also associate with the cytoskeleton through their PDZ domains [246-248]. Rad and Gem modulate the actin cytoskeleton as established inhibitors of Rho kinase [19], and overexpression of these RGK proteins leads to cell flattening and disassembly of stress fibers and focal adhesions [19, 20, 22].

Similarly, Enigma deletion in mouse embryonic fibroblasts inhibited stress fiber formation [249]. While it is unclear whether the roles of RGK proteins and of Enigma in the regulation of actin stress fibers are linked, it is notable that Enigma deletion, which we observed was correlated with an increase in Rad expression in the heart (**Figure 3.3**), results in a similar phenotype of impaired stress fiber formation as does Rad overexpression. Enigma is not the only PDZ-LIM family protein associated with the regulation of stress fiber assembly; CLP36 (*PDLIM1*), a protein with a PDZ domain and only one LIM domain, localizes to actin stress fibers [248], and its knock down results in the loss of stress fibers and focal adhesions with rescue of this phenotype requiring both the PDZ and LIM domains [250]. Furthermore, both Rad and Enigma have independently been reported to have roles in the translocation of glucose transporters to the plasma membrane and glucose uptake in response to insulin, a process that is known to involve rearrangement of the actin cytoskeleton [140, 251]. Notably, overexpression of full-length Enigma inhibited insulin-stimulated glucose transport, while deletion of the LIM domains, which are not required for cytoskeletal association but are involved in RGK association (**Figure 3.2**), abolished this effect [251]. *In vivo*, Rad overexpression in muscle resulted in more severe insulin resistance [252], which is consistent with the *in vitro* observation of decreased insulin-stimulated translocation of glucose transporters. Rad has also been reported to inhibit glucose transporter translocation in cancer cells [24-27]. Taken together, these reports in the literature suggest that the

interaction between Rad and Enigma may play a role in the regulation of Rad-mediated cytoskeletal remodeling in addition to calcium channel modulation.

Another key untested notion is that ubiquitin-mediated turnover might contribute to Rad regulation in the heart, particularly of Rad-mediated VDCC control. Should Enigma and Smurf1 play an important role in the regulation of Rad in cardiac myocytes, it will be important to consider the role of alternative splicing of Enigma in Rad activity. Full-length Enigma, or LIM mineralization protein-1, consists of an N-terminal PDZ domain and 3 C-terminal LIM domains as we have described here; however, alternative splicing can result in the generation of a shorter LIM mineralization protein-3 isoform that lacks the three LIM domains [170]. Since the data suggest that Rad associates via the LIM domains of Enigma, the implication is that this alternatively spliced isoform may exclude Rad. Interestingly, the related protein Enigma homolog (ENH) is alternatively spliced during heart development as well as cardiac hypertrophy [253]. Should the same be true for Enigma, this could explain the altered regulation of Rad protein levels in heart failure. In a similar vein, recent studies have reported increases in BMP-4 and 6 expression and signaling in heart failure [254, 255], presenting another potential means for Rad down regulation in this context. Bone morphogenetic protein-2 (BMP-2) was also shown to be required for cardiac contractility [256], which is in keeping with the phenotype of enhanced contractility that we observe in $Rad^{-/-}$ hearts [104]. While it remains unclear whether the down regulation of Rad in the context of heart failure is pathological or compensatory and whether proteostatic mechanisms are relevant to this regulation, understanding how Rad

levels are modulated and the role of Enigma and Smurf1 in this process could afford a potential therapeutic strategy for heart failure patients. Other interesting questions along these lines include whether Enigma or Smurf1 levels are altered in heart failure and whether and how the interaction between Rad and Enigma is regulated.

The studies in Chapter 4 of this dissertation suggest that β-adrenergic signaling promotes downstream Rad phosphorylation at Ser39 (**Figures 4.1-4.4**). While we were unable to demonstrate a change in Rad-mediated VDCC blockade in response to Rad Ser39 phosphorylation (**Figure 4.11**), co-immunoprecipitation studies suggested that Rad Ser39 phosphorylation may decrease its association with the $Ca_V\beta$2a subunit of the calcium channel and increase its association with 14-3-3 (**Figures 4.5-4.8**), and we have proposed studies in the Discussion section of Chapter 4 for further analysis of the potential regulatory role of phosphorylation in Rad-mediated calcium channel modulation.

The hypothesis that Rad Ser39 phosphorylation downstream of β-adrenergic signaling may abolish its calcium channel inhibitory properties is particularly attractive in light of the recent studies showing that mice with calcium channel knock-in mutations that eliminate phosphorylation of the channel complex through β-adrenergic signaling retain β-adrenergic responsiveness [199-201]. To determine whether Rad phosphorylation plays a key role in the acute increase in calcium current observed following β-adrenergic receptor stimulation, we could use CRISPR/Cas9 gene editing technology to mutate the endogenous Rad

Ser39 to alanine in mice, as we have successfully used this system recently to generate a floxed Rad mouse and a Flag-tagged Rad knock-in mouse (data not shown). If Rad phosphorylation at Ser39 is necessary for the β-adrenergic increases in calcium current, then the Rad S39A knock-in mouse would no longer be responsive to isoproterenol. In contrast, knocking in an S39D/E mutation into mice may be expected to generate a cardiac phenotype that mimics β-adrenergic activation in the absence of stimulus, similar to what we have reported in $Rad^{-/-}$ mice [104, 131].

While our preliminary results in Chapter 4 demonstrate Rad Ser39 phosphorylation downstream of β-adrenergic receptor and adenylyl cyclase activation using isoproterenol and forskolin, respectively (**Figures 4.1-4.3**), the endogenous kinase(s) responsible for Rad phosphorylation at this residue have not yet been identified. Namely, it is unclear whether PKA directly phosphorylates Rad or whether PKA signaling indirectly modulates Rad phosphorylation through regulation of downstream kinase(s) or phosphatase(s) that then act upon Rad. *In vitro* kinase assays would allow determination of a direct role for PKA, while a kinase siRNA library could be employed to identify kinase(s) that act upon Rad at Ser39.

Finally, the impact of β-adrenergic stimulation and Rad Ser39 phosphorylation on the subcellular localization of Rad has not yet been investigated. It is worth noting that our observation that Rad Ser39 phosphorylation enhances 14-3-3 binding reproduces what has been previously published [16, 118], but also

extends those studies as the first report of 14-3-3 association in response to a stimulus. RGK mutants deficient for 14-3-3 binding have altered subcellular distributions, and overexpression of 14-3-3 results in cytoplasmic redistribution of wildtype RGK proteins [16, 109, 113]. As mentioned above, we have recently generated a mouse with a Flag tag introduced in frame at the N-terminus of the endogenous Rad gene, and this mouse will be useful in studying the subcellular distribution of endogenous Rad protein in different cell types and in response to different stimuli, including isoproterenol and forskolin. In addition, anti-Flag immunoprecipitation from heart tissue from these mice coupled with mass spectrometry would allow analysis of the endogenous proteins that interact with Rad, with the expectation that we would observe co-immunoprecipitated Enigma and potentially other protein partners that may give further insight into Rad regulation.

Roles of Rad beyond calcium channel regulation: regulation of bone homeostasis

In Chapter 5, we demonstrated that genetic loss of Rad GTPase results in low bone mass accompanied by a dramatic expansion in bone marrow adipose tissue (BMAT) that is similar to the presentation of age-related osteoporosis in humans. We also showed that Rad is significantly down regulated during the adipogenic differentiation of primary calvarial cells, suggesting that Rad signaling may play a previously unrecognized role in directing osteogenic versus adipogenic differentiation.

An interesting area of future investigation will be the contributions of the known functions of Rad GTPase as well as the new insights made about Rad regulation in Chapters 3 and 4 of this dissertation to Rad-mediated regulation of bone homeostasis (**Figure 6.2**). Specifically, Rad-mediated calcium channel inhibition, Rad-mediated cytoskeletal modulation through regulation of Rho/ROK signaling, the interaction between Rad and Enigma, and the regulation of Rad phosphorylation through β-adrenergic signaling could each play a potential role in the $Rad^{-/-}$ phenotype of low bone density that we have reported in Chapter 5.

Does calcium channel regulation contribute to Rad's role in bone?

First, the role of Rad as an intrinsic negative regulator of calcium current has not yet been probed as a potential mechanism for Rad modulation of bone homeostasis. Importantly, both osteoblasts and osteoclasts express L-type VDCCs [257, 258]. Specifically, both mRNA and protein for the $Ca_V1.2$ subunit, the predominant $Ca_V\alpha$ subunit in the heart, have been detected in osteoblasts [259, 260]. However, since increased calcium current is correlated with an increase in bone density and a decrease in bone resorption [257], and we see a decrease in bone density in $Rad^{-/-}$ mice where we would expect increased calcium current, we do not expect calcium current to play a key role in the low bone density phenotype of $Rad^{-/-}$ mice. Nevertheless, calvarial osteoblasts from WT and $Rad^{-/-}$ mice could be isolated and subjected to voltage clamp analysis to determine whether calcium current is elevated in the absence of Rad in these cells, as we have established for cardiac myocytes [104]. In Chapter 5 of this

dissertation, we were unable to ask whether the $Rad^{-/-}$ phenotype might be complemented upon reintroduction of Rad protein. In preliminary studies, Rad overexpression not only failed to improve the deficit in calcium deposition in $Rad^{-/-}$ calvarial cells, but Rad overexpression in WT calvarial cells severely inhibited calcium deposition (data not shown). We postulate that Rad overexpression in these cells blocked calcium current and therefore interfered with osteoblast mineralization, and that Rad deletion likely impairs osteoblast differentiation and/or activity through a mechanism that is distinct from calcium channel regulation. We have previously demonstrated that the C-terminus of RGK proteins is required for calcium channel blockade [12], so we could ask whether introduction of Rad $\Delta\Delta$CT might rescue the mineralization defect in $Rad^{-/-}$ calvarial cells.

Does cytoskeletal reorganization contribute to Rad's role in bone?

While work in our laboratory has focused on the function of Rad in VDCC regulation [12, 104], the other key physiological role that has been documented for Rad is in regulation of cytoskeletal remodeling through regulation of Rho/Rho kinase signaling [19] as described in Chapter 1. Interestingly, Rho signaling plays a critical role in osteoclast-mediated bone resorption [261]. During bone resorption, osteoclasts undergo ordered cycles of migration and attachment that depend upon podosome assembly and disassembly [261]. Podosomes have an actin-rich core that is highly sensitive to actin regulatory pathways, including Rho signaling, and these structures cluster in a ring around the cell periphery [262].

Constitutively active Rho stimulates podosome formation, osteoclast motility, and bone resorption, while dominant negative Rho prevents these processes [263]. Hence, given the role of Rad as an inhibitor of Rho/ROK signaling [19], one hypothesis may be that loss of Rad results in enhanced Rho signaling to promote osteoclast-mediated resorption and lower bone density. While such a mechanism would fail to explain the decrease in bone formation observed in $Rad^{-/-}$ mice, it may be a contributing factor to the overall low bone density phenotype. In Chapter 5, we demonstrated that Rad deletion resulted in enhanced osteoclast differentiation *in vitro* that did not correlate to an increase in osteoclast surface area *in vivo*. However, future studies are necessary to probe the effects of Rad loss on osteoclast activity through either serum or urine ELISAs of bone resorption markers. If these markers are elevated in $Rad^{-/-}$ mice, altered Rho/ROK signaling should be considered as a likely contributor. Finally, Rho signaling has been implicated in the cytoskeletal rearrangements necessary for mononuclear precursors to migrate and fuse to form multinucleated osteoclasts during late stages of osteoclast differentiation [264], so enhanced Rho signaling in $Rad^{-/-}$ mononuclear cells could contribute to the increase in osteoclast differentiation observed *in vitro.*

Does the interaction with Enigma contribute to Rad's role in bone?

As outlined in the introduction to Chapter 5, the novel Rad-interacting protein Enigma/LIM mineralization protein (LMP) (Chapter 3) has an established role in osteoblast differentiation and bone homeostasis that may provide insight into the

role of Rad in these processes. Multiple studies have found that overexpression of Enigma/LMP enhances bone formation *in vitro* and *in vivo* [223-229]. Notably, there are three endogenous splice isoforms of Enigma/LMP [170]. The full-length, 457 amino acid Enigma-1/LMP-1 protein has a PDZ domain and 3 LIM domains [170] and was utilized for the studies in this dissertation. Enigma-2/LMP-2 is a 423 amino acid splice variant whose PDZ and LIM domains are intact but whose overexpression fails to induce bone formation [222]. Interestingly, Enigma-3/LMP-3 has only 153 amino acids and lacks all three LIM domains, yet it retains the property of bone formation upon overexpression [222]. Hence, the LIM domains of Enigma/LMP are dispensable for its stimulation of bone formation [222]. Since our analyses in **Figure 3.2** suggested that the LIM domains are required for Rad association with Enigma/LMP, it is possible that overexpression of the truncated Enigma-3/LMP-3 protein induces efficient bone formation through loss of regulation of Rad turnover. Studies of these three splice isoforms has indicated a 36 amino acid region within the Enigma/LMP protein that is necessary for the induction of bone formation [222]. We could ask whether the native splice isoform Enigma-2/LMP-2, which is unable to bind to Smurf1, also fails to bind to Rad. Our initial hypothesis is that overexpression of full length Enigma (LMP-1) induces bone formation through its ability to bind to both endogenous Rad and Smurf1, thereby sequestering these proteins from one another on separate Enigma scaffolds upon gross Enigma overexpression (**Figure 6.3A**). Likewise, overexpression of truncated Enigma lacking the LIM domains (LMP-3) may induce bone formation through binding to Smurf1 but not

to Rad, again effectively reducing the efficiency of Rad ubiquitination and turnover (**Figure 6.3C**). In contrast, overexpression of LMP-2 may fail to induce bone formation if it cannot bind to either Rad or Smurf1; hence, binding of Rad and Smurf1 to endogenous Enigma scaffolds would be unperturbed and Rad turnover would not be altered (**Figure 6.3B**).

Similarly, the Smurf1 E3 ubiquitin ligase that binds to Enigma and that we have demonstrated to regulate Rad ubiquitination and turnover *in vitro* (Chapter 3) plays a critical role in the regulation of osteogenesis through altering BMP/Smad signaling [187, 190]. Indeed, the potential contribution of Smurf1-mediated regulation of Rad turnover to the $Rad^{-/-}$ low bone density phenotype we have observed in Chapter 5 is highlighted by the observation in **Figure 5.10** that adipogenesis of WT calvarial cells results in a profound decrease in Rad protein levels. Further work is necessary to determine whether this decrease in Rad expression is at the transcriptional level, the post-transcriptional level, or a combination of the two. To address this issue, WT calvarial cells could be cultured in growth media or adipogenic media as described, followed by RNA isolation and qRT-PCR analysis to ask whether Rad mRNA levels are altered in this context. If adipogenic differentiation does not reduce Rad mRNA levels, then the decrease in Rad protein levels that we have observed is likely mediated through a post-transcriptional mechanism. Administration of proteasome inhibitor to WT calvarial cells in combination with the adipogenic media would aid in determining whether the decrease in Rad levels during adipogenesis is due to increased protein turnover. If proteasome inhibition would render protection of

Rad levels during adipogenesis, then we would conclude that Rad is likely subject to ubiquitination and proteasomal degradation during adipogenic differentiation. In such a case, the potential role of Smurf1 in regulating Rad protein ubiquitination and turnover during the physiological process of adipogenesis is an intriguing idea that could be tested by knocking down Smurf1 expression in these cells and asking whether Rad protein levels are reduced to the same extent during adipogenesis. Similarly, to test the role of Enigma as a scaffold that facilitates this process, calvarial osteoblasts should be isolated from $LMP^{-/-}$ mice and treated with adipogenic media to ask whether the same decline in Rad protein expression is observed.

Does β-adrenergic signaling contribute to Rad's role in bone?

The β-adrenergic signaling pathway also has established effects on bone homeostasis [265]. Both osteoblasts and osteoclasts express type 2 β-adrenergic receptors (β2ARs) [266, 267]. Studies in rodents suggest that β-adrenergic activation results in an increase in osteoclastogenesis and bone resorption [267-270], as well as a decrease in osteoblast proliferation [271, 272]. Conversely, global deletion of the three known β-adrenergic receptor subtypes results in an increase in bone mass [273], and β-adrenergic antagonism reduces bone loss following ovariectomy [274, 275], the chronic mild stress model of depression [276], and mechanical unloading [277]. In humans, some studies have correlated βAR-blocker treatment with increased bone density and a reduction in the risk of bone fractures [278-280], although not all studies have

yielded consistent results making overall conclusions about the effectiveness of beta-blockers difficult [281, 282]. Notably, patients with asthma or chronic obstructive pulmonary disease (COPD) using βAR agonists had an increased risk of bone fracture [283], and a study of pre- and post-menopausal women found an inverse correlation between sympathetic activity and bone density [284]. These studies collectively suggest that β-adrenergic signaling modulates bone homeostasis and raises the question of the role that proteins downstream of the β-adrenergic receptor may play in regulating bone formation and resorption. Administration of β-adrenergic agonists or antagonists to WT and $Rad^{-/-}$ mice followed by assessment of bone density may provide insight into the potential role that this signaling pathway may have in generating the $Rad^{-/-}$ low bone density phenotype we have observed. Measurement of circulating catecholamine levels in WT and $Rad^{-/-}$ mice by serum ELISA would also provide insights into whether sympathetic drive may contribute to the observed phenotype. Finally, the floxed Rad mouse that we have recently generated could be used to knock out Rad expression specifically in bone cells to determine whether the low bone density phenotype is intact; conversely, if the sympathetic nervous system is playing a critical role in generating the phenotype, then deletion of Rad specifically in osteoblasts, osteoclasts, adipocytes, or even MSC progenitors would be expected to have no effect on bone mineral density.

Parathyroid hormone signaling and matrix Gla protein

While β-adrenergic signaling is one candidate, the upstream pathways involved in regulating Rad signaling in bone still require elucidation. Future studies should also aim at determining whether signaling pathways known to direct bone marrow mesenchymal cell fate, such as parathyroid hormone (PTH), bone morphogenetic protein (BMP), and Wnt signaling, impact Rad expression levels and/or Rad function. Notably, the parathyroid receptor (PTH1R), like the β-adrenergic receptor, is a G-protein coupled receptor (GPCR) that signals through PKA [285]. PTH has complex effects in bone depending on the dose and the frequency of administration. Namely, continuous PTH treatment has a catabolic effect in bone through decreased osteoblast activity and increased bone resorption by osteoclasts, while intermittent PTH treatment results in increased bone formation [286]. PTH been reported to enhance osteoblast differentiation, potentially through enhanced BMP signaling [287, 288], and overexpression of PTH1R results in an increase in bone formation and a decrease in BMAT [289, 290]. More recently, Fan et al. has demonstrated that MSC-specific deletion of PTH1R results in a phenotype of increased BMAT and decreased bone density [291] that bears a resemblance to the $Rad^{-/-}$ bone phenotype described in Chapter 5. PTH administration to WT and $Rad^{-/-}$ calvarial cells, followed by assessment of mineralization, alkaline phosphatase activity, and adipogenesis, would provide a reasonable pilot study for the role of Rad in PTH-mediated osteogenesis. In addition, serum PTH levels in WT and $Rad^{-/-}$ mice could be assessed, as could plasma membrane expression of PTH1R in WT and $Rad^{-/-}$

calvarial cells. Furthermore, if Rad is required for the increase in osteogenesis downstream of PTH signaling, then overexpression of PTH1R in $Rad^{-/-}$ calvarial cells would be expected to fail to induce mineralization compared to WT.

As mentioned above, continuous PTH treatment has an opposing, catabolic effect on bone. Underscoring the potential relevance of altered PTH signaling to the $Rad^{-/-}$ bone phenotype, PTH treatment of the osteoblast-like cell line MC3T3E1 inhibited mineralization through induction of matrix Gla protein (MGP) expression [235, 236]. MGP is a 15-kDa secreted protein that was initially isolated and identified from demineralized bovine bone and whose name is derived from the presence of several mineral-binding γ-carboxyglutamic acid residues within the protein [234]. These modified amino acids, also present in osteocalcin or bone Gla protein, are generated via the action of a vitamin K-dependent γ-carboxylase enzyme on glutamic acid residues [292-294]. These Gla residues can bind to calcium and hydroxyapatite [292-294], but the precise mechanism by which MGP blocks mineralization remains unclear. We observed significant up regulation of MGP in $Rad^{-/-}$ calvarial osteoblasts at base line and in WT calvarial osteoblasts following adipogenic differentiation in **Figures 5.8** and **5.11**, suggesting that the role of Rad in PTH signaling should be further explored as expressed above. It would be worthwhile to ask whether PTH stimulation might alter Rad phosphorylation and/or ubiquitination and turnover in HEK293 cells and in primary calvarial osteoblasts. To probe the importance of the elevation in MGP expression to the $Rad^{-/-}$ phenotype of lower mineralization and spontaneous adipogenesis in calvarial osteoblast cultures, future studies should

aim at knocking down MGP expression in these primary cells to determine whether normalization of MGP expression to WT levels may rescue the observed phenotype. Conversely, we could ask whether elevated MGP expression is sufficient to drive the $Rad^{-/-}$ phenotype by overexpressing MGP in WT calvarial cells and asking whether adipogenesis is enhanced at the expense of mineralization.

Finally, the increase in the expression of MGP, an extracellular matrix protein, in $Rad^{-/-}$ calvarial cells is also intriguing in light of recent work suggesting that Rad deficiency can lead to increased cardiac fibrosis [41], which arises from excess deposition of extracellular matrix (ECM) in the heart. Specifically, loss of Rad enhanced C/EBP-δ activity and resulted in an increase in the expression of the target gene connective tissue growth factor and an increase in ECM deposition [41]. Taken together with our data, this study suggests that one role for Rad beyond calcium channel control may be regulation of the ECM. Indeed, altered ECM deposition may explain the unique mechanical phenotype of weaker but more elastic bones in $Rad^{-/-}$ mice (**Figure 5.3** and **Table 5.3**).

Does Rad regulate transcription?

Our data that Rad associates with R-Smad proteins (**Figure 3.7**) and C/EBP proteins (**Figure 5.14**), coupled with the reports that Rad associates with and regulates the transcriptional activity of the RelA subunit of NF-kB [40] and C/EBP-δ [41] and that Rad resides in the nucleus in certain settings [16, 40, 117], suggest that the function of Rad in transcriptional regulation should be further explored.

One intriguing hypothesis that could be tested is that Rad may bind to and sequester C/EBP proteins in the cytosol. In such a model, loss of Rad would increase basal C/EBP activity to promote adipogenesis. Billiard et al. demonstrated stimulus-dependent translocation of C/EBP-δ from the cytosol to the nucleus in osteoblasts [295]. Notably, this nuclear shuttling of C/EBP-δ required PKA activity, but C/EBP-δ was not itself a substrate for PKA [295]. Conversely, early *in vitro* kinase assays to characterize Rad phosphorylation indicated direct phosphorylation of Rad by PKA at an unknown site [49], and our studies in Chapter 4 of this dissertation indicate phosphorylation of Rad at serine-39 downstream of PKA signaling. Hence, we propose the idea that Rad may sequester C/EBP-δ in the cytoplasm, but that PKA activation may result in Rad phosphorylation and disassociation from C/EBP proteins, releasing C/EBPs to enter the nucleus and regulate target gene expression. Alternatively, phosphorylated Rad may remain associated with C/EBP proteins and may enter the nucleus along with C/EBPs, given the presence of NLS sequences within the

Rad protein and the reports in the literature of Rad nuclear shuttling [11, 16, 40, 117]. A first step in testing this model would be to determine whether the interaction between Rad and C/EBP-δ is direct or indirect. Next, the co-immunoprecipitation studies of Rad and C/EBP-δ in HEK293 cells (**Figure 5.14**) should be repeated using a stimulus such as isoproterenol or forskolin to activate PKA activity and induce Rad phosphorylation. If PKA-dependent phosphorylation of Rad triggers disassociation from C/EBP-δ, then we would expect these stimuli to reduce the co-immunoprecipitation of C/EBP-δ with Rad. Similarly, co-immunoprecipitation and/or binding of Rad WT with C/EBP-δ could be compared to that of phosphodeficient and phosphomimetic Rad mutants at S39 as well as other serine residues to establish the effects of Rad phosphorylation on C/EBP association as well as which phosphorylation sites are pertinent. To determine the relevance of C/EBP binding *in vivo,* we could probe for an interaction between endogenous Rad and C/EBP isoforms in calvarial cells and determine whether adipogenic treatment might abrogate this interaction to promote C/EBP-dependent gene expression. Finally, to determine the effects of Rad on C/EBP transcriptional activity, chromatin immunoprecipitation experiments could be performed to determine the promoter occupancy of C/EBP in WT versus $Rad^{-/-}$ calvarial cells, and C/EBP luciferase reporter assays could be utilized as well. We could also use the newly generated mouse line with Flag-tagged endogenous Rad to ask whether Rad is present at the promoter regions of C/EBP-regulated genes as well as to probe the subcellular localization of Rad and C/EBP-δ basally and in response to stimuli.

Clarifying the Rad$^{-/-}$ low bone density phenotype using conditional Rad-knockout mice

While the Rad$^{-/-}$ phenotype of low bone density and high bone marrow adiposity is quite striking, the deletion of Rad globally in these mice makes it difficult to draw conclusions about the underlying mechanism that drives the phenotype. Moreover, our observations that Rad deletion enhances osteoclast differentiation (**Figure 5.4**) and also decreases osteoblast mineralization *in vitro* (**Figure 5.7**) suggests that changes in both osteoblast and osteoclast activities may contribute to the low bone mass in these mice. We have recently used CRISPR/Cas9 to insert loxP sites around exons 2 and 3 of the *RRAD* gene to generate conditional Rad-knockout mice that can be combined with tamoxifen-inducible Cre recombinase expression globally or tissue specifically. These conditional Rad-knockout mice will allow selective loss of Rad in distinct cell types or lineages to probe the contributions of these cell types to the phenotype we have observed. For instance, Rad could be selectively deleted in osteoblasts by expressing Cre recombinase under the control of the type I collagen promoter (*Col1a1*-Cre) [296], while selective loss of Rad in osteoclasts could be achieved using tartrate-resistant acid phosphatase- or cathepsin K-driven Cre recombinase expression (*TRAP*-Cre or *Ctsk*-Cre, respectively) [297]. These mice would facilitate interrogation of the individual roles of osteoblasts and osteoclasts in generating the phenotype that we observe in the global Rad$^{-/-}$ mouse. Specifically, we could ask whether deletion of Rad in osteoblasts or osteoclasts alone is sufficient to recapitulate the low bone mass phenotype that we report in Chapter 5 to

determine whether the phenotype results from a decrease in bone formation, an increase in bone resorption, or a combination of the two.

Additionally, the conditional Rad-knockout mice could also be utilized in order to characterize the impact of Rad loss on osteogenic and adipogenic differentiation of mesenchymal stem cells (MSCs). Deletion of Rad in MSCs can be achieved by crossing the floxed Rad mice with *Prx1*-Cre animals [298]. We would then assess the bone density and bone marrow adiposity of these animals, with the expectation that if Rad loss indeed alters the differentiation potential of MSCs to favor adipogenesis, then we should observe a similar phenotype of low bone mass and high marrow adiposity as with global Rad deletion. We could also isolate MSCs from these animals and assess osteogenic versus adipogenic differentiation potential *in vitro*. Furthermore, MSC-specific Rad deletion could be compared to osteoblast-specific ablation of Rad expression to distinguish between the possible effects of Rad on osteoblast differentiation versus mature osteoblast function. Finally, tamoxifen injection of mice at various ages and stages in development to induce Cre expression and thus turn off Rad expression would allow us to look at the role of Rad in bone development as well as in aging.

Conclusions

In this dissertation, we have presented a novel interaction between Rad and Enigma that may regulate Rad ubiquitination and turnover, we have characterized Rad phosphorylation and altered protein interactions downstream of β-adrenergic signaling, and we have demonstrated that Rad deletion in mice perturbs bone homeostasis and the bone-fat balance. Given that Rad, unlike most Ras-related small GTPases, has not been shown to be controlled by classical GTP/GDP cycling, other mechanisms such as phosphorylation, ubiquitination, and alterations in Rad expression levels may represent key means of regulation.

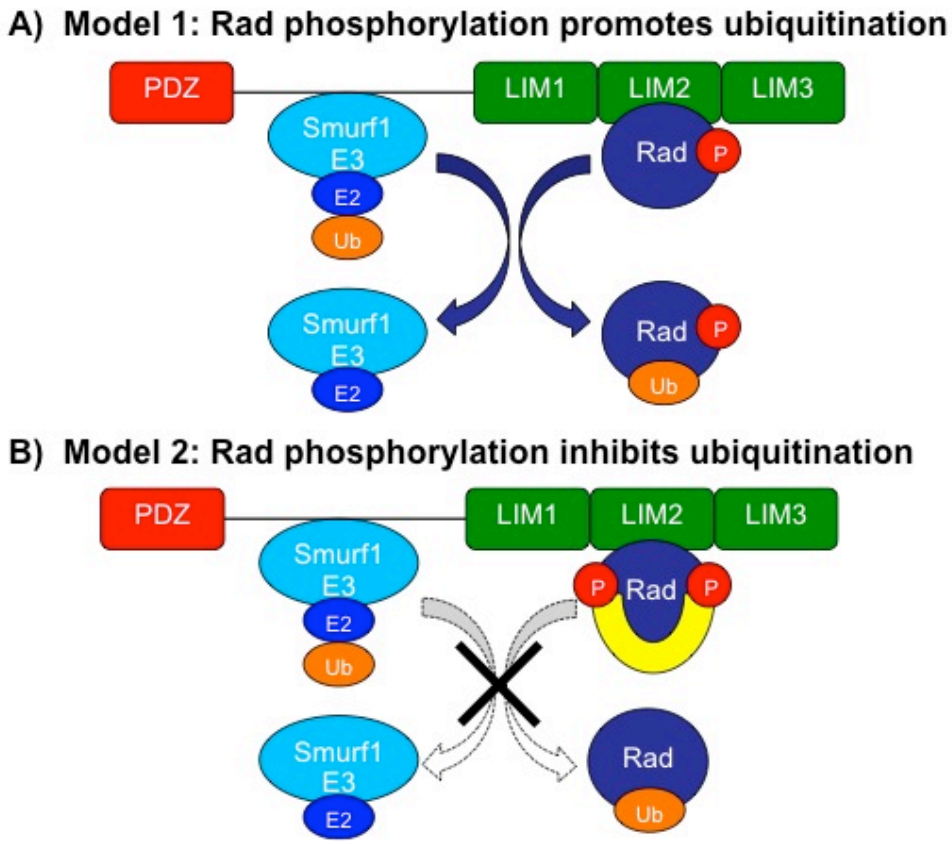

Figure 6.1: Models to integrate Rad phosphorylation and ubiquitination

Panel A) In the first model, Rad phosphorylation at Ser39 or other residues may facilitate Smurf1-mediated ubiquitination of Rad.

Panel B) In the second model, Rad phosphorylation at Ser39 (and Ser301), which is known to promote 14-3-3 binding, may impede Smurf1-mediated ubiquitination of Rad.

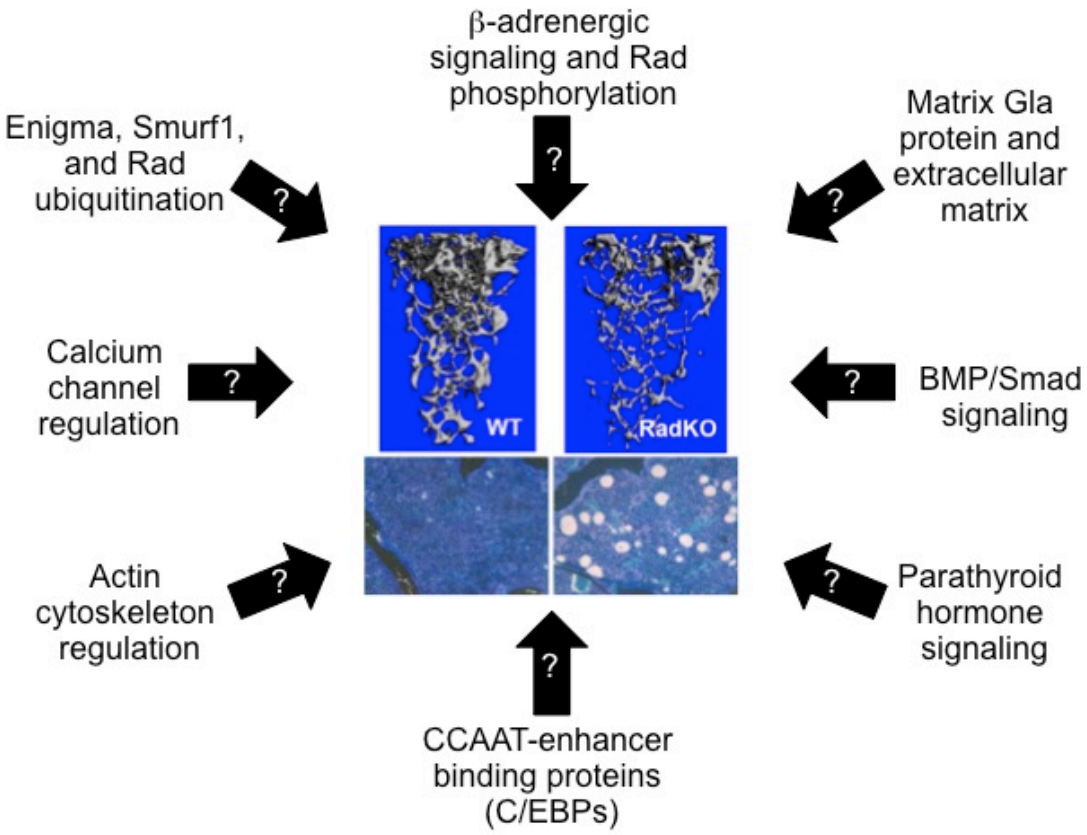

Figure 6.2: Potential contributors to the Rad$^{-/-}$ phenotype of low bone density and high bone marrow adiposity

A summary of many of the potential mechanisms that may contribute to the phenotype of low bone density and high bone marrow adiposity that we have reported in Rad$^{-/-}$ mice indicates that more work is needed to understand the role of Rad in regulating the bone-fat balance.

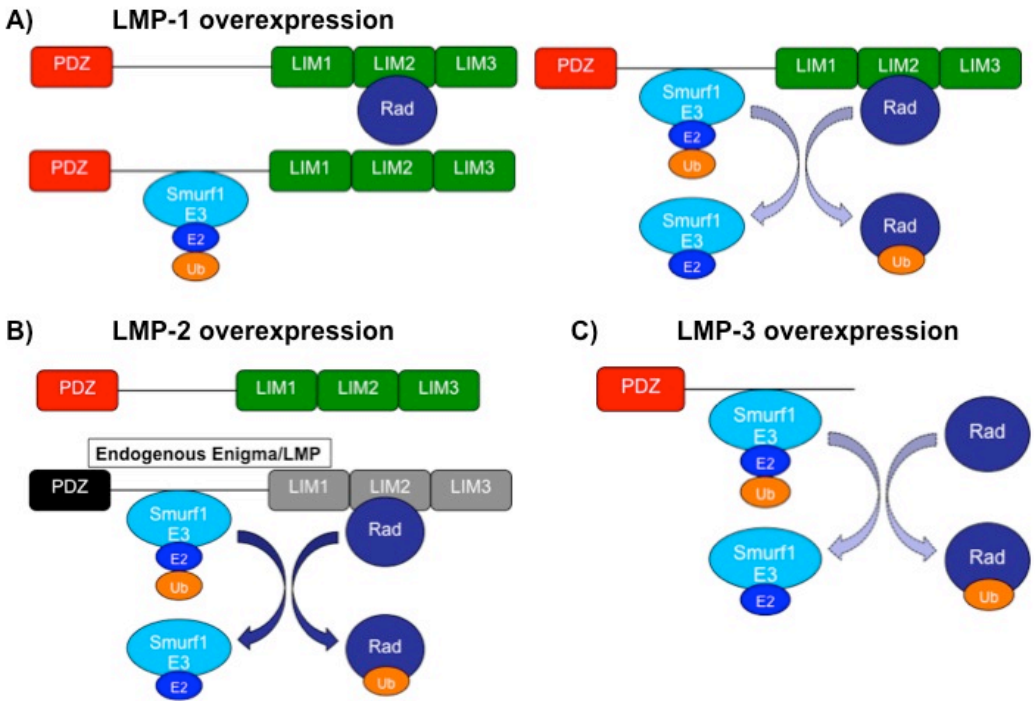

Figure 6.3: Proposed model for the role of Rad in the osteogenesis induced by overexpression of various LMP splice isoforms

Panel A) Enigma/LMP-1 overexpression induces mineralization. We propose that overexpression of LMP-1 may allow sequestration of Rad and Smurf1 on distinct LMP scaffolds to reduce the efficiency of Rad ubiquitination and turnover.

Panel B) Enigma/LMP-2 overexpression does not induce mineralization and does not bind to Smurf1. We propose that if LMP-2 also fails to bind to Rad, then Rad turnover may not be impacted by overexpression of this isoform, as Rad and Smurf1 would remain correctly localized to endogenous Enigma/LMP.

Panel C) Enigma/LMP-3 overexpression induces mineralization, despite the absence of LIM domains. We propose that overexpression of LMP-3 results in loss of regulation of Rad turnover through binding to Smurf1 but not Rad, sequestering the E3 ubiquitin ligase away from its substrate Rad.

Appendix

List of Abbreviations

AID: $Ca_V\alpha$ interaction domain

ALP: Alkaline phosphatase

AM: Adipogenic medium

Ap.Dens: Apparent density

AR: Adrenergic receptor

ARS: Alizarin Red S

ATP: Adenosine triphosphate

BCIP: 5-bromo-4-chloro-3'-indolyphosphate

BFR/BS: Bone formation rate/bone surface

BMAT: Bone marrow adipose tissue

BMP: Bone morphogenetic protein

BMPRI/II: Bone morphogenetic protein receptor I/II

BV: Bone volume

BV/TV: Bone volume fraction

CaMKII: Ca^{2+}/Calmodulin-dependent protein kinase II

cAMP: Cyclic adenosine monophosphate

cDNA: Complementary deoxyribonucleic acid

C/EBP: CCAAT-enhancer binding protein

Co-IP: Co-immunoprecipitation

Conn.D: Connectivity density

Co-Smad: Common partner Smad

CRISPR: Clustered regularly interspaced short palindromic repeats

Ct.Ar: Cortical bone area

Ct.Ar/Tt.Ar: Cortical area fraction

CTGF: Connective tissue growth factor

Ct.Th: Cortical thickness

DA: Degree of anisotropy

DAG: Diacylglycerol

DEPC: Diethyl pyrocarbonate

dLS: Double labeled surface

DMEM: Dulbecco's Modified Eagle Medium

DNA: Deoxyribonucleic acid

DNase: Deoxyribonuclease

ECM: Extracellular matrix

EDTA: Ethylene diamine tetraacetic acid

EGTA: Ethylene glycol tetraacetic acid

ELISA: Enzyme-linked immunosorbent assay

ENH: Enigma homolog

EV: Empty vector

FBS: Fetal bovine serum

GAP: GTPase activating protein

Gapdh: Glyceraldehyde 3-phosphate dehydrogenase

GDP: Guanosine diphosphate

GEF: Guanine exchange factor

Gem: Gene expressed in mitogen-stimulated T-cells

GM: Growth medium

GFP: Green fluorescent protein

Gmip: Gem-interacting protein

GPCR: G-protein coupled receptor

GK: Guanylate kinase

GSK-3: Glycogen synthase kinase-3

GST: Glutathione S-transferase

GTP: Guanosine triphosphate

HA: Hemagglutinin

HEK: Human embryonic kidney

HTN: Hypertension

HVA: High voltage-activated

I_{Ca}: Calcium current

IP_3: Inositol 1,4,5-trisphosphate

ISO: Isoproterenol

kD: Kilodaltons

Kir: Tyrosine kinase-inducible Ras-like

LIM: Lin11, Isl-1, Mec-3

LMP: LIM mineralization protein

LVA: Low voltage-activated

Ma.Ar: Medullary area

MAPK: Mitogen-activated protein kinase

MAR: Mineral apposition rate

Mat.Dens: Material density

M-CSF: Macrophage colony-stimulating factor

μCT: Microcomputed tomography

MEM: Modified Eagle Medium

MGP: Matrix Gla protein

MNC: Multinucleated cells

MRI: Magnetic resonance imaging

mRNA: Messenger RNA

MS/BS: Mineralizing surface/bone surface

MSC: Mesenchymal stem cell

NBT: Nitro blue tetrazolium

NFκB: Nuclear factor kappa-light-chain-enhancer of activated B cells

NLS: Nuclear localization signal

NMDA: N-methyl D-aspartate receptor

noLS: Unlabeled surface

Oc.S/BS: Osteoclast surface/bone surface

OD: Optical density

OM: Osteogenic medium

ORO: Oil Red O

Osx: Osterix

PBS: Phosphate buffered saline

PCR: Polymerase chain reaction

PDZ: PSD95, Dlg1, zo-1

PIP: Phosphatidyl inositol phospholipids

PIP_2: Phosphatidylinositol 4,5-bisphosphate

PKA: Protein kinase A

PKC: Protein kinase C

PKD1: Protein kinase D1

PMA: Phorbol 12-myristate 13-acetate

PTH: Parathyroid hormone

PTH1R: Parathyroid hormone receptor

Rad: Ras associated with diabetes

RadpS39: Rad phospho-serine-39

RANKL: Receptor activator of nuclear factor kappa-B ligand

Rem(2): Rad- and Gem-like (2)

RFP: Red fluorescent protein

RGK: Rad, Rem, Rem2, Gem/Kir

RNA: Ribonucleic acid

ROK: Rho kinase

R-Smad: Receptor-associated Smad

RT-PCR: Reverse transcriptase-polymerase chain reaction

Runx2: Runt-related transcription factor 2

SDS-PAGE: Sodium dodecyl sulfate-polyacrylamide gel electrophoresis

SEM: Standard error of the mean

SH3: Src homology 3

sLS: Single labeled surface

SMI: Structural model index

Smurf: Smad ubiquitin regulatory factor

SR: Sarcoplasmic reticulum

Tb.N: Trabecular number

Tb.Sp: Trabecular spacing

Tb.Th: Trabecular thickness

TGF-β: Transforming growth factor-β

TRAP: Tartrate-resistant acid phosphatase

Tt.Ar: Total cross-sectional area

TV: Total volume

Ub: Ubiquitin

VDCC: Voltage-dependent calcium channel

VKM: Von Kossa/MacNeal's stain

WB: Western blot

WT: Wildtype

References

1. Colicelli, J., *Human RAS superfamily proteins and related GTPases.* Sci STKE, 2004(250): p. RE13.
2. Bourne, H.R., Sanders, D.A., and McCormick, F., *The GTPase superfamily: a conserved switch for diverse cell functions.* Nature, 1990. **348**(6297): p. 125-32.
3. Reynet, C., and Kahn, C.R., *Rad: a member of the Ras family overexpressed in muscle of type II diabetic humans.* Science, 1993. **262**(5138): p. 1441-4.
4. Finlin, B.S., and Andres, D.A., *Rem is a new member of the Rad- and Gem/Kir Ras-related GTP-binding protein family repressed by lipopolysaccharide stimulation.* J Biol Chem, 1997. **272**(35): p. 21982-8.
5. Finlin, B.S., Shao, H., Kadono-Okuda K., Guo, N., and Andres, D.A., *Rem2, a new member of the Rem/Rad/Gem/Kir family of Ras-related GTPases.* Biochem J, 2000. **347 Pt 1**: p. 223-31.
6. Maguire, J., Santoro, T., Jensen, P., Siebenlist, U., Yewdell, J., and Kelly, K., *Gem: an induced, immediate early protein belonging to the Ras family.* Science, 1994. **265**(5169): p. 241-4.
7. Opatowsky, Y., Sasson, Y., Shaked, I., Ward, Y., Chomsky-Hecht, O., Litvak, Y., Selinger, Z., Kelly, K., and Hirsch, J.A., *Structure-function studies of the G-domain from human gem, a novel small G-protein.* FEBS Lett, 2006. **580**(25): p. 5959-64.
8. Splingard A., M.J., Perderiset M., Cicolari J., Regazzoni K., Hamoudi F., Cabanie L. El Marjou A., Wells A., Houdusse A., and de Gunzburg, J., *Biochemical and structural characterization of the gem GTPase.* J Biol Chem, 2007. **282**(3): p. 1905-15.
9. Yanuar, A., Sakurai, S., Kitano, K., and Hakoshima, T., *Crystal structure of human Rad GTPase of the RGK-family.* Genes Cells, 2006. **11**(8): p. 961-8.
10. Del Villar, K., Dorin, D., Sattler, I., Urano, J., Poullet, P., Robinson, N., Mitsuzawa, H., and Tamanoi, F., *C-terminal motifs found in Ras-superfamily G-proteins: CAAX and C-seven motifs.* Biochem Soc Trans, 1996. **24**(3): p. 709-13.
11. Correll, R.N., Pang, C., Niedowicz, D.M., Finlin, B.S., and Andres, D.A., *The RGK family of GTP-binding proteins: regulators of voltage-dependent calcium channels and cytoskeleton remodeling.* Cell Signal, 2008. **20**(2): p. 292-300.
12. Finlin, B.S., Crump, S.M., Satin, J., and Andres, D.A., *Regulation of voltage-gated calcium channel activity by the Rem and Rad GTPases.* Proc Natl Acad Sci U S A, 2003. **100**(24): p. 14469-74.
13. Finlin, B.S., Mosley, A.L., Crump, S.M., Correll, R.N., Ozcan, S., Satin, J., and Andres, D.A., *Regulation of L-type Ca2+ channel activity and insulin secretion by the Rem2 GTPase.* 2005.

14. Beguin, P., Nagashima, K., Gonoi, T., Shibasaki, T., Takahashi, K., Kashima, Y., Ozaki, N., Geering, K., Iwanaga, T., and Seino, S., *Regulation of Ca2+ channel expression at the cell surface by the small G-protein kir/Gem.* Nature, 2001. **411**(6838): p. 701-6.
15. Finlin, B.S., Correll, R.N., Pang, C., Crump, S.M., Satin, J., and Andres, D.A., *Analysis of the complex between Ca2+ channel beta-subunit and the Rem GTPase.* J Biol Chem, 2006. **281**(33): p. 23557-66.
16. Beguin, P., Mahalakshmi, R.N., Nagashima, K., Cher, D.H., Ikeda, H., Yamada, Y., Seino, Y., and Hunziker, W., *Nuclear sequestration of beta-subunits by Rad and Rem is controlled by 14-3-3 and calmodulin and reveals a novel mechanism for Ca2+ channel regulation.* J Mol Biol, 2006. **355**(1): p. 34-46.
17. Yang, T., Xu, X., Kernan, T., Wu, V., and Colecraft, H.M., *Rem, a member of the RGK GTPases, inhibits recombinant CaV1.2 channels using multiple mechanisms that require distinct conformations of the GTPase.* J Physiol, 2010. **588**(Pt 10): p. 1665-81.
18. Yang, T., Puckerin, A., and Colecraft, H.M., *Distinct RGK GTPases differentially use a1- and auxiliary b-binding-dependent mechanisms to inhibit CaV1.2/CaV2.2 channels.* PLoS One, 2012. **7**(5): p. e37079.
19. Ward, Y., Yap, S.F., Ravichandran, V., Matsumura, F., Ito, M., Spinelli, B., and Kelly, K., *The GTP binding proteins Gem and Rad are negative regulators of the Rho-Rho kinase pathway.* J Cell Biol, 2002. **157**(2): p. 291-302.
20. Fu, M., Zhang, J., Tseng, Y.H., Cui, T., Zhu, X., Xiao, Y., Mou, Y., De Leon, H., Chang, M.M., Hamamori, Y., Kahn, C.R., and Chen, Y.E., *Rad GTPase attenuates vascular lesion formation by inhibition of vascular smooth muscle cell migration.* Circulation, 2005. **111**(8): p. 1071-7.
21. Olson, M.F., *Gem GTPase: between a ROCK and a hard place.* Curr Biol, 2002. **12**(14): p. R496-8.
22. Hatzoglou, A., Ader, I., Splingard, A., Flanders, J., Saade, E., Leroy, I., Traver, S., Aresta, S., and de Gunzburg, J., *Gem associates with Ezrin and acts via the Rho-GAP protein Gmip to down-regulate the Rho pathway.* Mol Biol Cell, 2007. **18**(4): p. 1242-52.
23. Gunton, J.E., Sisavanh, M., Stokes, R.A., Satin, J., Satin, L.S., Zhang, M., Liu, S.M., Cai, W., Cheng, K., Cooney, G.J., Laybutt, D.R., So, T., Molero, J.C., Grey, S.T., Andres, D.A., Rolph, M.S., and Mackay, C.R., *Mice deficient in GEM GTPase show abnormal glucose homeostasis due to defects in beta-cell calcium handling.* PLoS One, 2012. **7**(6): p. e39462.
24. Zhang, C., Liu, J., Wu, R., Liang, Y., Lin, M., Liu, J., Chan, C.S., Hu, W., and Feng, Z., *Tumor suppressor p53 negatively regulates glycolysis stimulated by hypoxia through its target RRAD.* Oncotarget, 2014. **5**(14): p. 5535-46.
25. Liu, J., Zhang, C., Wu, R., Lin, M., Liang, Y., Liu, J., Wang, X., Yang, B., and Feng, Z., *RRAD inhibits the Warburg effect through negative regulation of the NF-kB signaling.* Oncotarget, 2015. **6**(17): p. 14982-92.

26. Shang, R., Wang, J., Sun, W., Dai, B., Ruan, B., Zhang, Z., Yang, X., Gao, Y., Qu, S., Lv, X., Tao, K., Wang, L., Dou, K., and Wang, D., *RRAD inhibits aerobic glycolysis, invasion, and migration and is associated with poor prognosis in hepatocellular carcinoma.* Tumour Biol, 2016. **37**(4): p. 5097-105.
27. Yan, Y., Xie, M., Zhang, L., Zhou, X., Xie, H., Zhou, L., Zheng, S., and Wang, W., *Ras-related associated with diabetes gene acts as a suppressor and inhibits Warburg effect in hepatocellular carcinoma.* Onco Targets Ther, 2016. **9**: p. 3925-37.
28. Tseng, Y.H., Vicent, D., Zhu, J., Niu, Y., Adeyinka, A., Moyers, J.S., Watson, P.H., and Kahn, C.R., *Regulation of growth and tumorigenicity of breast cancer cells by the low molecular weight GTPase Rad and nm23.* Cancer Res, 2001. **61**(5): p. 2071-9.
29. Lee, I., Yeom, S.Y., Lee, S.J., Kang, W.K., and Park, C., *A novel senescence-evasion mechanism involving Grap2 and Cyclin D interacting protein inactivation by Ras associated with diabetes in cancer cells under doxorubicin treatment.* Cancer Res, 2010. **70**(11): p. 4357-65.
30. Hsiao, B.Y., Chen, C.C., Hsieh, P.C., Chang, T.K., Yeh, Y.C., Wu, Y.C., Hsu, H.S., Wang, F.F., and Chou, T.Y., *Rad is a p53 direct transcriptional target that inhibits cell migration and is frequently silenced in lung carcinoma cells.* J Mol Med (Berl), 2011. **89**(5): p. 481-92.
31. Lin, Z.Y., and Chuang, W.L., *Genes responsible for the characteristics of primary cultured invasive phenotype hepatocellular carcinoma cells.* Biomed Pharmacother, 2012. **66**(6): p. 454-8.
32. Mo, Y., Midorikawa, K., Zhang, Z., Zhou, X., Ma, N., Huang, G., Hiraku, Y., Oikawa, S., and Murata, M., *Promoter hypermethylation of Ras-related GTPase gene RRAD inactivates a tumor suppressor function in nasopharyngeal carcinoma.* Cancer Lett, 2012. **323**(2): p. 147-54.
33. Yeom, S.Y., Lee, S.J., Kim, W.S., and Park, C., *Rad knockdown induces mitochondrial apoptosis in bortezomib resistant leukemia and lymphoma cells.* Leuk Res, 2012. **36**(9): p. 1172-8.
34. Szymanowska-Narloch, A., Jassem, E., Skrzypski, M., Muley, T., Meister, M., Dienemann, H., Taron, M., Rosell, R., Rzepko, R., Jarzab, M., Marjanski, T., Pawlowski, R., Rzyman, W., and Jassem, J., *Molecular profiles of non-small cell lung cancers in cigarette smoking and never-smoking patients.* Adv Med Sci, 2013. **58**(2): p. 196-206.
35. Jin, Z., Feng, X., Jian, Q., Cheng, Y., Gao, Y., Zhang, X., Wang, L., Zhang, Y., Huang, W., Fan, X., Chen, S., Yu, H., Zhao, Z., Dong, M., Liu, J., Mori, Y., and Meltzer, S.J., *Aberrant methylation of the Ras-related associated with diabetes gene in human primary esophageal cancer.* Anticancer Res, 2013. **33**(11): p. 5199-203.
36. Laurberg, J.R., Jensen, J.B., Schepeler, T., Borre, M., Orntoft, T.F., and Dyrskjot, L., *High expression of GEM and EDNRA is associated with metastasis and poor outcome in patients with advanced bladder cancer.* BMC Cancer, 2014. **14**: p. 638.

37. Huang, X., Cong, X., Yang, D., Ji, L., Liu, Y., Cui, X., Cai, J., He, S., Zhu, C., Ni, R., and Zhang, Y., *Identification of Gem as a new candidate prognostic marker in hepatocellular carcinoma.* Pathol Res Pract, 2014. **210**(11): p. 719-25.
38. Wang, Y., Li, G., Mao, F., Li, X., Liu, Q., Chen, L., Lv, L., Wang, X., Wu, J., Dai, W., Wang, G., Zhao, E., Tang, K.F., and Sun, Z.S., *Ras-induced epigenetic inactivation of the RRAD (Ras-related associated with diabetes) gene promotes glucose uptake in a human ovarian cancer model.* J Biol Chem, 2014. **289**(20): p. 14225-38.
39. Ma, J., Hou, X., Li, M., Ren, H., Fang, S., Wang, X., and He, C., *Genome-wide methylation profiling reveals new biomarkers for prognosis prediction of glioblastoma.* J Cancer Res Ther, 2015. **11 Suppl 2**: p. C212-5.
40. Hsiao, B.Y., Chang, T.K., Wu, I.T., and Chen, M.Y., *Rad GTPase inhibits the NFkB pathway through interacting with RelA/p65 to impede its DNA binding and target gene transactivation.* Cell Signal, 2014. **26**(7): p. 1437-44.
41. Zhang, J., Chang, L., Chen, C., Zhang, M., Luo, Y., Hamblin, M., Villacorta, L., Xiong, J.W., Chen, Y.E., Zhang, J., and Zhu, X., *Rad GTPase inhibits cardiac fibrosis through connective tissue growth factor.* Cardiovasc Res, 2011. **91**(1): p. 90-8.
42. Edel, M.J., Menchon, C., Menendez, S., Consiglio, A., Raya, A., and Izpisua Belmonte, J.C., *Rem2 GTPase maintains survival of human embryonic stem cells as well as enhancing reprogramming by regulating p53 and cyclin D1.* Genes Dev, 2010. **24**(6): p. 561-73.
43. Edel, M.J., Boue, S., Menchon, C., Sanchez-Danes, A., and Izpisua Belmonte, J.C., *Rem2 GTPase controls proliferation and apoptosis of neurons during embryo development.* Cell Cycle, 2010. **9**(17): p. 3414-22.
44. Satija, N.K., Sharma, D., Afrin, F., Tripathi, R.P., and Gangenahalli, G., *High throughput transcriptome profiling of lithium stimulated human mesenchymal stem cells reveals priming towards osteoblastic lineage.* PLoS One, 2013. **8**(1): p. e55769.
45. Pennings, J.L., van Dartel, D.A., Pronk, T.E., Hendriksen, P.J., and Piersma, A.H., *Identification by gene coregulation mapping of novel genes involved in embryonic stem cell differentiation.* Stem Cells Dev, 2011. **20**(1): p. 115-26.
46. Shimizu-Nishikawa, K., Tsuji, S., and Yoshizato, K., *Identification and characterization of newt rad (ras associated with diabetes), a gene specifically expressed in regenerating limb muscle.* Dev Dyn, 2001. **220**(1): p. 74-86.
47. Laville, M., Auboeuf, D., Khalfallah, Y., Vega, N., Riou, J.P., and Vidal, H., *Acute regulation by insulin of phosphatidylinositol-3-kinase, Rad, Glut 4, and lipoprotein lipase mRNA levels in human muscle.* J Clin Invest, 1996. **98**(1): p. 43-9.
48. Sonna, L.A., Gaffin, S.L., Pratt, R.E., Cullivan, M.L., Angel, K.C., and Lilly, C.M., *Effect of acute heat shock on gene expression by human peripheral blood mononuclear cells.* J Appl Physiol (1985), 2002. **92**(5): p. 2208-20.

49. Moyers, J.S., Zhu, J., and Kahn, C.R., *Effects of phosphorylation on function of the Rad GTPase.* Biochem J, 1998. **333**(Pt 3): p. 609-14.
50. Tan, F.L., Moravec, C.S., Li, J., Apperson-Hansen, C., McCarthy, P.M., Young, J.B., and Bond, M., *The gene expression fingerprint of human heart failure.* Proc Natl Acad Sci U S A, 2002. **99**(17): p. 11387-92.
51. Magnusson, C., Svensson, A., Christerson, U., and Tagerud, S., *Denervation-induced alterations in gene expression in mouse skeletal muscle.* Eur J Neurosci, 2005. **21**(2): p. 577-80.
52. Kannangai, R., Diehl, A.M., Sicklick, J., Rojkind, M., Thomas, D., and Torbenson, M., *Hepatic angiomyolipoma and hepatic stellate cells share a similar gene expression profile.* Hum Pathol, 2005. **36**(4): p. 341-7.
53. Wyatt, S.M., Kraus, F.T., Roh, C.R., Elchalal, U., Nelson, D.M., and Sadovsky, Y., *The correlation between sampling site and gene expression in the term human placenta.* Placenta, 2005. **26**(5): p. 372-9.
54. Hawke, T.J., Kanatous, S.B., Martin, C.M., Goetsch, S.C., and Garry, D.J., *Rad is temporally regulated within myogenic progenitor cells during skeletal muscle regeneration.* Am J Physiol Cell Physiol, 2006. **290**(2): p. C379-87.
55. Wu, X., Wang, J., Cui, X., Maianu, L., Rhees, B., Rosinski, J., So, W.V., Willi, S.M., Osier, M.V., Hill, H.S., Page, G.P., Allison, D.B., Martin, M., and Garvey, W.T., *The effect of insulin on expression of genes and biochemical pathways in human skeletal muscle.* Endocrine, 2007. **31**(1): p. 5-17.
56. Bierings, R., Beato, M., and Edel, M.J., *An endothelial cell genetic screen identifies the GTPase Rem2 as a suppressor of p19ARF expression that promotes endothelial cell proliferation and angiogenesis.* J Biol Chem, 2008. **283**(7): p. 4408-16.
57. Coletta, D.K., Balas, B., Chavez, A.O., Baig, M., Abdul-Ghani, M., Kashyap, S.R., Folli, F., Tripathy, D., Mandarino, L.J., Cornell, J.E., Defronzo, R.A., and Jenkinson, C.P., *Effect of acute physiological hyperinsulinemia on gene expression in human skeletal muscle in vivo.* Am J Physiol Endocrinol Metab, 2008. **294**(5): p. E910-7.
58. Jackson, A., McWilliams, C., Kaizer, E., Chaussabel, D., Glaser, C., Noguchi, H., Matsumoto, S., Levy, M.F., and Naziruddin, B., *Gene expression profiling of human pancreatic islets undergoing a simulated process of instant blood-mediated inflammatory reaction.* Transplant Proc, 2008. **40**(2): p. 430-2.
59. Porterfield, V.M.a.M., E.M., *Temporal patterns of light-induced immediate-early gene expression in the suprachiasmatic nucleus.* Neurosci Lett, 2009. **463**(1): p. 70-3.
60. Liu, L., Zhu, J., Glass, P.S., Brink, P.R., Rampil, I.J., and Rebecchi, M.J., *Age-associated changes in cardiac gene expression after preconditioning.* Anesthesiology, 2009. **111**(5): p. 1052-64.
61. Halter, B., Gonzalez de Aguilar, J.L., Rene, F., Petri, S., Fricker, B., Echaniz-Laguna, A., Dupuis, L., Larmet, Y., and Loeffler, J.P., *Oxidative stress in skeletal muscle stimulates early expression of Rad in a mouse*

model of amyotrophic lateral sclerosis. Free Radic Biol Med, 2010. **48**(7): p. 915-23.
62. Luo, Y., Zhang, M., Zhang, J., Zhang, J., Chen, C., Chen, Y.E., Xiong, J.W., and Zhu, X., *Platelet-derived growth factor induces Rad expression through Egr-1 in vascular smooth muscle cells.* PLoS One, 2011. **6**(4): p. e19408.
63. White, R.E., Palm, C., Xu, L., Ling, E., Ginsburg, M., Daigle, B.J., Han, R., Patterson, A., Altman, R.B., and Giffard, R.G., *Mice lacking the β2 adrenergic receptor have a unique genetic profile before and after focal brain ischaemia.* ASN Neuro, 2012. **4**(5): p. e00096.
64. Jhun, B.S., O-Uchi, J., Wang, W., Ha, C.H., Zhao, J., Kim, J.Y., Wong, C., Dirksen, R.T., Lopes, C.M., and Jin, Z.G., *Adrenergic signaling controls RGK-dependent trafficking of cardiac voltage-gating L-type Ca2+ channels through PKD1.* Circ Res, 2012. **110**(1): p. 59-70.
65. Jackson, A.M., Kanak, M.A., Grishman, E.K., Chaussabel, D., Levy, M.F., and Naziruddin, B., *Gene expression changes in human islets exposed to type 1 diabetic serum.* Islets, 2012. **4**(4): p. 312-9.
66. Wang, Y., Cheng, X., Zhou, Z., Wu, H., Long, L., Gu, X., and Xu, G., *Increased expression of Gem after rat sciatic nerve injury.* J Mol Histol, 2013. **44**(1): p. 27-36.
67. Pope, N.J., and Bresknick, E.H., *Establishment of a cell-type-specific genetic network by the mediator complex component Med1.* Mol Cell Biol, 2013. **33**(10): p. 1938-55.
68. Wen, H., Cao, J., Yu, X., Sun, B., Ding, T., Li, M., Li, D., Wu, H., Long, L., Xu, G., and Zhang, F., *Spatiotemporal patterns of Gem expression after rat spinal cord injury.* Brain Res, 2013. **1516**: p. 11-9.
69. Ghiretti, A.E., Moore, A.R., Brenner, R.G., Chen, L.F., West, A.E., Lau, N.C., Van Hooser, S.D., and Paradis, S., *Rem2 is an activity-dependent negative regulator of dendritic complexity in vivo.* J Neurosci, 2014. **34**(2): p. 392-407.
70. Xu, F., Huang, H., Wu, Y., Lu, L., Jiang, L., Chen, L., Zeng, S., Li, L., and Li, M., *Upregulation of Gem relates to retinal ganglion cells apoptosis after optic nerve crush in adult rats.* J Mol Histol, 2014. **45**(5): p. 565-71.
71. Rovsing, L., and Moller M., *Photic stimulation of the suprachiasmatic nucleus via the non-visual optic system. A gene expression study in the blind Crx-/- mouse.* Cell Tissue Res, 2014. **358**(1): p. 239-48.
72. Liao, W.L., Tan, M.W., Yuan, Y., Wang, G.K., Wang, C., Tang, H., and Xu, Z.Y., *Brahma-related gene 1 inhibits proliferation and migration of human aortic smooth muscle cells by directly up-regulating Ras-related associated with diabetes in the pathophysiologic processes of aortic dissection.* J Thorac Cardiovasc Surg, 2015. **150**(5): p. 1292-301.
73. Scamps, F., Sangari, S., Bowerman, M., Rousset, M., Bellis, M., Cens, T., and Charnet, P., *Nerve injury induces a Gem-GTPase-dependent downregulation of P/Q-type Ca2+ channels contributing to neurite plasticity in dorsal root ganglion neurons.* Pflugers Arch, 2015. **467**(2): p. 351-66.

74. Ghosh, S., Mitra, P.S., Loffredo, C.A., Trnovec, T., Murinova, L., Sovcikova, E., Ghimbovschi, S., Zang, S., Hoffman, E.P., and Dutta, S.K., *Transcriptional profiling and biological pathway analysis of human equivalence PCB exposure in vitro: indicator of disease and disorder development in humans.* Environ Res, 2015. **138**: p. 202-16.
75. Bourne, H.R., Sanders, D.A., and McCormick, F., *The GTPase superfamily: conserved structure and molecular mechanism.* Nature, 1991. **349**(6305): p. 117-27.
76. Zhu, J., Reynet, C., Caldwell, J.S., and Kahn, C.R., *Characterization of Rad, a new member of Ras/GTPase superfamily, and its regulation by a unique GTPase-activating protein (GAP)-like activity.* J Biol Chem, 1995. **270**(9): p. 4805-12.
77. Sasson, Y., Navon-Perry, L., Huppert, D., and Hirsch, J.A., *RGK family G-domain:GTP analog complex structures and nucleotide-binding properties.* J Mol Biol, 2011. **413**(2): p. 372-89.
78. Zhu, J., Tseng, Y.H., Kantor, J.D., Rhodes, C.J., Zetter, B.R., Moyers, J.S., and Kahn, C.R., *Interaction of the Ras-related protein associated with diabetes rad and the putative tumor metastasis suppressor NM23 provides a novel mechanism of GTPase regulation.* Proc Natl Acad Sci U S A, 1999. **96**(26): p. 14911-8.
79. Reymond, P., Coquard, A., Chenon, M., Zeghouf, M., El Marjou, A., Thompson, A., and Menetrey, J., *Structure of the GDP-bound G domain of the RGK protein Rem2.* Acta Crystallogr Sect F Struct Biol Cryst Commun, 2012. **68**(Pt 6): p. 626-31.
80. Pasqualato, S., Renault, L., and Cherfils, J., *Arf, Arl, Arp, and Sar proteins: a family of GTP-binding proteins with a structural device for 'front-back' communication.* EMBO Rep, 2002. **3**(11): p. 1035-41.
81. Scheffzek, K., Klebe, C., Fritz-Wolf, K., Kabsch, W., and Wittinghofer, A., *Crystal structure of the nuclear Ras-related protein Ran in its GDP-bound form.* Nature, 1995. **374**(6520): p. 378-81.
82. Feig, L.A., and Cooper, G.M., *Inhibition of NIH 3T3 cell proliferation by a mutant ras protein with preferential affinity for GDP.* Mol Cell Biol, 1988. **8**(8): p. 3235-43.
83. Feig, L.A., *Tools of the trade: use of dominant-inhibitory mutants of Ras-family GTPases.* Nat Cell Biol, 1999. **1**(2): p. E25-7.
84. Yamakawa, H., Murata, M., Suzuki, T., Yada, H., Ishida, H., Aizawa, Y., Adachi, T., Kamiya, K., and Fukuda, K., *Suppression of Rad leads to arrhythmogenesis via PKA-mediated phosphorylation of ryanodine receptor activity in the heart.* Biochem Biophys Res Commun, 2014. **452**(3): p. 701-7.
85. Yada, H., Murata, M., Shimoda, K., Yuasa, S., Kawaguchi, H., Ieda, M., Adachi, T., Murata, M., Ogawa, S., and Fukuda, K., *Dominant negative suppression of Rad leads to QT prolongation and causes ventricular arrhythmias via modulation of L-type Ca2+ channels in the heart.* Circ Res, 2007. **101**(1): p. 69-77.

86. Wang, G., Zhu, X., Xie, W., Han, P., Li, K., Sun, Z., Wang, Y., Chen, C., Song, R., Cao, C., Zhang, J., Wu, C., Liu, J., and Cheng, H., *Rad as a novel regulator of excitation-contraction coupling and beta-adrenergic signaling in heart.* Circ Res, 2010. **106**(2): p. 317-27.
87. Xu, X., Marx, S.O., and Colecraft, H.M., *Molecular mechanisms, and selective pharmacological rescue, of Rem-inhibited Cav1.2 channels in heart.* Circ Res, 2010. **107**(5): p. 620-30.
88. Chang, D.D., and Colecraft, H.M., *Rad and Rem are non-canonical G-proteins with respect to the regulatory role of guanine nucleotide binding in Ca(V)1.2 channel regulation.* J Physiol, 2015. **593**(23): p. 5075-90.
89. Pan, J.Y., Fieles, W.E., White, A.M., Egerton, M.M., and Silberstein, D.S., *Ges, A human GTPase of the Rad/Gem/Kir family, promotes endothelial cell sprouting and cytoskeleton reorganization.* J Cell Biol, 2000. **149**(5): p. 1107-16.
90. Sasaki, T., Shibasaki, T., Beguin, P., Nagashima, K., Miyazaki, M., and Seino, S., *Direct inhibition of the interaction between alpha-interaction domain and beta-interaction domain of voltage-dependent Ca2+ channels by Gem.* J Biol Chem, 2005. **280**(10): p. 9308-12.
91. Aresta, S., de Tand-Heim, M.F., Beranger, F., and de Gunzburg, J., *A novel Rho GTPase-activating-protein interacts with Gem, a member of the Ras superfamily of GTPases.* Biochem J, 2002. **367**(Pt 1): p. 57-65.
92. Andrieu, G., Quaranta, M., Leprince, C., Cuvillier, O., and Hatzoglou, A., *Gem GTPase acts upstream Gmip/RhoA to regulate cortical actin remodeling and spindle positioning during early mitosis.* Carcinogenesis, 2014. **35**(11): p. 2503-11.
93. Leone, A., Mitsiades, N., Ward, Y., Spinelli, B., Poulaki, V., Tsokos, M., and Kelly, K., *The Gem GTP-binding protein promotes morphological differentiation in neuroblastoma.* Oncogene, 2001. **20**(25): p. 3217-25.
94. Andrieu, G., Quaranta, M., Leprince, C., and Hatzoglou, A., *The GTPase Gem and its partner Kif9 are required for chromosome alignment, spindle length control, and mitotic progression.* FASEB J, 2012. **26**(12): p. 5025-34.
95. Piddini, E., Schmid, J.A., de Martin, R., and Dotti, C.G., *The Ras-like GTPase Gem is involved in cell shape remodelling and interacts with the novel kinesin-like protein KIF9.* EMBO J, 2001. **20**(15): p. 4076-87.
96. Oyama, F., Kotliarova, S., Harada, A., Ito, M., Miyazaki, H., Ueyama, Y., Hirokawa, N., Nukina, N., and Ihara, H., *Gem GTPase and tau: morphological changes induced by gem GTPase in cho cells are antagonized by tau.* J Biol Chem, 2004. **279**(26): p. 27272-7.
97. Ghiretti, A.E., and Paradis, S., *The GTPase Rem2 regulates synapse development and dendritic morphology.* Dev Neurobiol, 2011. **71**(5): p. 374-89.
98. Ghiretti, A.E., Kenny, K., Marr, M.T. 2nd, and Paradis, S., *CaMKII-dependent phosphorylation of the GTPase Rem2 is required to restrict dendritic complexity.* J Neurosci, 2013. **33**(15): p. 6504-15.

99. Moore, A.R., Ghiretti, A.E., and Paradis, S., *A loss-of-function analysis reveals that endogenous Rem2 promotes functional glutamatergic synapse formation and restricts dendritic complexity.* PLoS One, 2013. **8**(8): p. e74751.
100. Catterall, W.A., *Structure and regulation of voltage-gated Ca2+ channels.* Annu Rev Cell Dev Biol, 2000. **16**: p. 521-55.
101. Buraei, Z., and Yang, J., *Structure and function of the b subunit of voltage-gated Ca2+ channels.* Biochim Biophys Acta, 2013. **1828**(7): p. 1530-40.
102. Richards, M.W., Butcher, A.J., and Dolphin, A.C., *Ca2+ channel beta-subunits: structural insights AID our understanding.* Trends Pharmacol Sci, 2004. **25**(12): p. 626-32.
103. Chen, H., Puhl, H.L. 3rd, Niu, S.L., Mitchell, D.C., Ikeda, S.R., *Expression of Rem2, an RGK family small GTPase, reduces N-type calcium current without affecting channel surface density.* J Neurosci, 2005. **25**(42): p. 9762-72.
104. Manning, J.R., Yin, G., Kaminski, C.N., Magyar, J., Feng, H.Z., Penn, J., Sievert, G., Thompson, K., Jin, J.P., Andres, D.A., and Satin, J., *Rad GTPase deletion increases L-type calcium channel current leading to increased cardiac contraction.* J Am Heart Assoc, 2013. **2**(6): p. e000459.
105. Magyar, J., Kiper, C.E., Sievert, G., Cai, W., Shi, G.X., Crump, S.M., Li, L., Niederer, S., Smith, N., Andres, D.A., and Satin, J., *Rem-GTPase regulates cardiac myocyte L-type calcium current.* Channels (Austin), 2012. **6**(3): p. 166-73.
106. Correll, R.N., Botzet, G.J., Satin, J., Andres, D.A., and Finlin, B.S., *Analysis of the Rem2 - voltage dependant calcium channel beta subunit interaction and Rem2 interaction with phosphorylated phosphatidylinositide lipids.* Cell Signal, 2008. **20**(2): p. 400-8.
107. Pang, C., Crump, S.M., Jin, L., Correll, R.N., Finlin, B.S., Satin, J., and Andres, D.A., *Rem GTPase interacts with the proximal CaV1.2 C-terminus and modulates calcium-dependent channel inactivation.* Channels (Austin), 2010. **4**(3): p. 192-202.
108. Fan, M., Buraei, Z., Luo, H.R., Levenson-Palmer, R., and Yang, J., *Direct inhibition of P/Q-type voltage-gated Ca2+ channels by Gem does not require a direct Gem/Cavbeta interaction.* Proc Natl Acad Sci U S A, 2010. **107**(33): p. 14887-92.
109. Beguin, P., Mahalakshmi, R.N., Nagashima, K., Cher, D.H., Kuwamura, N., Yamada, Y., Seino, Y., and Hunziker, W., *Roles of 14-3-3 and calmodulin binding in subcellular localization and function of the small G-protein Rem2.* Biochem J, 2005. **390**(Pt 1): p. 67-75.
110. Correll, R.N., Pang, C., Finlin, B.S., Dailey, A.M., Satin, J., and Andres, D.A., *Plasma membrane targeting is essential for Rem-mediated Ca2+ channel inhibition.* J Biol Chem, 2007. **282**(39): p. 28431-40.
111. Flynn, R., Chen, L., Hameed, S., Spafford, J.D., and Zamponi, G.W., *Molecular determinants of Rem2 regulation of N-type calcium channels.* Biochem Biophys Res Commun, 2008. **368**(3): p. 827-31.

112. Wennerberg, K., Rossman, K.L,, and Der, C.J., *The Ras superfamily at a glance.* J Cell Sci, 2005. **118**(Pt 5): p. 843-6.
113. Beguin, P., Mahalakshmi, R.N., Nagashima, K., Cher, D.H., Takahashi, A., Yamada, Y., Seino, Y., and Hunziker, W., *14-3-3 and calmodulin control subcellular distribution of Kir/Gem and its regulation of cell shape and calcium channel activity.* J Cell Sci, 2005. **118**(Pt 9): p. 1923-34.
114. Flynn, R., Labrie-Dion, E., Bernier, N., Colicos, M.A., De Koninck, P., and Zamponi, G.W., *Activity-dependent subcellular cotrafficking of the small GTPase Rem2 and Ca2+/CaM-dependent protein kinase IIα.* PLoS One, 2012. **7**(7): p. e41185.
115. Liput, D.J., Lu, V.B., Davis, M.I., Puhl, H.L., and Ikeda, S.R., *Rem2, a member of the RGK family of small GTPases, is enriched in nuclei of the basal ganglia.* Sci Rep, 2016. **6**: p. 25137.
116. Mahalakshmi, R.N., Nagashima, K., Ng, M.Y., Inagaki, N., Hunziker, W., and Beguin, P., *Nuclear transport of Kir/Gem requires specific signals and importin alpha5 and is regulated by calmodulin and predicted serine phosphorylations.* Traffic, 2007. **8**(9): p. 1150-63.
117. Mahalakshmi, R.N., Ng, M.Y., Guo, K., Qi, Z., Hunziker, W., and Beguin, P., *Nuclear localization of endogenous RGK proteins and modulation of cell shape remodeling by regulated nuclear transport.* Traffic, 2007. **8**(9): p. 1164-78.
118. Finlin, B.S., and Andres, D.A., *Phosphorylation-dependent association of the Ras-related GTP-binding protein Rem with 14-3-3 proteins.* Arch Biochem Biophys, 1999. **368**(2): p. 401-12.
119. Fischer, R., Wei, Y., Anagli, J., and Berchtold, M.W., *Calmodulin binds to and inhibits GTP binding of the ras-like GTPase Kir/Gem.* J Biol Chem, 1996. **271**(41): p. 25067-70.
120. Moyers, J.S., Bilan, P.J., Zhu, J., and Kahn, C.R., *Rad and Rad-related GTPases interact with calmodulin and calmodulin-dependent protein kinase II.* J Biol Chem, 1997. **272**(18): p. 11832-9.
121. Ward, Y., Spinelli, B., Quon, M.J., Chen, H., Ikeda, S.R., and Kelly, K., *Phosphorylation of critical serine residues in Gem separates cytoskeletal reorganization from down-regulation of calcium channel activity.* Mol Cell Biol, 2004. **24**(2): p. 651-61.
122. Crump, S.M., Correll, R.N., Schroder, E.A., Lester, W.C., Finlin, B.S., Andres, D.A., and Satin, J., *L-type calcium channel alpha-subunit and protein kinase inhibitors modulate Rem-mediated regulation of current.* Am J Physiol Heart Circ Physiol, 2006. **291**(4): p. H1959-71.
123. Moritz, A., *CST Curation Set: 9063; Year: 2010; Biosample/Treatment: cell line, K-562/Peroxide; Disease: chronic myelogenous leukemia; Specificities of antibodies Used to Purify Peptides prior to LCMS: Ub(K-e-GG).* 2010.
124. Moritz, A., *CST Curation Set: 9062; Year: 2010; Biosample/Treatment: cell line, HeLa/untreated; Disease: cervical adenocarcinoma; Specificities of Antibodies Used to Purify Peptides prior to LCMS: Ub(K-e-GG).* 2010.

125. Cohen, L., Mohr, R., Chen, Y.Y., Huang, M., Kato, R., Dorin, D., Tamanoi, F., Goga, A., Afar, D. Rosenberg, N., et al., *Transcriptional activation of a rase-like gene (kir) by oncogenic tyrosine kinases.* Proc Natl Acad Sci U S A, 1994. **91**(26): p. 12448-52.
126. Ohsugi, M., Cras-Meneur, C., Zhou, Y., Warren, W., Bernal-Mizrachi, E., and Permutt, M.A., *Glucose and insulin treatment of insulinoma cells results in transcriptional regulation of a common set of genes.* Diabetes, 2004. **53**(6): p. 1496-508.
127. Schroder, E., Magyar, J., Burgess, D., Andres, D., and Satin, J., *Chronic verapamil treatment remodels ICa,L in mouse ventricle.* Am J Physiol Heart Circ Physiol, 2007. **292**(4): p. H1906-16.
128. Paulik, M.A., Hamacher, L.L., Yarnall, D.P., Simmons, C.J., Maianu, L., Pratley, R.E., Garvey, W.T., Burns, D.K., and Lenhard, J.M., *Identification of Rad's effector-binding domain, intracellular localization, and analysis of expression in Pima Indians.* J Cell Biochem, 1997. **65**(4): p. 527-41.
129. Garvey, W.T., Maianu, L., Kennedy, A., Wallace, P., Ganaway, E., Hamacher, L.L., Yarnall, D.P., Lenhard, J.M., and Burns, D.K., *Muscle Rad expression and human metabolism: potential role of the novel Ras-related GTPase in energy expenditure and body composition.* Diabetes, 1997. **46**(3): p. 444-50.
130. Bilan, P.J., Moyers, J.S., and Kahn, C.R., *The ras-related protein rad associates with the cytoskeleton in a non-lipid-dependent manner.* Exp Cell Res, 1998. **242**(2): p. 391-400.
131. Levitan, B.M., Manning, J.R., Withers, C.N., Smith, J.D., Shaw, R.M., Andres, D.A., Sorrell, V.L., and Satin, J., *Rad-deletion phenocopies tonic sympathetic stimulation of the heart.* J Cardiovasc Transl Res, 2016. **9**(5-6): p. 432-44.
132. Chang, L., Zhang, J., Tseng, Y.H., Xie, C.Q., Ilany, J., Bruning, J.C., Sun, Z., Zhu, X., Cui, T., Youker, K.A., Yang, Q., Day, S.M., Kahn, C.R., and Chen, Y.E., *Rad GTPase deficiency leads to cardiac hypertrophy.* Circulation, 2007. **116**(25).
133. Lynch, R.A., Wagoner, L., Li, S., Sparks, L., Molkentin, J., and Dorn, G.W. 2nd, *Novel and nondetected human signaling protein polymorphisms.* Physiol Genomics, 2002. **10**(3): p. 159-68.
134. Meza, U., Beqollari, D., Romberg, C.F., Papadopoulos, S., and Bannister, R.A., *Potent inhibition of L-type Ca2+ currents by a Rad variant associated with congestive heart failure.* Biochem Biophys Res Commun, 2013. **439**(2): p. 270-4.
135. Sun, Z., Zhang, J., Zhang, J., Chen, C., Du, Q., Chang, L., Cao, C., Zheng, M., Garcia-Barrio, M.T., Chen, Y.E., Xiao, R.P., Mao, J., and Zhu, X., *Rad GTPase induces cardiomyocyte apoptosis through the activation of p38 mitogen-activated protein kinase.* Biochem Biophys Res Commun, 2011. **409**(1): p. 52-7.
136. Manning, J.R., Withers, C.N., Levitan, B., Smith, J.D., Andres, D.A., and Satin, J., *Loss of Rad-GTPase produces a novel adaptive cardiac*

phenotype resistant to systolic decline with aging. Am J Physiol Heart Circ Physiol, 2015. **309**(8): p. H1336-45.
137. Wei, C.C., Nie, F.Q., Jiang, L.L., Chen, Q.N., Chen, Z.Y., Chen, X., Pan, X., Liu, Z.L., Lu, B.B., and Wang, Z.X., *The pseudogene DUXAP10 promotes an aggressive phenotype through binding with LSD1 and repressing LATS2 and RRAD in non small cell lung cancer.* Oncotarget, 2017. **8**(3): p. 5233-46.
138. Sova, P., Feng, Q., Geiss, G., Wood, T., Strauss, R., Rudolf, V., Lieber, A., and Kiviat, N., *Discovery of novel methylation biomarkers in cervical carcinoma by global demethylation and microarray analysis.* Cancer Epidemiol Biomarkers Prev, 2006. **15**(1): p. 114-23.
139. Yeom, S.Y., Nam, D.H., and Park, C., *RRAD promotes EGFR-mediated STAT3 activation and induces temozolomide resistance of malignant glioblastoma.* Mol Cancer Ther, 2014. **13**(12): p. 3049-61.
140. Moyers, J.S., Bilan, P.J., Reynet, C., and Kahn, C.R., *Overexpression of Rad inhibits glucose uptake in cultured muscle and fat cells.* J Biol Chem, 1996. **271**(38): p. 23111-6.
141. Raisz, L.G., *Physiology and Pathophysiology of Bone Remodeling.* Clin Chem, 1999. **45**(8 Pt 2): p. 1353-8.
142. Raggatt, L.J., and Partridge, N.C., *Cellular and molecular mechanisms of bone remodeling.* J Biol Chem, 2010. **285**(33): p. 25103-8.
143. Miller, S.C., de Saint-Georges, L., Bowman, B.M., and Jee, W.S., *Bone lining cells: structure and function.* Scanning Microsc, 1989. **3**(3): p. 953-60.
144. Aarden, E.M., Burger, E.H., and Nijweide, P.J., *Function of osteocytes in bone.* J Cell Biochem, 1994. **55**(3): p. 287-99.
145. Boyle, W.J., Simonet, W.S., and Lacey, D.L., *Osteoclast differentiation and activation.* Nature, 2003. **423**(6937): p. 337-42.
146. Jiang, Y., Jahagirdar, B.N., Reinhardt, R.L., Schwartz, R.E., Keene, C.D., Ortiz-Gonzalez, X.R., Reyes, M., Lenvik, T., Lund, T., Blackstad, M., Du, J., Aldrich, S., Lisberg, A., Low, W.C., Largaespada, D.A., Verfaillie, C.M., *Pluripotency of mesenchymal stem cells derived from adult bone marrow.* Nature, 2002. **418**(6893): p. 41-9.
147. Stein, G.S., and Lian, J.B., *Molecular mechanisms mediating proliferation/differentiation interrelationships during progressive development of the osteoblast phenotype.* Endocr Rev, 1993. **14**(4): p. 424-42.
148. Otto, F., Thornell, A.P., Crompton, T., Denzel, A., Gilmour, K.C., Rosewell, I.R., et al., *Cbfa1, a candidate gene for cleidocranial dysplasia syndrome, is essential for osteoblast differentiation and bone development.* Cell, 1997. **89**(5): p. 765-71.
149. Kern, B., Shen, J., Starbuck, M., and Karsenty, G., *Cbfa1 contributes to the osteoblast-specific expression of type I collagen genes.* J Biol Chem, 2001. **276**(10): p. 7101-7.
150. Harada, H., Tagashira, S., Fujiwara, M., Ogawa, S., Katsumata, T., Yamaguchi, A., Komori, T., and Nakatsuka, M., *Cbfa1 isoforms exert*

functional differences in osteoblast differentiation. J Biol Chem, 1999. **274**(11): p. 6972-8.
151. Nakashima, K., Zhou, X., Kunkel, G., Zhang, Z., Deng, J.M., Behringer, R.R., and de Crombrugghe, B., *The novel zinc finger-containing transcription factor osterix is required for osteoblast differentiation and bone formation.* Cell, 2002. **108**(1): p. 17-29.
152. Suda, T., Takahashi, N., Udagawa, N., Jimi, E., Gillespie, M.T., and Martin, T.J., *Modulation of osteoclast differentiation and function by the new members of the tumor necrosis factor receptor and ligand families.* Endocr Rev, 1999. **20**(3): p. 345-57.
153. Urist, M.R., *Bone: formation by autoinduction.* Science, 1965. **150**(698): p. 893-9.
154. Gazzerro, E., and Canalis, E., *Bone morphogenetic proteins and their antagonists.* Rev Endocr Metab Disord, 2006. **7**(1-2): p. 51-65.
155. Chen, D., Zhao, M., and Mundy, G.R., *Bone morphogenetic proteins.* Growth Factors, 2004. **22**(4): p. 233-41.
156. van Dinther, M., Visser, N., de Gorter, D.J.J., Doorn, J., Goumans, M.J., de Boer, J., et al., *ALK2 R206H mutation linked to fibrodysplasia ossificans progressiva confers constitutive activity to the BMP type I receptor and sensitizes mesenchymal cells to BMP-induced osteoblast differentiation and bone formation.* J Bone Miner Res, 2010. **25**(6): p. 1208-15.
157. Gautschi, O.P., Frey, S.P., and Zellweger, R., *Bone morphogenetic proteins in clinical applications.* ANZ J Surg, 2007. **77**(8): p. 626-31.
158. Sapkota, G., Alarcon, C., Spagnoli, F.M., Brivanlou, A.H., and Massague, J., *Balancing BMP signaling through integrated inputs into the Smad1 linker.* Mol Cell, 2007. **25**(3): p. 441-54.
159. Fuentealba, L.C., Eivers, E., Ikeda, A., Hurtado, C., Kuroda, H., Pera, E.M., and De Robertis, E.M., *Integrating patterning signals: Wnt/GSK3 regulates the duration of the BMP/Smad1 signal.* Cell, 2007. **131**(5): p. 980-93.
160. Gary, M.F., Viggeswarapu, M., Oliver, C., Teklemariam, M., Sangadala, S., Titus, L., and Boden, S.D., *Lim mineralization protein-1 knockout mice have reduced spine trabecular bone density on microcomputed tomography due to decreased bone morphogenetic protein responsiveness.* Neurosurgery, 2014. **61 Suppl 1**: p. 182-6.
161. Jepsen, K.J., Silva, M.J., Vashishth, D., Guo, X.E., and van der Meulen, M.C., *Establishing biomechanical mechanisms in mouse models: practical guidelines for systematically evaluating phenotypic changes in the diaphyses of long bones.* J Bone Miner Res, 2015. **30**(6): p. 951-66.
162. Wallace, J.M., Burr, D.B., and Allen, M.R., *Chapter 6-skeletal hard tissue biomechanics*, in *Basic and applied bone biology*. 2014, Academic Press: San Diego. p. 115-30.
163. Berman, A.G., Wallace, J.M., Bart, Z.R., and Allen, M.R., *Raloxifene reduces skeletal fractures in an animal model of osteogenesis imperfecta.* Matrix Biol, 2015. **52-54**: p. 19-28.

164. Erlebacher, A., and Derynck, R., *Increased expression of TGF-beta 2 in osteoblasts results in an osteoporosis-like phenotype.* J Cell Biol, 1996. **132**(1-2): p. 195-210.
165. Schenck, R.K., Olah, A.J., and Herrmann, W., *Preparation of calcified tissues for light microscopy*, in *Methods of calcified tissue preparation*, D. G., Editor. 1984, Elsevier: Amsterdam. p. 1-56.
166. Rolland, T., Tasan, M., Charloteaux, B., et al., *A proteome-scale map of the human interactome network.* Cell, 2014. **159**(5): p. 1212-26.
167. te Velthius, A.J., and Bagowski, C.P., *PDZ and LIM domain-encoding genes: molecular interactions and their role in development.* ScientificWorldJournal, 2007. **7**: p. 1470-92.
168. Jemth, P., and Gianni, S., *PDZ domains: folding and binding.* Biochemistry, 2007. **46**(30): p. 8701-8.
169. Bach, I., *The LIM domain: regulation by association.* Mech Dev, 2000. **91**(1-2): p. 5-17.
170. Zheng, M., Cheng, H., Benerjee, I., and Chen, J., *ALP/Enigma PDZ-LIM domain proteins in the heart.* J Mol Cell Biol, 2010. **2**(2): p. 96-102.
171. Wu, R.Y., and Gill, G.N., *LIM domain recognition of a tyrosine-containing tight turn.* J Biol Chem, 1994. **269**(40): p. 25085-90.
172. Kuroda, S., Tokunaga, C., Kiyohara, Y., Higuchi, O., Konishi, H., Mizuno, K., Gill, G.N., and Kikkawa, U., *Protein-protein interaction of zinc finger LIM domains with protein kinase C.* J Biol Chem, 1996. **271**(49): p. 31029-32.
173. Faulkner, G., Pallavicini, A., Formentin, E., Comelli, A., Ievolella, C., Trevisan, S., Bortoletto, G., Scannapieco, P., Salamon, M., Mouly, V., Valle, G., and Lanfranchi, G., *ZASP: a new Z-band alternatively spliced PDZ-motif protein.* J Cell Biol, 1999. **146**(2): p. 465-75.
174. Ueki, N., Seki, N., Yano, K., Masuho, Y., Saito, T., and Muramatsu, M., *Isolation, tissue expression, and chromosomal assignment of a human LIM protein gene, showing homology to rat enigma homologue (ENH).* J Hum Genet, 1999. **1999**(44): p. 4.
175. Niederlander, N., Fayein, N.A., Auffray, C., and Pomies, P., *Characterization of a new human isoform of the enigma homolog family specifically expressed in skeletal muscle.* Biochem Biophys Res Commun, 2004. **325**(4): p. 1304-11.
176. Maeno-Hikichi, Y., Chang, S., Matsumura, K., Lai, M., Lin, H., Nakagawa, N., Kuroda, S., and Zhang, J.F., *A PKC epsilon-ENH-channel complex specifically modulates N-type Ca2+ channels.* Nat Neurosci, 2003. **6**(5): p. 468-75.
177. Chen, Y., Lai, M., Maeno-Hikichi, Y., and Zhang, J.F., *Essential role of the LIM domain in the formation of the PKCepsilon-ENH-N-type Ca2+ channel complex.* Cell Signal, 2006. **18**(2): p. 215-24.
178. Maturana, A.D., Walchli, S., Iwata, M., Ryser, S., Van Lint, J., Hoshijima, M., Schlegel, W., Ikeda, Y., Tanizawa, K., and Kuroda, S., *Enigma homolog 1 scaffolds protein kinase D1 to regulate the activity of the*

cardiac L-type voltage-gated calcium channel. Cardiovasc Res, 2008. **78**(3): p. 458-65.
179. Lin, C., Guo, X., Lange, S., Liu, J., Ouyang, K., Yin, X., Jiang, L., Cai, Y., Mu, Y., Sheikh, F., Ye, S., Chen, J., Ke, Y., and Cheng, H., *Cypher/ZASP is a novel A-kinase anchoring protein.* J Biol Chem, 2013. **288**(41): p. 29403-13.
180. Zheng, M., Cheng, H., Li, X., Zhang, J., Cui, L., Ouyang, K., Han, L., Zhao, T., Gu, Y., Dalton, N.D., Bang, M.L., Peterson, K.L., and Chen, J., *Cardiac-specific ablation of Cypher leads to a severe form of dilated cardiomyopathy with premature death.* Hum Mol Genet, 2009. **18**(4): p. 701-13.
181. Cheng, H., Kimura, K., Peter, A.K., Cui, L., Ouyang, K., Shen, T., Liu, Y., Gu, Y., Dalton, N.D., Evans, S.M., Knowlton, K.U., Peterson, K.L., and Chen, J., *Loss of enigma homolog protein results in dilated cardiomyopathy.* Circ Res, 2010. **107**(3): p. 348-56.
182. Mu, Y., Jing, R., Peter, A.K., Lange, S., Lin, L., Zhang, J., Ouyang, K., Fang, X., Veevers, J., Zhou, X., Evans, S.M., Cheng, H., and Chen, J., *Cypher and Enigma homolog protein are essential for cardiac development and embryonic survival.* J Am Heart Assoc, 2015. **4**(5): p. e001950.
183. Krcmery, J., Gupta, R., Sadleir, R.W., Ahrens, M.J., Misener, S., Kamide, C., Fitchev, P., Losordo, D.W., Crawford, S.E., and Simon, H.G., *Loss of cytoskeletal protein Pdlim7 predisposes mice to heart defects and hemostatic dysfunction.* PLoS One, 2013. **8**(11): p. e80809.
184. Sangadala, S., Boden, S.D., Viggeswarapu, M., Liu, Y., and Titus, L., *LIM mineralization protein-1 potentiates bone morphogenetic protein responsiveness via a novel interaction with Smurf1 resulting in decreased ubiquitination of Smads.* J Biol Chem, 2006. **281**(25): p. 17212-9.
185. Jung, C.R., Lim, J.H., Choi, Y., Kim, D.G., Kang, K.J., Noh, S.M., and Im, D.S., *Enigma negatively regulates p53 through MDM2 and promotes tumor cell survival in mice.* J Clin Invest, 2010. **120**(12): p. 4493-506.
186. Kales, S.C., Nau, M.M., Merchant, A.S., and Lipkowitz, S., *Enigma prevents Cbl-c mediated ubiquitination and degradation of RETMEN2A.* PLoS One, 2014. **9**(1): p. e87116.
187. Yamashita, M., Ying, S.X., Zhang, G.M., Li, C., Cheng, S.Y., Deng, C.X., and Zhang, Y.E., *Ubiquitin ligase Smurf1 controls osteoblast activity and bone homeostasis by targeting MEKK2 for degradation.* Cell, 2005. **121**(1): p. 101-13.
188. Sangadala, S., Boden, S.D., Metpally, R.P., and Reddy, B.V., *Modeling and analysis of molecular interaction between Smurf1-WW2 domain and various isoforms of LIM mineralization protein.* Proteins, 2007. **68**(3): p. 690-701.
189. Fei, Q., Boden, S.D., Sangadala, S., Viggeswarapu, M., Liu, Y., and Titus, L., *Truncated human LMP-1 triggers differentiation of C2C12 cells to an osteoblastic phenotype in vitro.* Acta Biochim Biophys Sin (Shanghai), 2007. **39**(9): p. 693-700.

190. Zhu, H., Kavsak, P., Abdollah, S., Wrana, J.L., and Thomsen, G.H., *A SMAD ubiquitin ligase targets the BMP pathway and affects embryonic pattern formation.* Nature, 1999. **400**(6745): p. 687-93.
191. Tang, L.Y., Yamashita, M., Coussens, N.P., Tang, Y., Wang, X., Li, C., Deng, C.X., Cheng, S.Y., and Zhang, Y.E., *Ablation of Smurf2 reveals an inhibition in TGF-β signalling through multiple mono-ubiquitination of Smad3.* EMBO J, 2011. **30**(23): p. 4777-89.
192. Fukuchi, M., Imamura, T., Chiba, T., Ebisawa, T., Kawabata, M., Tanaka, K., and Miyazono, K., *Ligand-dependent degradation of Smad3 by a ubiquitin ligase complex of ROC1 and associated proteins.* Mol Biol Cell, 2001. **12**(5): p. 1431-43.
193. Shi, Y., Hata, A., Lo, R.S., Massague, J., and Pavletich, N.P., *A structural basis for mutational inactivation of the tumour suppressor Smad4.* Nature, 1997. **388**(6637): p. 87-93.
194. Wozney, J.M., *The bone morphogenetic protein family and osteogenesis.* Mol Reprod Dev, 1992. **32**(2): p. 160-7.
195. Endoh, M., *Cardiac alpha(1)-adrenoceptors that regulate contractile function: subtypes and subcellular signal transduction mechanisms.* Neurochem Res, 1996. **21**(2): p. 217-29.
196. Xiao, R.P., *Beta-adrenergic signaling in the heart: dual coupling of the beta2-adrenergic receptor to G(s) and G(i) proteins.* Sci STKE, 2001. **2001**(104): p. re15.
197. Osterrieder, W., Brum, G., Hescheler, J., Trautwein, W., Flockerzi, V., and Hofmann, F., *Injection of subunits of cyclic AMP-dependent protein kinase into cardiac myocytes modulates Ca2+ current.* Nature, 1982. **298**(5874): p. 576-8.
198. Hartzell, H.C., Mery, P.F., Fischmeister, R., and Szabo, G., *Sympathetic regulation of cardiac calcium current is due exclusively to cAMP-dependent phosphorylation.* Nature, 1991. **351**(6327): p. 573-6.
199. Lemke, T., Welling, A., Christel, C.J., Blaich, A., Bernhard, D., Lenhardt, P., Hofmann, F., and Moosmang, S., *Unchanged beta-adrenergic stimulation of cardiac L-type calcium channels in Ca v 1.2 phosphorylation site S1928A mutant mice.* J Biol Chem, 2008. **283**(50): p. 34738-44.
200. Ganesan, A.N., Maack, C., Johns, D.C., Sidor, A., and O'Rourke, B., *Beta-adrenergic stimulation of L-type Ca2+ channels in cardiac myocytes requires the distal carboxyl terminus of alpha1C but not serine 1928.* Circ Res, 2006. **98**(2): p. e11-8.
201. Brandmayr, J., Poomvanicha, M., Domes, K., Ding, J., Blaich, A., Wegener, J.W., Moosmang, S., and Hofmann, F., *Deletion of the C-terminal phosphorylation sites in the cardiac β-subunit does not affect the basic β-adrenergic response of the heart and the Ca(v)1.2 channel.* J Biol Chem, 2012. **287**(27): p. 22584-92.
202. Sundram, V., Chauhan, S.C., and Jaggi, M., *Emerging role of protein kinase D1 in cancer.* Mol Cancer Res, 2011. **9**(8): p. 985-96.
203. Weintz, G., Olsen, J.V., Fruhauf, K., Niedzielska, M., Amit, I., Jantsch, J., Mages, J., Frech, C., Dolken, L., Mann, M., and Lang, R., *The*

phosphoproteome of toll-like receptor-activated macrophages. Mol Syst Biol, 2010. **6**: p. 371.
204. Mertins, P., Mani, D.R., Ruggles, K.V., et al., *Proteogenomics connects somatic mutations to signalling in breast cancer.* Nature, 2016. **534**(7605): p. 55-62.
205. Parker, B.L., Yang, G., Humphrey, S.J., Chaudhuri, R., Ma, X., Peterman, S., and James, D.E., *Targeted phosphoproteomics of insulin signaling using data-independent acquisition mass spectrometry.* Sci Signal, 2015. **8**(380): p. rs6.
206. Humphrey, S.J., Yang, G., Yang, P., Fazakerley, D.J., Stockli, J., Yang, J.Y., and James, D.E., *Dynamic adipocyte phosphoproteome reveals that Akt directly regulates mTORC2.* Cell Metab, 2013. **17**(6): p. 1009-20.
207. Lundby, A., Andersen, M.N., Steffensen, A.B., Horn, H., Kelstrup, C.D., Francavilla, C., Jensen, L.J., Schmitt, N., Thomsen, M.B., and Olsen, J.V., *In vivo phosphoproteomics analysis reveals the cardiac targets of β-adrenergic receptor signaling.* Sci Signal, 2013. **6**(278): p. rs11.
208. Williams, G.R., Bethard, J.R., Berkaw, M.N., Nagel, A.K., Luttrell, L.M., and Ball, L.E., *Exploring G protein-coupled receptor signaling networks using SILAC-based phosphoproteomics.* Methods, 2016. **92**: p. 36-50.
209. Schweppe, D.K., Rigas, J.R., and Gerber, S.A., *Quantitative phosphoproteomic profiling of human non-small cell lung cancer tumors.* J Proteomics, 2013. **91**: p. 286-96.
210. Scheller, E.L., Cawthorn, W.P., Burr, A.A., Horowitz, M.C., and MacDougald, O.A., *Marrow adipose tissue: trimming the fat.* Trends Endocrinol Metab, 2016. **27**(6): p. 392-403.
211. (NOF), N.O.F., *America's bone health: the state of osteoporosis and low bone mass in our nation.* 2002.
212. Bredella, M.A., Fazeli, P.K., Miller, K.K., Misra, M., Torriani, M., Thomas, B.J., Ghomi, R.H., Rosen, C.J., and Klibanski, A., *Increased bone marrow fat in anorexia nervosa.* J Clin Endocrinol Metab, 2009. **94**(6): p. 2129-36.
213. LeBlanc, A.D., Spector, E.R., Evans, H.J., and Sibonga, J.D., *Skeletal responses to space flight and the bed rest analog: a review.* J Musculoskelet Neuronal Interact, 2007. **7**(1): p. 33-47.
214. Verma, S., Rajaratnam, J.H., Denton, J., Hoyland, J.A., and Byers, R.J., *Adipocytic proportion of bone marrow is inversely related to bone formation in osteoporosis.* J Clin Pathol, 2002. **55**(9): p. 693-8.
215. Yeung, D.K., Griffith, J.F., Antonio, G.E., Lee, F.K., Woo, J., and Leung, P.C., *Osteoporosis is associated with increased marrow fat content and decreased marrow fat unsaturation: a proton MR spectroscopy study.* J Magn Reson Imaging, 2005. **22**(2): p. 279-85.
216. Scheller, E.L., and Rosen, C.J., *What's the matter with MAT? Marrow adipose tissue, metabolism, and skeletal health.* Ann N Y Acad Sci, 2014. **1311**: p. 14-30.
217. Veldhuis-Vlug, A.G.a.R., C.J., *Mechanisms of marrow adiposity and its implications for skeletal health.* Metabolism, 2017. **67**: p. 106-14.

218. Lefterova, M.I., Zhang, Y., Steger, D.J., Schupp, M., Schug, J., Cristancho, A., Feng, D., Zhuo, D., Stoeckert, C.J. Jr, Liu, X.S., and Lazar, M.A., *PPARgamma and C/EBP factors orchestrate adipocyte biology via adjacent binding on a genome-wide scale.* Genes Dev, 2008. **22**(21): p. 2941-52.
219. Komori, T., Yagi, H., Nomura, S., Yamaguchi, A., Sasaki, K., Deguchi, K., Shimizu, Y., Bronson, R.T., Gao, Y.H., Inada, M., Sato, M., Okamoto, R., Kitamura, Y., Yoshiki, S., and Kishimoto, T., *Targeted disruption of Cbfa1 results in a complete lack of bone formation owing to maturational arrest of osteoblasts.* Cell, 1997. **89**(5): p. 755-64.
220. Song, L., Liu, M., Ono, N., Bringhurst, F.R., Kronenberg, H.M., and Guo, J., *Loss of wnt/β-catenin signaling causes cell fate shift of preosteoblasts from osteoblasts to adipocytes.* J Bone Miner Res, 2012. **27**(11): p. 2344-58.
221. Chen, J., Shi, Y., Regan, J., Karuppaiah, K., Ornitz, D.M., and Long, F., *Osx-Cre targets multiple cell types besides osteoblast lineage in postnatal mice.* PLoS One, 2014. **9**(1): p. e85161.
222. Liu, Y., Hair, G.A., Boden, S.D., Viggeswarapu, M., and Titus, L., *Overexpression LIM mineralization proteins do not require LIM domains to induce bone.* J Bone Miner Res, 2002. **17**(3): p. 406-14.
223. Boden, S.D., Liu, Y., Hair, G.A., Helms, J.A., Hu, D., Racine, M., Nanes, M.S., and Titus, L., *LMP-1, a LIM-domain protein, mediates BMP-6 effects on bone formation.* Endocrinology, 1998. **139**(12): p. 5125-34.
224. Viggeswarapu, M., Boden, S.D., Liu, Y., Hair, G.A., Louis-Ugbo, J., Murakami, H., Kim, H.S., Mayr, M.T., Hutton, W.C., and Titus, L., *Adenoviral delivery of LIM mineralization protein-1 induces new-bone formation in vitro and in vivo.* J Bone Joint Surg Am, 2001. **83-A**(3): p. 364-76.
225. Boden, S.D., Titus, L., Hair, G., Liu, Y., Viggeswarapu, M., Nanes, M.S., and Baranowski, C., *Lumbar spine fusion by local gene therapy with a cDNA encoding a novel osteoinductive protein (LMP-1).* Spine (Phila Pa 1976), 1998. **23**(23): p. 2486-92.
226. Pola, E., Gao, W., Zhou, Y., Pola, R., Lattanzi, W., Sfeir, C., Gambotto, A., and Robbins, P.D., *Efficient bone formation by gene transfer of human LIM mineralization protein-3.* Gene Ther, 2004. **11**(8): p. 683-93.
227. Lattanzi, W., Parrilla, C., Fetoni, A., Logroscino, G., Straface, G., Pecorini, G., Stigliano, E., Tampieri, A., Bedini, R., Pecci, R., Michetti, F., Gambotto, A., Robbins, P.D., and Pola, E., *Ex vivo-transduced autologous skin fibroblasts expressing human Lim mineralization protein-3 efficiently form new bone in animal models.* Gene Ther, 2008. **15**(19): p. 1330-43.
228. Strohbach, C.A., Rundle, C.H., Wergedal, J.E., Chen, S.T., Linkhart, T.A., Lau, K.H., and Strong, D.D., *LMP-1 retroviral gene therapy influences osteoblast differentiation and fracture repair: a preliminary study.* Calcif Tissue Int, 2008. **83**(3): p. 202-11.

229. Jiang, X., Chen, Y., Fan, X., Zhang, H., and Kun, L., *Osteogenesis and mineralization in a rabbit mandibular distraction osteogenesis model is promoted by the human LMP-1 gene.* J Orthop Res, 2015. **33**(4): p. 521-6.
230. Lin, Z., Navarro, V.P., Kempeinen, K.M., Franco, L.M., Jin, Q., Sugai, J.V., and Giannobile, W.V., *LMP1 regulates periodontal ligament progenitor cell proliferation and differentiation.* Bone, 2010. **47**(1): p. 55-64.
231. Minamide, A., Boden, S.D., Viggeswarapu, M., Hair, G.A., Oliver, C., and Titus, L., *Mechanism of bone formation with gene transfer of the cDNA encoding for the intracellular protein LMP-1.* J Bone Joint Surg Am, 2003. **85-A**(6): p. 1030-9.
232. Yoon, S.T., Park, J.S., Kim, K.S., Li, J., Attallah-Wasif, E.S., Hutton, W.C., and Boden, S.D., *ISSLS prize winner: LMP-1 upregulates intervertebral disc cell production of proteoglycans and BMPs in vitro and in vivo.* Spine (Phila Pa 1976), 2004. **29**(23): p. 2603-11.
233. Pan, H., Li, X., Wang, J., Zhang, K., Yang, H., Li, Z., Zheng, Z., and Liu, H., *LIM Mineralizaiton Protein-1 Enhances Bone Morphogenetic Protein-2-Mediated Osteogenesis Through Activation of ERK1/2 MAPK Pathway and Upregulation of Runx2 Transactivity.* J Bone Miner Res, 2015. **30**(8): p. 1523-35.
234. Price, P.A., Urist, M.R., and Otawara, Y., *Matrix Gla protein, a new gamma-carboxyglutamic acid-containing protein which is associated with the organic matrix of bone.* Biochem Biophys Res Commun, 1983. **117**(3): p. 765-71.
235. Gopalakrishnan, R., Ouyang, H., Somerman, M.J., McCauley, L.K., and Franceschi, R.T., *Matrix gamma-carboxyglutamic acid protein is a key regulator of PTH-mediated inhibition of mineralization in MC3T3-E1 osteoblast-like cells.* Endocrinology, 2001. **142**(10): p. 4379-88.
236. Gopalakrishnan, R., Suttamanatwong, S., Carlson, A.E., and Franceschi, R.T., *Role of matrix Gla protein in parathyroid hormone inhibition of osteoblast mineralization.* Cells Tissues Organs, 2005. **181**(3-4): p. 166-75.
237. Mutch, D.M., Rouault, C., Keophiphath, M., Lacasa, D., and Clement, K., *Using gene expression to predict the secretome of differentiating human preadipocytes.* Int J Obes (Lond), 2009. **33**(3): p. 354-63.
238. Yeh, W.C., Cao, Z., Classon, M., and McKnight, S.L., *Cascade regulation of terminal adipocyte differentiation by three members of the C/EBP family of leucine zipper proteins.* Genes Dev, 1995. **9**(2): p. 168-81.
239. Darlington, G.J., Ross, S.E., and MacDougald, O.A., *The role of C/EBP genes in adipocyte differentiation.* J Biol Chem, 1998. **273**(46): p. 30057-60.
240. Lin, F.T., and Lane, M.D., *CCAAT/enhancer binding protein alpha is sufficient to initiate the 3T3-L1 adipocyte differentiation program.* Proc Natl Acad Sci U S A, 1994. **91**(19): p. 8757-61.
241. Murshed, M., Schinke, T., McKee, M.D., and Karsenty, G., *Extracellular matrix mineralization is regulated locally; different roles of two gla-containing proteins.* J Cell Biol, 2004. **165**(5): p. 625-30.

242. Luo, G., Ducy, P., McKee, M.D., Pinero, G.J., Loyer, E., Behringer, R.R., and Karsenty, G., *Spontaneous calcification of arteries and cartilage in mice lacking matrix GLA protein.* Nature, 1997. **386**(6620): p. 78-81.
243. El-Maadawy, S., Kaartinen, M.T., Schinke, T., Murshed, M., Karsenty, G., and McKee, M.D., *Cartilage formation and calcification in arteries of mice lacking matrix Gla protein.* Connect Tissue Res, 2003. **44 Suppl 1**: p. 272-8.
244. Zhu, J., Bilan, P.J., Moyers, J.S., Antonetti, D.A., and Kahn, C.R., *Rad, a novel Ras-related GTPase, interacts with skeletal muscle beta-tropomyosin.* J Biol Chem, 1996. **271**(2): p. 768-73.
245. Guy, P.M., Kenny, D.A., and Gill, G.N., *The PDZ domain of the LIM protein enigma binds to beta-tropomyosin.* Mol Biol Cell, 1999. **10**(6): p. 1973-84.
246. Nakagawa, N., Hoshijima, M., Oyasu, M., Saito, N., Tanizawa, K., and Kuroda, S., *ENH, containing PDZ and LIM domains, heart/skeletal muscle-specific protein, associates with cytoskeletal proteins through the PDZ domain.* Biochem Biophys Res Commun, 2000. **272**(2): p. 505-12.
247. Zhou, Q., Ruiz-Lozano, P., Martone, M.E., and Chen, J., *Cypher, a striated muscle-restricted PDZ and LIM domain-containing protein, binds to alpha-actinin-2 and protein kinase C.* J Biol Chem, 1999. **274**(28): p. 19807-13.
248. Bauer, K., Kratzer, M., Otte, M., de Quintana, K.L., Hagmann, J., Arnold, G.J., Eckerskorn, C., Lottspeich, F., and Siess, W. , *Human CLP36, a PDZ-domain and LIM-domain protein, binds to alpha-actinin-1 and associates with actin filaments and stress fibers in activated platelets and endothelial cells.* Blood, 2000. **96**(13): p. 4236-45.
249. Urban, A.E., Quick, E.O., Miller, K.P., Krcmery, J., and Simon, H.G., *Pdlim7 regulates Arf6-dependent actin dynamics and is required for platelet-mediated thrombosis in mice.* PLoS One, 2016. **11**(10): p. e0164042.
250. Tamura, N., Ohno, K., Katayama, T., Kanayama, N., and Sato, K., *The PDZ-LIM protein CLP36 is required for actin stress fiber formation and focal adhesion assembly in BeWo cells.* Biochem Biophys Res Commun, 2007. **364**(3): p. 589-94.
251. Barres, R., Gremeaux, T., Gual, P., Gonzalez, T., Gugenheim, J., Tran, A., Le Marchand-Brustel, Y., and Tanti, J.F., *Enigma interacts with adaptor protein with PH and SH2 domains to control insulin-induced actin cytoskeleton remodeling and glucose transporter 4 translocation.* Mol Endocrinol, 2006. **20**(11): p. 2864-75.
252. Ilany, J., Bilan, P.J., Kapur, S., Caldwell, J.S., Patti, M.E., Marette, A., and Kahn, C.R., *Overexpression of Rad in muscle worsens diet-induced insulin resistance and glucose intolerance and lowers plasma triglyceride level.* Proc Natl Acad Sci U S A, 2006. **103**(12): p. 4481-6.
253. Yamazaki, T., Walchli, S., Fujita, T., Ryser, S., Hoshijima, M., Schlegel, W., Kuroda, S., and Maturana, A.D., *Splice variants of enigma homolog,*

differentially expressed during heart development, promote or prevent hypertrophy. Cardiovasc Res, 2010. **86**(3): p. 374-82.
254. Guo, W.T., and Dong, D.L., *Bone morphogenetic protein-4: a novel therapeutic target for pathological cardiac hypertrophy/heart failure.* Heart Fail Rev, 2014. **19**(6): p. 781-8.
255. Banach, J., Gilewski, W., Slomka, A., Buszko, K., Blazejewski, J., Karasek, D., Rogowicz, D., Zekanowska, E., and Sinkiewicz, W., *Bone morphogenetic protein 6-a possible new player in the pathophysiology of heart failure.* Clin Exp Pharmacol Physiol, 2016. **43**(12): p. 1247-50.
256. Wang, Y.X., Qian, L.X., Liu, D., Yao, L.L., Jiang, Q., Yu, Z., Gui, Y.H., Zhong, T.P., and Song, H.Y., *Bone morphogenetic protein-2 acts upstream of myocyte-specific enhancer factor 2a to control embryonic cardiac contractility.* Cardiovasc Res, 2007. **74**(2): p. 290-303.
257. Guggino, S.E., Lajeunesse, D., Wagner, J.A., and Snyder, S.H., *Bone remodeling signaled by a dihydropyridine- and phenylalkylamine-sensitive calcium channel.* Proc Natl Acad Sci U S A, 1989. **86**(8): p. 2957-60.
258. Teti, A., Grano, M., Colucci, S., Argentino, L., Barattolo, R., Miyauchi, A., Teitelbaum, S.L., Hruska, K.A., and Zambonin Zallone, A., *Voltage dependent calcium channel expression in isolated osteoclasts.* Boll Soc Ital Biol Sper, 1989. **65**(12): p. 1115-8.
259. Shao, Y., Czymmek, K.J., Jones, P.A., Fomin, V.P., Akanbi, K., Duncan, R.L., and Farach-Carson, M.C., *Dynamic interactions between L-type voltage-sensitive calcium channel Cav1.2 subunits and ahnak in osteoblastic cells.* Am J Physiol Cell Physiol, 2009. **296**(5): p. C1067-78.
260. Wang, X.T., Nagaba, S., Nagaba, Y., Leung, S.W., Wang, J., Qiu, W., Zhao, P.L., and Guggino, S.E., *Cardiac L-type calcium channel alpha 1-subunit is increased by cyclic adenosine monophosphate: messenger RNA and protein expression in intact bone.* J Bone Miner Res, 2000. **15**(7): p. 1275-85.
261. Chellaiah, M.A., Soga, N., Swanson, S., McAllister, S., Alvarez, U., Wang, D., Dowdy, S.F., and Hruska, K.A., *Rho-A is critical for osteoclast podosome organization, motility, and bone resorption.* J Biol Chem, 2000. **275**(16): p. 11993-12002.
262. Linder, S., and Aepfelbacher, M., *Podosomes: adhesion hot-spots of invasive cells.* Trends Cell Biol, 2003. **13**(7): p. 376-85.
263. Chellaiah, M.A., *Regulation of actin ring formation by rho GTPases in osteoclasts.* J Biol Chem, 2005. **280**(38): p. 32930-43.
264. Touaitahuata, H., Blangy, A., and Vives, V., *Modulation of osteoclast differentiation and bone resorption by Rho GTPases.* Small GTPases, 2014. **5**: p. e28119.
265. Elefteriou, F., Campbell, P., and Ma, Y., *Control of bone remodeling by the peripheral sympathetic nervous system.* Calcif Tissue Int, 2014. **94**(1): p. 140-51.
266. Moore, R.E., Smith, C.K. 2nd, Bailey, C.S., Voelkel, E.F., and Tashijan, A.H. Jr., *Characterization of beta-adrenergic receptors on rat and human osteoblast-like cells and demonstration that beta-receptor agonists can*

stimulate bone resorption in organ culture. Bone Miner, 1993. **23**(3): p. 301-15.
267. Aitken, S.J., Landao-Bassonga, E., Ralston, S.H., and Idris, A.I., *Beta2-adrenoreceptor ligands regulate osteoclast differentiation in vitro by direct and indirect mechanisms.* Arch Biochem Biophys, 2009. **482**(1-2): p. 96-103.
268. Takeda, S., Elefteriou, F., Levasseur, R., Liu, X., Zhao, L., Parker, K.L., Armstrong, D., Ducy, P., and Karsenty, G., *Leptin regulates bone formation via the sympathetic nervous system.* Cell, 2002. **111**(3): p. 305-17.
269. Elefteriou, F., Ahn, J.D., Takeda, S., Starbuck, M., Yang, X., Liu, X., Kondo, H., Richards, W.G., Bannon, T.W., Noda, M., Clement, K., Vaisse, C., and Karsenty, G., *Leptin regulation of bone resorption by the sympathetic nervous system and CART.* Nature, 2005. **434**(7032): p. 514-20.
270. Kondo, H., Takeuchi, S., and Togari, A., *β-Adrenergic signaling stimulates osteoclastogenesis via reactive oxygen species.* Am J Physiol Endocrinol Metab, 2013. **304**(5): p. E507-15.
271. Kajimura, D., Hinoi, E., Ferron, M., Kode, A., Riley, K.J., Zhou, B., Guo, X.E., and Karsenty, G., *Genetic determination of the cellular basis of the sympathetic regulation of bone mass accrual.* J Exp Med, 2011. **208**(4): p. 841-51.
272. Fu, L., Patel, M.S., Bradley, A., Wagner, E.F., and Karsenty, G, *The molecular clock mediates leptin-regulated bone formation.* Cell, 2005. **122**(5): p. 803-15.
273. Bouxsein, M.L., Devlin, M.J., Glatt, V., Dhillon, H., Pierroz, D.D., and Ferrari, S. , *Mice lacking beta-adrenergic receptors have increased bone mass but are not protected from deleterious skeletal effects of ovariectomy.* Endocrinology, 2009. **150**(1): p. 144-52.
274. Bonnet, N., Benhamou, C.L., Malaval, L., Goncalves, C., Vico, L., Eder, V., Pichon, C., and Courteix, D., *Low dose beta-blocker prevents ovariectomy-induced bone loss in rats without affecting heart functions.* J Cell Physiol, 2008. **217**(3): p. 819-27.
275. Bonnet, N., Laroche, N., Vico, L., Dolleans, E., Benhamou, C.L., and Courteix, D., *Dose effects of propanolol on cancellous and cortical bone in ovariectomized adult rats.* J Pharmacol Exp Ther, 2006. **318**(3): p. 1118-27.
276. Yirmiya, R., Goshen, I., Bajayo, A., Kreisel, T., Feldman, S., Tam, J., Trembovler, V., Csernus, V., Shohami, E., and Bab, I., *Depression induces bone loss through stimulation of the sympathetic nervous system.* Proc Natl Acad Sci U S A, 2006. **103**(45): p. 16876-81.
277. Kondo, H., Nifuji, A., Takeda, S., Ezura, Y., Rittling, S.R., Denhardt, D.T., Nakashima, K., Karsenty, G., and Noda, M., *Unloading induces osteoblastic cell suppression and osteoclastic cell activation to lead to bone loss via sympathetic nervous system.* J Biol Chem, 2005. **280**(34): p. 30192-200.

278. Bonnet, N., Gadois, C., McCloskey, E., Lemineur, G., Lespessailles, E., Courteix, D., and Benhamou, C.L., *Protective effect of beta blockers in postmenopausal women: influence on fractures, bone density, micro and macroarchitecture.* Bone, 2007. **40**(5): p. 1209-16.
279. Paso, J.A., Henry, M.J., Sanders, K.M., Kotowicz, M.A., Seeman, E., and Nicholson, G.C., *Beta-adrenergic blockers reduce the risk of fracture partly by increasing bone mineral density: Geelong Osteoporosis Study.* J Bone Miner Res, 2004. **19**(1): p. 19-24.
280. Graham, S., Hammond-Jones, D., Gamie, Z., Polyzois, I., Tsiridis, E., and Tsiridis, E., *The effect of beta-blockers on bone metabolism as potential drugs under investigation for osteoporosis and fracture healing.* Expert Opin Investig Drugs, 2008. **17**(9): p. 1281-99.
281. Reid, I.R., *Effects of beta-blockers on fracture risk.* J Musculoskelet Neuronal Interact, 2008. **8**(2): p. 105-10.
282. Reid, I.R., Gamble, G.D., Grey, A.B., Black, D.M., Ensrud, K.E., Browner, W.S., and Bauer, D.C., *beta-Blocker use, BMD, and fractures in the study of osteoporotic fractures.* J Bone Miner Res, 2005. **20**(4): p. 613-8.
283. de Vries, F., Pouwels, S., Bracke, M., Leufkens, H.G., Cooper, C., Lammers, J.W., and van Staa, T.P., *Use of beta-2 agonists and risk of hip/femur fracture: a population-based case-control study.* Pharmacoepidemiol Drug Saf, 2007. **16**(6): p. 612-9.
284. Farr, J.N., Charkoudian, N., Barnes, J.N., Monroe, D.G., McCready, L.K., Atkinson, E.J., Amin, S., Melton, L.J. 3rd, Joyner, M.J., and Khosla, S., *Relationship of sympathetic activity to bone microstructure, turnover, and plasma osteopontin levels in women.* J Clin Endocrinol Metab, 2012. **97**(11): p. 4219-27.
285. Partridge, N.C., Bloch, S.R., and Pearman, A.T., *Signal transduction pathways mediating parathyroid hormone regulation of osteoblastic gene expression.* J Cell Biochem, 1994. **55**(3): p. 321-7.
286. Tam, C.S., Heersche, J.N., Murray, T.M., and Parsons, J.A., *Parathyroid hormone stimulates the bone apposition rate independently of its resorptive action: differential effects of intermittent and continuous administration.* Endocrinology, 1982. **110**(2): p. 506-12.
287. Ishizuya, T., Yokose, S., Hori, M., Noda, T., Suda, T., Yoshiki, S., and Yamaguchi, A., *Parathyroid hormone exerts disparate effects on osteoblast differentiation depending on exposure time in rat osteoblastic cells.* J Clin Invest, 1997. **99**(12): p. 2961-70.
288. Yu, B., Zhao, X., Yang, C., Crane, J., Xian, L., Lu, W., Wan, M., and Cao, X., *Parathyroid hormone induces differentiation of mesenchymal stromal/stem cells by enhancing bone morphogenetic protein signaling.* J Bone Miner Res, 2012. **27**(9): p. 2001-14.
289. Calvi, L.M., Sims, N.A., Hunzelman, J.L., Knight, M.C., Giovannetti, A., Saxton, J.M., Kronenberg, H.M., Baron, R., and Schipani, E., *Activated parathyroid hormone/parathyroid hormone-related protein receptor in osteoblastic cells differentially affects cortical and trabecular bone.* J Clin Invest, 2001. **107**(3): p. 277-86.

290. Tascau, L., Gardner, T., Anan, H., Yongpravat, C., Cardozo, C.P., Bauman, W.A., Lee, F.Y., Oh, D.S., and Tawfeek, H.A., *Activation of protein kinase A in mature osteoblasts promotes a major bone anabolic response.* Endocrinology, 2016. **157**(1): p. 112-26.
291. Fan, Y., Hanai, J.I., Le, P.T., Bi, R., Maridas, D., DeMambro, V., Figueroa, C.A., Kir, S., Zhou, X., Mannstadt, M., Baron, R., Bronson, R.T., Horowitz, M.C., Wu, J.Y., Bilezikian, J.P., Dempster, D.W., Rosen, C.J., and Lanske, B., *Parathyroid Hormone Directs Bone Marrow Mesenchymal Cell Fate.* Cell, 2017. **25**(3): p. 661-72.
292. Roy, M.E., and Nishimoto, S.K., *Matrix Gla protein binding to hydroxyapatite is dependent on the ionic environment: calcium enhances binding affinity but phosphate and magnesium decrease affinity.* Bone, 2002. **31**(2): p. 296-302.
293. Price, P.A., and Williamson, M.K., *Primary structure of bovine matrix Gla protein, a new vitamin K-dependent bone protein.* J Biol Chem, 1985. **260**(28): p. 14971-5.
294. Hauschka, P.V., Lian, J.B., Cole, D.E., and Gundberg, C.M., *Osteocalcin and matrix Gla protein: vitamin K-dependent proteins in bone.* Physiol Rev, 1989. **69**(3): p. 990-1047.
295. Billiard, J., Umayahara, Y., Wiren, K., Centrella, M., McCarthy, T.L., and Rotwein, P., *Regulated nuclear-cytoplasmic localization of CCAAT/enhancer-binding protein delta in osteoblasts.* J Biol Chem, 2001. **276**(18): p. 15354-61.
296. Zha, L., Hou, N., Wang, J., Yang, G., Gao, Y., Chen, L., and Yang, X., *Collagen1alpha1 promoter drives the expression of Cre recombinase in osteoblasts of transgenic mice.* J Genet Genomics, 2008. **35**(9): p. 525-30.
297. Chiu, W.S., McManus, J.F., Notini, A.J., Cassady, A.I., Zajac, J.D., and Davey, R.A., *Transgenic mice that express Cre recombinase in osteoclasts.* Genesis, 2004. **39**(3): p. 178-85.
298. Zhong, Z.A., Kot, A., Lay, Y.E., Zhang, H., Jia, J., Lane, N.E., and Yao, W., *Sex-Dependent, Osteoblast Stage-Specific Effects of Progesterone Receptor on Bone Acquisition.* J Bone Miner Res, 2017. **Epub ahead of print**.

Vita

Catherine Nicole Kaminski Withers

Education

Asbury University, Wilmore, KY 2007-2011

B.A. in Biochemistry

Minors in Spanish and Mathematics

Awards and Fellowships

P.E.O. Scholar Award 2015-2016

Evelyn K. Aitken Named Scholar 2015-2016

National Science Foundation Graduate Research Fellowship 2014-2017

NIH T32 Interdisciplinary Training Grant 2012-2014

Research and Professional Experience

Graduate Student 2011-2017

University of Kentucky

Mentor: Douglas Andres, Ph.D.

Summer Undergraduate Research Fellowship 2010

Cincinnati Children's Hospital Medical Center

Mentor: Sean Moore, M.D.

Research Experience for Undergraduates 2009

New Mexico Institute of Mining and Technology

Mentors: Wim Steelant, Ph.D., and Severine van Slambrouck, Ph.D.

Teaching Experience

University of Kentucky, Lexington, KY

Teaching Assistant, Critical Scientific Readings (IBS610)	Fall 2016
Teaching Assistant, Critical Scientific Readings (IBS610)	Fall 2014
Teaching Assistant, Principles of Biochemistry (BCH401G)	Fall 2012

Asbury University, Wilmore, KY

Lab Assistant, Organic Chemistry Laboratory (CHE 202)	Spring 2011
Lab Assistant, Organic Chemistry Laboratory (CHE 201)	Fall 2010
Lab Assistant, General Chemistry Laboratory (CHE 124)	Spring 2010
Lab Assistant, General Chemistry Laboratory (CHE 123)	Fall 2009

Publications

Levitan BM, Manning JR, **Withers CN**, Smith JD, Shaw RM, Andres DA, Sorrell VL, and Satin J. Rad-deletion phenocopies tonic sympathetic stimulation of the heart. *J Cardiovasc Transl Res.* 2016;9(5-6):432-44.

Manning JR, **Withers CN**, Levitan B, Smith JD, Andres DA, and Satin J. Loss of Rad-GTPase produces a novel adaptive cardiac phenotype resistant to systolic decline with aging. *Am J Physiol Heart Circ Physiol*. 2015;309(8):H1336-45.

Shi GX and **Kaminski CN**. Analysis of the Rit subfamily GTPase-mediated signaling and neuronal differentiation and survival. *Methods Mol. Biol.* 2014;1120:217-40.

Manning JR, Yin G, **Kaminski CN**, Magyar J, Feng HZ, Penn J, Sievert G, Jin JP, Andres DA, and Satin J. Rad GTPase deletion increases L-type

calcium channel current leading to increased cardiac contraction. *J Am Heart Assoc.* 2013;2(6):e000459.

Kaminski CN, Ferrey SL, Lowrey T, Guerra L, van Slambrouck S, and Steelant WFA. In vitro anticancer activity of Anemopsis californica. *Oncol Lett.* 2010;1(4):711-5.

Janser RFJ, Meka RK, Bryant ZE, Adogla EA, Vogel EK, Wharton JL, Tilley CM, **Kaminski CN**, Ferrey SL, van Slambrouck S, Steelant WFA, and Janser I. Ethacrynic acid analogues lacking the α,β-unsaturated carbonyl unit – potential anti-metastatic drugs. *Bioorg Med Chem Lett.* 2010;20(6):1848-50.

Presentations

American Society for Bone and Mineral Research (Poster Presentation)

September 2016, Atlanta, GA

Biochemistry Department Student Seminar Series (Oral Presentation)

September 2016, University of Kentucky, Lexington, KY

Bluegrass Molecular Biophysics Symposium (Poster Presentation)

May 2016, University of Kentucky, Lexington, KY

Postdoctoral Research Symposium (Poster Presentation)

May 2016, University of Kentucky, Lexington, KY

2ND PLACE AWARD

Biochemistry Department Retreat (Poster Presentation)

May 2016, University of Kentucky, Lexington, KY

2ND PLACE AWARD

Biochemistry Department Student Seminar Series (Oral Presentation)

January 2016, University of Kentucky, Lexington, KY

Biochemistry Department Retreat (Oral Presentation)

May 2015, University of Kentucky, Lexington, KY

American Society for Biochemistry and Molecular Biology (Poster Presentation)

April 2015, Boston, MA

STUDENT TRAVEL AWARD

Biochemistry Department Student Seminar Series (Oral Presentation)

January 2015, University of Kentucky, Lexington, KY

Biochemistry Student Data Club (Oral Presentation)

December 2014, University of Kentucky, Lexington, KY

Appalachian Regional Cell Conference (Oral Presentation)

November 2014, Marshall University, Huntington, WV

BEST ABSTRACT AWARD WINNER

Gill Heart Institute Cardiovascular Research Day (Poster Presentation)

October 2014, University of Kentucky, Lexington, KY

Biochemistry Student Data Club (Oral Presentation)

February 2014, University of Kentucky, Lexington, KY

Biochemistry Department Student Seminar Series (Oral Presentation)

December 2013, University of Kentucky, Lexington, KY

Gill Heart Institute Cardiovascular Research Day (Oral Presentation)

October 2013, University of Kentucky, Lexington, KY

Biochemistry Department Retreat (Oral Presentation)

June 2013, University of Kentucky, Carrollton, KY

1ST PLACE AWARD

Biochemistry Department Retreat (Poster Presentation)

June 2013, University of Kentucky, Carrollton, KY

American Society for Biochemistry and Molecular Biology (Poster Presentation)

April 2013, Boston, MA

STUDENT TRAVEL AWARD

Biochemistry Student Data Club (Oral Presentation)

March 2013, University of Kentucky, Lexington, KY

Biochemistry Department Student Seminar Series (Oral Presentation)

January 2013, University of Kentucky, Lexington, KY

Gill Heart Institute Cardiovascular Research Day (Oral Presentation)

October 2012, University of Kentucky, Lexington, KY

Biochemistry Department Retreat (Oral Presentation)

June 2012, University of Kentucky, Carrollton, KY

Kentucky Academy of Sciences Meeting (Oral Presentation)

November 2010, Western Kentucky University, Bowling Green, KY

Undergraduate Research Symposium (Oral Presentation)

July 2009, New Mexico Tech, Socorro, NM